

COMPARISON OF FILTRATION EFFICIENCY OF
PLEATED FILTERS FOR DIFFERENT
PARTICLE SIZES

By

PUNBET SAXENA

Bachelor of Engineering

University of Mysore

Mysore, India

1994

Submitted to the faculty of the
Graduate College of the
Oklahoma State University
in partial fulfillment of
the requirements for
the Degree of
MASTER OF SCIENCE
July, 1998

ACKNOWLEDGMENTS

I would like to express my gratitude to my major advisor Dr. R. L. Dougherty for his continued guidance, advice and encouragement throughout my two years as a graduate student at the Oklahoma State University. My sincere appreciation extends to Dr. F. W. Chambers for his valuable suggestions and help. I would like to thank Dr. A. J. Ghajar for agreeing to be on my committee.

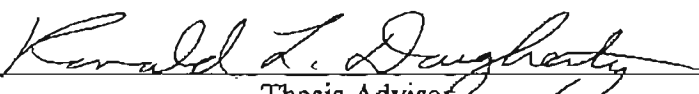
I would like to offer my sincere thanks to my colleague T. Gebreegziabher with whom I conducted the consistency measurements and some of the filtration efficiency measurements. I would like to express my heartfelt appreciation for the cooperation extended to me by my other colleagues S. H. Yao and A. Al-Sarkhi. I would also like to thank James Davis and other MAE North Lab personnel for their support.

I want to take this opportunity to thank my parents Arun Saxena and Deepika Arun for guiding me through my life and being there for me when I needed them. A special word of appreciation to my brother Navneet for being a wonderful friend and brother.

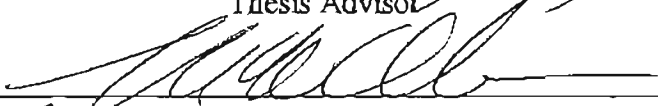
Finally, I extend my gratitude to Dayco-Purolator Products, Inc., and the Oklahoma Center for the Advancement of Science and Technology (OCAST) for financially supporting this study.

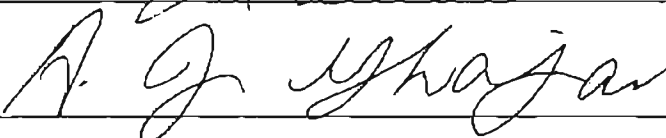
COMPARISON OF FILTRATION EFFICIENCY OF
PLEATED FILTERS FOR DIFFERENT
PARTICLE SIZES

Thesis Approved:



Thesis Advisor







Dean of the Graduate College

TABLE OF CONTENTS

Chapter	Page
1. INTRODUCTION.....	1
1.1 Summary of the Present Research.....	2
1.2 Thesis Layout	3
2. LITERATURE REVIEW	4
2.1 Introduction	4
2.2 Mechanisms of Particle Deposition	6
2.2.1 Diffusion Deposition	6
2.2.2 Direct Interception	8
2.2.3 Inertial Mechanism	9
2.2.4 Gravitational Mechanism	10
2.2.5 Electrostatic Mechanism.....	11
2.2.6 Deposition due to London-van der Waals Forces	12
2.3 Combined Filtration Mechanisms	14
2.4 Interference Effect	15
2.5 Characteristics of Filters	17
2.5.1 Selective Characteristics	17
2.5.2 Velocity	18
2.5.3 Pressure and Temperature	19
2.6 Experimental Analysis	21
2.6.1 Verification of Theoretical Models	22
2.6.1.1 Research at OSU	25
2.6.2 Evaluation of Filter Media	30
2.7 Standard Testing Methods	34
2.7.1 SAE J726 Test Code	34
2.7.2 SAE J1669 Passenger Compartment Air Filtration Code	35
2.8 Present Work	36

3.	FLOW AND EXPERIMENTAL SETUP	37
	3.1 Summary	37
	3.2 Laser Setup	38
	3.3 Data Collection and Processing Unit	48
	3.4 Flow System	49
	3.4.1 Small Angle Diffuser Housing	51
	3.4.2 Standard J726 Housing	51
	3.4.3 Simulated Automotive Filter Housing	52
4.	CONSISTENCY MEASUREMENTS	57
	4.1 Laser Power	58
	4.2 Atomizer Consistency Tests	64
	4.3 Experimental Procedure	66
5.	RESULTS AND DISCUSSION	69
	5.1 Summary of the Experiments	69
	5.2 Small Angle Diffuser Housing Measurements	71
	5.3 SAE Housing Measurements	91
	5.4 Simulated Automotive Filter Housing Measurements	97
	5.5 Glass Beads	104
6.	SUMMARY AND CONCLUSIONS	105
	6.1 Summary	105
	6.2 Recommendations for Future Work	107
	REFERENCES	112
	APPENDIXES	119
	APPENDIX A - STOKES NUMBER CALCULATION	120
	APPENDIX B - RESULTS FOR 0.497 μm DIAMETER PSL PARTICLES IN THE SMALL ANGLE DIFFUSER HOUSING	122
	APPENDIX C - RESULTS FOR 2.04 μm DIAMETER PSL PARTICLES IN THE SMALL ANGLE DIFFUSER HOUSING	142
	APPENDIX D - RESULTS FOR 0.966 μm DIAMETER PSL PARTICLES IN THE SAE J726 HOUSING	160

APPENDIX E - RESULTS FOR 0.966 μm DIAMETER PSL PARTICLES IN THE SIMULATED AUTOMOTIVE FILTER HOUSING	172
APPENDIX F - CONSISTENCY MEASUREMENTS FOR THE LASER, THE ATOMIZER AND THE GLASS BEADS	181
APPENDIX G - EXPERIMENTS CONDUCTED TO VERIFY THE REPEATABILITY OF THE MEASUREMENTS	200
APPENDIX H - SWEEPED VOLUME TECHNIQUE	205
APPENDIX I - ERROR ANALYSIS	207
APPENDIX J - LIST OF EQUIPMENT	209

LIST OF TABLES

Table		Page
3.1	A13192 Pleated Filter Dimensions	54
5.1	Comparison of Laser Power Exiting the Transceiver Before and After Maintenance (@ 0.8 W from the Laser)	70
5.2	Summary of Small Angle Diffuser Housing Results for 2.04 and 0.497 μm Diameter Particles	73
5.3	Summary of Small Angle Diffuser Housing Results for 0.966 μm Diameter Particles for Comparison with Those of Jadbabaei [1997]	90
5.4	Summary of SAE Housing Results for 0.966 μm Diameter Particles	92
5.5	Summary of Simulated Automotive Filter Housing Results for 0.966 μm Particles	103
TF-1a	Data for Figure F-1a (Date: May 28 - May 29, 1997)	183
TF-1b	Data for Figure F-1b (Date: June 16 - June 22, 1997)	183
TF-1c	Data for Figure F-1c (Date: June 23 - July 07, 1997)	184
TF-2a	Data for Figure F-2a (Date: May 21 - May 23, 1997)	186
TF-2b	Data for Figure F-2b (Date: May 25 - May 27, 1997)	186
TF-2c	Data for Figure F-2c (Date: June 06 - June 10, 1997)	187
TF-3a	Data for Figure F-3a (Date: May 29 - June 01, 1997)	189
TF-3b	Data for Figure F-3b (Date: June 02 - June 03, 1997)	189
TF-3c	Data for Figure F-3c (Date: June 04 - June 07, 1997)	190
TF-4a	Data for Figure F-4a (Date: July 11 - July 12, 1997)	192
TF-4b	Data for Figure F-4b (Date: July 14 - July 15, 1997)	192
TF-4c	Data for Figure F-4c (Date: July 17 - July 18, 1997)	193
TF-5a	Sampling Rate for 2.04 Micron Particles (November 07, 1997 - March 28, 1998)	195
TF-5b	Sampling Rate for 0.497 Micron Particles (November 11, 1997 - March 28, 1998)	196
TF-5c	Sampling Rate for 0.966 Micron Particles (November 26, 1997 - November 27, 1997)	197
TF-6a	Data for Figure F-6 for Glass Beads	199

LIST OF FIGURES

Figure		Page
2.1	Particle Capture Mechanisms: A, Particle Capture by Interception; B, Particle Capture by Inertial Impaction; C, Particle Capture by Diffusional Deposition [Brown, 1993]	7
2.2	Schematic Diagram of the Collection Efficiencies of Different Particle Capture Mechanisms [Liu et al., 1985]	14
2.3	Influence of High Temperature Exposure on Charged Filter Media Efficiency [Ptak et al., 1994]	21
2.4	Influence of Humidity on Charged Filter Media Efficiency, with Initial RH = 50% [Ptak et al., 1994].	22
2.5	Illustration of the Concept of Single Fiber Efficiency [Brown, 1993]	23
2.6	Comparison of Experimental Efficiency Measurements with the Theory of Harrop [1969] in the Inertial Impaction Regime [Lee, 1977]	24
2.7	Elemental Efficiencies over A13192 Filter (Duran's Model, Packing Density = 0.49) [Natarajan, 1995]	26
2.8	Elemental Efficiencies over A13192 Filter (Duran's Model, Packing Density = 0.345) [Natarajan, 1995]	27
2.9	Overall Filter Efficiencies [Anand, 1997] Compared to Lee [1977]	28
2.10	Comparison of Filter Efficiencies [Jadabaei, 1997]	29
2.11	Typical Dust Capacity Performance Levels of Air Induction Filters (AIF) [Bugli, 1997]	31
2.12	Typical Initial Efficiency Performance Levels of Air Induction Filters (AIF) [Bugli, 1997]	31

2.13	Ability of Tests to Discriminate Between Filter Media [McDonald et al., 1997]	32
2.14	Pressure Drop of FA6005 with Dust Loading [Poon and Liu, 1997]	33
2.15	Pressure Drop of KE1351 with Dust Loading [Poon and Liu, 1997]	34
3.1	Schematic Diagram of the Fiber Drive	38
3.2	Layout of the 7 x 5 Measurement Grid on the Filter	40
3.3	A Typical Laser Doppler Signal	41
3.4	Cylindrical Instrument for Holding the Pinhole Aperture	42
3.5	Comparison of Laser Power Variation [June 16 - June 22, 1997]	44
3.6	Laser Setup	44
3.7	Room Layout	45
3.8	Variation of Laser Power at the Transceiver for Uncontrolled Temperature Inside the Plexiglas Box [May 21 - June 10, 1997]	46
3.9	Variation of Laser Power at the Transceiver for Uncontrolled Temperature Inside the Plexiglas Box, with Sensors Interchanged [May 28 - May 29, 1997]	47
3.10	Laser Power Variation at Constant Temperature [May 28 - May 29, 1997]	48
3.11	Data Collection and Processing Unit	49
3.12	Small Angle Diffuser Housing	52
3.13	Standard J726 Housing	53
3.14	Simulated Automotive Filter Housing	53
3.15	Flow By-pass System	54
3.16	Experimental Setup	55

3.17	Absolute Filter Used for Preventing the Release of Particles into the Atmosphere	56
4.1	Setup for Isolation of Vibration from the Blower [Anand, 1997]	59
4.2	Variation of Laser Power at the Transceiver for a Constant Temperature Inside the Plexiglas Box, Test Stand's Blower Shut Off	60
4.3	Variation of Laser Power at the Transceiver for a Constant Temperature Inside the Plexiglas Box, Test Stand's Blower in Operation	60
4.4	Variation of Laser Power at the Transceiver for Uncontrolled Temperature Inside the Plexiglas Box, Test Stand's Blower in Operation	61
4.5	Variation of Laser Power at the Transceiver for Uncontrolled Temperature Inside the Plexiglas Box, Test Stand's Blower Shut Off	61
4.6	Variation in Laser Power When the Temperature Inside the Plexiglas Box Was Allowed to Fluctuate	63
4.7	Variation in Laser Power When the Temperature Inside the Plexiglas Box Was Kept Constant	63
4.8	Consistency Test Setup for the Atomizer	64
4.9	Atomizer Consistency Results for 0.966 μm Particles	65
5.1	Upstream Number Density for Test SAH10_05_1 at 13.61 m^3/hr	76
5.2	Downstream Number Density for Test SAH10_05_1 at 13.61 m^3/hr	77
5.3	Upstream Velocity Profile for Test SAH10_05_1 at 13.61 m^3/hr	78
5.4	Downstream Velocity Profile for Test SAH10_05_1 at 13.61 m^3/hr	79
5.5	Pleated Filter Efficiency for Test SAH10_05_1 at 13.61 m^3/hr	80
5.6	Upstream Number Density for Test SAH50_05_1 at 77.07 m^3/hr	81
5.7	Downstream Number Density for Test SAH50_05_1 at 77.07 m^3/hr	81

5.8	Upstream Velocity Profile for Test SAH50_05_1 at 77.07 m ³ /hr	82
5.9	Downstream Velocity Profile for Test SAH50_05_1 at 77.07 m ³ /hr	82
5.10	Pleated Filter Efficiency for Test SAH50_05_1 at 77.07 m ³ /hr	83
5.11	Variation of Filtration Efficiency with Stokes Number	85
5.12	Variation of Filtration Efficiency with Flow Rate	86
5.13	Comparison of Experimental Results of Present Study with Theoretical Model Based on Perfect Adhesion Theory (Duran, 1995) for Interception Parameter = 0.01, Fiber Diameter D _r = 38 μm, Packing Density = 0.23	87
5.14	Comparison of Local Filtration Efficiency Measurements in Small Angle Diffuser Housing at 103.69 m ³ /hr with Jadbabaei [1997]	88
5.15	Local Filtration Efficiency Measurements in Small Angle Diffuser Housing at a Flow Rate 188.45 m ³ /hr [Jadbabaei, 1997]	89
5.16	Local Filtration Efficiency Measurements in Small Angle Diffuser Housing at a Flow Rate of 188.45 m ³ /hr [Present Study]	89
5.17	Upstream Number Density for Test SAE200_1_2 at 314.73 m ³ /hr	93
5.18	Downstream Number Density for Test SAE200_1_2 at 314.73 m ³ /hr	93
5.19	Upstream Velocity Profile for Test SAE200_1_2 at 314.73 m ³ /hr	94
5.20	Downstream Velocity Profile for Test SAE200_1_2 at 314.73 m ³ /hr	94
5.21	Pleated Filter Efficiency for Test SAE200_1_2 at 314.73 m ³ /hr	95
5.22	Variation of Filtration Efficiency with Stokes Number for SAE J726 Housing	96
5.23	Overall Efficiency vs. Flow Rate for the SAE Housing (0.966 μm Particles) [Natarajan, 1995]	97
5.24	Upstream Number Density for Test SAF15_1_1 at 21.55 m ³ /hr	98
5.25	Downstream Number Density for Test SAF15_1_1 at 21.55 m ³ /hr	98

5.26	Upstream Velocity Profile for Test SAF15_1_1 at 21.55 m ³ /hr	100
5.27	Downstream Velocity Profile for Test SAF15_1_1 at 21.55 m ³ /hr	100
5.28	Pleated Filter Efficiency for Test SAF15_1_1 at 21.55 m ³ /hr	101
5.29	Variation of Filtration Efficiency with Stokes Number for Simulated Automotive Filter (SAF) Housing	102
5.30	Variation of Filtration Efficiency with Flow Rate for SAF Housing	104
B-1	Pleated Filter Efficiency for Test SAH10_05_2 at 13.61 m ³ /hr	123
B-2	Pleated Filter Efficiency for Test SAH15_05_1 at 21.55 m ³ /hr	124
B-3	Pleated Filter Efficiency for Test SAH15_05_2 at 21.55 m ³ /hr	125
B-4	Pleated Filter Efficiency for Test SAH20_05_1 at 29.48 m ³ /hr	126
B-5	Pleated Filter Efficiency for Test SAH20_05_2 at 29.48 m ³ /hr	127
B-6	Pleated Filter Efficiency for Test SAH25_05_1 at 37.42 m ³ /hr	128
B-7	Pleated Filter Efficiency for Test SAH25_05_2 at 37.42 m ³ /hr	129
B-8	Pleated Filter Efficiency for Test SAH30_05_1 at 45.35 m ³ /hr	130
B-9	Pleated Filter Efficiency for Test SAH30_05_2 at 45.35 m ³ /hr	131
B-10	Pleated Filter Efficiency for Test SAH50_05_2 at 77.07 m ³ /hr	132
B-11	Pleated Filter Efficiency for Test SAH75_05_1 at 104.26 m ³ /hr	133
B-12	Pleated Filter Efficiency for Test SAH75_05_2 at 104.26 m ³ /hr	134
B-13	Pleated Filter Efficiency for Test SAH100_05_1 at 146.36 m ³ /hr	135
B-14	Pleated Filter Efficiency for Test SAH100_05_2 at 146.36 m ³ /hr	136
B-15	Pleated Filter Efficiency for Test SAH100_05_3 at 146.36 m ³ /hr	137
B-16	Pleated Filter Efficiency for Test SAH125_05_1 at 188.45 m ³ /hr	138
B-17	Pleated Filter Efficiency for Test SAH125_05_2 at 188.45 m ³ /hr	139

B-18	Pleated Filter Efficiency for Test SAH150_05_1 at 230.54 m ³ /hr	140
B-19	Pleated Filter Efficiency for Test SAH150_05_2 at 230.54 m ³ /hr	141
C-1	Pleated Filter Efficiency for Test SAH12_2_1 at 16.78 m ³ /hr	143
C-2	Pleated Filter Efficiency for Test SAH12_2_2 at 16.78 m ³ /hr	144
C-3	Pleated Filter Efficiency for Test SAH12_2_3 at 16.78 m ³ /hr	145
C-4	Pleated Filter Efficiency for Test SAH15_2_1 at 21.55 m ³ /hr	146
C-5	Pleated Filter Efficiency for Test SAH15_2_2 at 21.55 m ³ /hr	147
C-6	Pleated Filter Efficiency for Test SAH20_2_1 at 29.48 m ³ /hr	148
C-7	Pleated Filter Efficiency for Test SAH20_2_2 at 29.48 m ³ /hr	149
C-8	Pleated Filter Efficiency for Test SAH25_2_1 at 37.42 m ³ /hr	150
C-9	Pleated Filter Efficiency for Test SAH25_2_2 at 37.42 m ³ /hr	151
C-10	Pleated Filter Efficiency for Test SAH40_2_1 at 61.20 m ³ /hr	152
C-11	Pleated Filter Efficiency for Test SAH40_2_2 at 61.20 m ³ /hr	153
C-12	Pleated Filter Efficiency for Test SAH50_2_1 at 77.07 m ³ /hr	154
C-13	Pleated Filter Efficiency for Test SAH50_2_2 at 77.07 m ³ /hr	155
C-14	Pleated Filter Efficiency for Test SAH75_2_1 at 104.26 m ³ /hr	156
C-15	Pleated Filter Efficiency for Test SAH75_2_2 at 104.26 m ³ /hr	157
C-16	Pleated Filter Efficiency for Test SAH125_2_1 at 188.45 m ³ /hr	158
C-17	Pleated Filter Efficiency for Test SAH125_2_2 at 188.45 m ³ /hr	159
D-1	Pleated Filter Efficiency for Test SAE10_1_1 at 13.61 m ³ /hr	161
D-2	Pleated Filter Efficiency for Test SAE10_1_2 at 13.61 m ³ /hr	162
D-3	Pleated Filter Efficiency for Test SAE25_1_1 at 37.42 m ³ /hr	163
D-4	Pleated Filter Efficiency for Test SAE25_1_2 at 37.42 m ³ /hr	164

D-5	Pleated Filter Efficiency for Test SAE40_1_1 at 61.20 m ³ /hr	165
D-6	Pleated Filter Efficiency for Test SAE40_1_2 at 61.20 m ³ /hr	166
D-7	Pleated Filter Efficiency for Test SAE120_1_1 at 180.03 m ³ /hr	167
D-8	Pleated Filter Efficiency for Test SAE125_1_1 at 188.45 m ³ /hr	168
D-9	Pleated Filter Efficiency for Test SAE125_1_2 at 188.45 m ³ /hr	169
D-10	Pleated Filter Efficiency for Test SAE200_1_1 at 314.73 m ³ /hr	170
D-11	Pleated Filter Efficiency for Test SAE200_1_3 at 314.73 m ³ /hr	171
E-1	Pleated Filter Efficiency for Test SAF15_1_2 at 21.55 m ³ /hr	173
E-2	Pleated Filter Efficiency for Test SAF20_1_1 at 29.48 m ³ /hr	174
E-3	Pleated Filter Efficiency for Test SAF25_1_1 at 37.42 m ³ /hr	175
E-4	Pleated Filter Efficiency for Test SAF25_1_2 at 37.42 m ³ /hr	176
E-5	Pleated Filter Efficiency for Test SAF45_1_1 at 70.07 m ³ /hr	177
E-6	Pleated Filter Efficiency for Test SAF60_1_1 at 79 m ³ /hr	178
E-7	Pleated Filter Efficiency for Test SAF60_1_2 at 79 m ³ /hr	179
E-8	Pleated Filter Efficiency for Test SAF100_1_1 at 146.36 m ³ /hr	180
F-1	Laser Power Measured at the Transceiver When the Temperature in the Plexiglas Box Is Controlled	182
F-2	Laser Power Measured at the Transceiver When the Temperature in the Plexiglas Box Is Not Controlled	185
F-3	Laser Power Measured at Different Points Before the Transceiver	188
F-4	Laser Power Measured for Verifying the Effects of Air Current and Alignment of Couplers	191
F-5	Atomizer Consistency Measurements for 0.497, 0.966, 2.04 Micron Particles	194

F-6	Consistency Measurements for 1.59 Micron Glass Beads at 103.69 m ³ /hr	198
G-1	Comparison of Local Efficiency, Upstream Velocity and Number Density Profiles with Jadbabaei [1997] at 77.07 m ³ /hr	201
G-2	Comparison of Local Efficiency, Upstream Velocity and Number Density Profiles with Jadbabaei [1997] at 103.69 m ³ /hr	202
G-3	Comparison of Local Efficiency, Upstream Velocity and Number Density Profiles with Jadbabaei [1997] at 188.45 m ³ /hr	203
G-4	Comparison of Local Filtration Efficiencies for Tests SAH75_05_1 and SAH75_05_2	204
H-1	Swept Volume [Liang, 1997]	206

NOMENCLATURE

a	particle radius (m)
A	cross-sectional area of the LDV probe volume (m^2)
A_f	filter surface area (m^2)
A^*	a constant
B^*	a constant
C	a constant
C_n	Cunningham slip correction factor
C_s	a constant ($^{\circ}K$)
C_q	charge constant ($N\cdot m^2/Coulomb^2$)
d_{pm}	particle minimum diameter (m)
D	diffusion coefficient of the particle (m^2/s)
D_f	diameter of fiber (m)
D_p	diameter of particle (m)
D_2	dielectric constant of the fiber (at 1 MHz)
E_D	capture coefficient for particle deposition due to diffusion
E_{DRI}	capture coefficient for the simultaneous action of diffusion, interception, and inertia

E_f	total capture coefficient for the fiber
E_{β}	effective capture coefficient with an unknown dependence on β
E_j	capture coefficient of a fiber in a filter due to an individual mechanism
E_k	kinetic energy of the particle (kJ)
E_G	capture coefficient of a fiber due to gravitation
E_L	layer efficiency (m^{-1})
E_M	capture coefficient of the fiber due to London-van der Waals force
E_{Oq}	capture coefficient for electrostatic mechanism
E_s	single fiber efficiency
F	London van der Waals attraction force (N)
$F(L')$	interaction between the charge on an aerosol and its image on the fiber (N)
g	acceleration due to gravity (m/s^2)
g_c	gravitational constant ($kg\cdot m/N\cdot s^2$)
G_1	flux of particles into the filter (particles/ m^2)
G_2	flux of particles from the filter (particles/ m^2)
k	Boltzmann's constant ($10^{-23} J \text{ deg}^{-1}$)
K	hydrodynamic factor of Kuwabara flow
L	filter thickness (m)
L'	distance between the particle and the fiber (m)
L''	distance between the particle center and a plane (m)
m	mass of the particle (kg)
n_0	particle concentration (particles/ m^3)
n_i	measured local particle number density (particles/ m^3)

n_{down}	local number density of particles downstream of the filter (m^{-3})
n_{up}	local number density of particles upstream of the filter (m^{-3})
n_u	upstream number density (m^{-3})
n_d	downstream number density (m^{-3})
N	particle count
N_i	number of particles counted at a particular grid point location
N_D	dimensionless parameter for diffusion mechanism ($= \text{Pe}^{-1}$)
N_G	dimensionless parameter for gravitational mechanism (Eq. 2.13)
N_{Oq}	dimensionless parameter for electrostatic mechanism (Eq. 2.16)
N_M	dimensionless parameter for London-van der Waals force (Eq. 2.19)
N_R	dimensionless parameter for direct interception mechanism ($= D_p/D_f$)
p	pressure (Pa)
Pe	Peclet number ($= U_0 \frac{D_f}{D}$)
q	particle charge (Coulomb)
Q	charge per unit length of the fiber (Coulomb/m)
Q^*	a constant
$Q_{\text{flow nozzle}}$	volumetric flow rate measured by ASME flow nozzle (Scfm)
Q_0	Hamaker's constant of interaction (J)
Q_{TSI}	volumetric flow rate measured by TSI flow meter (Scfm)
Q_{flow}	volumetric flow rate of fluid/particle suspension being atomized in the atomizer (m^3/s)
R_f	fiber radius (m)

R_D	the ratio of the particle diameter D_p to the fiber diameter D_f
Re	Reynolds number of the cylinder (fiber) $(= \frac{D_f U_0 \rho_g}{\mu_a})$
Re_p	particle Reynolds Number $(= \frac{D_p U_0 \rho_g}{\mu_a})$
Re_ϕ	Reynolds number of the cylinder (as calculated by this author) $(= D_f/D_p C_n)$
R_{nd}	ratio of upstream and downstream number densities
S'	solidarity factor
Sc	Schmidt Number (ν/D)
St	Stokes number $(= \frac{C_n D_p^2 \rho_p U_0}{18 \mu_s D_f})$
t	time (s)
t_i	time taken by LDV to count N_i particles at a particular grid point location "i" (s)
T_0	LDV data acquisition time (s)
t_{sol}	total duration of the full experiment to map efficiencies over a filter surface (s)
T	temperature (K)
T_m	temperature minimum characteristic (K)
U_0	velocity of the flow approaching the filter (m/s)
v_i	average particle velocity at a particular grid point location (m/s)
y	Cartesian coordinate (m)

α	coefficient of absorption of particles by the filter
β	filter solidity or packing density (= volume of fibers/total volume of filter)
δx	thickness of a layer of the filter (m)
Δp	pressure drop across the filter (mm of water)
η	filter efficiency
η_{12}	resultant efficiency due to any two different mechanisms
η_i	local filter efficiency
η_D	collection efficiency due to diffusion
η_{DR}	collection efficiency due to interaction of interception and diffusion
η_I	collection efficiency due to inertial impaction
η_{max}	maximum efficiency due to variation in number density
η_{min}	minimum efficiency due to variation in number density
η_R	collection efficiency due to interception
η_s	single fiber efficiency
λ	mean free path of molecules at Normal Temperature and Pressure (m)
μ_a	dynamic viscosity of air (Pa-s)
ν	kinematic viscosity of the fluid (m ² /s)
ρ	distance between the particle and the fiber (m)
ρ'	distance between the particle center and a plane (m)
ρ_a	density of air (kg/m ³)
ρ_g	density of the fluid flowing through the filter (kg/m ³)

ρ_p	density of seeding particles (kg/m^3)
ϕ_r	number of particles captured by the filter in unit time (particles/s)
ϕ^*	inertial parameter when Stokes Number is not valid

Chapter 1

INTRODUCTION

Filtration is both a process of major contemporary importance and one with its beginnings rooted in antiquity. Hardly a modern industry exists without some dependence on a filtering operation. The earliest Chinese writings describe a crude form of filtration, as do Hebrew scrolls [Matteson, 1987]. The first patent on a filter may be that issued by the French government in 1789 to one Joseph Amy [Matteson, 1987]. A British patent of 1791 describes an operation identified as filtration by ascent, the invention here being a vessel containing coarse gravel at the bottom followed by graded sand above.

The complete evaluation of an air filter or filtration installation involves more than a single measurement of its efficiency in retaining particles of a standard test material, although it is the particulate efficiency which is generally of prime importance and to which most of this study and thesis is devoted. Other factors requiring attention are [Matteson, 1987]:

1. Resistance to air flow.

2. Loading capacity before a resistance to airflow increases to too high a level for proper functioning of the equipment.
3. Chemical and physical characteristics; for example, mechanical strength, capability to withstand acid mists.
4. Size, cost, ease of replacement.

1.1 Summary of the Present Research

This study involved the measurement of local filtration efficiency at 35 points over the face of a panel filter. The measurements were carried out at different flow rates and for different particle sizes. The tests were conducted in a housing related to the J1669 housing (Small Angle Diffuser (SAH) housing), the standard J726 housing (SAE housing), and a representative model of the actual filter housing (referred to as the Simulated Automotive Filter (SAF) housing in the later chapters of this thesis) from a Chrysler minivan. All of the tests were conducted on the Dayco-Purolator A13192 filters. The results were then compared with those of Jadbabaei [1997] for experimental comparison and Duran [1995] for theoretical comparison.

A Laser Doppler Velocimetry (LDV) system was used to make the measurements. Before taking the efficiency measurements on the filters, several experiments were carried out to measure the consistency of the equipment that was used during the measurements. This was essential to ascertain the reliability and the repeatability of the measurements. These included consistency measurements on the power of the laser, which has been

shown to be significantly dependent on the room temperature [Anand, 1997; Jadbabaei, 1997], and on the atomizer which feeds particles at a particular rate during the course of the experiment. To maintain the accuracy of the measurements and prevent any potential factor for discrepancy in the results, a new Small Angle Diffuser housing (SAH) was built, since the old housing had several old glued joints and thus were potential places of leakage in the housing.

1.2 Thesis Layout

Chapter 2 of this thesis is devoted to the literature review on the subject and discusses certain theoretical predictions based on models developed and results of previous researchers on the project. The LDV system details are discussed in Chapter 3 of this thesis. Chapter 4 gives a brief description of the consistency measurements that were made in order to verify the accuracy and repeatability of the measurements. Some of the filtration efficiency results are presented and discussed in Chapter 5. The conclusions based on the results of this study, and certain suggestions about areas of future research are discussed in Chapter 6. Additional results, graphs, and equipment are listed in the appendices. The data from the consistency measurements has been tabulated in the Appendix F.

Chapter 2

LITERATURE REVIEW

2.1 Introduction

The process of separating dispersed particles from a dispersed fluid by means of porous media is known as filtration. While the dispersing media may be a gas or a liquid, the medium can be either aerosols or lyosols [Pich, 1987]. As part of this literature review, attention has been limited to aerosol filtration. In the case of a clean filter, the pressure drop across a filter, Δp , is dependent on the properties of the fluid and the porous filtration media only. As the filter gets dirty, the pressure drop is also dependent on the properties of the particles on or in the filter. For a mono-disperse system of particles, the filter efficiency η is defined as

$$\eta = \frac{G_1 - G_2}{G_1} \quad (2.1)$$

where G_1 is the flux of particles into the filter and G_2 is the flux of particles exiting from the filter. The process of filtration involves three objects: the dispersed particles, the

dispersing medium and the porous filter medium. The characteristics of the dispersed particles include the diameter of the particle (D_p), the mass and the density (ρ_p) of the particle, the electric charge, dielectric constant and the chemical composition. The fluid flow is characterized by the velocity U_0 , density ρ_g , temperature T , pressure p , dynamic viscosity μ_a , and humidity. The filter media is dependent on its geometrical dimensions - the filter surface area A_f , filter thickness L , distribution of the media in the filter, porosity, electric charge, and dielectric constant. The pressure drop Δp and the filter efficiency η are dependent on nearly all of the factors mentioned above [Pich, 1987].

Theoretically, there are two distinguished phases in the process of filtration [Pich, 1987]. The first phase, known as the stationary phase, involves the deposition of the particles on a clean filter of a certain structure. This deposition does not change the basic structure of the filter and hence does not significantly affect the basic parameters of the filter: the pressure drop Δp and the filter efficiency η . Both Δp and η do not vary with time during this phase. This study involved the efficiency measurements during the stationary phase of the filtration process. However in reality, once the filter is being used, the particles get deposited on the filter, and it is not possible to maintain the stationary phase of the filtration process. There was no appreciable change in the pressure drop across the filter during the course of the experiments. It is therefore assumed that, during these experiments the filter did not enter the second phase of the filtration process known as the non-stationary filtration - which occurs, when the filter is partially plugged. This chapter introduces the reader to the various aspects of filtration and previous theoretical

and experimental studies in aerosol filtration with fibrous filters in general and the work done at Oklahoma State University in particular.

2.2 Mechanisms of Particle Deposition

Essentially, the deposition of particles from a flowing fluid onto bodies of simple geometry involves an interfacial mass transfer of small particles. In systems with a simple geometry, the interfacial mass transfer between the gas suspension and a solid body (filter fiber) is usually described by two quantities: a capture coefficient E_f and a local capture coefficient [Pich, 1987]. The capture coefficient of the body (fiber) is defined by

$$\phi_f = E_f n_0 U_0 D_f \quad (2.2)$$

Where ϕ_f is the number of particles captured by the fiber in a unit time, n_0 is the particle concentration, U_0 is the velocity of fluid flow, D_f is the diameter of the fiber placed perpendicular to the fluid flow.

The particle deposition on the filter medium takes place by several mechanisms: the most important of which are described below:

2.2.1 Diffusion Deposition

The trajectories of the small particles do not coincide with the streamlines of the fluid [Fig. 2.1]. This is because the Brownian motion increases with the decrease in particle diameter causing a corresponding increase in the intensity of diffusion deposition.

The capture coefficient E_D for particle deposition due to diffusion is a function of the Peclet number

$$Pe = \frac{D_f U_0}{D} \quad (2.3)$$

Peclet number is also defined as

$$Pe = Re Sc \quad (2.4)$$

where $Sc = \nu/D$ is the Schmidt Number and D is the diffusion coefficient of the particle.

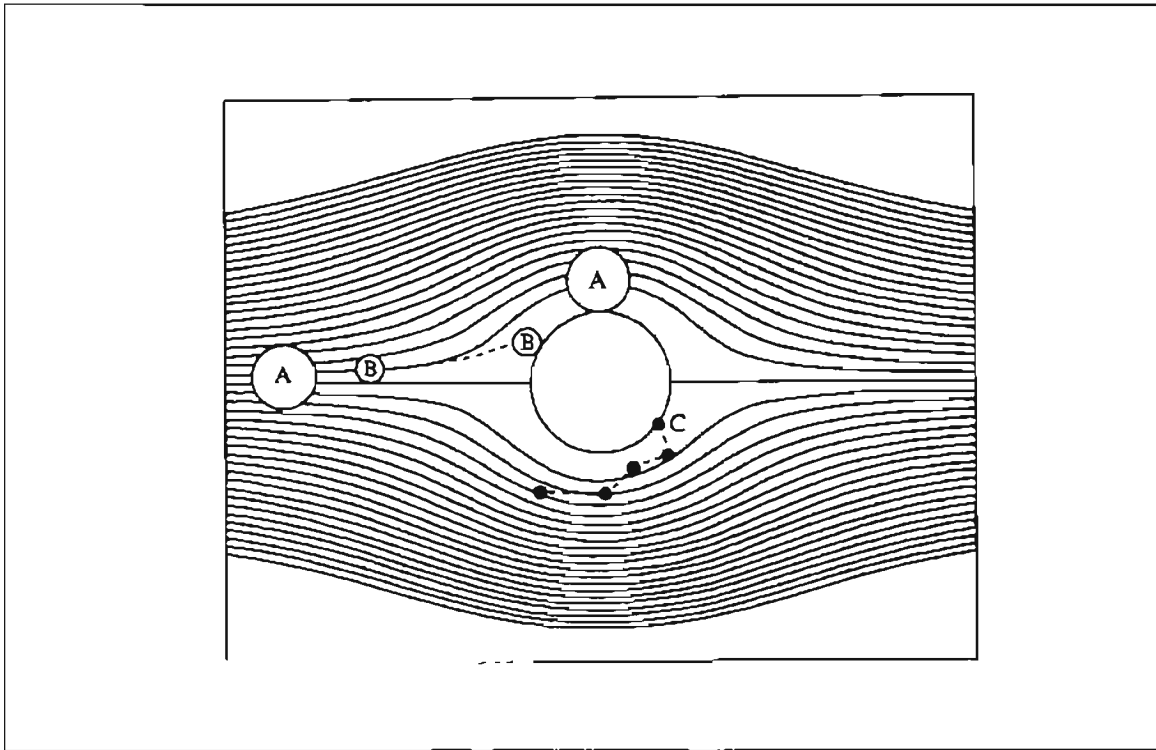


Figure 2.1: Particle Capture Mechanisms: A, Particle Capture by Interception; B, Particle Capture by Inertial Impaction; C, Particle Capture by Diffusional Deposition [Brown, 1993]

There are three regions for theoretical investigation. As shown in Pich [1987], Stechkina [1964] derived the following equation for small Pe numbers ($Pe \ll 1$) and viscous flow ($Re < 1$)

$$E_D = \frac{2\pi}{Pe(1.502 - \ln Pe)} \quad (2.5)$$

For $Pe \gg 1$ and $Re < 1$ (a condition usually satisfied in the case of fibrous filters), Friedlander [1958] has the following relation for this mechanism

$$E_D = \frac{2.22}{(2 - \ln Re)^{1/3}} Pe^{-2/3} \quad (2.6)$$

Making use of the Kuwabara - Happel velocity field, Stechkina deduced the following equation for $Pe \gg 1$, $Re \gg 1$

$$E_D = \frac{2.9}{(-C - \ln \beta)^{1/3}} Pe^{-2/3} \quad (2.7)$$

where β is the packing density of the filter and $C = 0.75$.

2.2.2 Direct Interception

This mechanism considers the finite size of the particles. This takes place as the particle approaches the collecting surface (following a streamline) and reaches a distance (from the fiber) equal to its radius [Fig. 2.1]. A special case of this mechanism, called the sieve effect, occurs when the distance between the fibers is less than the particle diameter D_p . The interception regime overlaps with the diffusion regime (0.1-0.5 μm) and the

impaction regime ($\geq 0.5 \mu\text{m}$), respectively. The efficiency due to this mechanism is described by [Lee and Liu, 1982]:

$$\eta_R = \left(\frac{1-\beta}{K} \right) \frac{R_D^2}{1+R_D} \quad (2.8)$$

Where R_D is the ratio of the particle diameter D_p to the fiber diameter D_f ; K is Kuwabara's hydrodynamic factor $\left(= -\frac{1}{2} \ln \beta - \frac{3}{4} + \beta - \frac{1}{4} \beta^2 \right)$

2.2.3 Inertial Mechanism

In a flowing fluid, the presence of a body results in a curvature of streamlines in the neighborhood of the body [Fig. 2.1]. However the particles due to their inertia do not follow the streamlines and instead are impinged on the body and are deposited there. The particle deposition due to this mechanism increases with increase in the particle size and flow velocity. At constant conditions, there is a limiting trajectory separating the trajectories of particles that are captured, from the trajectories of particles that miss the fiber and are not captured. The capture coefficient for particles of finite size due to their inertia, E_{IR} , is defined as the ratio of the number of captured particles to the number of particles that would be captured if the particles moved only in a straight line [Pich, 1987]. This coefficient is dependent upon several parameters; the most important of which is the Stokes number or the inertial parameter.

$$St = \frac{C_n \rho_p D_p^2 U_0}{18 \mu_a D_f} \quad (2.9)$$

For instances where the velocity or particles sizes are so great that the particle drag cannot be described Stokes' law, another parameter (ϕ^*) is used ($\phi^* = 0$ for particles obeying the Stokes' law) [Pich, 1987]

$$\phi^* = \frac{Re_p}{St} = 18 \frac{\rho_g}{\rho_p} Re_\phi \quad (2.10)$$

where Re_ϕ is the Reynolds number of the cylinder (fiber) which, as calculated by this author, is $D_f/(D_p C_n)$ (for Eq. 2.10 to be true, Re_ϕ does not appear to be a true Reynolds number), and Re_p is the particle Reynolds number and is given by

$$Re_p = \frac{D_p U_0 \rho_g}{\mu_a} \quad (2.11)$$

There have been several experimental investigations of the inertial deposition of particles. Pich [1987] reports that Landahl and Hermann [1949] expressed their results for $Re = 10$ by the empirical relationship

$$\eta_i = \frac{St^3}{St^3 + 0.77St^2 + 0.22} \quad (2.12)$$

2.2.4 Gravitational Mechanism

Particles can deposit from a flowing gas on collector surfaces under the influence of gravity. This deposition of particles due to gravitational force is expected to be

considerable for large particles and small flow velocities. The importance of the mechanism is described by a dimensionless parameter N_G (as calculated by this author N_G has dimensions of m^{-1}), which, for Stokes particles is given by [Pich, 1987]

$$N_G = \frac{D_p \rho_p g}{18 \mu_o U_o g_c} \quad (2.13)$$

The capture coefficient of a fiber E_G describing the rate of particle deposition due to gravitational forces is a function of this parameter i.e. $E_G = E_G(N_G)$.

2.2.5 Electrostatic Mechanism

Aerosol particles and the fibers of a filter often carry electrostatic charges that may influence the particle deposition. The electrostatic charge usually is unstable. This charge decreases with time mainly due to fiber conductivity, passage of ionized gas, radioactive radiation, deposition of charged particles and humidity. A charge on the particle or the fiber alters the particle trajectory and the extent of particle adherence to the fiber and hence affects the filtration process. The deviation of the filtration process varies, depending upon whether the particle, or the fiber, or both carry a charge. In the case of a neutral fiber and charged particle, Pich [1987] reports that Gillespie [1955] gives the interaction between the charge on an aerosol and its image on the fiber as follows

$$F(\dot{L}) = \frac{q^2}{4(\dot{L} - R_F)^2} \frac{D_2 - 1}{D_2 + 1} \quad (2.14)$$

where F is the force, D_2 is the dielectric constant of the fiber, q is the particle charge, R_F is the fiber radius, L' is the distance between the particle and the fiber. When both the particle and the fiber carry a charge that is opposite to each other, then we have the following relation [Gillespie, 1955 as reported by Pich, 1987]

$$F(L') = \frac{2qQ}{L} \quad (2.15)$$

where Q is the charge per unit length of the fiber. The electrostatic mechanism may be described by a dimensionless parameter (N_{0q}) describing the magnitude of this mechanism. The dimensionless parameter is described in terms of the ratio between the electrostatic forces and the drag forces. The dimensionless parameter N_{0q} (valid only for Stokes particles) describing the deposition due to the like forces in a system composed of neutral fibers and charged particles [Pich, 1987] is

$$N_{0q} = C_1 \frac{q^2}{3\pi\mu_a D_p D_f^2 U_0} \frac{D_2 - 1}{D_2 + 1} \quad (2.16)$$

The capture coefficient E_{0q} for this system for a viscous flow is given by

$$E_{0q} = \frac{2}{(2 - \ln \text{Re})^{1/2}} N_{0q}^{1/2} \quad (2.17)$$

2.2.6 Deposition due to London-van der Waals Forces

Molecular interaction between particles and a fiber may affect the deposition rate when the distance between the fiber and the particle is very small. Like electrostatic

forces, these forces, besides influencing the process of particle deposition, may enable the particle to stick continuously to the fiber. Pich [1987] mentions that the London van der Waals attraction force between a plane and a sphere is given by [Hamaker, 1937]

$$F = \frac{2}{3} \frac{Q_0 a^3}{(L^2 - R^2)^2} \quad (2.18)$$

and that Natanson [1957] derived the dimensionless parameter N_M characterizing the intensity of particle deposition due to these forces and described it as

$$N_M = \frac{Q_0 a^2}{9\pi R_F^4 U_0 \mu_0} \quad (2.19)$$

where R_F is the fiber radius and Q_0 is Hamaker's constant of interaction and is typically of the order of 10^{-20} to 10^{-19} J. Pich [1987] explains that the capture coefficient of the fiber E_M , due to this force is a function of this dimensionless parameter for a viscous flow is as described by Natanson [1957] below

$$E_M = \left[\frac{3\pi}{2} \right]^{-1/3} \frac{1}{(2 - \ln \text{Re})^{2/3}} N_M^{1/3} \quad (2.20)$$

For small particle sizes, diffusion is the dominant mechanism for particle collection by the fiber as seen in Fig. 2.2. The importance of this mechanism decreases for higher particle sizes and for particles between sizes 0.1 - 0.5 μm the direct interception also accounts for the particle collection phenomenon. Particle diameter is critical since large particles, in effect, reach out to intercept the fibers. Particles with diameter $\geq 0.5 \mu\text{m}$ have high inertia and also have a large Stokes drag exerted by the air, resulting in the increased importance of the inertial impaction mechanism as a method of particle collection. The

importance of different efficiency mechanisms for different particle sizes is shown in Fig.

2.2.

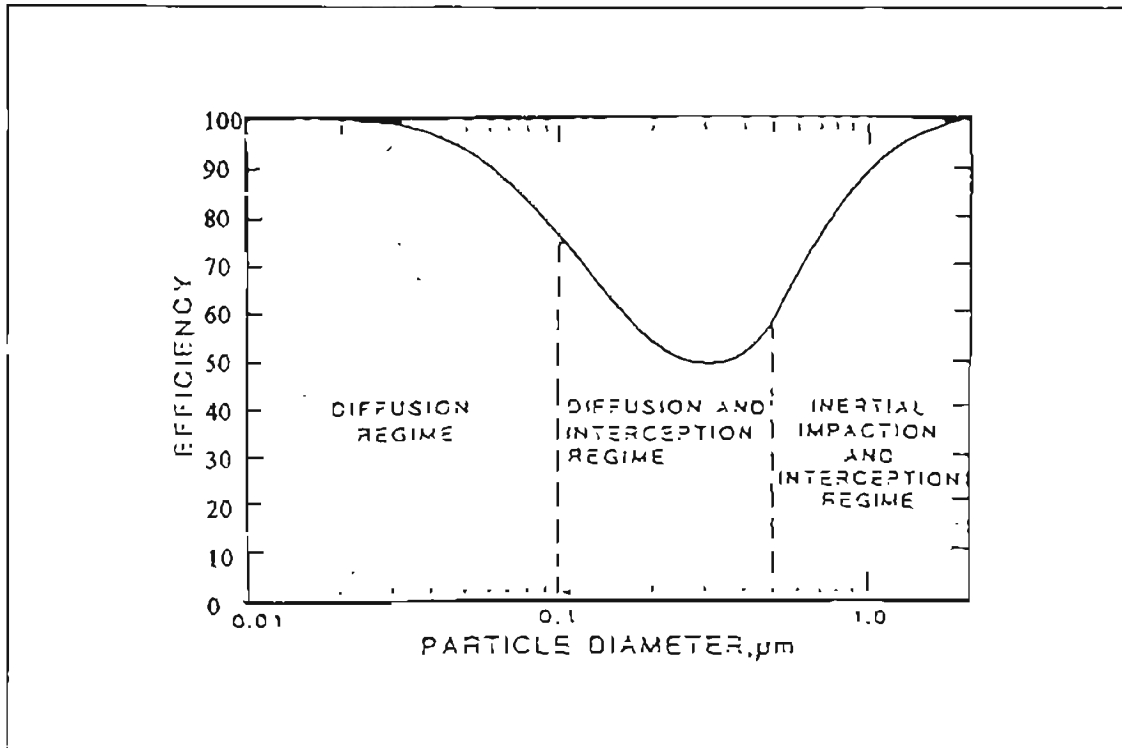


Figure 2.2 Schematic Diagram of the Collection Efficiencies of Different Particle Capture Mechanisms [Liu et al., 1985]

2.3 Combined Filtration Mechanisms

During the actual filtration process, particles may be subjected to the simultaneous effect of all the deposition mechanisms; with each one of them playing different roles under different conditions. The most widespread approach toward finding the total capture coefficient of a fiber E_T is to assume that the individual capture coefficients E_i ($i = 1, 2, \dots, n$) corresponding to different mechanisms are additive [Pich, 1987] i.e.

$$E_T = E_1 + E_2 + E_3 + \dots + E_n \quad (2.21)$$

Chen and Yu [1993] have proposed the following relation for the combined effect of any two mechanisms, where η_1 and η_2 are the individual deposition efficiencies for the two mechanisms.

$$\eta_{12} = \sqrt{\eta_1^2 + \eta_2^2 - (\eta_1 \eta_2)^2} \quad (2.22)$$

Davies [1952] derived the following equation for the simultaneous action of diffusion, interception, inertia for the simultaneous capture coefficient E_{DRI}

$$E_{DRI} = 0.16 \left[N_R + (0.5 + 0.8 N_R) (Pe^{-1} + St) - 0.105 N_R (Pe^{-1} + St)^2 \right] \quad (2.23)$$

where $N_R = D_p/D_f$ is the dimensionless parameter for direct interception mechanism.

2.4 Interference Effect

The capture coefficient of a fiber in a filter $E_{j\beta}$ differs from the capture coefficient of an isolated fiber E_j [$j = D, R, I, G$ and corresponds to different collection mechanisms (diffusion, interception, inertial, gravitational)] for two main reasons:

- a) the velocity field around the individual fibers differs.

This is so because the fibers embedded in a filter cannot be treated as being identical to each other, further their environments will vary considerably in a filter due to the irregular structure of the filter by itself.

- b) the median gas velocity in the filter is higher than that corresponding to an isolated fiber.

In the case of an isolated fiber, a limiting trajectory can be defined in such a way that the particles nearer to this trajectory will be captured by this fiber while the others will not. However, in the case of fiber in the filter, this trajectory is not defined and the velocity of the particle and the consequent particle capture phenomenon is affected by the presence of other fibers in the filter.

The resulting influence of neighboring fibers on the deposition process for any selected fiber is called an interference effect. Pich [1987] explains that Davies [1952] using experimental data, concluded that the effect on the filtration process due to a particular mechanism (e.g. interception) due to the presence of other fibers is expressed as follows

$$E_{j,\beta} = E_j(0.16 + 10.9\beta - 17\beta^2) \quad (2.24)$$

He also proved that this relation for interference effect is true for different filtration mechanisms considered individually. Chen [1955] corroborated the concept of the interference effect on the filtration efficiency by proving that the presence of neighboring filters led to an increase of filtration efficiency, the increase being a function of the filter porosity (packing density).

The total capture coefficient of the individual fiber in the filter E_{fp} (effective capture coefficient with an unknown dependence on β) is related to the filter efficiency η by the following relation [Pich, 1987]

$$\eta = 1 - e^{-\alpha} \quad \text{where } \alpha = S E_{\text{fp}} \text{ and } S = \frac{4}{\pi} \left(\frac{\beta}{1-\beta} \right) \frac{L}{D_f} \quad (2.25)$$

Here α is the coefficient of absorption of particles by the filter, S' is the solidarity factor [Whitby, 1965], and L is the filter thickness [Pich, 1987].

2.5 Characteristics of Filters

As mentioned in Section 2.1 of this chapter, three factors take part in the filtration process. These dependencies or characteristics can be divided into three groups. The first group includes the particle properties. The second group includes the dependencies of Δp and η on the fluid flow. The third group includes the dependencies of Δp and η on the properties of the filter.

2.5.1 Selective Characteristic

The selective characteristic of a fiber, or that of a filter, is defined as the dependence of the filtration on the particle size. If only the mechanisms of diffusion, interception, and inertial deposition are assumed to be dominant, then we have the dimensionless diffusion parameter Pe^{-1} which decreases with increasing particle size, and the interception parameter N_R and inertial deposition (dependent on Stokes number, St) which increase with the particle size. These mechanisms act simultaneously, and hence the respective capture coefficients increase with the increase in their parameters. It is therefore expected that the selective characteristic will exhibit a minimum efficiency. Pich [1987] reports that this was shown theoretically by Langmuir [1942] and experimentally determined by Fitzgerald and Detwiller [1957]. Pich [1987] reports on one of his earlier

works [Pich, 1966] wherein the position of the minimum was given by the following equation

$$d_{pm} = \frac{0.85(kT)^{1/4} D_f^{3/8} \nu^{1/8}}{(3\pi\mu_a)^{1/4} U_0^{5/8}} \quad (2.26)$$

where ν is the kinematic viscosity of the fluid, and T is the absolute temperature. The position of the selectivity d_{pm} therefore depends both on the fiber diameter and flow velocity. Therefore with increasing velocity, the position of d_{pm} shifts towards small particle sizes.

In most filtration theories, it has been assumed that the particles are spherical in shape. However, according to Pich [1987], Benarie [1963] theoretically concluded that, for particle Reynolds numbers $Re_p \leq 2$, acicular (pointed) particles reach the fibers completely unoriented and behave like spheres of the same mass having a diameter equal to the particle length multiplied by 0.285.

2.5.2 Velocity

With increasing velocity, the value of $N_D (= Pe^{-1})$ decreases and so does the capture coefficient of diffusion deposition. The interception parameter is independent of velocity, and parameter St increases with velocity. Therefore there is a velocity characteristic minimum (in efficiency) here too. Pich [1987] quotes an earlier work [Pich, 1966] wherein he derived the value of the minimum velocity characteristic as follows:

$$U_{0,m} = \frac{2(kT)^{2/3} D_f v^{1/3}}{(3\pi\mu_o)^{2/3} D_p^{2/3}} \quad (2.27)$$

Hence, the position of the minimum is dependent on particle size and fiber diameter. Stern et al. [1960] experimented on IPC (Institute of Paper Chemistry) fibrous filters of average diameter 17 μm and monodisperse polystyrene particles with D_p from 0.026 to 1.71 μm , and found a distinct minimum for all investigated fibers. He, like Chen [1955], reported a unique velocity where filter efficiency was the same for all particle sizes, i.e., the existence of an isoefficiency point at a velocity of about 0.178 m/s at ambient pressure and which shifted to lower velocity values with a reduction in gas pressure. Pich [1987] reports that Lindeken et al. [1963] measured the velocity characteristics of Whatman No. 41 paper, using monodisperse polystyrene latex particles with particle diameters of $D_p = 0.088, 0.188, 0.264, 0.365, \text{ and } 0.557 \mu\text{m}$. He found a well-developed minimum (in efficiency) in the velocity characteristics in the velocity range of 0.102 to 0.152 m/s. These are the effects of the particle size, fiber diameter and the filter porosity on the capture coefficient E_T or the filter efficiency η .

2.5.3 Pressure and Temperature

The dependence of both basic parameters, Δp and η , on the pressure of the filtered fluid is denoted as the pressure characteristic of the filter. The temperature characteristic of a filter is defined as the efficiency dependence on the temperature of the filtered fluid while the other conditions remain constant. This dependence was studied by Pich [1971] (as mentioned by Pich [1987]) based upon the following assumptions:

- a) relatively dry air passes through the filter.
- b) the particles are not subjected to evaporation or condensation.
- c) there is no change in the structure of the filter on account of high temperature.

He concluded that the minimum (in filtration efficiency) of the temperature characteristics is given by the following relationship

$$T_m = \frac{1}{k} E_k + \frac{1}{2} C_s + \sqrt{\frac{1}{k^2} E_k^2 + 7 \frac{C_s E_k}{k} + \frac{1}{4} C_s^2} \quad (2.28)$$

where $E_k = mU^2 / 2$ is the kinetic energy of the particle with velocity U , and C_s is a constant. The position of the minimum is dependent on the particle size and on the flow velocity. With increasing particle size and increasing velocity, the minimum is shifted toward a higher temperature. The filter efficiency decreases with an increase in temperature, but this decrease is not significant for the temperature (of the flow) range from -20° to 200°C [Matteson, 1987]. If charged filter media is used, the charge on the media deteriorates, causing a significant reduction in efficiency as shown in Fig. 2.3. It is seen that the decrease in efficiency, especially for small particles, is a result of the charge deterioration. The uncharged filter media however has different efficiency characteristics and thus responds differently to the temperature variation [Ptak et al., 1994].

Humidity, another factor influencing the filtration, affects the density and viscosity of the air and hence the pressure drop and the filtration efficiency. High humidity influences the adhesive forces between the dust particles and the fibers besides affecting the charge on the media. An increase in the relative humidity increases the adhesive forces because of the capillary factors [Ptak et al., 1994].

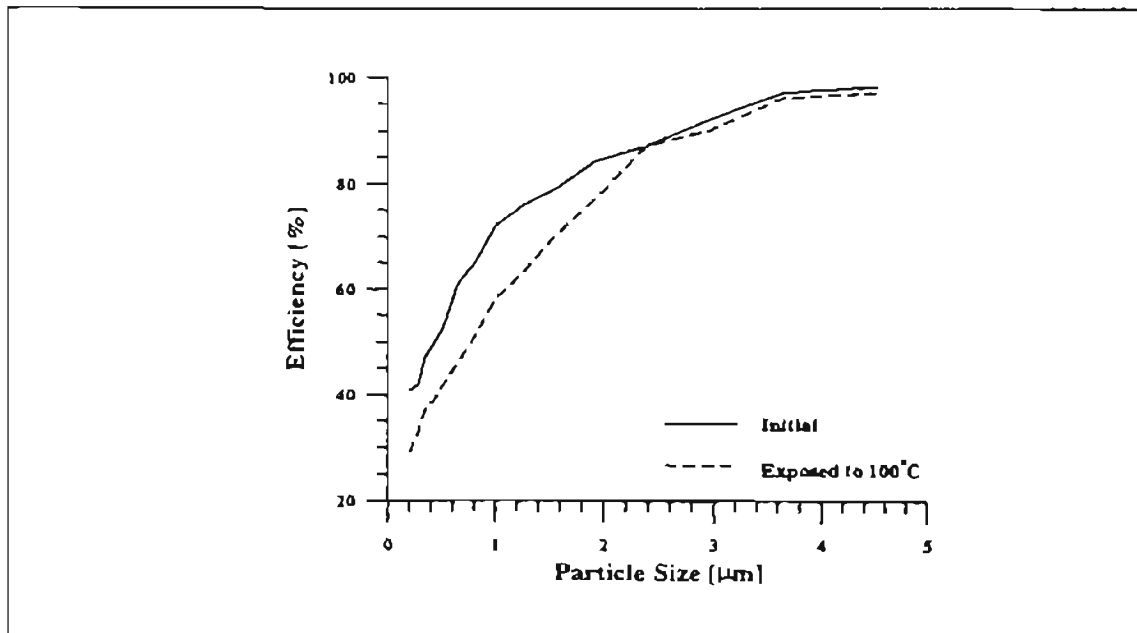


Figure 2.3: Influence of High Temperature Exposure on Charged Filter Media Efficiency [Ptak et al., 1994]

A strong adhesive force reduces the particle rebound and the re-entrainment, thereby increasing the filtration efficiency. However a very high humidity reduces the charge on the fiber and thus the efficiency. The effect of humidity as measured by Ptak et al. [1994] is shown in Fig. 2.4, where it is seen that, for small particles, the efficiency decreased slightly with an increase in humidity.

2.6 Experimental Analysis

The majority of the experimental evaluations may be classified under two headings:

1. Verification of theoretical models.
2. Evaluation of filter media.

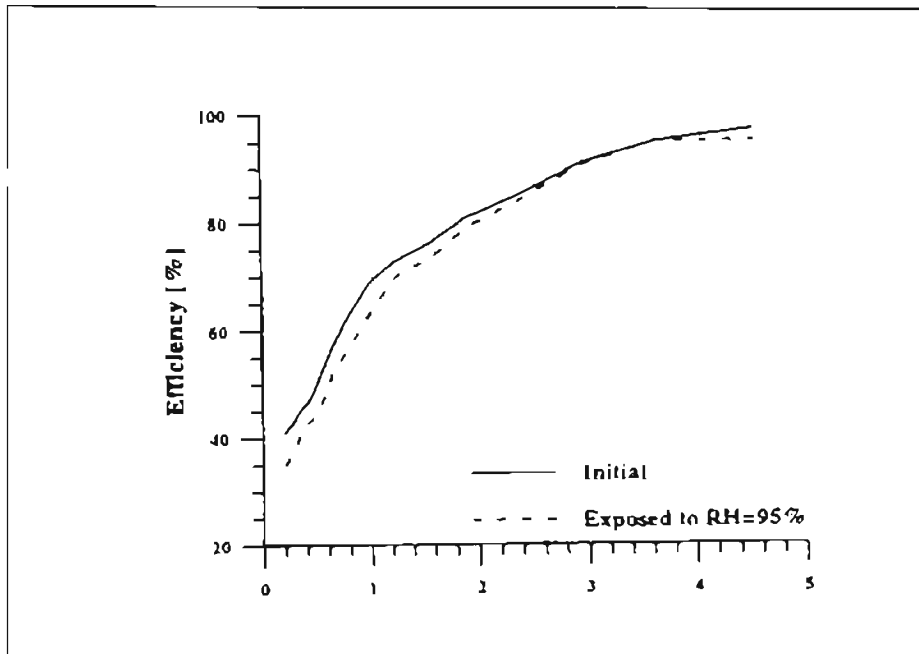


Figure 2.4: Influence of Humidity on Charged Filter Media Efficiency, with Initial RH = 50% [Ptak et al., 1994].

2.6.1 Verification of Theoretical Models

Several experimental studies have been carried out using aerosols and dust particles as the contaminant. In order to study the effect of the structure of the filter, the method of single fiber efficiency is used. If a fiber in filter is oriented at right angles to the flow, the area presented to the flow is equal to the product of the length and the diameter of the fiber. A fiber that has an efficiency of unity removes from the air all of the particles that would lie within the volume swept out by its area and the velocity vector of the air, assumed to be flowing uniformly as illustrated in Fig. 2.5. However a fiber does not remove all of the particles. The single fiber efficiency is defined as the quotient of the number of particles actually removed to the number that would be removed by a 100%

efficient fiber [Brown, 1993]. Single fiber efficiency, E_s , which is dimensionless, is related to the layer efficiency as follows

$$E_s = \frac{E_L \pi D_f}{4\beta} \quad (2.29)$$

where E_s is the single fiber efficiency, E_L is the layer efficiency (m^{-1}) which is related to the number of particles captured by a layer of filter of thickness δx , assuming that the filter is made up of a large number of layers. Yeh [1972] and Lee [1977] used a condensation aerosol generator to seed DOP (Triphenyl Phosphate Dioctyl Phthalate) particles and Dacron filters with different packing densities as the test filters.

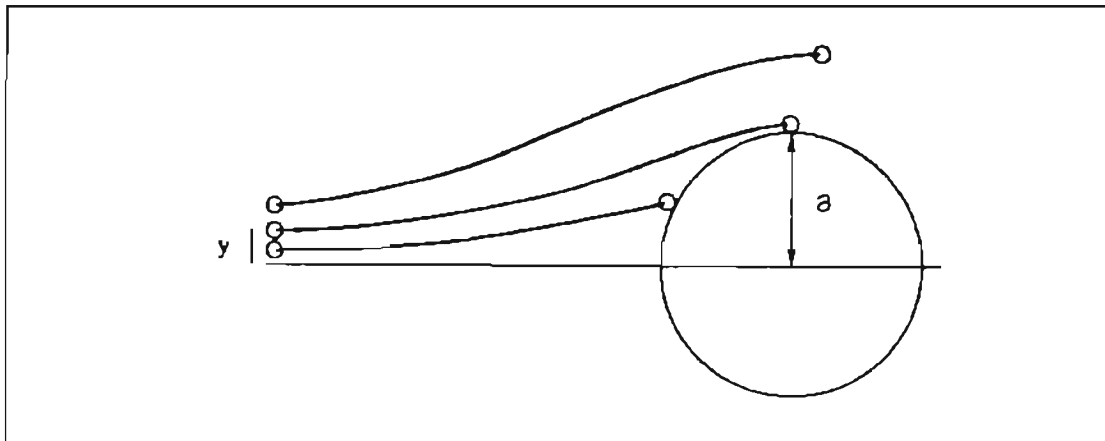


Figure 2.5 Illustration of the Concept of Single Fiber Efficiency [Brown, 1993]

Using the single fiber efficiency, Lee compared the experimental results with the theoretical results of Harrop [1969] in the inertial impaction region (Fig. 2.6). The results were in good agreement with theory for $Re = 0.94$, and $D_p = 0.7 \mu m$ particles. Maus and Umbauer [1996] made use of two optical particle counters to measure the particle flux

upstream and downstream simultaneously with different aerosols (latex spheres, bacteria aerosol, and limestone dust) and then found the fractional efficiency for the EUROVENT class of filters. They had neutralized the charge on the particles after generation and varied the relative humidity of the air from 10% to 90%. Though they make the efficiency measurements by making the number density calculations, they assume that the velocity upstream and downstream of the filter was the same, whereas the results of the present study and results of previous researchers on this project show that it is not.

The Society of Automotive Engineers (SAE) has defined two types of dust particles, SAE fine dust and SAE coarse dust. Several experiments were carried out by Jaroszczyk [1987] using polyacrylonitrile fibers with an average diameter of 27 μm and different packing densities from 0.0188 to 0.0612.

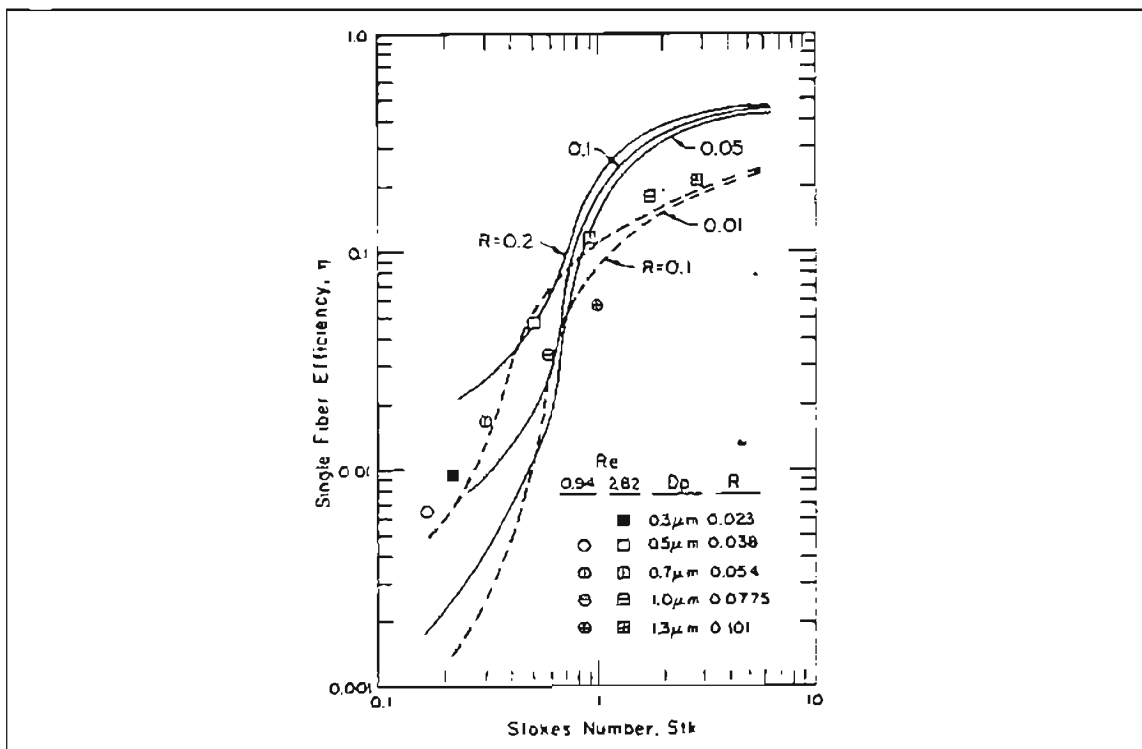


Figure 2.6 Comparison of Experimental Efficiency Measurements with the Theory of Harrop [1969] in the Inertial Impaction Regime [Lee, 1977]

He showed that the efficiency measurements using dust particles were higher than those obtained by using aerosol particles of smaller diameters. He explained that this may be due to accumulation of the dust particles on the filter, thus forming a dust cake across the filter and consequently creating a higher pressure drop across the filter.

The filter efficiency increases until the weight of the collected dust is less than the dust holding capacity of the filter. When this is exceeded, the dust cake breaks, and there is a drop in the efficiency. This is known as re-entrainment. Jaroszczyk et al. [1994] showed the effect of the type of dust [ASHRAE and SAE fine] on the pressure drop across the filter. They also explained the influence of dust [SAE fine] loading on the fractional efficiency of the charged media.

2.6.1.1 Research at OSU

Jadbabaei [1997] and Anand [1997] conducted measurements for finding the local filtration efficiencies for the pleated and flat filters respectively using the same setup as in the present study. They measured the pressure drop several times during the course of the experiment. These were taken at the start of the experiment, at the end of downstream measurements, and at the end of the experiment.

Jadbabaei [1997] and Natarajan [1995] conducted experiments on the A13192 pleated filters. Natarajan took measurements on pleated filters, but his results suffered from inconsistency. He had problems with repeatability of the results and the laser power variation. He used the model of Duran [1995] to compare with his results and used an

arbitrary value of 0.49 and 0.345 (as recommended by Duran) for the packing density.

His results are shown in Figs. 2.7 and 2.8.

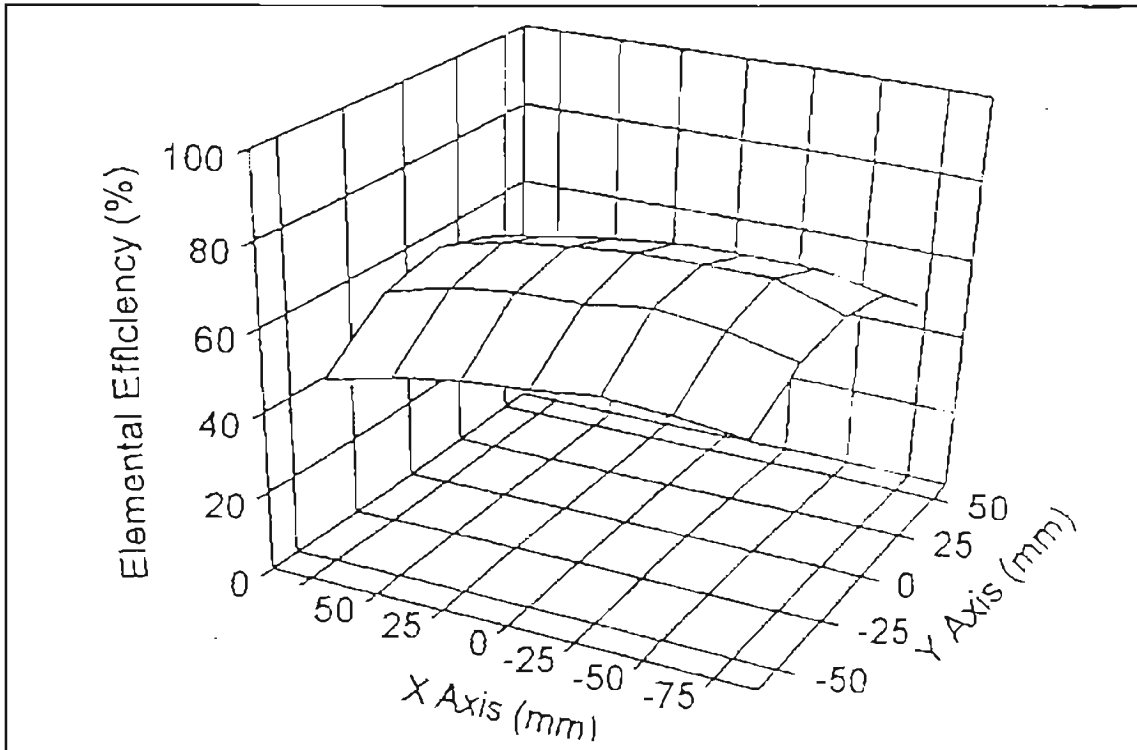


Figure 2.7: Elemental Efficiencies over A13192 Filter (Duran's Model, Packing Density = 0.49) [Natarajan, 1995]

Natarajan used the actual flow velocity inside the housing to calculate the Stokes number for different flow rates. The Stokes number obtained by dividing the flow rate by the cross-sectional area of the opened (unfolded pleats) filter was about 5% of the value obtained by Natarajan for the same flow rate [Anand, 1997].

As was explained by Jadbabaei and Anand, the laser power was affected by the temperature variation in the room, and laser power significantly affects the measured number density by the LDV. Anand and Jadbabaei made certain improvements in the

measurement setup and showed repeatability of their results from experiments on the flat and pleated filters, respectively. Anand compared his results with Lee [1977] as shown in Fig. 2.9. He showed that the local filtration efficiency values near the center of the filter were quite close to the actual values of the overall filtration values

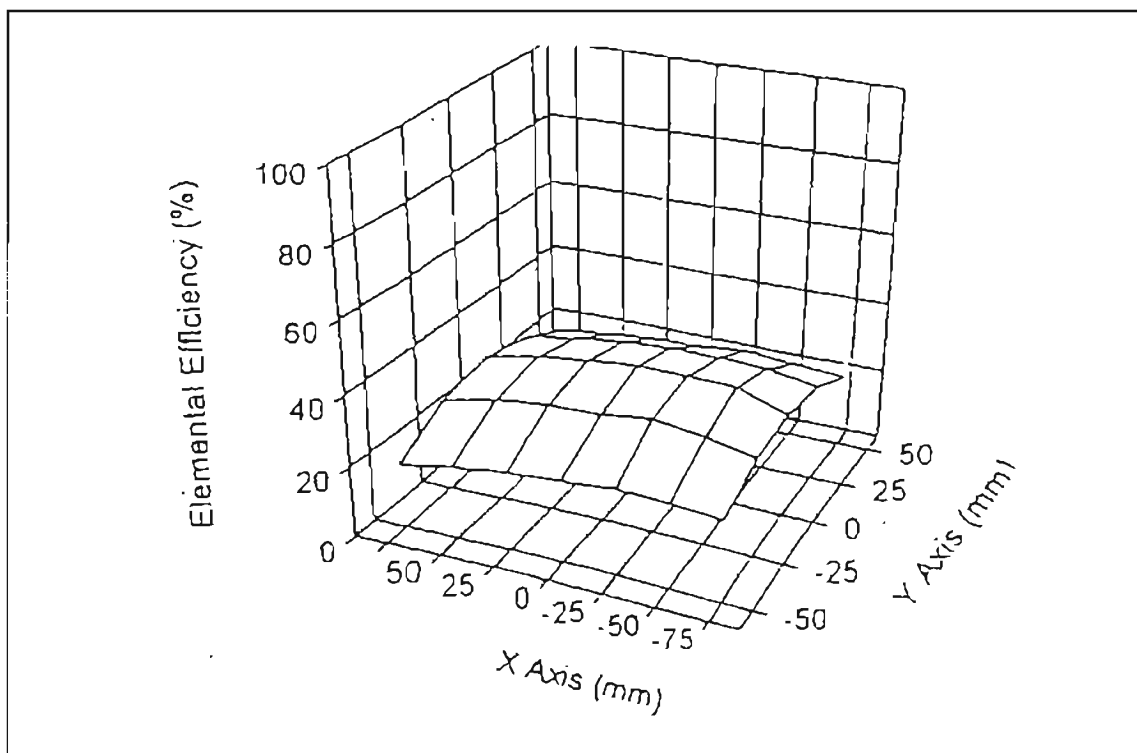


Figure 2.8: Elemental Efficiencies over A13192 Filter (Duran's Model, Packing Density = 0.345) [Natarajan, 1995]

Jadbabaei [1997] conducted experiments on the pleated filter in the Small Angle Diffuser housing with $0.966 \mu\text{m}$ particles. He compared his velocity profiles with those of Liang [1997] who conducted his experiments on the SAE J726 housing, and showed that the velocity profiles for the diffuser housing exhibited smaller local variation than those measured in the SAE J726 housing. Natarajan [1995] had shown similar results.

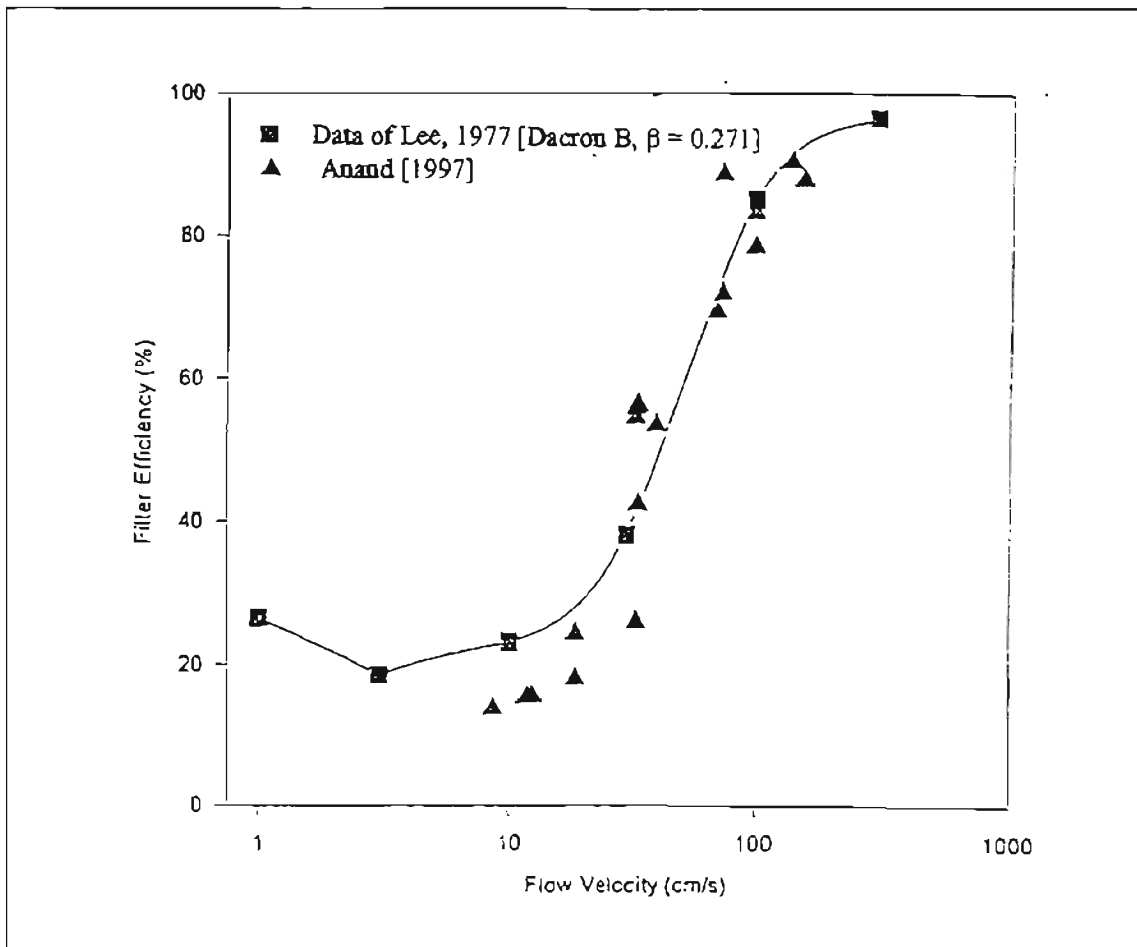


Figure 2.9: Overall Filter Efficiencies [Anand, 1997] Compared to Lee [1977]

Jadbabaei had compared his experimental results with the theoretical model of Duran [1995] who had predicted the overall efficiency of the A13192 filter using a packing density of 0.235 and for 0.966 μm particles. The elemental efficiency as predicted by Duran was 0.25% for a flow rate of 204 m^3/hr . Even though the trend as predicted by Duran was similar to the trend exhibited by the results of Jadbabaei, the actual values (72.56%) were different. The experimental values from Duran's model for 2.5 μm particle

size, packing density of 0.345 and fiber diameter of 51.75 μm were close to the experimental values of Jadbabaei for 0.966 μm . This difference was unexplained.

Anand compared his results with the three point measurements (measurements at points located to the left and right of the center of the filter, and located at the center; the traverse moved along the $X = 0.00$ axis) of Jadbabaei. The comparison showed [Fig. 2.10] that the trend was similar, provided that the pleated curve was shifted to the right approximately by a factor of 4.

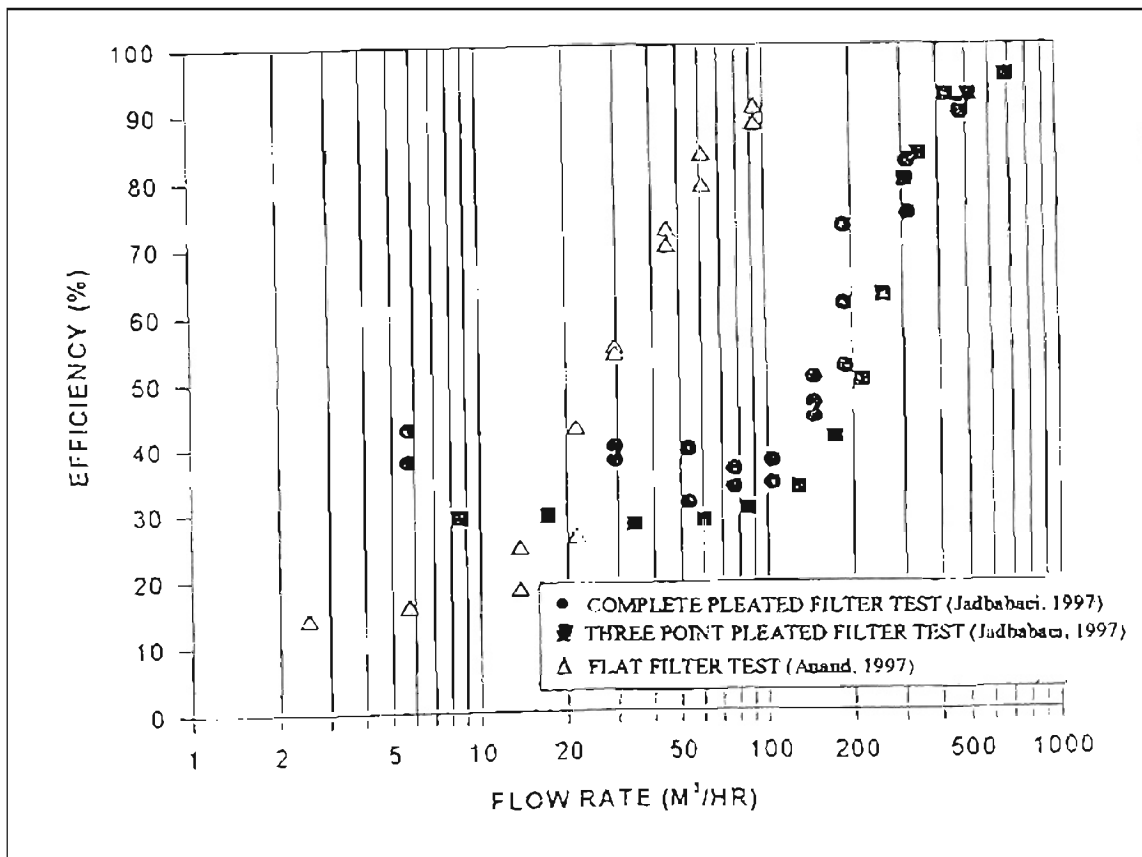


Figure 2.10: Comparison of Filter Efficiencies [Jadbabaei, 1997]

Anand had studied the Stokes number calculation for the 204 m³/hr and the actual velocity measured inside the housing corresponding to this flow rate. He concluded that neither of the two velocities actually represented the velocity to be used for the Stokes number calculation. According to him, the correct velocity to be used for that purpose was about 4 times the velocity calculated using the unfolded filter area, which was about 20% of the average duct velocity.

2.6.2 Evaluation of Filter Media

The SAE J726 procedure is used in North and South America to evaluate engine air filters [Bugli, 1997]. Japan follows the JIS-D-1612, while the ISO-5011 test procedure is followed in Europe [Bugli, 1997]. Though these test procedures are essentially the same and yield comparable results, there is a need to have a common standard. There is an ongoing effort to commonize the SAE J726 procedure with the ISO standard.

Bugli [1997] compared the efficiencies of the three common filter media, Synthetic / Felt media, Treated Paper media, and Dry Paper media. The experimental results [Figure 2.11] show that the dust capacity measured using the SAE fine dust was about half the dust capacity measured with SAE coarse dust for the dry and the treated paper media. The synthetic media showed only a 20% reduction in dust capacity which is possibly due to the depth loading and the gradient density characteristics which are less sensitive to the dust size distributions. In the case of the paper media, the loading capacity depends on the formation of the dust cake which is affected by the face velocity and the dust size

distribution [Bugli, 1997]. The initial filtration efficiency for the treated paper media is better than that of dry and synthetic media with the SAE coarse dust as shown in Figure 2.12.

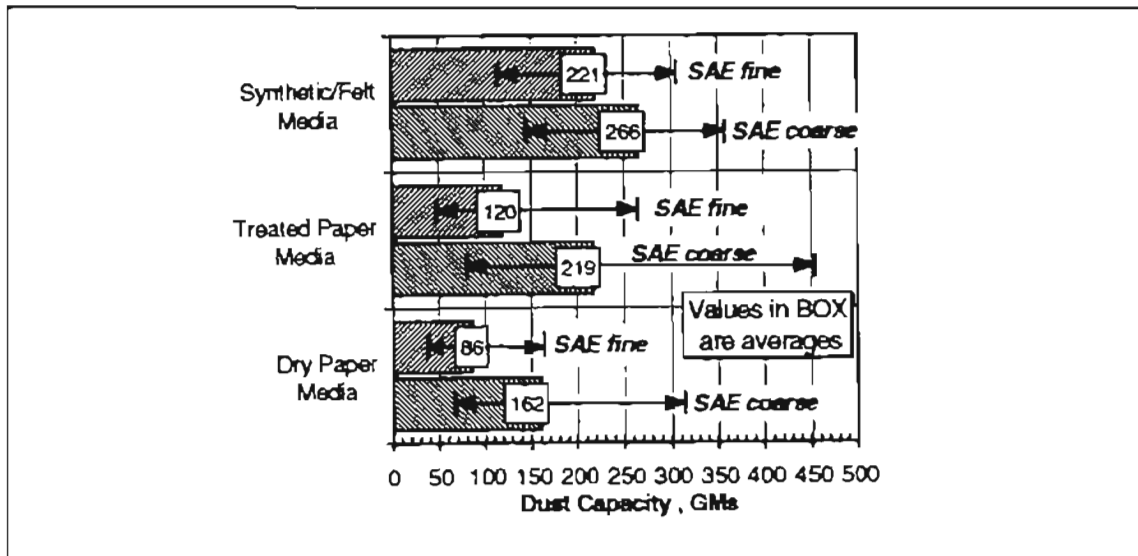


Figure 2.11: Typical Dust Capacity Performance Levels of Air Induction Filters (AIF) [Bugli, 1997]

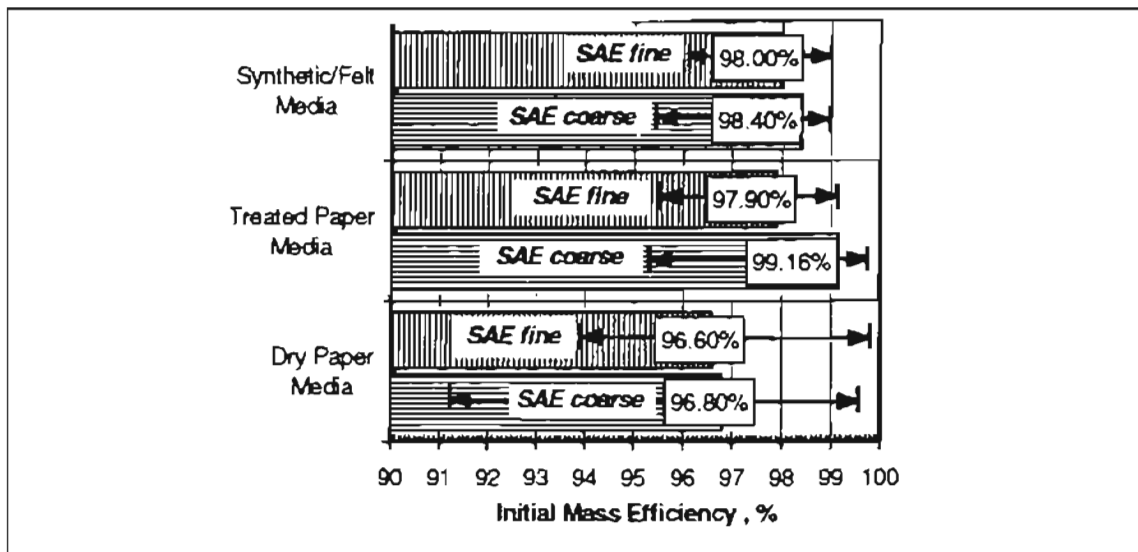


Figure 2.12: Typical Initial Efficiency Performance Levels of Air Induction Filters (AIF) [Bugli, 1997]

Typically filters are evaluated in the laboratory with manipulated (controlled) conditions, however the actual conditions on the road are different [Gustavsson, 1996]. The SAE recommended test procedure does not take into account the actual driving conditions, which are difficult to simulate in the laboratory. McDonald et al. [1997] carried out several tests [Fig. 2.13] in order to determine the test method that best simulates actual environmental exposure. These tests were shown to discriminate between various types of filter media that might be used in automobile cabin air filter applications. According to these tests, it was concluded that exposure to liquid hydrocarbon aerosol was the most discriminating of the tests explored (see Fig. 2.13).

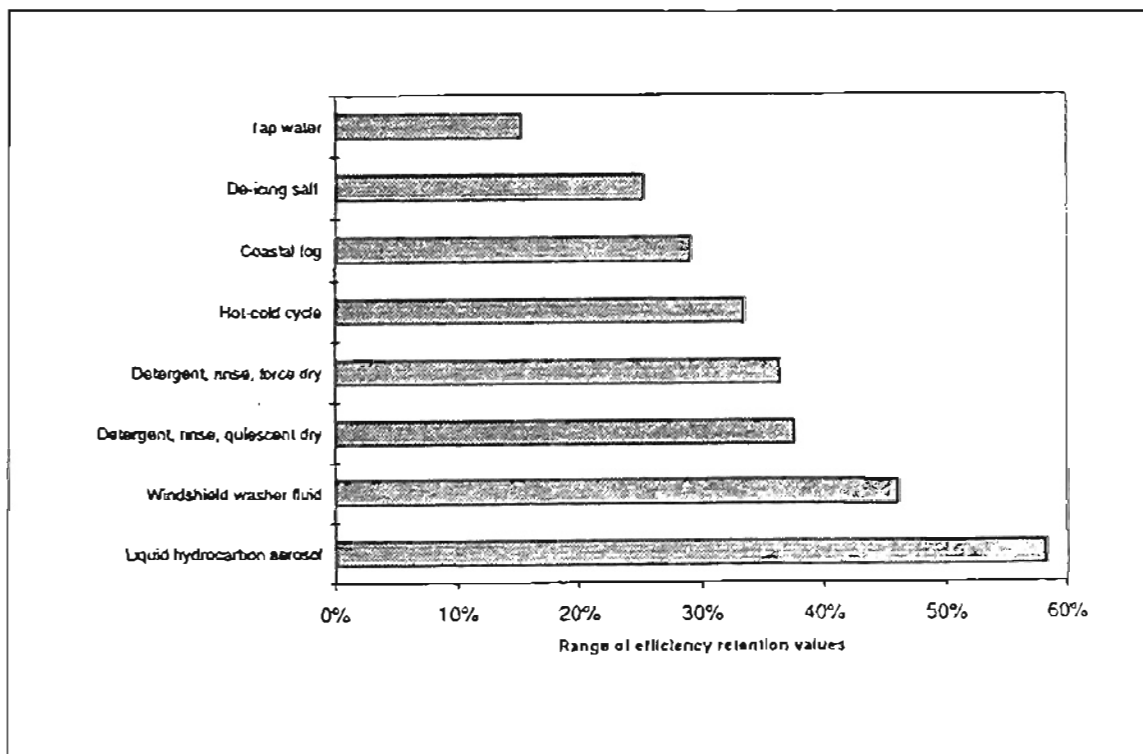


Figure 2.13: Ability of Tests to Discriminate Between Filter Media [McDonald et al., 1997]

The capacity of the filter for dust holding is dependent upon the size distribution of the particles. Several researchers, Whitby [1973], Wilson [1977] and Poon and Liu [1997] have demonstrated the bi-modal nature of the atmospheric aerosols. These are the coarse particles [2.5 - 30 μm] generated due to grinding and re-suspension of particles and the fine particles [0.1 - 2.5 μm] generated directly or indirectly from the combustion processes [Poon and Liu, 1997]. Since the relative proportion of these particles in the atmosphere varies with location, it is necessary to evaluate a bi-modal test dust for a filter housing which will be more representative of the atmospheric aerosols. Making use of different proportion of SAE fine and coarse test dusts, Poon and Liu [1997] showed [Figs. 2.14 and 2.15] that even a small percentage of fine particles could substantially increase the pressure drop as compared to the 100% coarse dust.

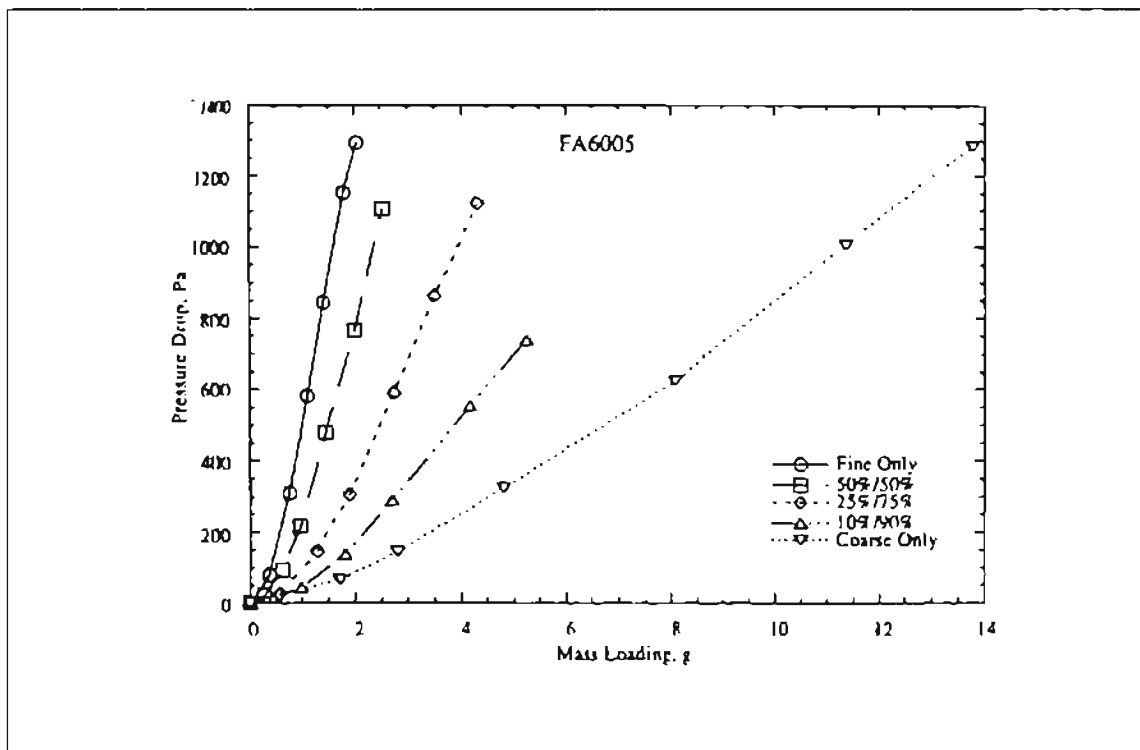


Figure 2.14: Pressure Drop of FA6005 with Dust Loading [Poon and Liu, 1997]

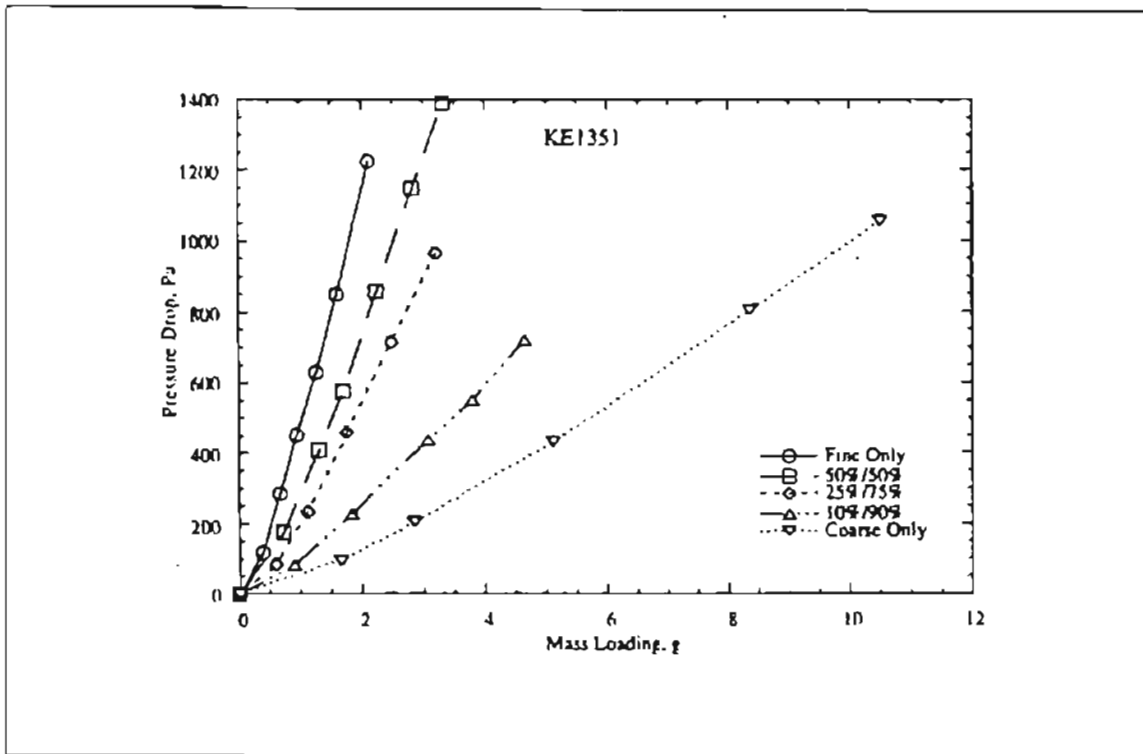


Figure 2.15: Pressure Drop of KE1351 with Dust Loading [Poon and Liu, 1997]

2.7 Standard Testing Methods

2.7.1 SAE J726 Test Code

In order to provide a uniform testing method for different engine air cleaners, the SAE J726 Test code [Society of Automotive Engineers, 1987], was established. This enables a performance report, which permits direct comparison of the basic performance characteristics of these air filters: overall dust collection weight efficiency; dust capacity to reach terminal pressure drop; airflow restriction characteristics; and structural integrity. This code specifies uniform test procedures and test conditions, and standardized test dust – Arizona Road Dust (SAE) (coarse and fine) with specified chemical analysis and particle

size distributions. It allows the usage of either one of the two types of test road dusts for the single stage air cleaner - depending on the application, while the SAE coarse test dust is used for the multistage air cleaner. The efficiency of an engine air cleaner is expressed by the percentage of dust captured by the filter element. The dust holding capacity of an engine air cleaner is the total amount of dust fed to the filter to reach a terminal pressure drop (approximately 1 - 2.5 kPa) [Stinson et al., 1988] or airflow restriction. The test code specifies a dust feed rate of 28 grams per 1000 cfm for a single stage filter and 56 grams per 1000 cfm for a multistage filter.

2.7.2 SAE J1669 Passenger Compartment Air Filtration Code

The objective of this test [SAE, 1993] was to maintain a uniform test method for evaluating performance characteristics, like pressure drop, overall and fractional efficiencies, and holding capacity, for airborne particles. This SAE recommended practice describes the laboratory test methods, consistent test procedures, conditions, equipment, and performance reports. This test recommends the usage of the SAE J726 procedure, gravimetric efficiency, for measuring the filter resistance. This test recommends the use of SAE ultrafine test dust. It recommends the conditioning of the filter before the test and heating of the test dust in some cases.

A major difference between the two SAE recommended tests mentioned above, which has been observed as a result of this study and that of Natarajan [1995] is that, that the filter is placed in a relatively uniform flow field in the SAE J1669 recommended housing, but in a non-uniform flow in the SAE J726 housing. Even though the housing in

the present study (Small Angle Diffuser housing) is not exactly as per the recommended specifications of J1669, it is similar to the intent of the SAE J1669 housing; and the results can be compared to those of J1669.

2.8 Present Work

The present study measures the local filtration efficiency of an automotive air filter (Dayco-Purolator A13192) for different particle sizes (0.497, 0.966, and 2.04 μm particles), at different flow rates (17.1 to 342 m^3/hr) and in different housings (Small Angle Diffuser housing, standard J726 housing, and Simulated Automotive Filter housing). The experimental work studied as a part of this literature review invariably has centered around dust loaded filters and has relied on the overall efficiencies for their respective cases. This study has tried to examine the process of filtration from a local viewpoint, in the sense that it has measured the efficiencies at different points on the filter to determine to what extent the different parts of the filter participate in the process. The study has compared the local filtration efficiencies for different particle sizes in order to determine the effect of particle size on the filtration process.

Chapter 3

FLOW AND EXPERIMENTAL SETUP

3.1 Summary

This chapter explains the Laser Doppler Velocimeter (LDV) system [Aerometrics, 1992]. The construction of different types of housing used for taking the measurements is also explained. The experimental setup is divided into three parts

1. laser setup;
2. data collection and processing unit;
3. flow setup;

Previous researchers on this project have observed that the power of the laser was inconsistent with time. This variation of power affected the data collection and reliability of the results. The variation of power was eventually traced to the variation in the room temperature [Anand 1997; Jadbabaei 1997]. Several experiments were conducted to understand how the temperature affects the measured laser power. These are explained in this chapter.

3.2 Laser Setup

The laser setup includes a 5 watt Argon-Ion laser manufactured by Coherent. This laser generates a multi-line, multi-wavelength beam of light at wavelengths between 457.9 nm and 514.5 nm. The laser is then guided via two steering mirrors into the fiber optic drive as shown in Fig. 3.1.

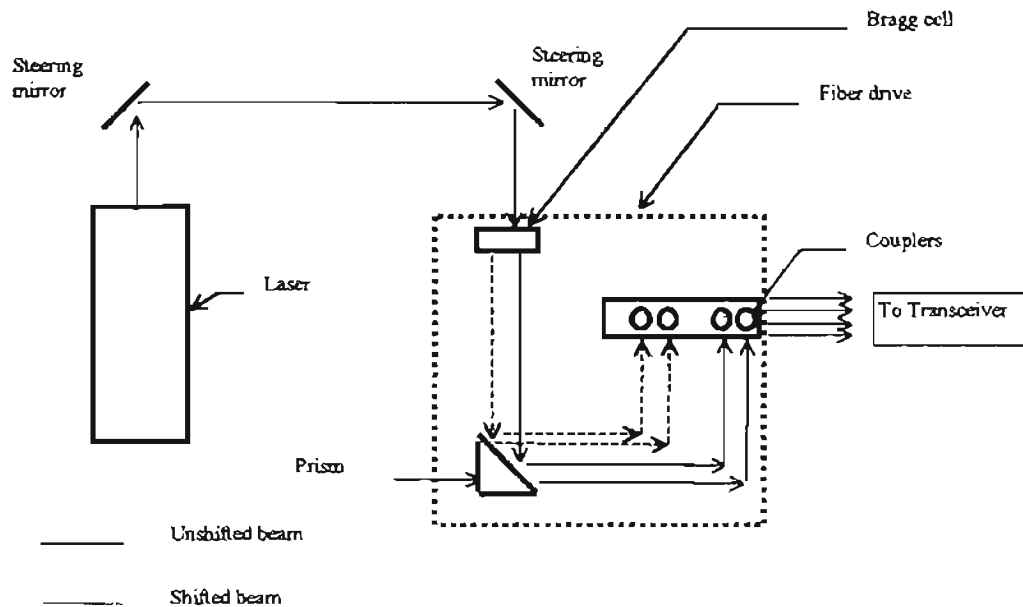


Figure 3.1 Schematic Diagram of the Fiber Drive

The single blue colored beam exiting from the laser is split into two separate beams by a dispersion prism in the fiber drive. Only the 488 nm (blue) and the 514.5 nm (green) beams are used for the two component LDV. These two beams are further split by a Bragg cell into two beams - shifted and unshifted, both of them having the same color but having a frequency shift of 40 MHz. This shift in frequency is used to detect the direction of particle motion in the probe volume [Liang, 1997].

The four beams are then directed into the optical couplers by means of mirrors. In the couplers, the beams are focused into the fiber optical cables (each of 4 μm diameter)

with the help of focusing lenses housed in the couplers. The beams travel through the fiber optic cables to the transceiver head. The transmitted beams form a probe volume where the signals are generated by the particles crossing the probe volume. This probe volume concept makes use of the 'swept volume technique' (explained in Appendix G of this thesis), developed by Liang [1997]. These signals are reflected back to the transceiver.

The transceiver head is so named since it functions both as a transmitter of the four beams and also as a receptor of the scattered signals generated by the particles. After the reflected signals are processed, information about the average particle velocity (v_i), number of particles counted (N_i) and the time taken (t_i) to count these particles is obtained. This information is used in calculating the particle concentration above or below the filter. These measurements are taken at 35 points on a 7x5 matrix as shown in Fig. 3.2, upstream and downstream of the filter. The swept volume technique gives the particle concentration in units of particles/m³ by the following formula:

$$n_i = \frac{N_i}{v_i t_i A} \quad (3.1)$$

where $A = 3.257 \times 10^{-11} \text{ m}^2$ is the cross-sectional area of the probe volume [Liang, 1997].

The number density thus calculated gives the local filtration efficiency at that particular grid location by the following expression:

$$\eta_i = 1 - \frac{n_{i\text{down}}}{n_{i\text{up}}} \quad (3.2)$$

$n_{i\text{down}}$ and $n_{i\text{up}}$ are the downstream and upstream number densities at that location.

The layout of the 35 grid point locations is as follows.

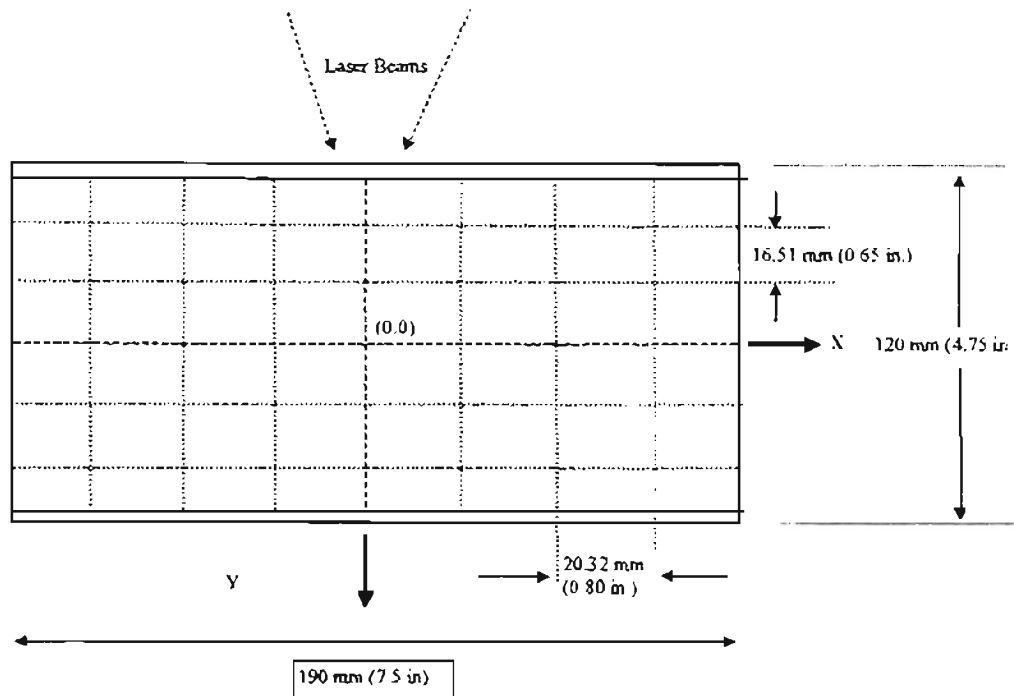


Figure 3.2: Layout of the 7 x 5 Measurement Grid on the Filter

At the point of intersection of the shifted and the unshifted beams of the same color, interference patterns in the form of dark and bright fringes are observed. When a seeding particle crosses the probe volume, it scatters the light in the form of bright and dark fringe patterns superimposed on a low frequency high amplitude pedestal as shown in Figure 3.3.

The direction of the flow pattern is determined by virtue of the 40 MHz shift in the frequency of the two beams - which results in the formation of a moving fringe pattern. A movement by the particle in the direction of the fringe movement results in a smaller frequency of the detected signals. On the other hand, a movement in the opposite direction results in higher frequency signals. It is imperative that the light intensity of the probe volume is consistent during the course of the experiment. This is required since the

edge of the probe volume has to be well defined in order to get good signals and keep the rate of data collection constant throughout the duration of the experiment.

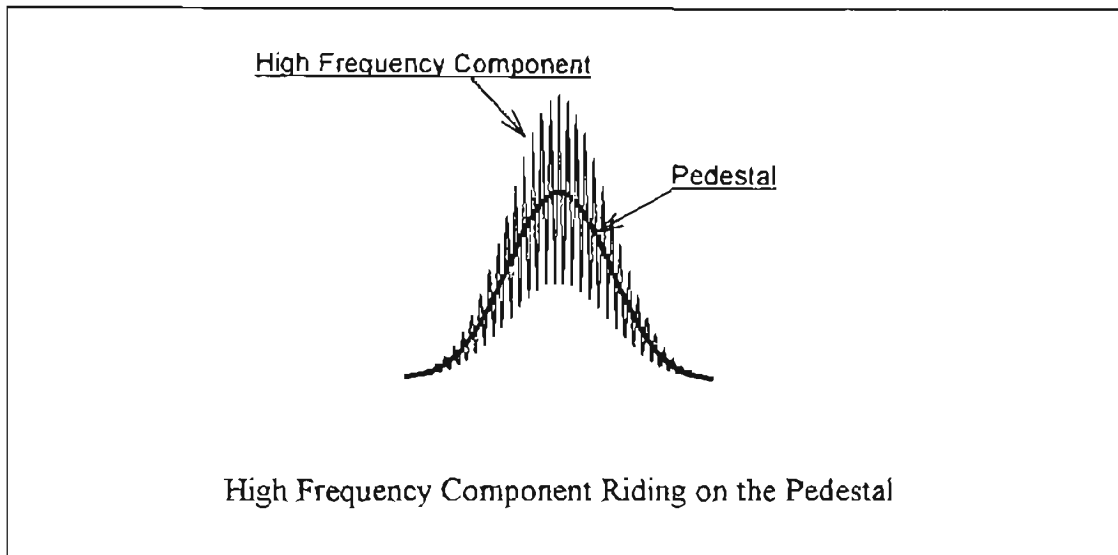


Figure 3.3: A Typical Laser Doppler Signal

A decrease in the power of the laser during the course of the experimental results in the gradual reduction of the probe volume and hence the rate of data collection [Anand, 1997]. A change in the intensity of the laser beam causes the number density to vary, since the probe volume changes and thus the sample rate at the upstream and the downstream points of measurement changes. This variation does not provide a consistent basis for comparison of the number densities at different locations on the grid. Also the particles scatter less at lower power and more at higher power. Hence it is necessary to maintain a consistent laser power during the course of the experiment.

Several experiments were carried out to determine the effects of various factors causing a variation in laser power, as measured at the transceiver head. Measurements were taken at the exit of the laser head to find out whether the power of the generated

laser beam varied with time. The power of the beam was measured after the steering mirrors for studying the effects of any movement of the steering mirrors on the laser power. The couplers were removed and measurements were taken to find out if the alignment of the reflecting mirrors and the prism changed with temperature, and thus caused the power to vary before the laser beam entered the fiber optic cable.

For these measurements, a special cylindrical instrument was fabricated to hold two pinholes separated at a distance so that a very narrow beam of laser light was visible to the power meter. This instrument was placed after the fiber drive so that the beam was measured just before it entered into the optical cable. Any change in the power would be attributed to the fact that the beam actually shifted in alignment and thus did not focus at the same spot on the optical fiber at all times.

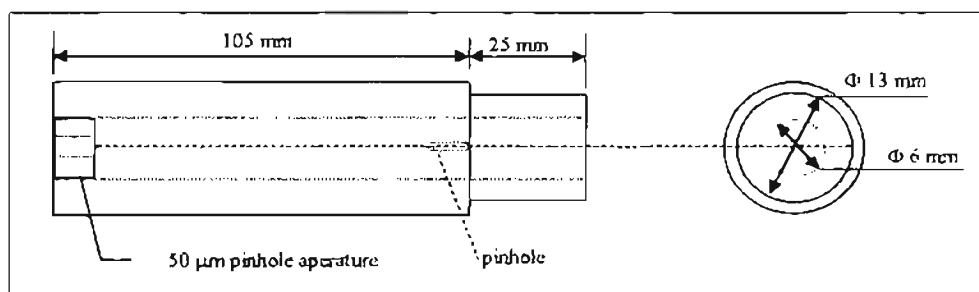


Figure 3.4: Cylindrical Instrument for Holding the Pinhole Aperture

With the variation of temperature, the alignment of the beam is affected and it does not focus on the same spot on the optical fiber. The pinhole apertures used were of diameters 200 μm and 50 μm. Any diameter smaller than 50 μm truncated the beam substantially, resulting in a very small reading by the power meter. The measured changes in the power were not significant to definitely find out the cause of the deterioration of power with time. However, the results did help in explaining that how the alignment of

the beam was affected by the temperature fluctuations and thus disturbed the power setting (Appendix F).

Small changes in the power settings can be controlled by three knobs on the coupler, which individually control the movement of the X, Y and Z axes [Aerometrics, 1992]. It was believed that the blower of the test stand produced strong air currents and also caused vibrations, which affected the alignment. However after performing the tests, both when the blower was running and when it was not, the variation in power appeared unaffected as is seen in Fig. 3.5, when the power remained constant whether the blower was running or not. It was then concluded that the blower, with the vibration isolation around it and the cork sheet on the laser table, did not significantly affect the power consistency in any way (also see Appendix F).

The laser, external mirrors and the optical fiber drive were mounted on an optical breadboard as shown in Fig. 3.6. The breadboard, with a honeycomb structure, was placed on a sheet of cork that helped isolate it from any vibration from the ground. The cork was glued to the slate top of a heavy metal table base as illustrated in Figure 3.6. In order to isolate the laser setup, a Plexiglas box was built. This box was helpful in isolating the laser setup thermally and from air currents, while also protecting the delicate optical system from dust. The room layout is shown in Figure 3.7. In order to find out if air currents adversely affected the power consistency, a fan was run near the beams. It was observed that running the fan did not cause changes in the laser power [Appendix F]. All of the collected data has been tabulated and plotted in Appendix F.

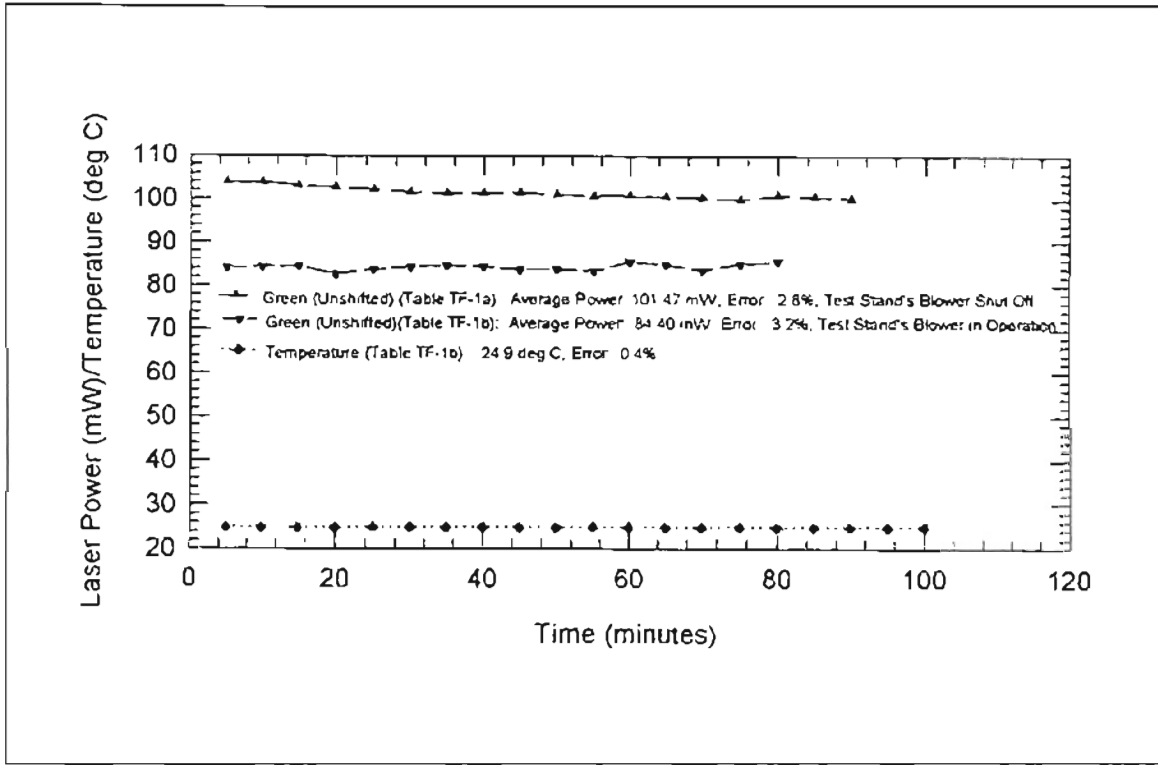


Figure 3.5: Comparison of Laser Power Variation [June 16 - June 22, 1997]

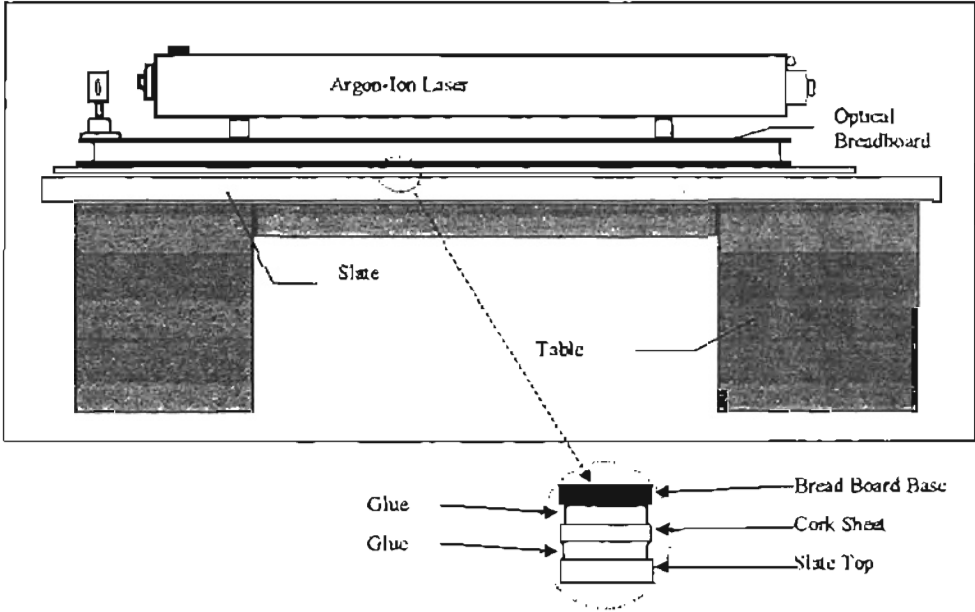


Figure 3.6: Laser Setup

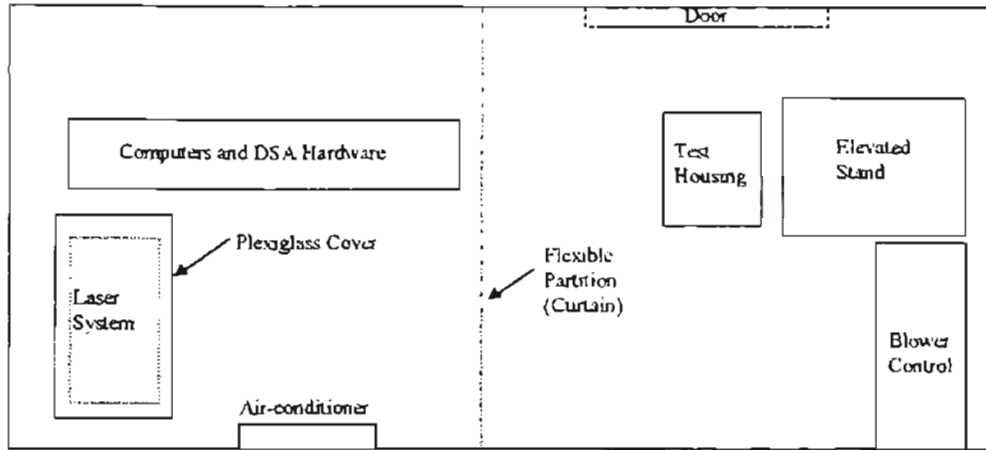


Figure 3.7: Room Layout

When the blower was running, the room temperature rose by about 2-4 °C, due to an inadequate air-conditioning system in the room. An additional room air-conditioner was installed in the room, and a partition was installed so as to reduce the volume of the room (Fig. 3.7) where the air-conditioner was required to maintain the temperature. This proved to be very effective in maintaining the room temperature constant and helped in checking the laser power variation. A thermometer (Appendix H) with a range of -20°C to 80°C was used to monitor the temperature in the Plexiglas box.

Several experiments were conducted wherein the room temperature was increased and the effect on the beam intensities was noted. These experiments were carried on for about 3-4 hours at a time - the time taken for an approximate run of an actual experiment. The temperature increased gradually, and the corresponding plot for different beams showed a drop in power. It was observed that the drop in power was not the same for all of the four beams for the same variation in temperatures (Fig. 3.8).

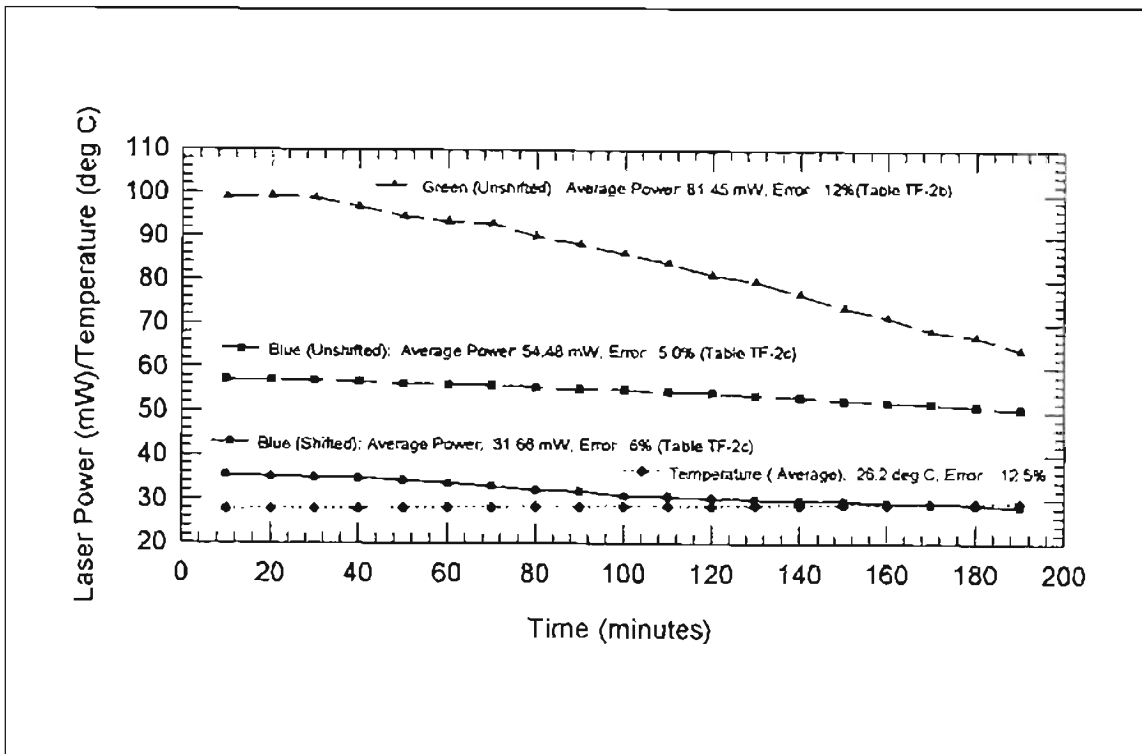


Figure 3.8: Variation of Laser Power at the Transceiver for Uncontrolled Temperature Inside the Plexiglas box [May 21 – June 10, 1997]

Two power meters with the capacity to measure power levels from 0.1 pW to 2W [Newport Catalog, 1993] were used simultaneously on different beams, and thus, for the same environmental conditions, the measurements were taken together. The power meters were then interchanged but the same results were obtained (Fig. 3.9).

The power drop was evidently caused by the misalignment of the external steering mirrors and couplers, since realigning the mirrors, and adjusting the knobs on the couplers attained the original power. When only the steering mirrors were realigned, there was a significant improvement in power; however the original power could not be restored.

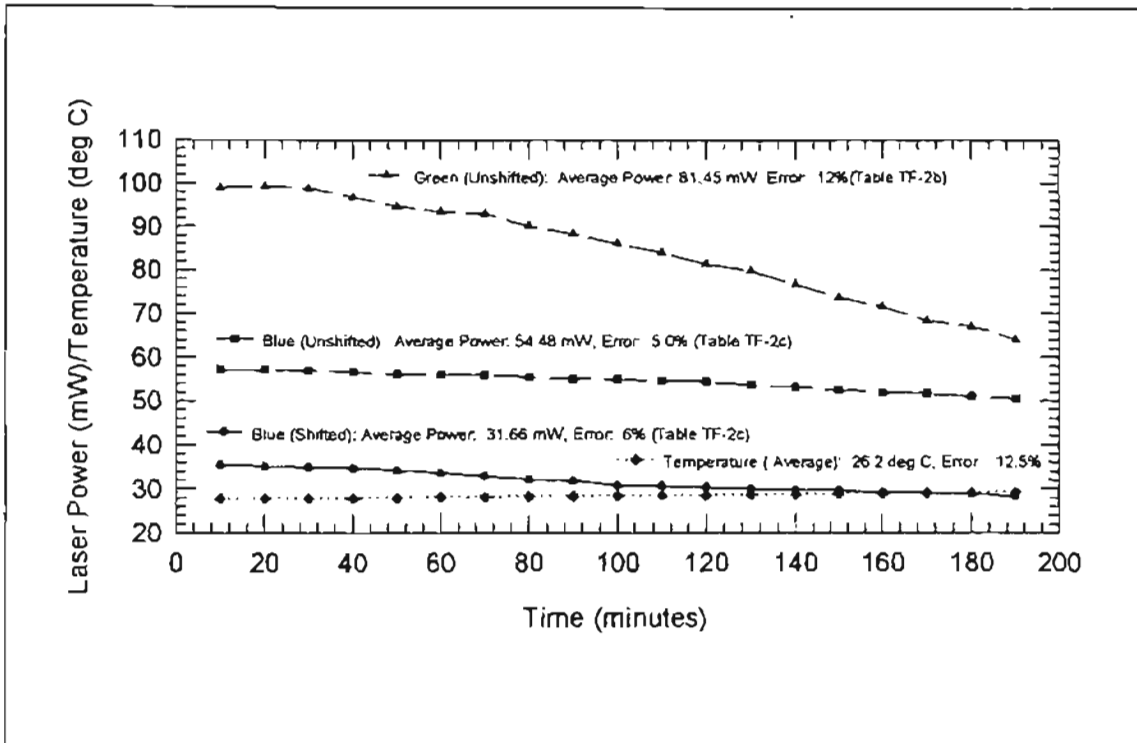


Figure 3.9: Variation of Laser Power at the Transceiver for Uncontrolled Temperature Inside the Plexiglas box, with Sensors Interchanged [May 28 – May 29, 1997]

Several experiments were carried where the temperature was kept constant, both when the blower was running and when it was not. It was observed that the power was almost constant during these times (Fig. 3.10). Since it is very difficult to keep the room temperature constant, these experiments were conducted for as long as the room temperature could be kept constant. This time varied between 30 to 90 minutes.

These experiments were helpful in concluding that if the temperature in the room and in the Plexiglas box was kept constant, then the variation in the laser power during the course of the experiment would be minimal.

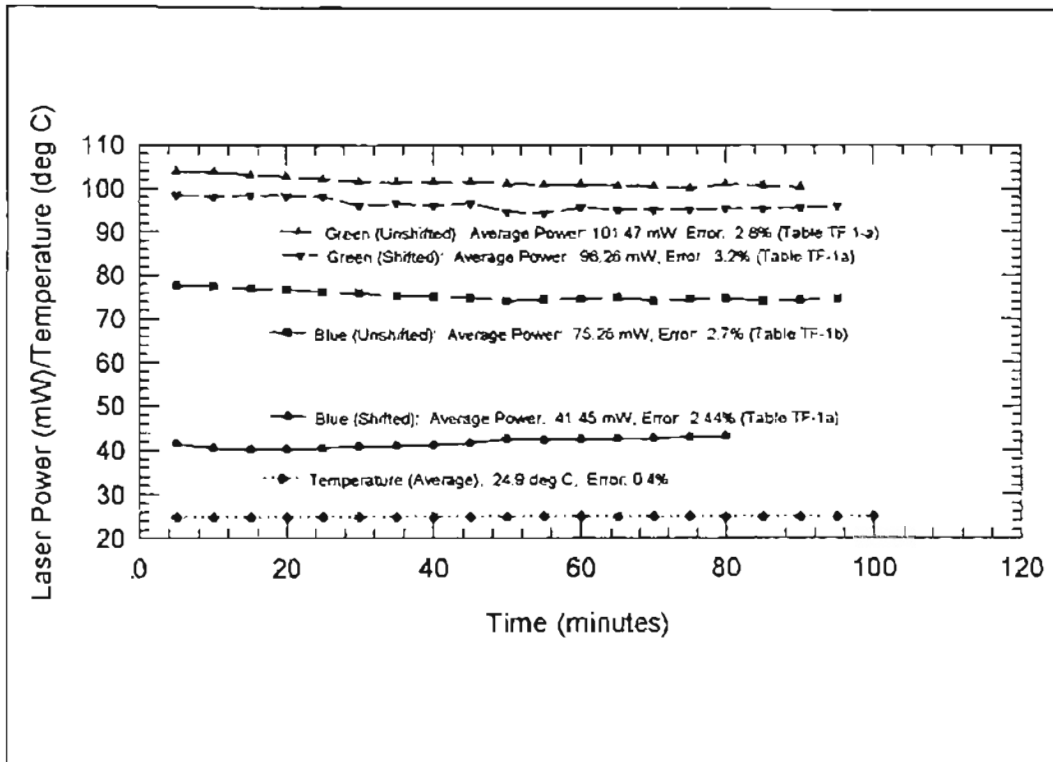


Figure 3.10: Laser Power Variation at Constant Temperature [May 28 – May 29, 1997]

3.3 Data Collection and Processing Unit

The Digital Signal Analyzer (DSA) has two main components, the hardware and the software [Fig. 3.11]. The signals that are obtained when the particles cross the probe volume need to be processed. The back-scattered signals are picked up by the transceiver and taken back to the Photo Multiplier Tube (PMT). The PMT converts the optical signal into an electronic signal, which can be handled by the processing hardware present inside the DSA hardware box [Fig. 3.11]. In order to monitor the signal processing and aid the adjustment of processing parameters, the signal at various stages of processing is displayed on an oscilloscope. The software has the process parameters settings which are needed for controlling the hardware and thus developing the signals to get the requisite information [Aerometrics, 1992].

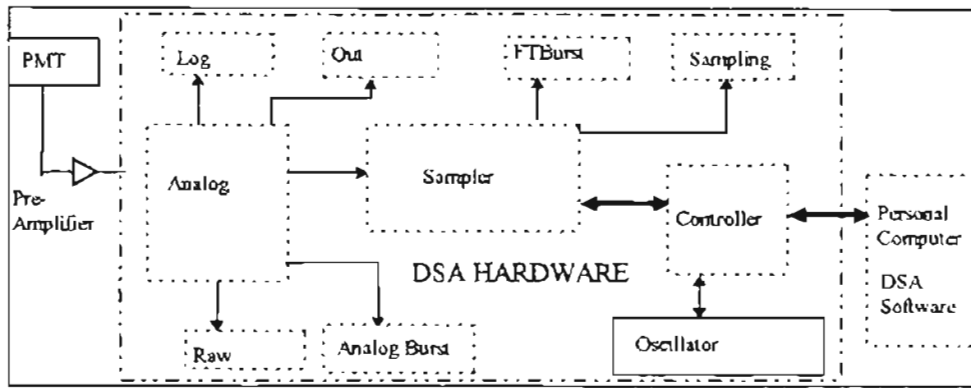


Figure 3.11: Data Collection and Processing Unit

The oscilloscope displays four different types of signals. These include the raw unprocessed signal after the PMT and the amplifier. It displays on the same screen the Doppler burst without the Gaussian pedestal. In order to increase the amplitude of the signals caused by the particles, a logarithmic amplification of the signal is carried out and is displayed on the screen of the oscilloscope. The burst detector serves to locate the signal and issue a signal to the controller, which then transfers the sampled signal to the First In First Out (FIFO) buffer. The burst detector operates on the logarithmically amplified signal after it is rectified and squared. Here, the power of the signal is used for burst detection. The system uses a Fast Fourier Transform for processing the signal and calculating the velocity of the corresponding particle. Anand [1997] demonstrated the effects of various parameter settings on the data collection.

3.4 Flow System

A blower generated the required airflow. The housing was installed on the suction side of the blower. The room air was taken in through a heater, which was also used to evaporate the water droplets in the solution. The flow rate was controlled by a pneumatic

flow control system. A six-jet atomizer was used to seed the particles. For the purpose of this thesis, three different particle sizes were used. They were 2.04 μm , 0.966 μm , and 0.497 μm . These particles, which are available in the form of a 10% concentrated solution by volume, are further diluted by using distilled water. The typical dilution ratio used was as follows:

- 2.04 μm : 20 ml of particles and 980 ml of water for making 1000 ml of solution
- 0.966 μm : 10 ml of particles and 980 ml of water for making 1000 ml of solution
- 0.497 μm : 5 ml of particles and 980 ml of water for making 1000 ml of solution

At different flow rates, the number density observed is different. For example, at high flow when the filtration efficiency is high, the number density below the filter is very low. Therefore, in order to get measurable data in a reasonable time period, depending on the flow rate, these concentrations were varied in order to get a greater number of signals. Compressed air at pressure of 40 psig was supplied to the atomizer. The air actually used in the atomizer was at a pressure of 36 psig. The solution was atomized by passing through the jet nozzles. Before the actual atomization process, it is possible to mix the solution with air and then atomize the mixture. This control in the atomizer can also be used to control the rate at which the particles are seeded into the system.

The solution then passed through a mixing chamber which was helpful in providing a uniform flow for the Small Angle Diffuser Housing (Fig. 3.12). As a part of this thesis, the experiments were carried out using three different housings, the construction of which is explained below.

3.4.1 Small Angle Diffuser Housing

This housing, which has a small diffuser angle, has been built similar to the one recommended in the SAE J1669 cabin air filtration code [SAE, 1993] (Fig. 3.12). Though not built exactly to the specifications of the code, it has its largest cross-sectional area less than 13.5% larger than the area of the filter being tested [against less than 10%, as required by the code] and has diverging wall angles of 1° and 3° for each pair of diverging walls [against less than 7° , as required by the code]. This small diffuser angle helps in providing a uniform flow at the filter plane. Two pressure taps are mounted in the housing in order to study the effect of the pressure drop across the filter on the efficiency of the filter. One tap is in the upstream section while the other is on the downstream section. These are then connected to a U-tube manometer to determine the pressure drop across the filter at different times during the course of the experiment.

3.4.2 Standard J726 Housing

This housing has been specified under the SAE J726 code [SAE, 1987] for automotive filter testing. The J726 housing (Fig. 3.13) provides a rapid expansion at the inlet due to the presence of a large diffuser angle. This housing provides a vertical entrance for the flow above the filter and a horizontal outlet below the filter. The presence of a large diffuser angle causes a separation and a non-uniform highly recirculating flow field as was documented by Sabnis [1993] and then by Natarajan [1995].

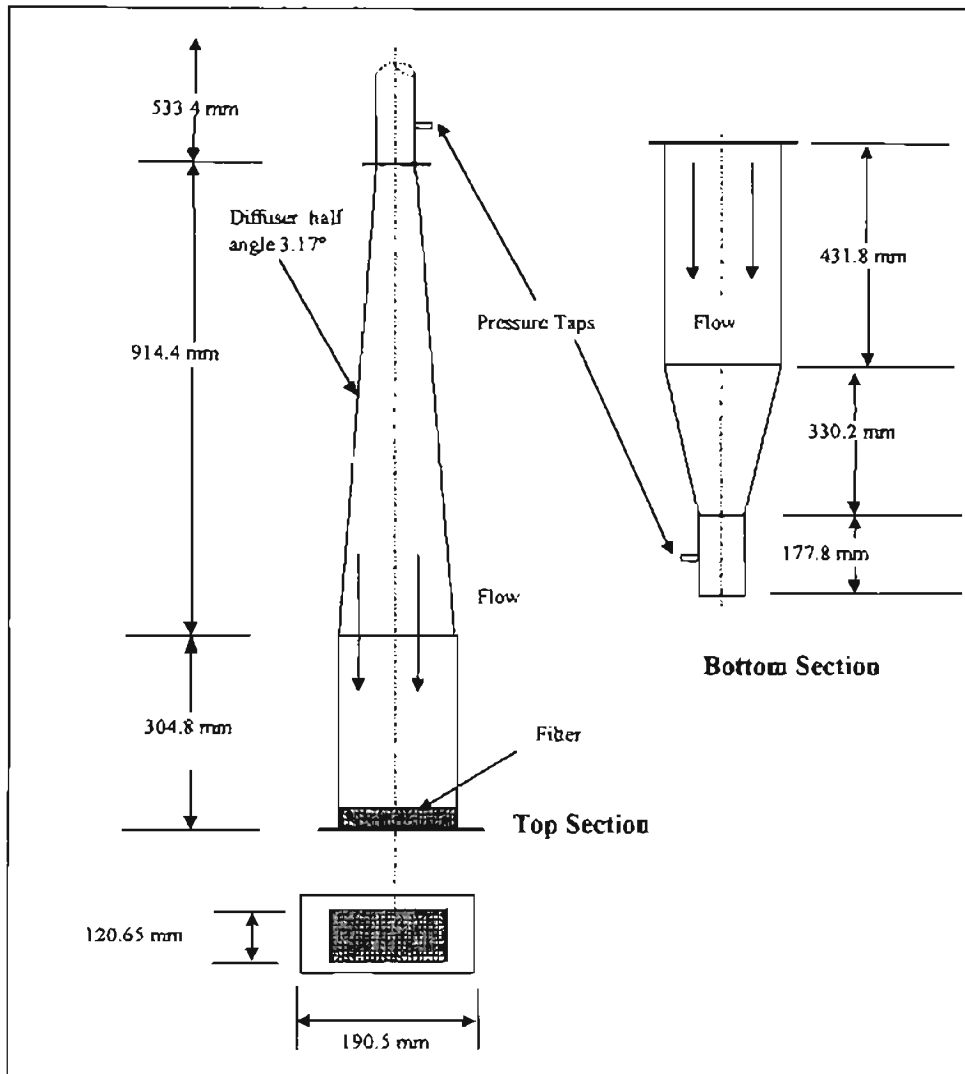


Figure 3.12: Small Angle Diffuser Housing

3.4.3 Simulated Automotive Filter Housing

This housing has been designed by other researchers on this project for testing the CFD models of the flow pattern over the filter [Al Sarkhi et al., 1997]. This housing has a long rectangular duct, which provides a horizontal entrance for the flow above the filter (Fig. 3.14). This housing provides a cross velocity (Fig. 3.14) which is almost equal to or more than the downward velocity above the filter. The lower half of the housing is the same as that as used for the Small Angle Diffuser Housing.

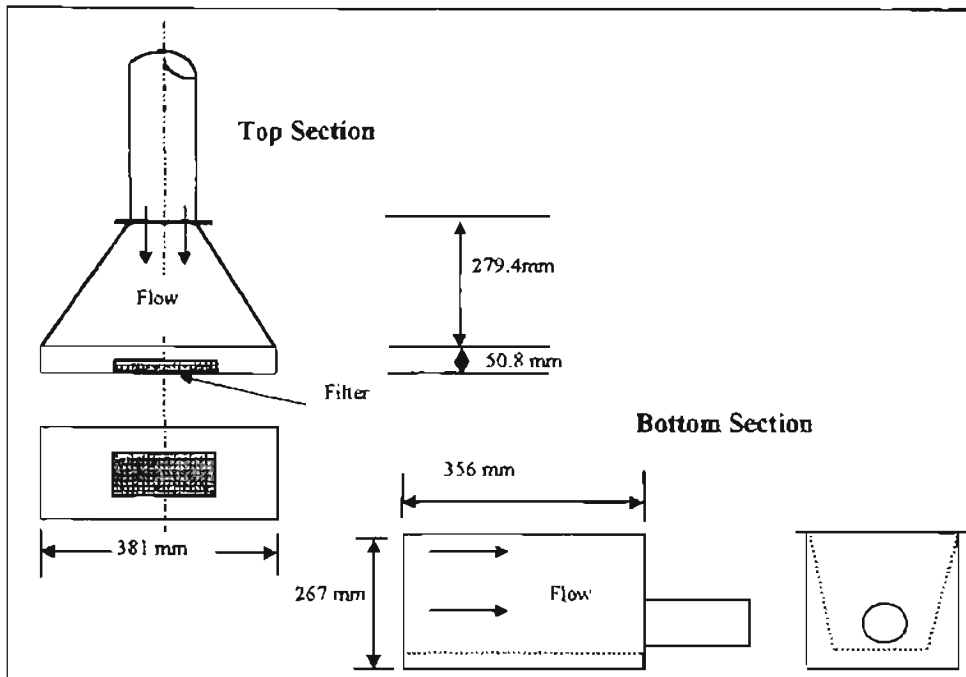


Figure 3.13: Standard J726 Housing

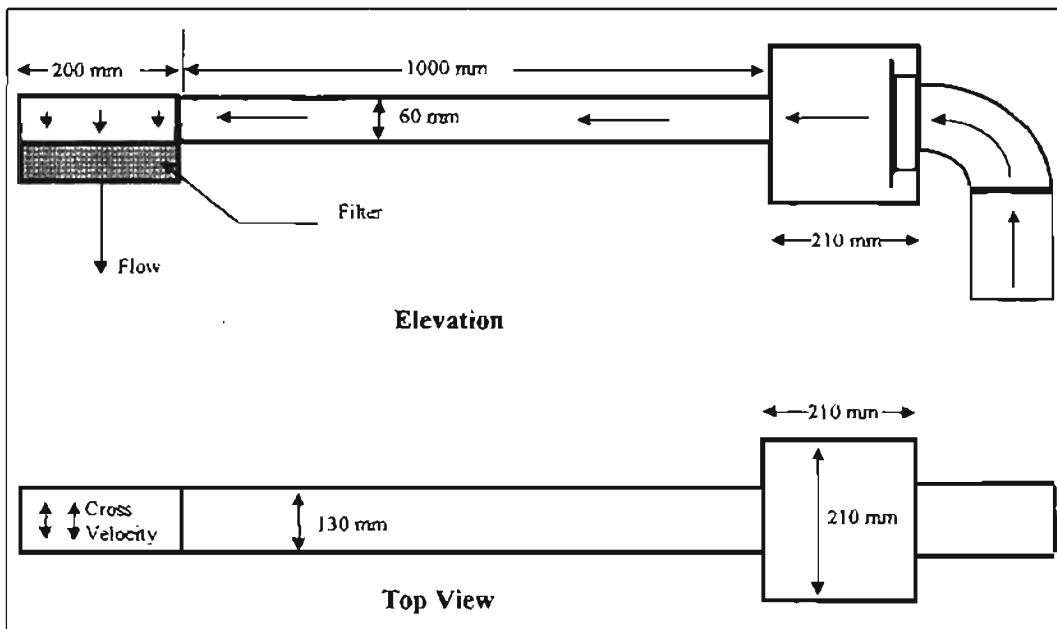


Figure 3.14: Simulated Automotive Filter Housing

A flow bypass system was installed, as shown in Figs. 3.15 and 3.16, by Jadbabaei [1997] for testing the efficiency at flow rates lower than 25 scfm, which is the lowest flow

rate, provided by the blower. This arrangement allows a lower flow rate from the filter by adjusting the bypass valves.

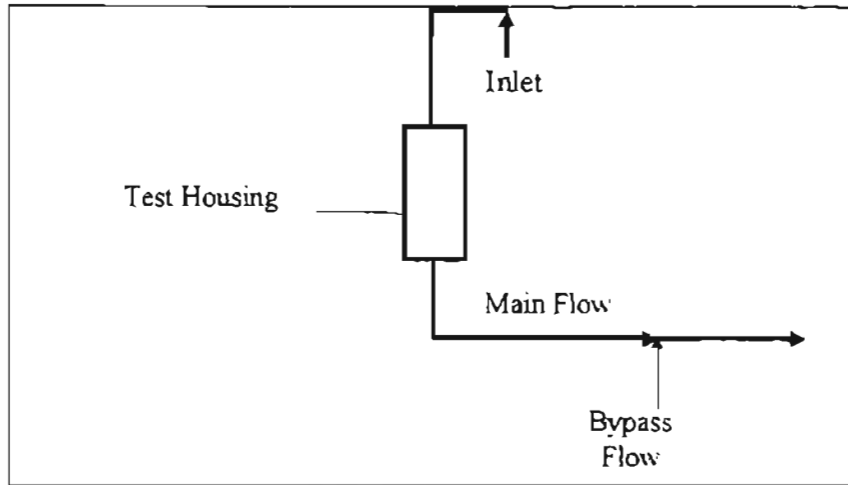


Figure 3.15: Flow By-pass System.

The following table from Jadbabaei [1997] gives the dimensions of the filter supplied by Dayco-Purolator, which is used in the experiments. The packing density of the filter and the average fiber density are from Duran [1995].

Table 3.1: A13192 Pleated Filter Dimensions

Overall dimensions	193 mm x 121 mm
Pleat pitch	3.125 mm
Pleat height	30 mm
Estimated average fiber diameter	51.78 μm (Approximately)
Estimated packing density	0.345 (Approximately)

The experimental set up that was used during the course of the experiment is as shown in Fig. 3.16. The solution of PSL particles was made in distilled water. The

prepared solution was placed in the atomizer. During the test, the solution after atomization enters the flow system through a bypass above the atomizer as shown in Fig. 3.16.

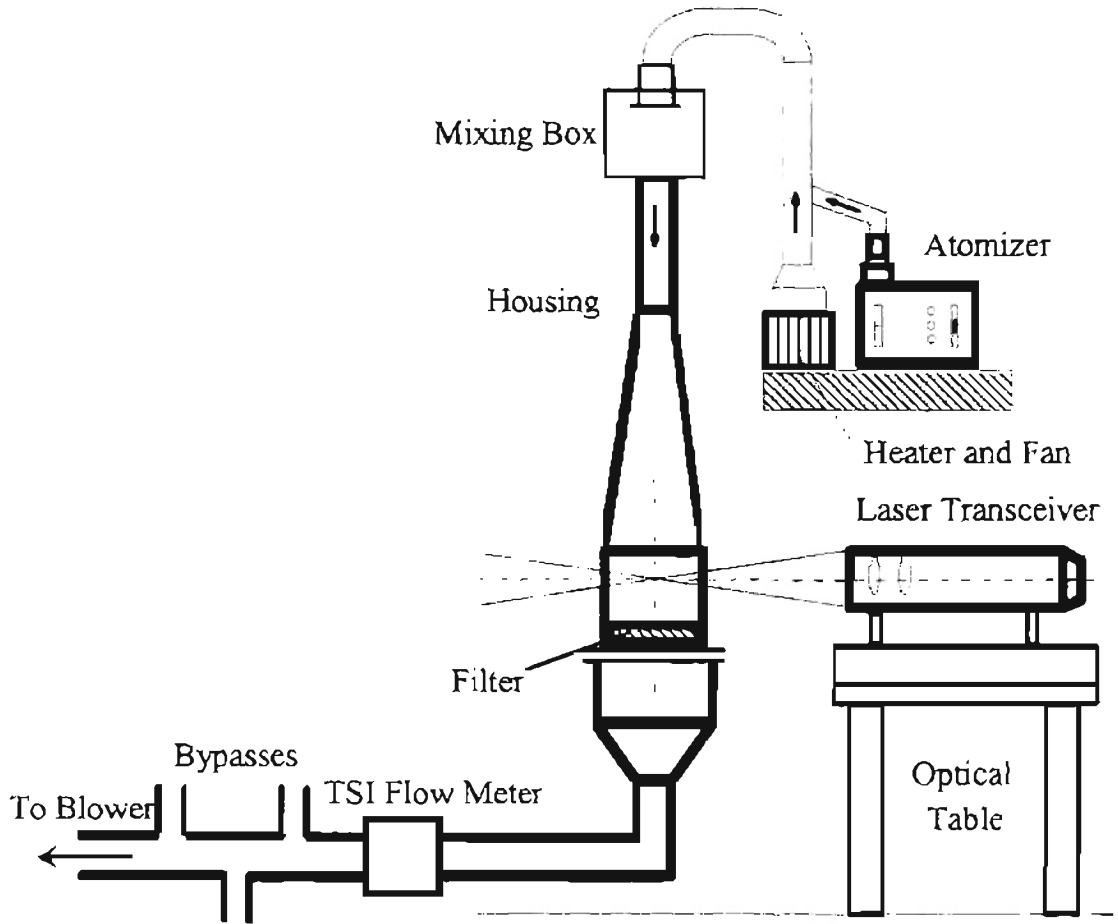


Figure 3.16: Experimental Setup

The heater evaporates the water droplets in order to remove all the water droplets from the atomized solution. The atomized solution passes through the mixing box (only in the case of the Small Angle Diffuser Housing) for proper mixing and then enters into the housing before crossing the filter. The TSI Flow meter was installed downstream of the housing. Anand [1997] and Jadbabaei [1997] calibrated the flow meter. After the test filter, there are still some particles in the air, which need to be removed. An absolute filter

[Fig. 3.17] is provided in the system, which prevents the release of the particles into the atmosphere.

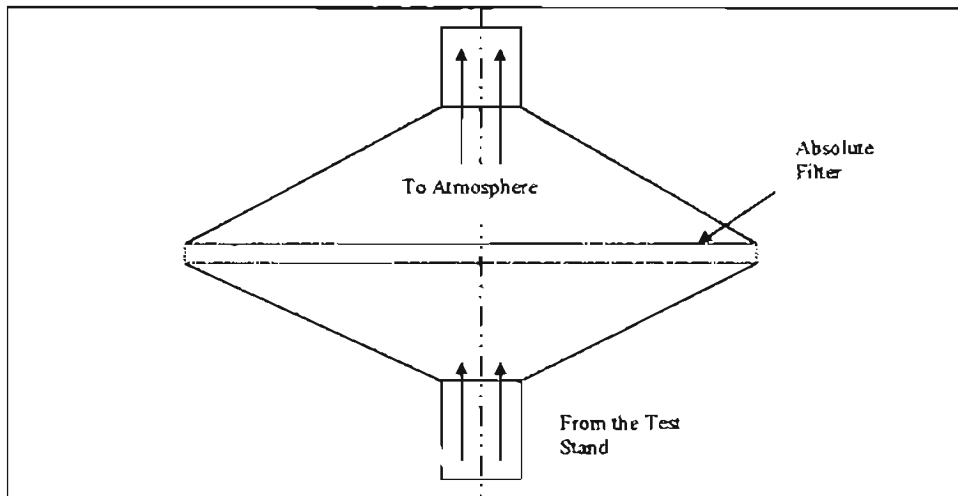


Figure 3.17: Absolute Filter Used for Preventing the Release of Particles into the Atmosphere

Chapter 4

CONSISTENCY MEASUREMENTS

Before any data is deemed to be correct, it is imperative that the data from the experiments be repeatable and the results be consistent. In the past, though the results obtained by earlier researchers Natarajan [1995] and Williams [1996] on this project were reflective of the expected trend, they had experienced considerable difficulty in providing consistent results. In a typical case the measured efficiency varied from 28% to 79% when the same flow rate was run twice.

Anand [1997] and Jadbabaei [1997] had performed several experiments on the laser to find out the cause of variation of the laser power during the course of the experiment. This variation of laser power had been shown by Williams [1996] to affect the number density of the particles. Though he was unable to point to the cause of the power variation, it was apparent that the fluctuation in the number density was caused by the power variation. Anand and Jadbabaei reasoned, after carrying out several experiments, that temperature variation in the room was the cause for the deterioration of the laser power. They made certain changes (as explained in Chapter 3) in the experimental setup and the procedure of data collection by optimizing the parameter settings on the DSA software. They carried out several experiments to check the

consistency of the atomizer. As a result of these experiments, they were able to explain the inconsistencies of the previous results. Though they were able to maintain the laser power constant by holding the temperature constant, the power of the laser had worsened considerably with the power of the blue beams being almost negligible as illustrated in Chapter 5. Most of the experiments during this study were conducted during the second half of 1997, and the laser system had been sent to the manufacturer (Aerometrics) for maintenance during February 1997. After the maintenance, the laser power improved substantially. The power of the laser before and after the maintenance work, at Aerometrics, is compared in Chapter 5.

The following experiments were carried out after the laser system was received from Aerometrics' maintenance to ensure the consistency of the test data and the results:

1. laser power consistency (these experiments were carried out with author's research partner T. Gebreegziabher [1998])
2. particle seeding rate

4.1 Laser Power

Jadbabaei [1997] had suggested that the vibration from the test stand's blower (when the blower was running) may be affecting the laser power and hence had installed vibration isolators below the optical bread board as shown in Fig. 4.1. As part of the present study, the pneumatic vibration isolators were removed and a cork sheet was used instead as a vibration isolator as illustrated in Fig 3.6. As part of the consistency measurements, five experiments were carried out to determine the effect (if any) of vibration on the laser power as measured at the transceiver head. Two of these

experiments were performed with the blower shut-off [Fig. 4.2], and in three experiments, the blower was operating [Fig. 4.3]. The temperature was controlled during all of these experiments. On comparing Figs. 4.2 and 4.3, it appears that there was no appreciable change in the laser power due to vibrations from the blower.

Next these experiments were carried out with no control over the temperature [Figs. 4.4 and 4.5]. It was observed that the variation in the laser power was very similar, whether the blower was running or not.

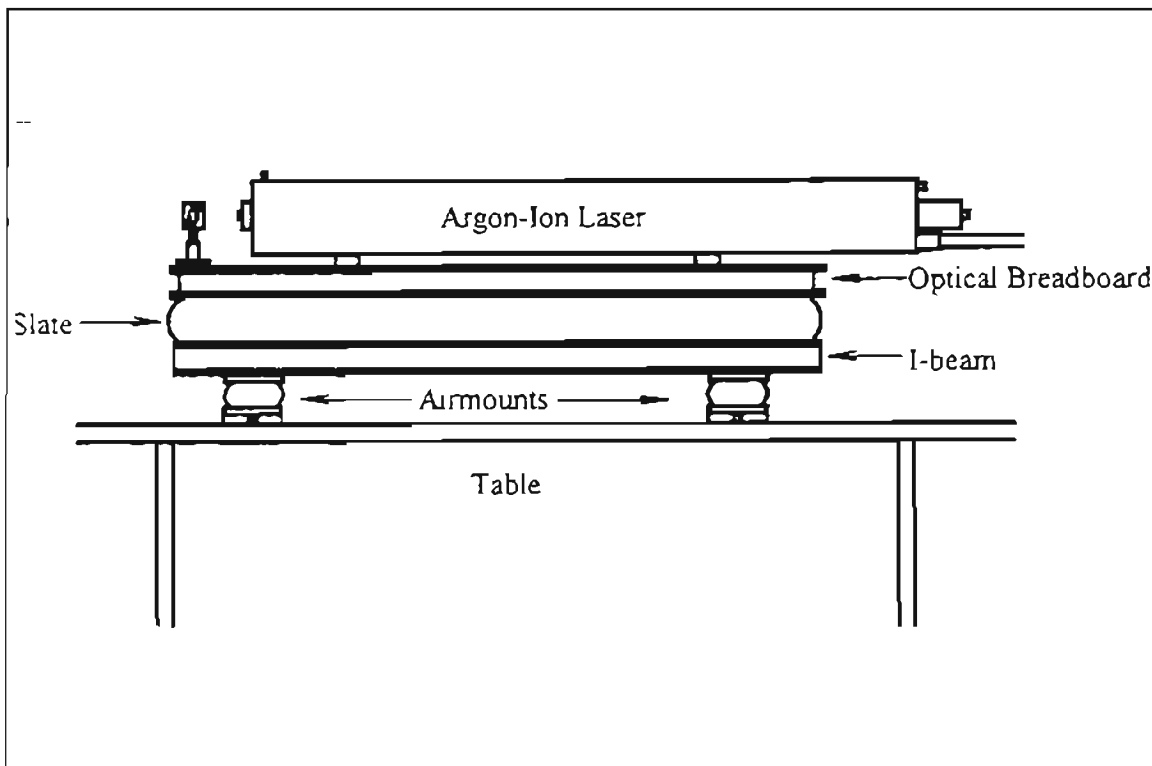


Figure 4.1: Setup for Isolation of Vibration from the Blower [Anand, 1997]

This showed that either the cork sheet that was being used for vibration isolation was capable of stopping vibration (if any) from the blower, or that the vibration of the blower did not appear to have any effect on the laser power. The actual data and the other plots for the consistency measurements have been provided in Appendix F.

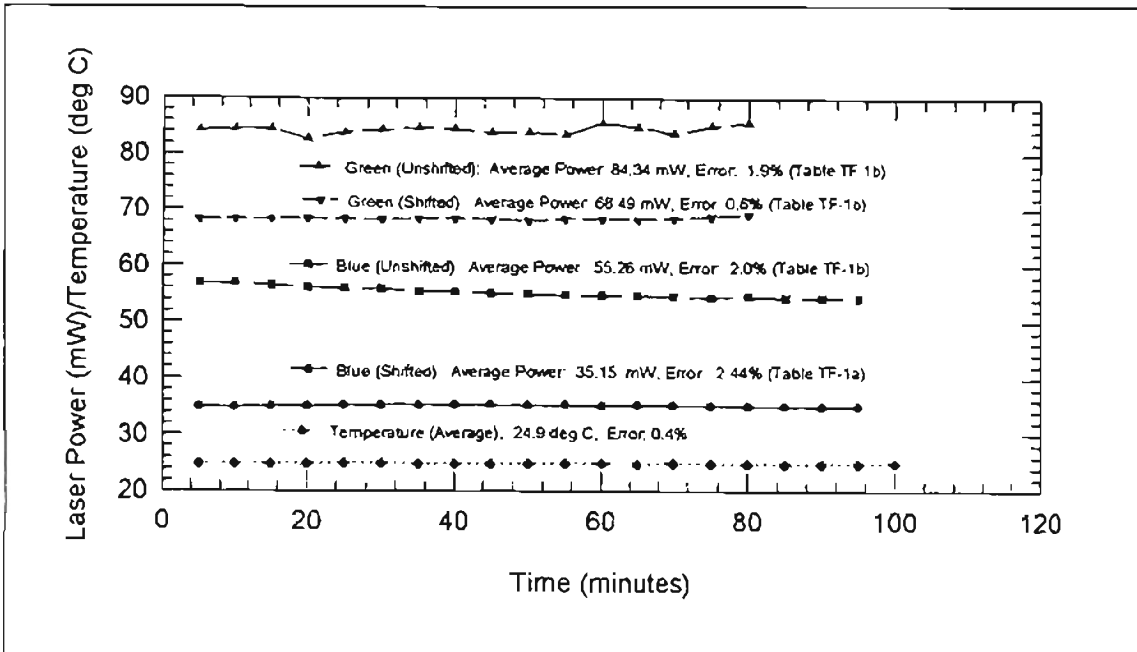


Figure 4.2: Variation of Laser Power at the Transceiver for a Constant Temperature Inside the Plexiglas Box, Test Stand's Blower Shut Off

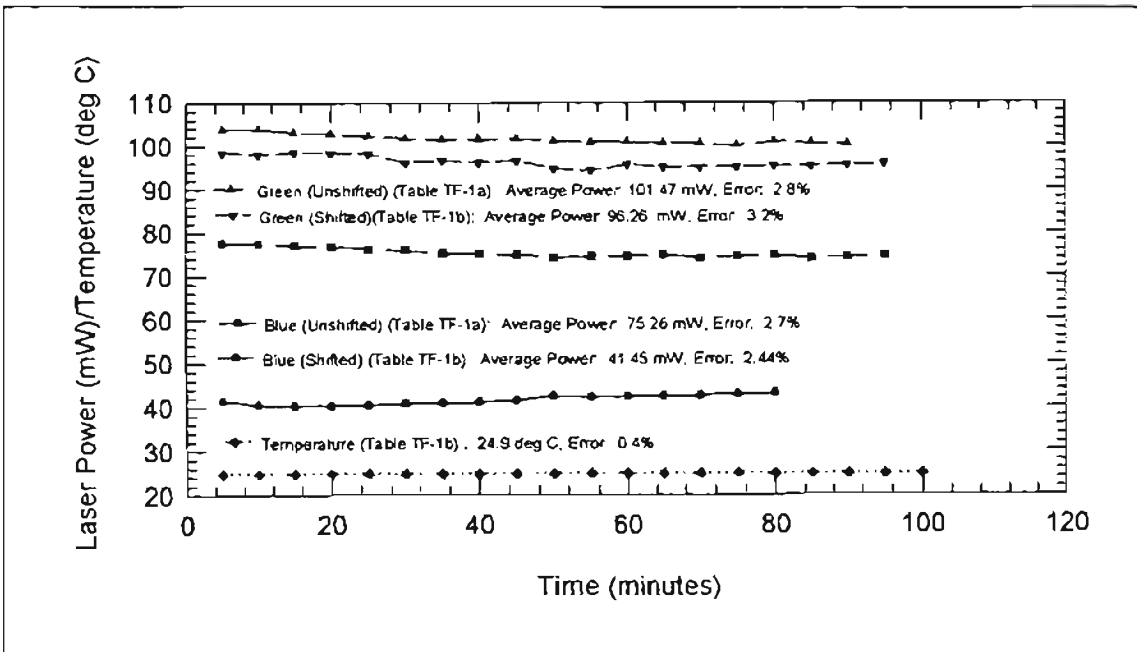


Figure 4.3: Variation of Laser Power at the Transceiver for a Constant Temperature Inside the Plexiglas Box, Test Stand's Blower in Operation

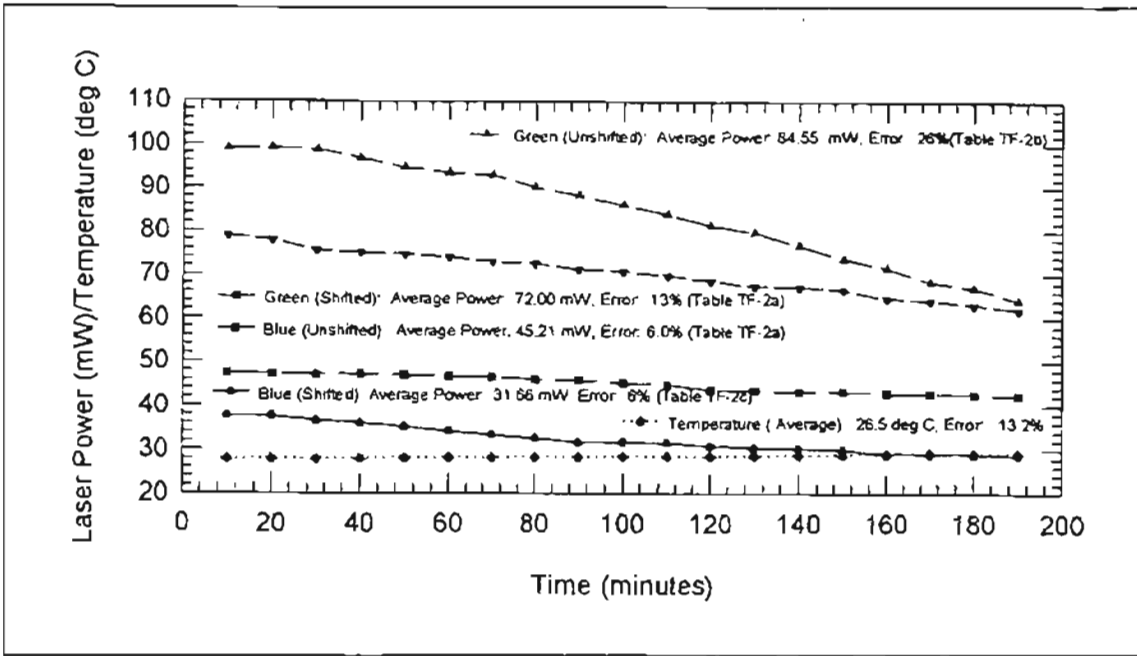


Figure 4.4: Variation of Laser Power at the Transceiver for Uncontrolled Temperature Inside the Plexiglas Box, Test Stand's Blower in Operation

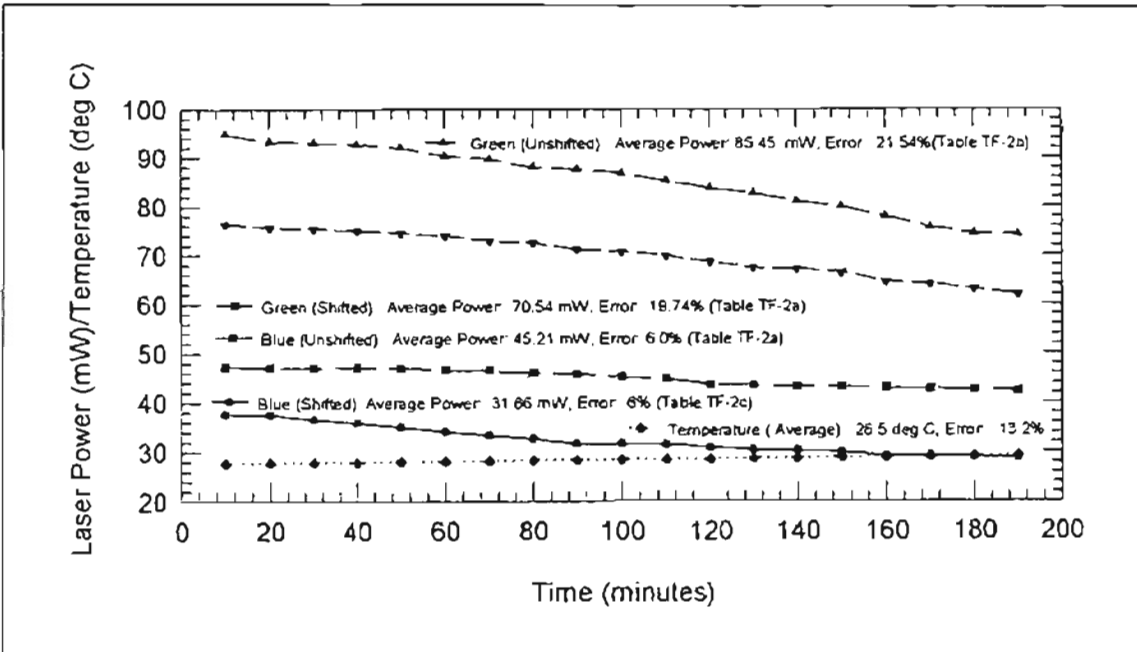


Figure 4.5: Variation of Laser Power at the Transceiver for Uncontrolled Temperature Inside the Plexiglas Box, Test Stand's Blower Shut Off

In order to maintain a constant temperature in the room, a room air conditioner was installed as was described in Chapter 3 (Fig. 3.7). The purpose of the room air conditioner was to aid in maintaining the room temperature constant. In addition it was desired to lower the working room temperature. Anand and Jadbabaei had worked at elevated room temperatures of approximately 29°C. Previously the room temperature increased when the blower was running, and in order to arrest the fluctuation in the room temperature, Anand [1997] had suggested working at relatively higher room temperature (29 - 30°C). Despite working at these temperatures, they had considerable difficulty in maintaining the room temperature constant, since they did not have any means of cooling the room once the temperature started to increase.

As part of the present study, several experiments were conducted in order to ensure that the laser power remained constant during the course of the experiment. It was observed that the laser power varied by only about 3-5% when the temperature within the Plexiglas box was kept within a variation of ± 0.2 °C as indicated by the thermocouple (response time 60 s Omega, [1997]). When no steps were taken to control the temperature within the Plexiglas box, the laser power variation was in some cases as high as 30% as shown in Figs. 4.6 and 4.7. As mentioned earlier, Anand and Jadbabaei had considerable difficulty in maintaining the room temperature constant; therefore a room air conditioner was installed in the room in order to assist in maintaining the room temperature constant. Several experiments were conducted in order to ascertain if the presence of the air currents from the air conditioner affected the laser power consistency. It was found that that the air currents did not have any significant effect on the laser

power. All of the data and some other plots for these consistency measurements have been provided in Appendix F.

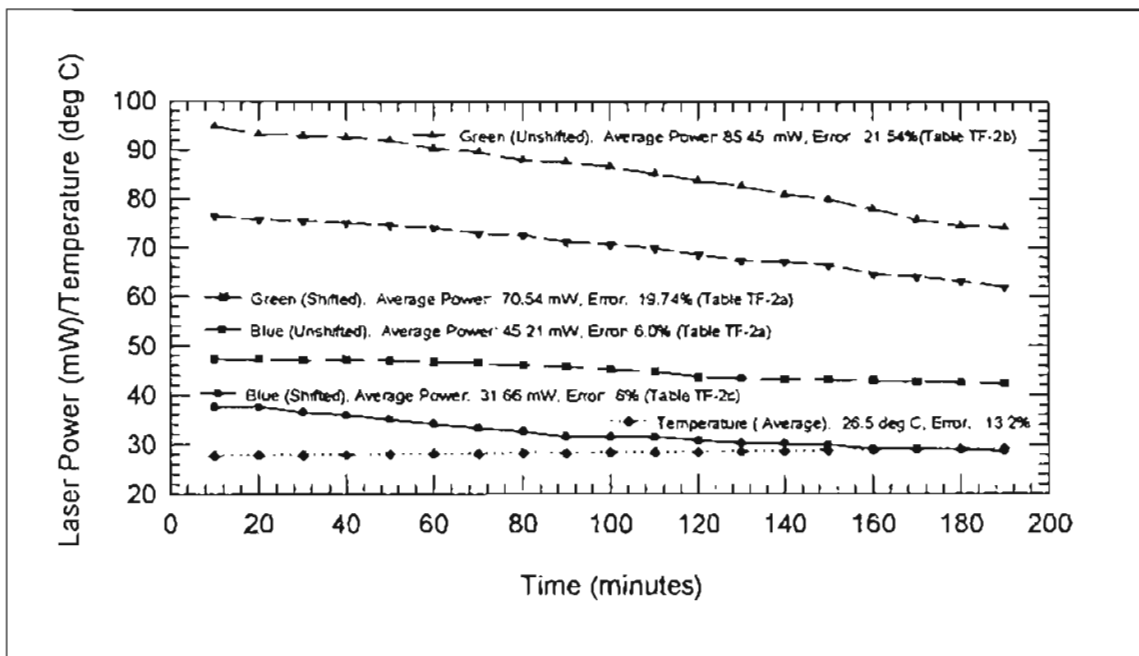


Figure 4.6: Variation in Laser Power When the Temperature Inside the Plexiglas Box Was Allowed to Fluctuate

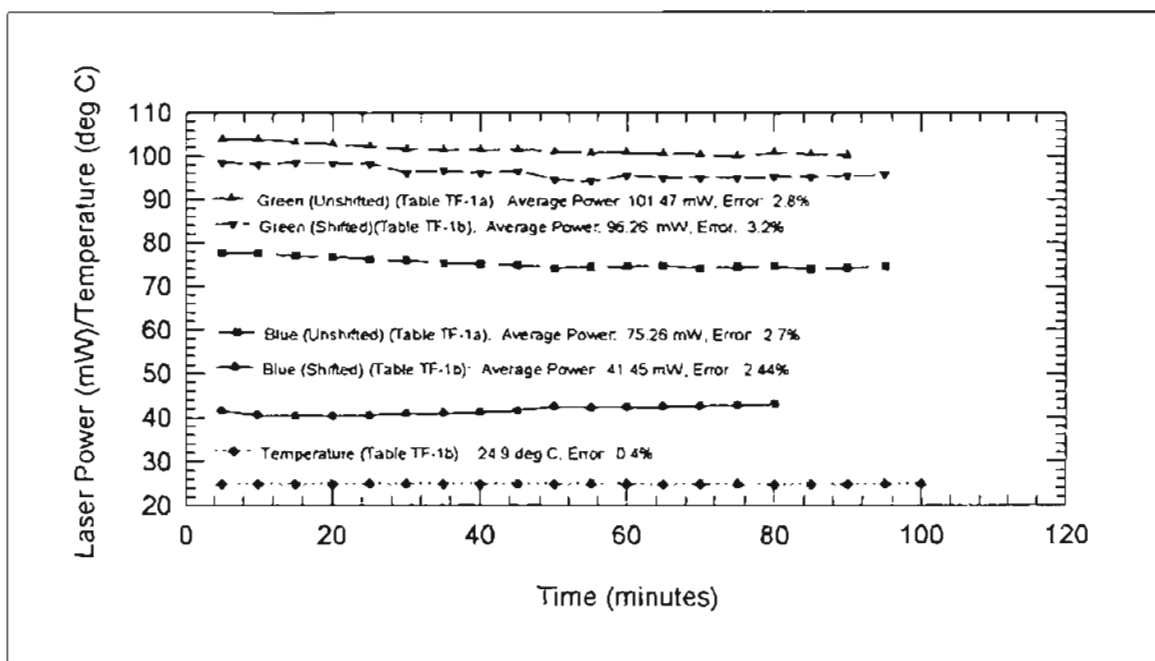


Figure 4.7: Variation in Laser Power When the Temperature Inside the Plexiglas Box Was Kept Constant

4.2 Atomizer Consistency Tests

Measurements were taken on the spray leaving directly from the atomizer. These measurements were taken directly in front of the atomizer. These tests were performed because it was possible that the rate of the particle generation from the atomizer itself was varying and thus providing inconsistent particle count to the system. These tests were conducted in order to determine whether the atomizer was generating particles at a constant rate or not. These tests were required to monitor the sampling rate, since the measurements were taken at a single point in front of the atomizer as shown in Fig. 4.8.

The number of samples determines the frequency and velocity resolution of the instrument (LDV). For the LDV the relationship between record length, sampling rate and the number of samples is given as [Anand, 1997]

$$\text{Record Length} = \frac{\text{Number of Samples}}{\text{Sampling Rate}} \quad (4.1)$$

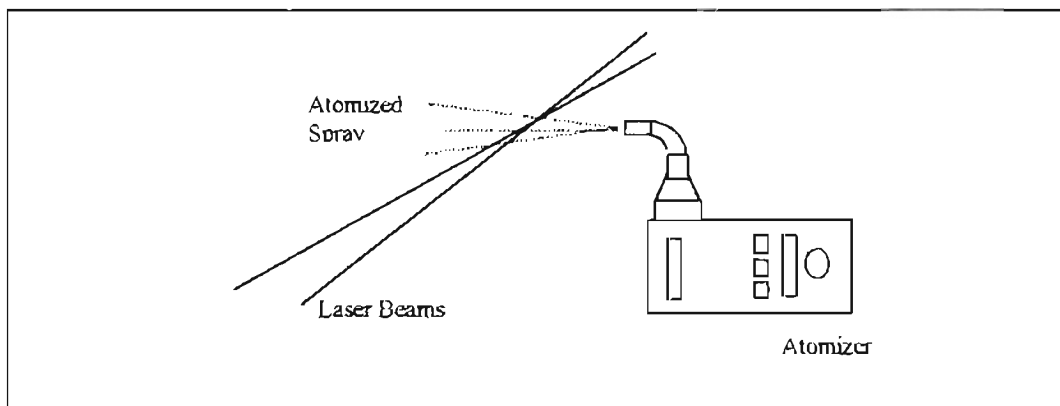


Figure 4.8: Consistency Test Setup for the Atomizer

Almost all of the data taken was within a range of $\pm 5\%$ as is illustrated for $0.966 \mu\text{m}$ size particles in Fig. 4.9. This is a fairly narrow bandwidth. Two sets of data each

were taken for 0.497, 0.966 and 0.497 μm size particles. All of the experimental data showed similar trends. All of the actual data and some other plots for these measurements have been provided in Appendix F

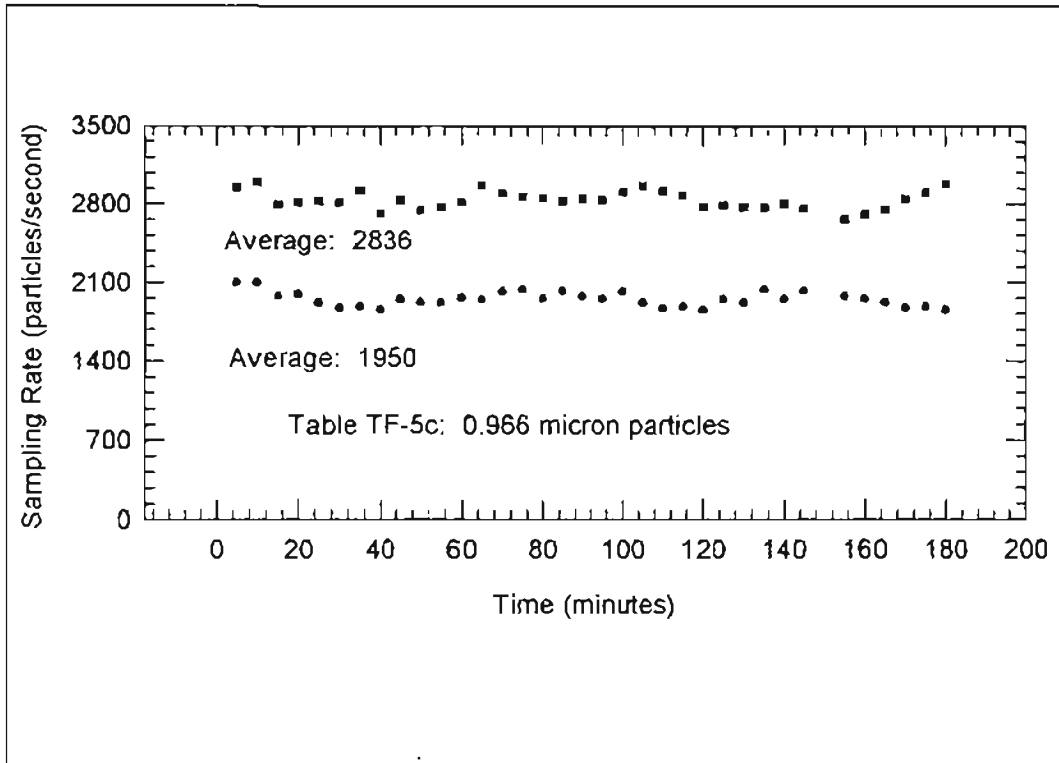


Figure 4.9: Atomizer Consistency Results for 0.966 μm Particles

Jadbabaei [1997] showed that a $\pm 5\%$ error in the sampling results in a higher error in the measured efficiencies as explained below. The local filtration efficiency is given by Eq. (3.2).

$$\eta = 1 - R_{nd} \quad (4.2)$$

The highest efficiency evaluated will be when the value of n_{down} is lower by 5% and that of $n_{upstream}$ is higher by 5%. Then the value of the efficiency will be

$$\eta_{max} = 1 - \frac{0.95}{1.05} R_{nd} \cong 1 - 0.9 R_{nd} \quad (4.3)$$

Similarly the minimum efficiency is calculated when n_{down} is higher by 5% and $n_{upstream}$ is lower by 5%.

$$\eta_{\min} = 1 - \frac{1.05}{0.95} R_{nd} \cong 1 - 1.1 R_{nd} \quad (4.4)$$

where R_{nd} is the ratio of the number densities of particles upstream and downstream. The actual error will therefore depend upon the ratio R_{nd} . The sampling rates were normalized with the mean of all the measurements in order that different sets of data could be compared

4.3 Experimental Procedure

The following procedure was followed for data collection for both consistency tests (explained in this chapter) and filtration efficiency tests (Chapter 5) as part of this study [see Appendix H for list of equipment]:

1. The filter was changed (for every experiment a new filter was used), and the flow setup was assembled.
2. The blower was started and the desired flow rate set and the initial pressure drop reading taken.
3. The heater was started.
4. After the temperature in the room had stabilized to about 23-25°C (depending on the outside weather conditions), the laser and the LDV system were started and the laser beams aligned at the fiber drive. The room temperature at the time of alignment was noted.

5. The traverse was started and the probe volume was brought to the center position of the filter.
6. The required solution was prepared and the atomizer was connected to the compressed air supply after filling the atomizer with solution.
7. The DSA parameters were set. The readings were first taken downstream of the filter and then upstream of the filter. This was done because, at the beginning of the experiment, the filter is clean and the pressure drop is a minimum. So when the particle counts are first taken downstream of the filter, the effect of any change in efficiency of the filter due to particle deposition on the filter is minimized.
8. During the course of the experiment, care was taken to minimize the room temperature fluctuation ($\pm 0.1^{\circ}\text{C}$ as indicated by the thermometer kept in the Plexiglas cover for the laser system). After all of the readings (35 points) downstream of the filter were taken, the laser power was checked again and adjustments made to restore the original laser power. The power was restored to the original value, to the extent possible. However no record was kept as to the extent of the adjustments made to achieve realignment. The drop in the power was typically on the order of 5-10% (for example, the green shifted beam would drop from about 65 mW to about 60 mW).
9. The pressure drop at the end of the experiment was noted.
10. During the experiment, when the temperature ($+0.1^{\circ}\text{C}$ as indicated by the thermocouple in the Plexiglas box) started to rise, the air conditioner was started. Once the thermocouple (kept in the Plexiglas box) showed a deviation of -0.1°C from the original value, the air conditioner was stopped. It took about 15-20

minutes for the thermometer device to show a temperature deviation of $\pm 0.1^{\circ}\text{C}$ from the original value (alignment temperature). So the air conditioner had to be started or stopped as the case may be.

11. All of the data was tabulated in an Excel spreadsheet on the 486 MHz computer in the C:\AUSERS\NEWTEST\\mu\text{m} particles) for experiments conducted in the Small Angle Diffuser Housing. The directory was named as "05 micron" for the 0.497 μm particles. The directory was named according to the name of the housing for the other housings (standard SAE Housing and the Simulated Automotive Filter Housing). The directory was named as "SAE" for the standard SAE Housing. The experiments on these two housings were conducted only on 0.966 μm ; therefore they were not classified according to their particle size. All of these experiments have then been named according to the flow rates and the test run for that particular flow rate. Some experiments were repeated for comparison with the results of Jadbabaei [1997] and were saved under C:\AUSERS\NEWTEST\REPEAT. SAH75_1_1 is the name of the file for the test run at 75 cfm (103.69 m^3/hr), the first "1" stands for 0.966 μm particles, and the second "1" stands for the test run at that flow rate. The tabulated parameters (by experiment name and date) for each of these experiments will be presented in Chapter 5.

Chapter 5

RESULTS AND DISCUSSION

5.1 Summary of the Experiments

The experiments on the Dayco-Purolator A13192 filters were conducted for various flow rates on the standard SAE J726 using 0.966 μm particles, Small Angle Diffuser housing using 0.497 μm , 0.966 μm and 2.04 μm particles, and Simulated Automotive Filter housing using 0.966 μm particles. The LDV parameter settings for different test conditions were selected as recommended by Anand [1997]. In order to be assured of the accuracy and repeatability of the measurements, several consistency measurements, (outlined in Chapter 4 of this thesis and detailed in Appendix F) were carried out.

The experimental results of this study are also compared with those of Jadbabaei [1997] for 0.966 μm particles. However during the period when Jadbabaei and Anand conducted their experiments, the power of the laser beam had deteriorated considerably; and even though the laser power remained fairly constant during the course of a

experiment, the power of the four beams was quite low [Table 5.1]. All the experiments by Jadbabaei and Anand and those in the present study were conducted at a laser power 0.8 W. However the powers as measured exiting the transceiver by Jadbabaei and Anand, and that in the present study were quite different and are tabulated below for comparison.

Table 5.1: Comparison of Laser Power Exiting the Transceiver Before and After Maintenance (@ 0.8 W from the Laser)

Beam	Laser Power (mW)	
	Jadbabaei and Anand [1997]	Present Study [1998]
Blue (Shifted)	1.78	31.82
Blue (Unshifted)	3.69	56.28
Green (Shifted)	19.55	64.10
Green (Unshifted)	16.7	80.28

As mentioned in Chapter 4, before the experiments were conducted on the Small Angle Diffuser housing and the Simulated Automotive Filter housing, the laser system had been sent to the manufacturer [Aerometrics] during February of 1997 for maintenance. Therefore in order to ensure that the present results could be compared to those of previous researchers on this project, another purpose of this study was to find out if there was any change in the filtration efficiencies as measured by Jadbabaei [1997] from those in the present work. In order to do this verification, three different flow rates, that had been run by Jadbabaei, were also run by the author as part of this study.

The experiments were conducted at several different flow rates from 13.61 m³/hr to 314.73 m³/hr. These and other results of the experiments in the different housings are discussed in Sections 5.2 - 5.4.

5.2 Small Angle Diffuser Housing Measurements

For particle diameters of 2.04 μm and 0.497 μm , two runs were recorded at each location [35 points as shown in Figure 3.2] on the filter. During each of these runs, 300-1000 particles were counted (as described in Section 3.2). This was varied depending upon the flow rate and the particle size. At higher flow rates, when the number density was low, the sample size number was 300, since every run took a long time (approximately 150 seconds for 300 particles). The number densities were calculated based on the mean of the particle velocities.

The Swept Volume Technique (Appendix H) was used to calculate the number densities. At low flow rates, the pressure drop was very low, and any small change in the pressure drop was not discernible. At high flow rates, the initial pressure drop was about 50 - 70 mm of water and the final pressure drop increased by about 5-7 mm of water. The number density, velocity profile, and local filtration efficiency plots for all of the flow rates [not presented in this chapter] are presented in Appendix B for 0.497 μm and Appendix C for 2.04 μm . The overall results for the Small Angle Diffuser are summarized in Table 5.2. Flow rate given in Table 5.2 is the corrected flow rate based on the TSI calibration [Anand, 1997 and Jadbabaei, 1997]. The expected upstream number density (n_0) has been calculated as follows

$$n_0 = \frac{\text{Number of Particles Consumed in Time, } t_{sol}}{t_{sol} Q_{flow}}$$

The pressure drop was measured by the manometer at the start of the measurements and at the end of the measurements is tabulated along with the number of samples taken and the approximate LDV sampling time taken for each measurement.

The tests have alphanumeric designations, which specify the housing, flow rates, particle size and the repeat number. SAH75_05_2 stands for the Small Angle Housing experiment for 75 cfm (cubic feet per minute) with 0.497 μm particles (rounded to 0.5) and is the second experiment conducted for that flow rate. The Stokes number calculation [Appendix A] has been based on the mean velocities of the particles as measured by the LDV system (using housing cross-section, not unfolded filter area) [Jadbabaei, 1997] at the 35 points. The velocities calculated from the flow rate are obtained by uniformly distributing the flow over the entire pleated filter sheet (dimensions 114.30 mm x 184.15 mm). The average particle velocity (LDV measurements) is different from the velocity as measured by the TSI flow meter, since the LDV measurements were taken on a grid that covered only approximately 55% of the total area [Anand, 1997]. The areas very close to the housing wall were not considered (the velocities are lower in this region), and thus the LDV measurements covered only the central region of the filter (velocities are higher). All local measurement results in this chapter are based on the corrected flow rates as per the calibration of the TSI flow meter [Anand, 1997 and Jadbabaei, 1997]. The local filtration efficiency, velocity of the particles, and the upstream and downstream number densities of the particles were plotted and are illustrated in the figures in this chapter and in the Appendices as explained earlier.

Table 5.2: Summary of Small Angle Diffuser Housing Results for 2.04 and 0.497 μm Diameter Particles

Test Number	Test Date	Flow Rate (m^3/hr) [TSI]	Upstream No. Density Expected (Actual) ($\#/ \text{m}^3$)	Samples Taken	Time Taken for Data Collection (seconds)	Pressure Drop Initial (Final) (mm of water)	Upstream Average Particle Velocity TSI [LDV] (m/s)	Stokes Number Based on LDV Velocity	Average Overall Efficiency 2.04 μm	Average Overall Efficiency 0.497 μm
SAH10_05_1**	11/05/97	13.61	2.15 (2.08) $\times 10^9$	1000	25	2.54 (2.54)	0.218 (0.17)	0.0038		55.38
SAH10_05_2	11/05/97	13.61	2.15 (1.84) $\times 10^9$	1000	25	2.54 (2.54)	0.218 (0.19)	0.0043		58.18
SAH12_2_1	11/28/97	16.78	1.97 (2.00) $\times 10^9$	1000	30	2.54 (2.54)	0.262 (0.33)	0.0802	63.63	
SAH12_2_2	12/07/97	16.78	1.97 (1.93) $\times 10^9$	500	30	2.54 (2.54)	0.262 (0.33)	0.1058	46.57	
SAH12_2_3	12/07/97	16.78	1.97 (1.40) $\times 10^9$	500	30	2.54 (5.00)	0.262 (0.36)	0.1155	56.68	
SAH15_05_1	11/02/97	21.55	9.54 (7.12) $\times 10^8$	500	25	2.54 (2.54)	0.320 (0.30)	0.0068		33.83
SAH15_05_2	11/05/97	21.55	4.36 (3.3) $\times 10^9$	500	25	5.00 (7.50)	0.320 (0.24)	0.0054		56.84
SAH15_2_1	09/21/97	21.55	1.09 (0.908) $\times 10^9$	500	30	2.54 (2.54)	0.320 (0.43)	0.1389	48.53	
SAH15_2_2	11/23/97	21.55	1.09 (1.18) $\times 10^9$	500	30	5.00 (5.00)	0.320 (0.52)	0.1668	40.84	
SAH20_05_1**	11/02/97	29.48	7.15 (5.31) $\times 10^8$	500	25	7.50 (10.2)	0.436 (0.45)	0.0102		48.82
SAH20_05_2	03/27/98	29.48	7.15 (9.05) $\times 10^8$	500	25	7.50 (10.2)	0.438 (0.43)	0.0097		54.5
SAH20_2_1	08/16/97	29.48	3.87 (3.29) $\times 10^8$	500	30	7.50 (10.2)	0.436 (0.68)	0.2181	40.58	
SAH20_2_2	03/26/98	29.48	1.12 (1.12) $\times 10^9$	500	30	7.50 (10.2)	0.436 (0.60)	0.1924	37.87	
SAH25_05_1	10/03/97	37.42	7.15 (4.54) $\times 10^8$	500	30	7.50 (10.2)	0.545 (0.98)	0.0222		48.21

Table 5.2 (contd.): Summary of Small Angle Diffuser Housing Results for 2.04 and 0.497 μm Diameter Particles

Test Number	Test Date	Flow Rate (m ³ /hr) [TSI]	Upstream No. Density Expected (Actual) (#/m ³)	Samples Taken	Time Taken for Data Collection (seconds)	Pressure Drop Initial (Final) (mm of water)	Upstream Average Particle Velocity TSI [LDV] (m/s)	Stokes Number Based on LDV Velocity	Average Overall Efficiency 2.04 μm	Average Overall Efficiency 0.497 μm
SAH25_05_2**	10/31/97	37.42	7.15 (4.34) x 10 ⁸	500	30	10.2 (13.30)	0.545 (0.528)	0.0120		44.34
SAH25_2_1	09/22/97	37.42	1.08 (1.06) x 10 ⁹	500	35	10.2 (16.50)	0.545 (0.68)	0.2181	46.04	
SAH25_2_2	09/22/97	37.42	9.82 (4.68) x 10 ⁸	500	35	10.2 (13.30)	0.545 (0.75)	0.2405	61.05	
SAH30_05_1	10/02/97	45.35	5.96 (4.04) x 10 ⁸	500	30	10.2 (16.50)	0.654 (1.095)	0.0248		48.69
SAH30_05_2	03/25/98	45.35	5.96 (5.64) x 10 ⁸	500	30	10.2 (13.30)	0.654 (1.16)	0.0283		37.48
SAH40_2_1	09/27/97	61.20	4.09 (4.26) x 10 ⁸	500	50	25.4 (27.5)	0.873 (0.76)	0.2438	66.15	
SAH40_2_2	03/28/98	61.20	4.09 (3.34) x 10 ⁸	500	50	25.4 (25.4)	0.873 (1.52)	0.4875	53.08	
SAH50_05_1	10/04/97	77.07	3.58 (2.38) x 10 ⁸	500	70	34.3 (38.1)	1.09 (2.30)	0.0523		41.3
SAH50_05_2	10/31/97	77.07	1.59 (1.11) x 10 ⁸	500	70	34.3 (34.3)	1.09 (2.98)	0.0523		43.8
SAH50_2_1	09/14/97	77.07	3.84 (3.72) x 10 ⁸	500	50	34.3 (34.3)	1.09 (1.35)	0.4342	74.06	
SAH50_2_2	09/19/97	77.07	3.27 (3.31) x 10 ⁸	500	50	34.3 (38.1)	1.09 (1.63)	0.5228	70.14	
SAH75_05_1	11/01/97	104.26	3.05 (1.54) x 10 ⁸	500	90	42.6 (45.7)	1.64 (2.29)	0.0518		41.29
SAH75_05_2	03/25/98	104.26	1.91 (2.92) x 10 ⁸	500	90	45.54 (45.54)	1.64 (3.10)	0.0702		43.58

Table 5.2 (contd.): Summary of Small Angle Diffuser Housing Results for 2.04 and 0.497 μm Diameter Particles

Test Number	Test Date	Flow Rate (m ³ /hr) [TSI]	Upstream No. Density Expected (Actual) (#/m ³)	Samples Taken	Time Taken for Data Collection (seconds)	Pressure Drop Initial (Final) (mm of water)	Upstream Average Particle Velocity TSI [LDV] (m/s)	Stokes Number Based on LDV Velocity	Average Overall Efficiency 2.04 μm	Average Overall Efficiency 0.497 μm
SAH75_2_1	08/11/97	104.26	2.18 (1.57) $\times 10^8$	300	70	43.6 (45.7)	1.636 (2.15)	0.6889	83.56	
SAH75_2_2	09/25/97	104.26	2.55 (2.06) $\times 10^8$	300	70	53.3 (55.6)	1.636 (2.98)	0.9558	80.48	
SAH100_05_1	10/05/97	146.36	1.79 (1.11) $\times 10^8$	500	120	58.7 (61.0)	2.18 (2.97)	0.0672		43.8
SAH100_05_2	10/31/97	146.36	1.59 (0.979) $\times 10^8$	500	150	58.7 (61.0)	2.18 (3.30)	0.0747		37.25
SAH100_05_3**	11/06/97	146.36	1.43 (1.73) $\times 10^8$	500	150	56.2 (61.0)	2.18 (2.97)	0.0672		33.64
SAH125_05_1	11/08/97	188.45	1.11 (0.942) $\times 10^8$	300	120	60.8 (63.2)	2.73 (3.98)	0.0907		48.81
SAH125_05_2	11/09/97	188.45	8.58 (3.64) $\times 10^7$	300	150	63.2 (65.4)	2.73 (4.00)	0.0901		43.29
SAH125_2_1	08/12/97	188.45	1.09 (1.01) $\times 10^8$	300	150	61.1 (63.1)	2.73 (3.67)	1.1771	86.48	
SAH125_2_2**	03/26/98	188.45	1.09 (.820) $\times 10^8$	300	150	63.58 (67.5)	2.73 (5.09)	1.16325	92.05	
SAH150_05_1	11/01/97	230.54	1.43 (5.74) $\times 10^8$	300	150	68.5 (71.28)	3.27 (4.71)	0.1084		75.53
SAH150_05_2	11/08/97	230.54	1.43 (1.42) $\times 10^8$	300	150	68.5 (73.25)	3.27 (4.79)	0.1066		64.92

** For these tests, the traverse had to be moved 0.1 inch away from the edge, towards the center of the filter, because of negative velocities along that particular edge.

The upstream number density as shown in Fig. 5.1 is fairly uniform for the low flow rates. The number density at low flow rates ($7.96 \text{ m}^3/\text{hr}$) is high ($\sim 10^9 \text{ particles/m}^3$) and reduces to a low value ($\sim 10^7 \text{ particles/m}^3$) for high flow rates ($213.75 \text{ m}^3/\text{hr}$). Very low number densities led to an increase in the data collection time; and hence at these flow rates, the sample size was reduced from 1000 to 300 samples for $2.04 \text{ }\mu\text{m}$ particles and to 500 samples for $0.497 \text{ }\mu\text{m}$ particles. The average number density for a flow rate was calculated by taking the non-weighted average of the number densities at all of the 35 points upstream or downstream of the filter as the case may be.

A relatively regular upstream number density profile is observed for the Small Angle Diffuser Housing [Fig. 5.1]. After the flow passes through the filter, the flow gets disturbed, and as a consequence, the number density profile downstream of the filter [Fig. 5.2] is relatively irregular.

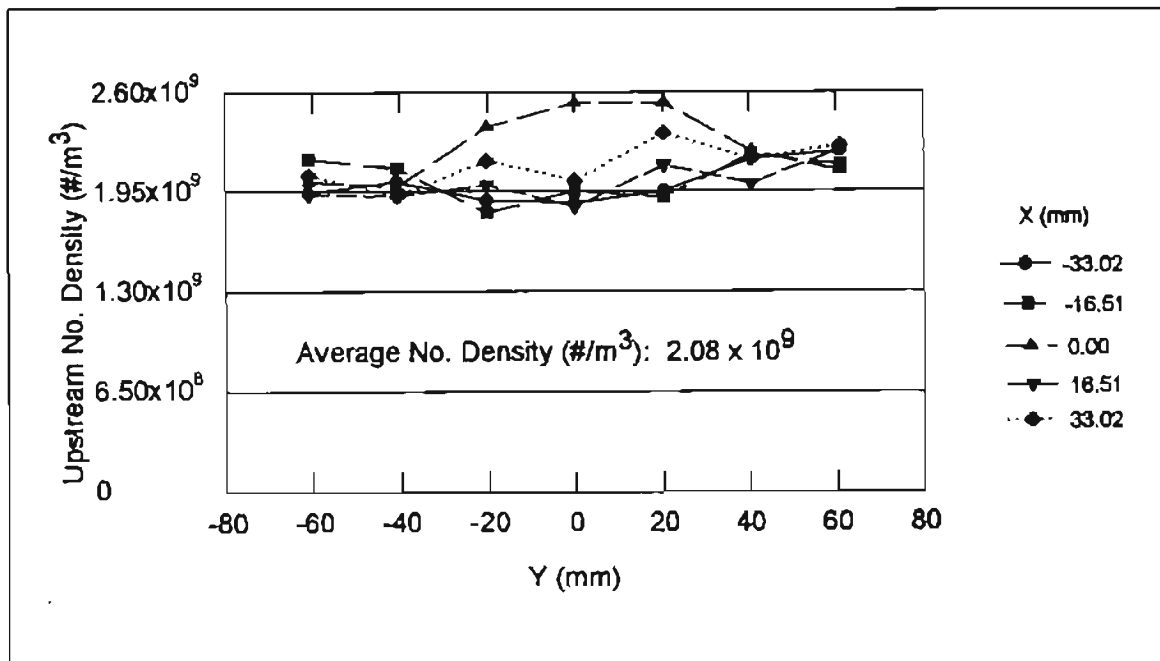


Figure 5.1: Upstream Number Density for Test SAH10_05_1 at $13.61 \text{ m}^3/\text{hr}$

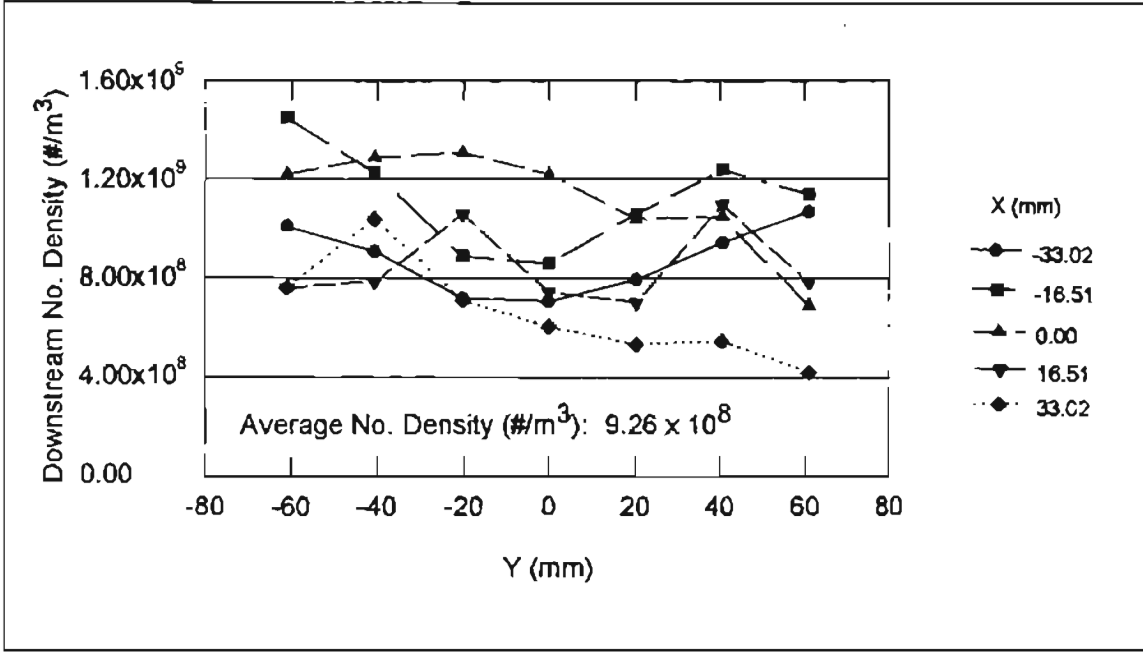


Figure 5.2: Downstream Number Density for Test SAH10_05_1 at 13.61 m³/hr

The flow profile is regular upstream of the filter [Fig. 5.3]. This regular velocity profile results in uniform number densities above the filter. The downstream number densities are affected by the change in the velocity profile [compare Figs. 5.3 and 5.4] after the filter. The housing wall is situated at locations approximately $Y = \pm 95$ mm, and thus the velocities (and hence the local number densities) around this location are affected by the presence of the housing wall. Further there is some interference caused due to the presence of the rubber beading of the filter on the lower side of the filter (this rubber beading is provided for supporting the pleated filter and has an embedded wire mesh that supports the filter). The downstream number density is therefore not as regular as the upstream number density [compare Fig. 5.1 with Fig. 5.2].

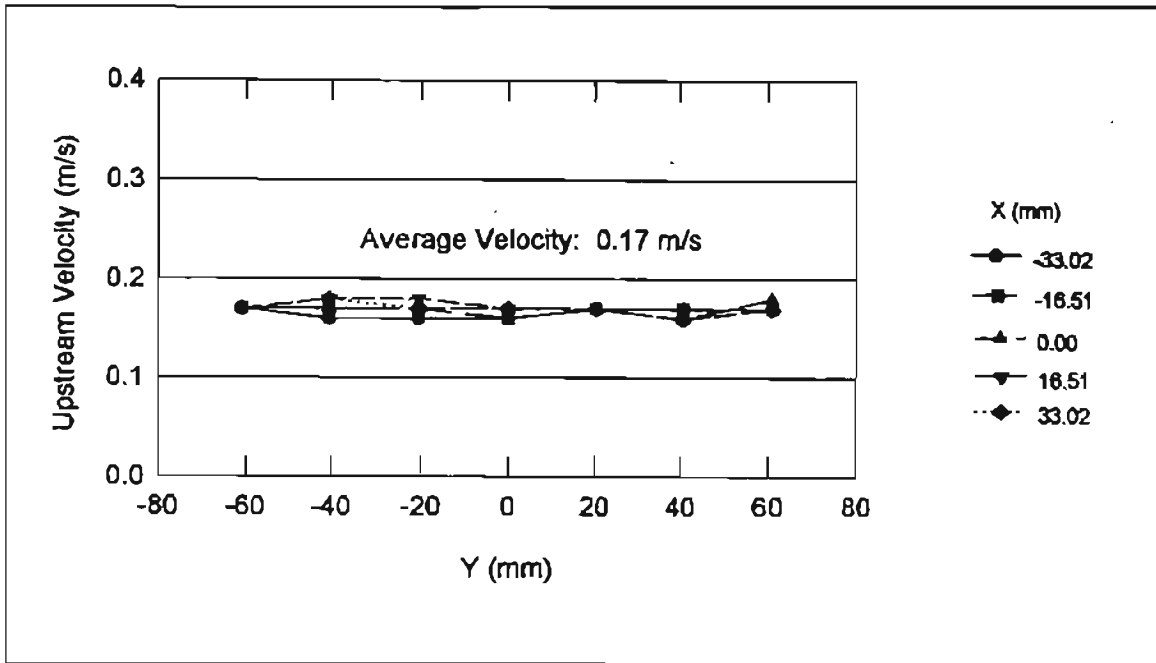


Figure 5.3: Upstream Velocity Profile for Test SAH10_05_1 at 13.61 m³/hr

The velocity profile measured above the filter exhibits a very regular profile. In some test runs, the velocities in certain instances, near the wall or edge rows downstream of the filter were irregular. This was due to the presence of recirculation zones near the edge of the filter as explained earlier and due to the housing walls, which affected the velocity profile. When the recirculation zone was found to be strong at a particular location, the position of the probe volume was shifted slightly away into the center of the filter (never more than 5 mm). Since this happened only at locations along the edge downstream of the filter, the corresponding upstream position of the probe volume was also shifted. The measurements presented herein are therefore representative of the values at that location. Recirculation zones affected a total of about 8-10 measurements out of all of the experiments conducted. Some of these experiments have been marked with “***” in Table 5.2. Others have not been marked since records were not kept for all cases.

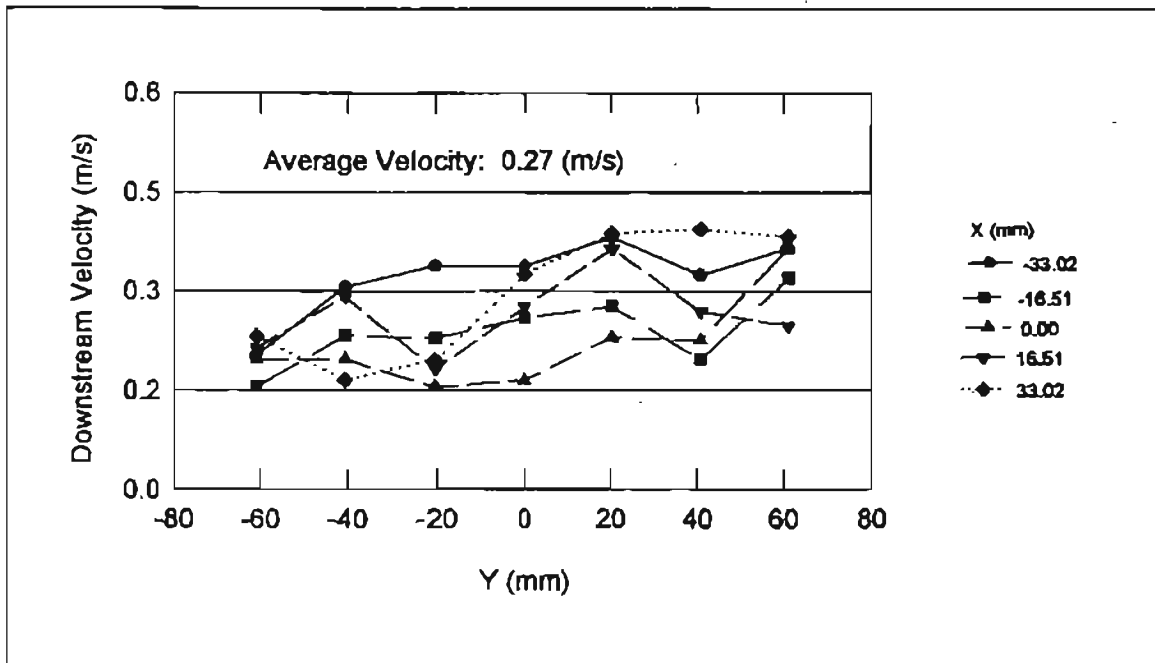


Figure 5.4: Downstream Velocity Profile for Test SAH10_05_1 at 13.61 m³/hr

The pressure drop was monitored during the course of the experiment. As part of these experiments, for every test, a new filter was used, since small particles tend to clog the filter quickly. The pressure drop was noted at the start of the test and after the end of the test. After the end of the downstream data was taken, the pressure drop was observed to find out if the filter was getting clogged. This gave an indication of the restriction caused by the particles.

The filter efficiency variation over the surface of the filter or the local filtration efficiency for the flow rate 13.61 m³/hr is shown in Fig. 5.5.

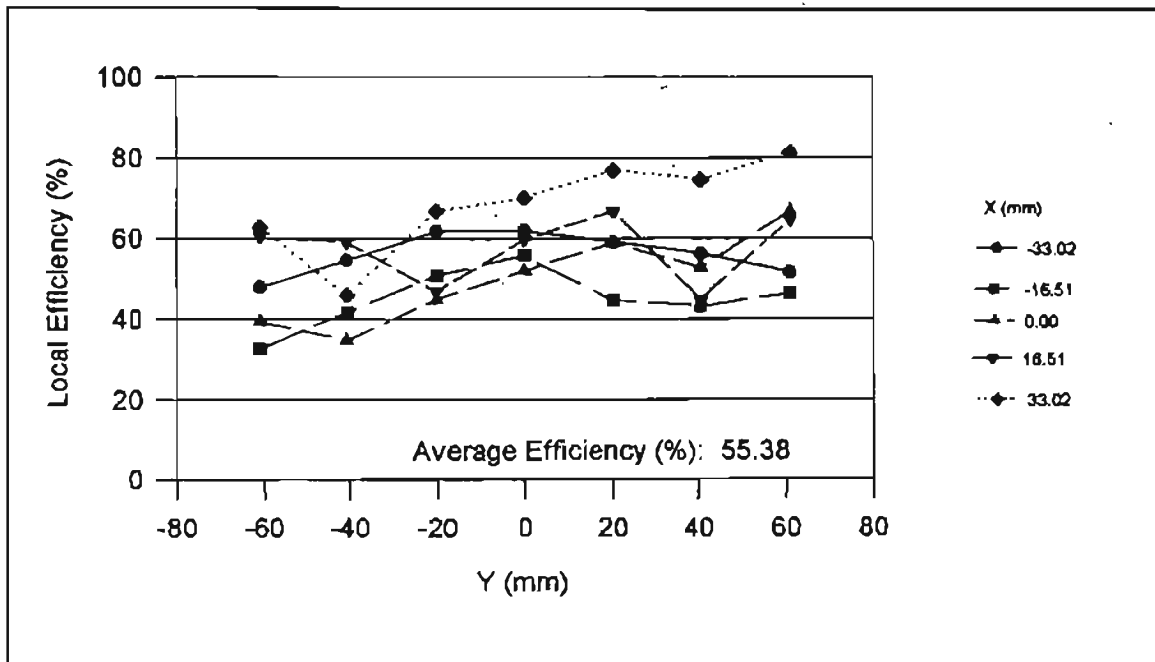


Figure 5.5: Pleated Filter Efficiency for Test SAH10_05_1 at 13.61 m³/hr

A set of similar data for number a flow rate of 77.07 m³/hr is shown from Figs 5.6 - 5.10. A comparison of the number densities upstream of the filter, for the two flow rates shows that, as the flow rate increases, the number density profile becomes flatter. This is probably because at low flow rates, even a small variation in the flow rate makes a large change in the number densities. At low flow rates, a change of only 0.05 m/s in the velocity of the particle [Fig. 5.3] is equal to a change of 25% in the velocity of the particle. This velocity change causes a corresponding approximate change in the number density by about 25%, thus causing a more variable number density profile than in the case of a higher flow rate [Fig. 5.7].

Plots for local filtration efficiency measurements are given in Appendix B & C for 0.497 and 2.04 μm particles. A comparison of the number density profiles and the velocity profiles for different flow rates further reaffirms the conclusion drawn above.

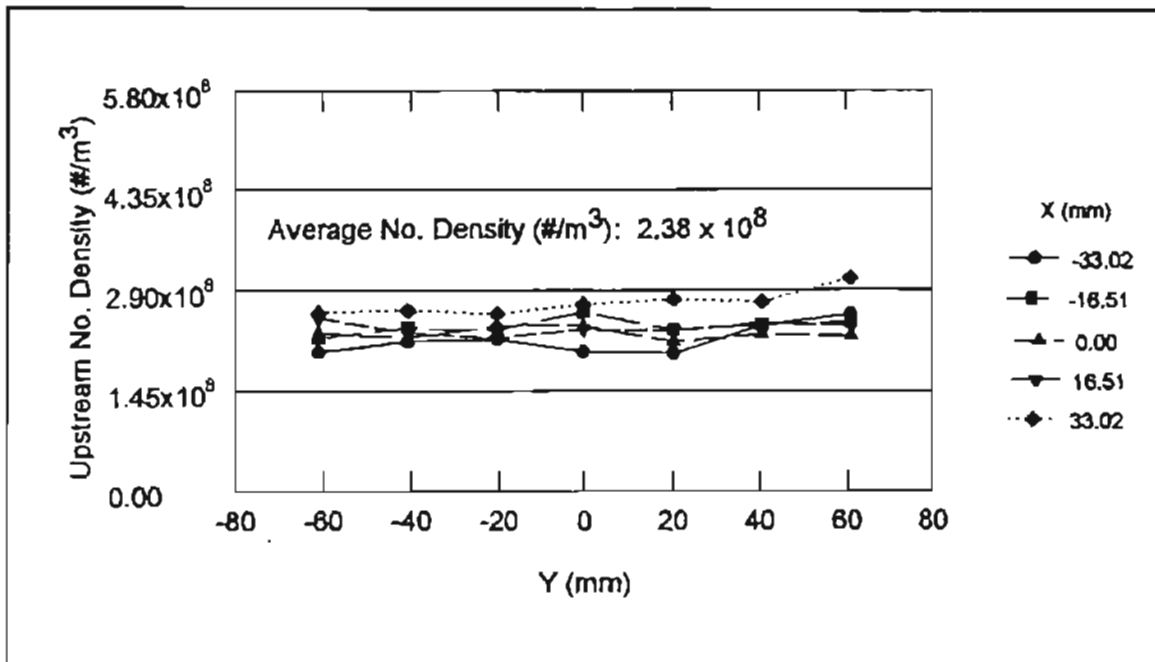


Figure 5.6: Upstream Number Density for Test SAH50_05_1 at 77.07 m^3/hr

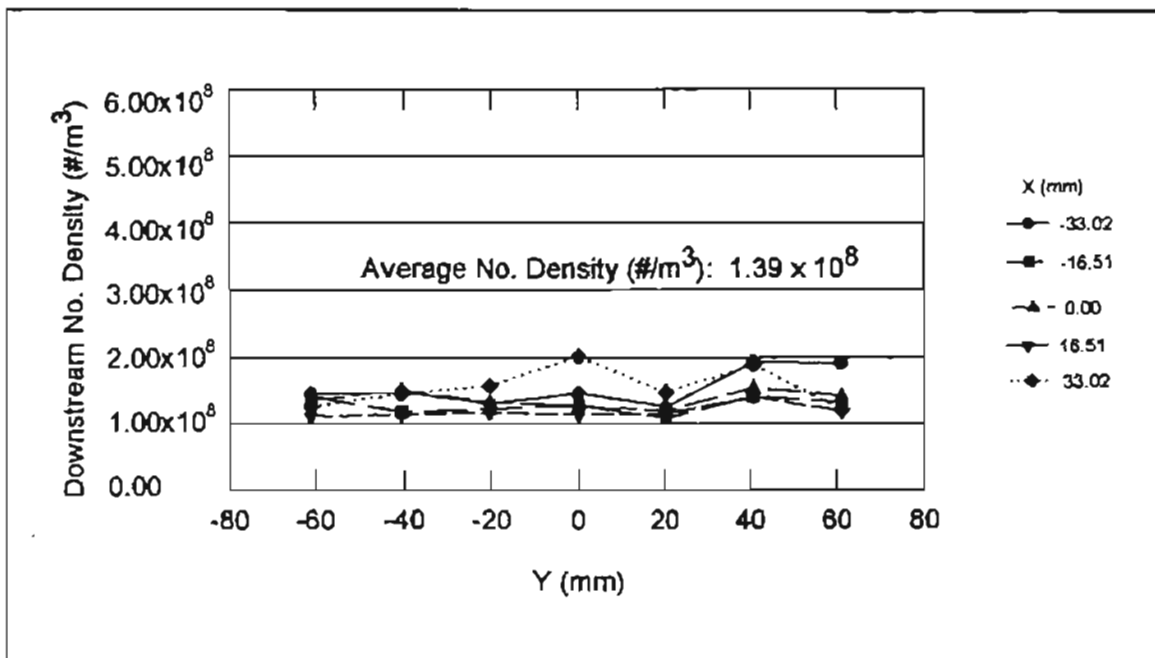


Figure 5.7: Downstream Number Density for Test SAH50_05_1 at 77.07 m^3/hr

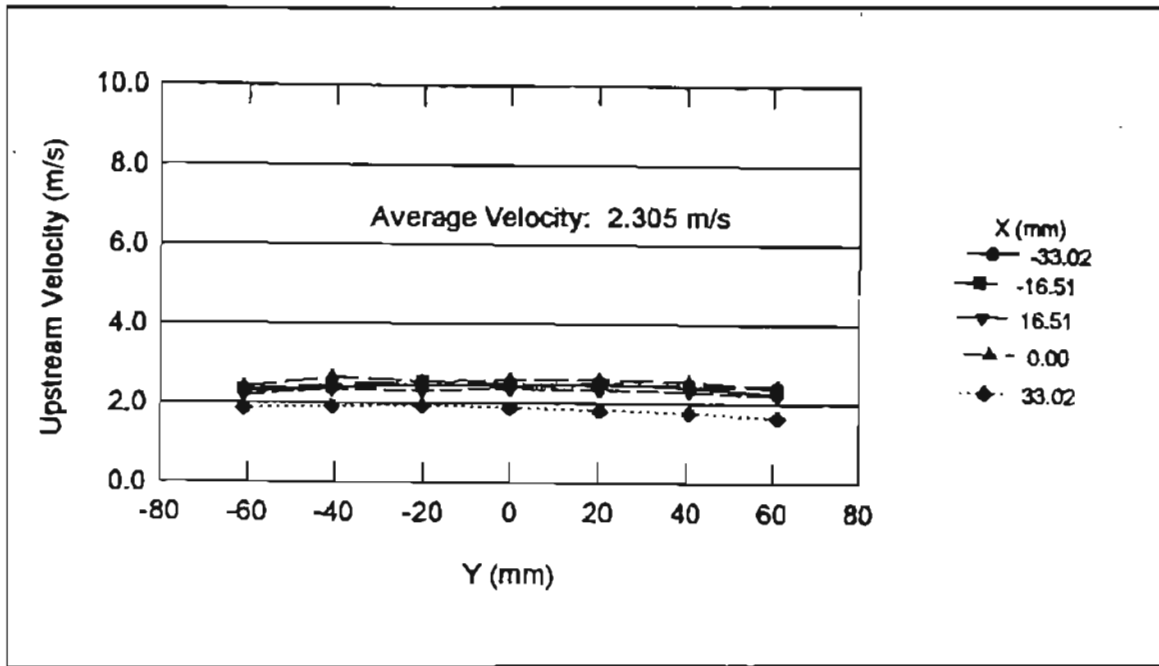


Figure 5.8: Upstream Velocity Profile for Test SAH50_05_1 at 77.07 m³/hr

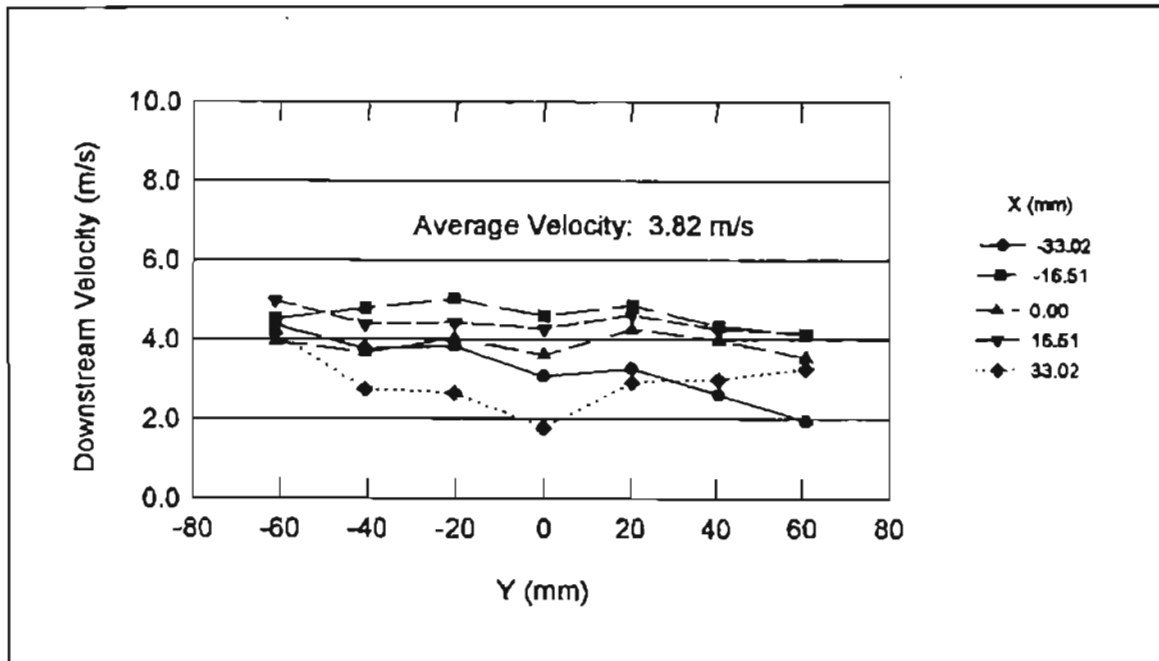


Figure 5.9: Downstream Velocity Profile for Test SAH50_05_1 at 77.07 m³/hr

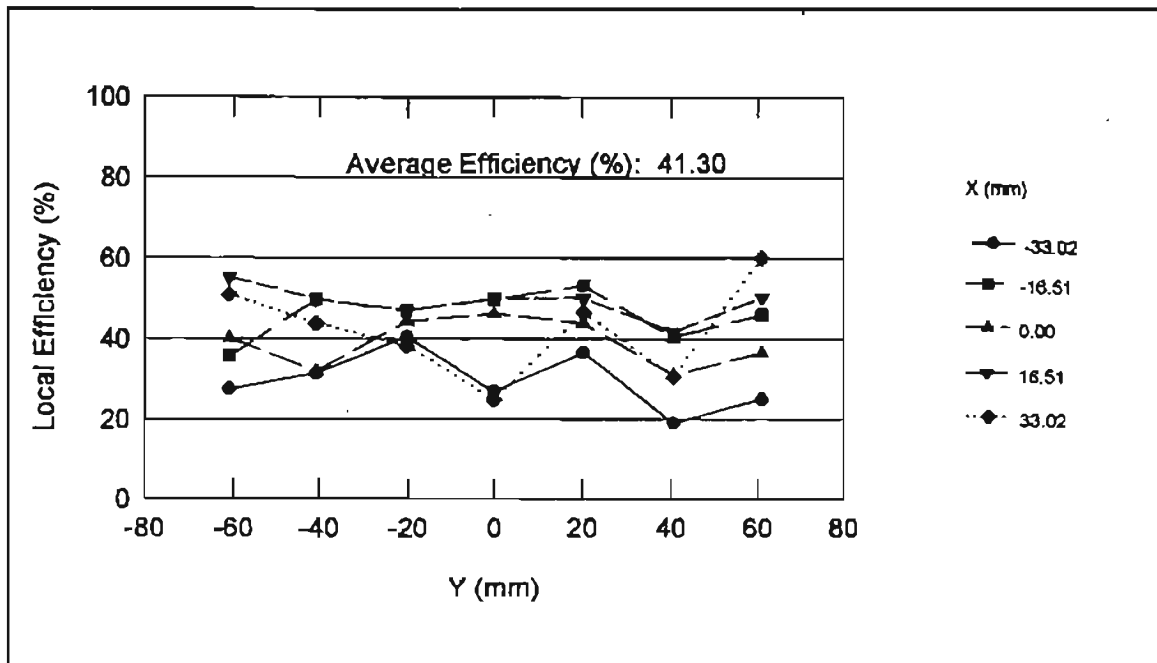


Figure 5.10: Pleated Filter Efficiency for Test SAH50_05_1 at 77.07 m³/hr

The trend in the efficiencies shows that the bandwidth for the local efficiency plot is quite narrow for high flow rates while for low flow rates, the measured local efficiencies are not in a very narrow band [compare Figs. 5.5 and 5.10 and Appendixes B & C].

Figure 5.11 shows the variation in the overall filtration efficiency with Stokes number and Fig. 5.12 shows the variation in the filtration efficiency with the flow rate. The Stokes number is a function of the particle diameter and velocity as given by Eq. (2.9), and the overall efficiency is given by Eq. (2.12). In this study, both the particle size and the velocity were changed. The Stokes number has been calculated using the average particle velocity [Jadbabaei, 1997] from the LDV measurements. The Stokes number for a particle diameter of 2.04 μm is larger than that of a 0.966 μm particle by a factor of about 4 for the same flow rate, since the Stokes number is proportional to the square of the diameter.

Theoretical studies (as given in Fig. 2.8) have shown that the curve for efficiency versus Stokes number shows dip at lower values and a plateau at high Stokes number. The efficiencies for 0.497 μm particles increase very fast after 104.26 m^3/hr ($St = 0.04466$). This trend is not expected [Fig. 5.13]. However small particles clog the filter very quickly and at high flow rates, the efficiencies increase. More particles are being deposited on the filter, which causes a faster clogging of the filter. This is also been demonstrated by the increase in the pressure drop by 9.75 mm of water [Table 5.2]. Some of the possible reasons for this abnormality are discussed in the next chapter. The variation in the measured filtration efficiencies for 2.04 μm particles are consistent with the theoretical predictions for flow rates between 29.48 m^3/hr and 188.45 m^3/hr [Fig. 5.13]. However, for lower flow rates (lower than 16.78 m^3/s), the efficiency increases significantly. This may be due to the fact that, at low flow rates, the filtration process due to diffusion can become important and this possibility needs to be considered and further investigated.

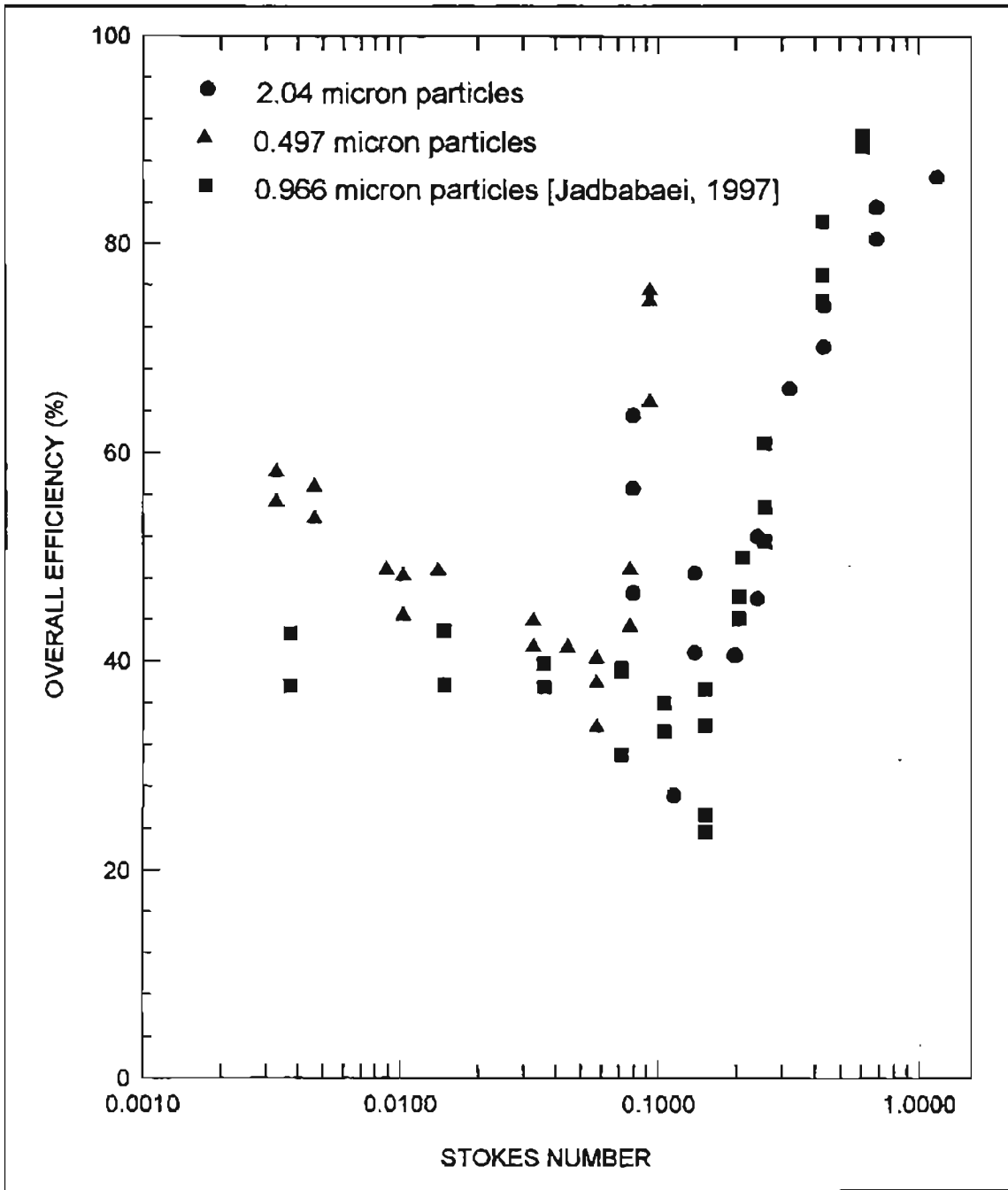


Figure 5.11: Variation of Filtration Efficiency with Stokes Number

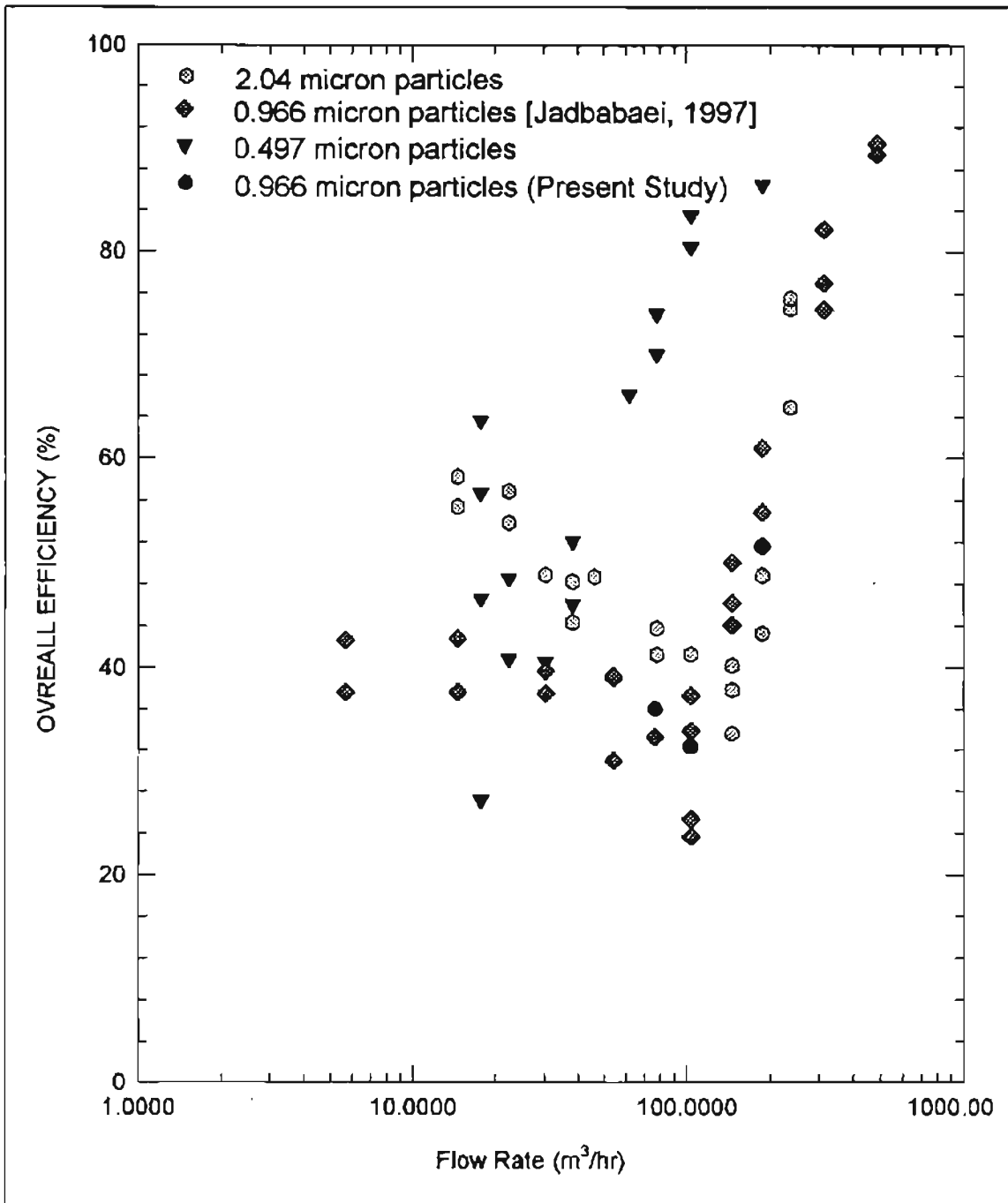
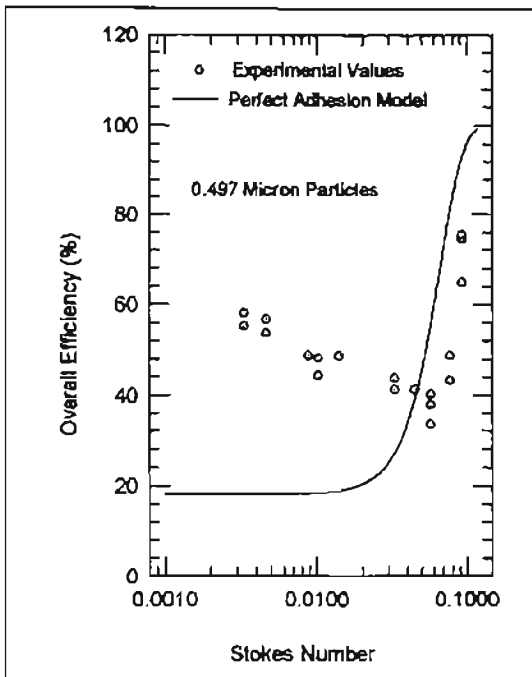
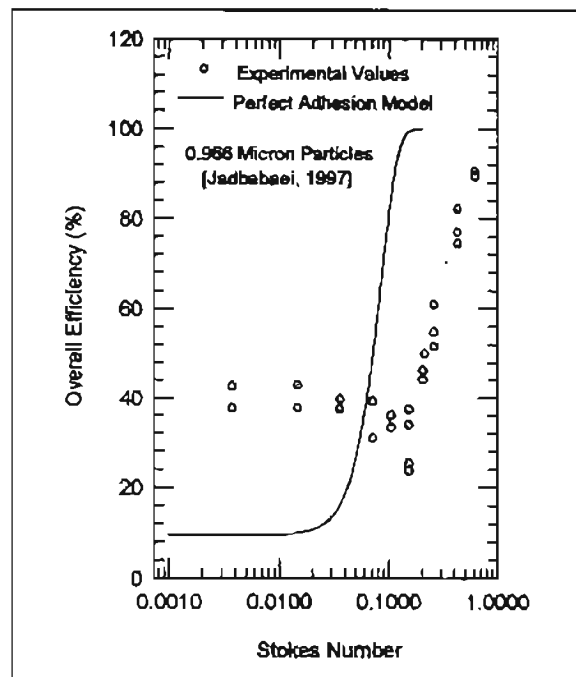


Figure 5.12: Variation of Filtration Efficiency with Flow Rate

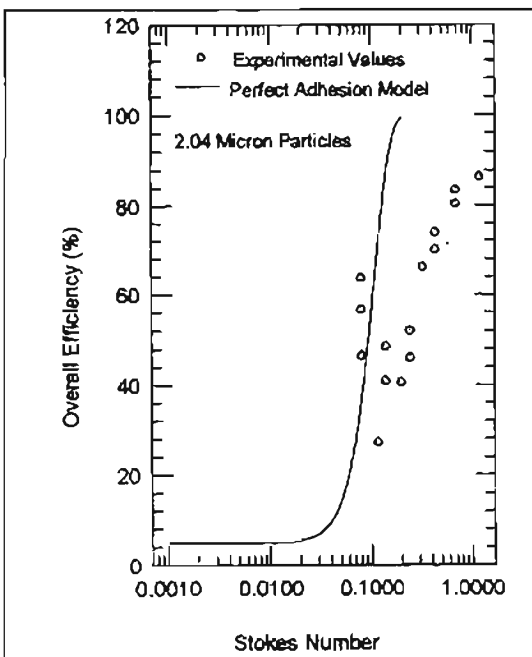
Filtration efficiencies for different particle sizes have been plotted individually against Stokes number in Fig. 5.13.



(a)



(b)



(c)

Figure 5.13: Comparison of Experimental Results of Present Study with Theoretical Model Based on Perfect Adhesion Theory (Duran, 1995) for Interception Parameter = 0.01, Fiber Diameter $D_f = 38 \mu\text{m}$, Packing Density = 0.23

Table 5.3 compares the results of the experiments carried out on the Small Angle Diffuser Housing using 0.966 μm particles with those of Jadbabaei [1997]. This comparison was required because of the modifications the system had undergone, and that the increase in the laser power might have affected the measured efficiencies. Only three tests were conducted, since the results from Jadbabaei were found to be in agreement within about 8% of the measured efficiencies with the results obtained in the present study. The local efficiency measurements (for the present study and Jadbabaei, 1997) for the flow rate of 103.69 m^3/hr have been plotted in Fig. 5.14 and those for 188.45 m^3/hr in Figs. 5.15 - 5.16. Other plots for these experiments are shown in Appendix G.

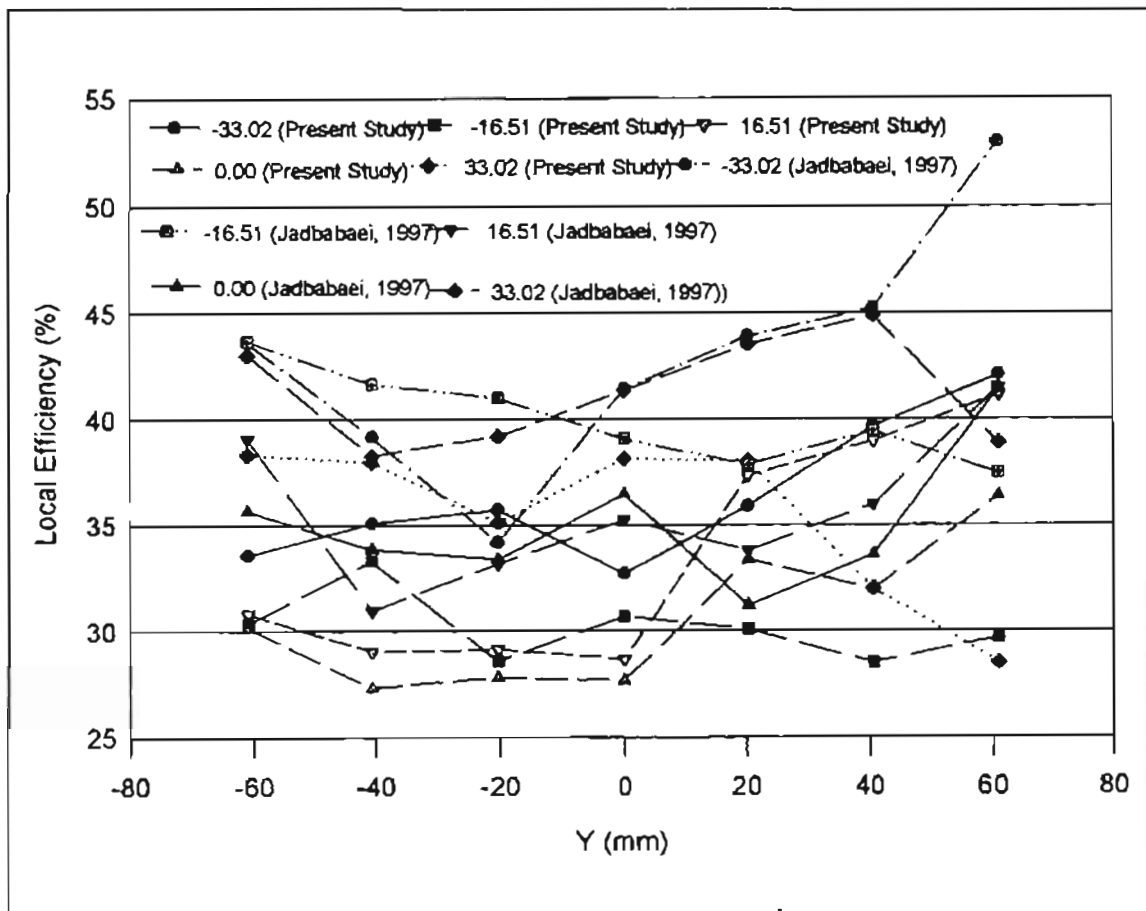


Figure 5.14: Comparison of Local Filtration Efficiency Measurements in Small Angle Diffuser Housing at 103.69 m^3/hr with Jadbabaei [1997]

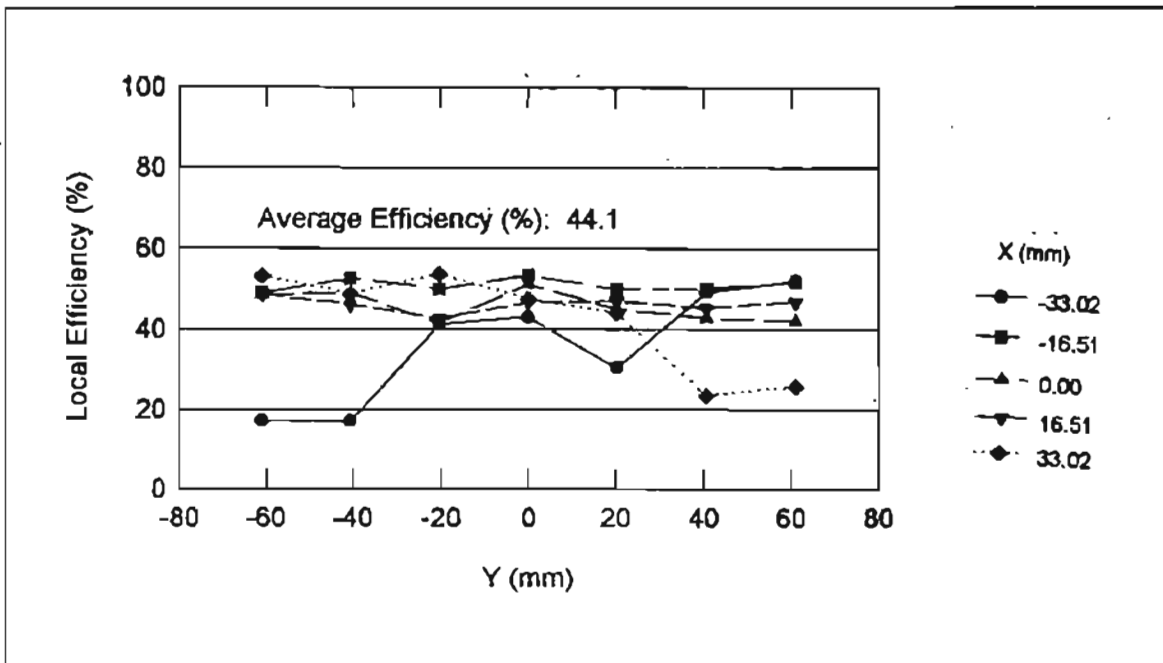


Figure 5.15: Local Filtration Efficiency Measurements in Small Angle Diffuser Housing at a Flow Rate of 188.45 m³/hr [Jadbabaei, 1997]

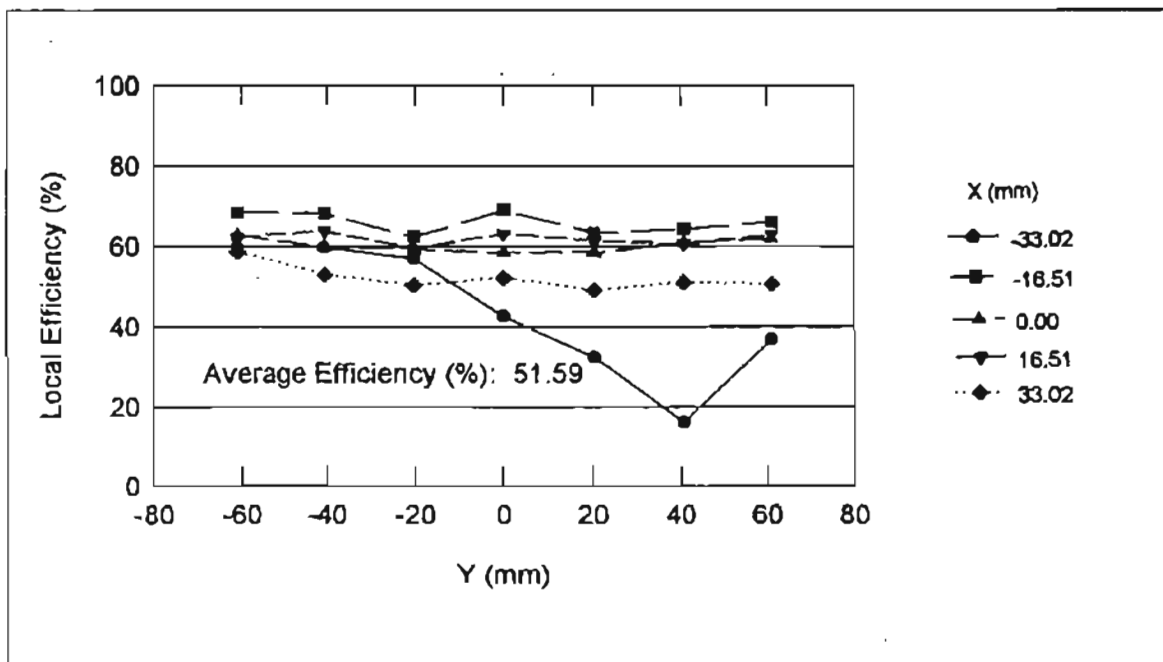


Figure 5.16: Local Filtration Efficiency Measurements in Small Angle Diffuser Housing at a Flow Rate of 188.45 m³/hr [Present Study]

Table 5.3: Summary of Small Angle Diffuser Housing Results for 0.966 μm Diameter Particles for Comparison with Those of Jadbabaei [1997]

Test Number	Test Date	Flow Rate (m ³ /hr) [TSI]	Samples Taken	Time Taken for Data Collection (seconds)	Pressure Drop Initial (Final) (mm of water)	Upstream Average Particle Velocity TSI [LDV] (m/s)	Stokes Number Based on LDV Velocity	Average Efficiency (Jadbabaei [1997])	Average Efficiency (Present Study)
F9	06/19/96	77.07	1000	25	N/A	1.09 (1.38)	0.0792	33.26	
SAH50_1_1	10/05/97	77.07	1000	30	58.7 (61.0)	1.09 (1.64)	0.1049		36.01
F19	07/05/96	103.69	1000	35	N/A	1.64 (2.39)	0.1526	37.34	
SAH75_1_1	10/31/97	103.69	1000	35	58.7 (61.0)	1.64 (2.97)	0.1533		32.3
F1	05/08/96	188.45	1000	40	58.2 (61.0)	2.73 (3.30)	0.1995	44.1	
SAH125_1_1	11/08/97	188.45	1000	40	60.8 (63.2)	2.73 (3.98)	0.2589		51.59

5.3 SAE Housing Measurements

Efficiency measurements were carried out on the SAE J726 Housing [Fig. 3.13]. Table 5.4 shows the flow rates and the efficiencies measured. The plots for SAE200_1_2 are presented in Figs. 5.17 – 5.21, and the remaining plots are presented in Appendix D.

Typical upstream and downstream number density profiles for the SAE housing have been shown in Figs. 5.17 and 5.18, respectively. The upstream and downstream velocity profiles for the SAE housing shown in Figs. 5.19 and 5.20 portray a irregular flow pattern over the filter surface in this housing [Fig. 5.19]. Near the center of the filter, the velocity is the highest, and the number density is the lowest in the respective rows across the filter. As seen in Figure 5.19, the velocity near the edges above the filter is very high and causes recirculation zones near the walls of the filter [Natarajan, 1995]. The effect of the velocity on the number density at a point has a corresponding effect on the local filtration efficiency value. A typical local filtration efficiency profile for the SAE J726 housing is shown in Fig. 5.21. Though the number density profile is affected by the velocity profile over the filter surface, it is seen from Fig. 5.21 that the local efficiency profile is unlike the trend apparent in Figs. 5.17 and 5.19. This shows that the flow over the filter surface is location dependent, even though the overall efficiency of the filter is not substantially affected. There is a large unexplained difference in the velocities at the flow rate of 314.73 m³/hr. It is possible that this is due to the presence of recirculation zones at that flow rate which affected the local velocities for some runs at that flow rate and not for others at that flow rate.

Table 5.4: Summary of SAE Housing Results for 0.966 μm Diameter Particles

Test Number	Test Date	Flow Rate TSI (m ³ /hr)	Upstream Average Particle Velocity TSI* [LDV] (m/s)	Samples Taken	Time Taken for Data Collection (seconds)	Average Upstream Actual Number Density (#/m ³)	Average Efficiency (%)	Stokes Number Based on LDV Velocity	Initial Pressure Drop (mm of water)	Final Pressure Drop (mm of water)
SAE10_1_1	04/08/98	13.61	0.0388 [0.399]	1000	20	7.59×10^9	49.9	0.0293	2.54	2.54
SAE10_1_2	04/09/98	13.61	[0.471]	1000	20	5.29×10^9	41.95	0.0345	2.54	2.54
SAE25_1_1	04/08/98	37.42	0.107 [1.39]	1000	25	1.50×10^9	44.61	0.1020	2.54	2.54
SAE25_1_2	04/09/98	37.42	[1.45]	1000	25	1.46×10^9	38.73	0.1064	2.54	2.54
SAE40_1_1	09/03/96	61.20	0.174 [1.67]	1000	30	6.82×10^8	32.4	0.1225	2.54	3.81
SAE40_1_2	11/08/96	61.20	[1.63]	1000	25	2.11×10^9	45.22	0.1130	2.54	3.81
SAE120_1_1	11/09/96	180.03	0.342 [4.20]	500	30	4.97×10^8	62.91	0.3081	38.10	45.72
SAE125_1_1	09/25/96	188.45	0.356 [4.51]	1000	30	3.99×10^8	46.17	0.3308	38.10	48.26
SAE125_1_2	04/08/98	188.45	[7.14]	500	30	3.73×10^8	75.55	0.5237	43.18	48.26
SAE200_1_1	09/24/96	314.73	0.570 [5.25]	1000	30	3.23×10^8	78.35	0.3851	68.58	75.8
SAE200_1_2	11/26/96	314.73	[6.48]	1000	30	3.91×10^8	86.32	0.4753	76.20	80.2
SAE200_1_3	04/08/98	314.73	[10.10]	1000	30	3.2×10^8	88.68	0.7408	68.58	73.66

*TSI velocity values are not repeated for test cases with the same flow rate.

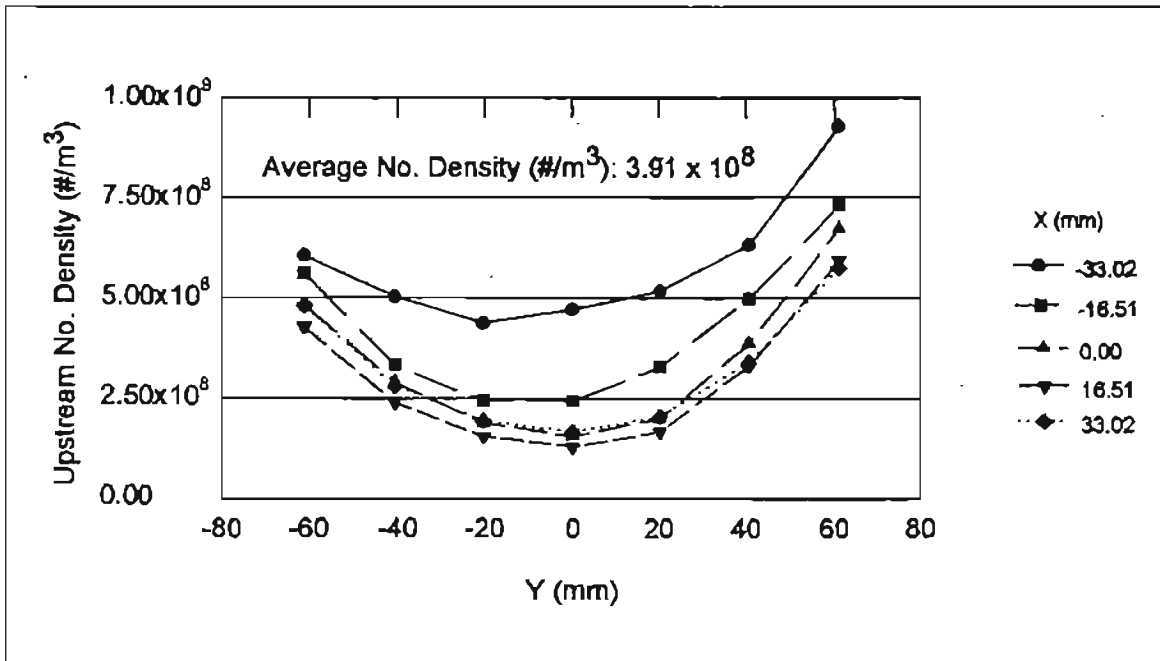


Figure 5.17: Upstream Number Density for Test SAE 200_1_2 at $314.73 \text{ m}^3/\text{hr}$

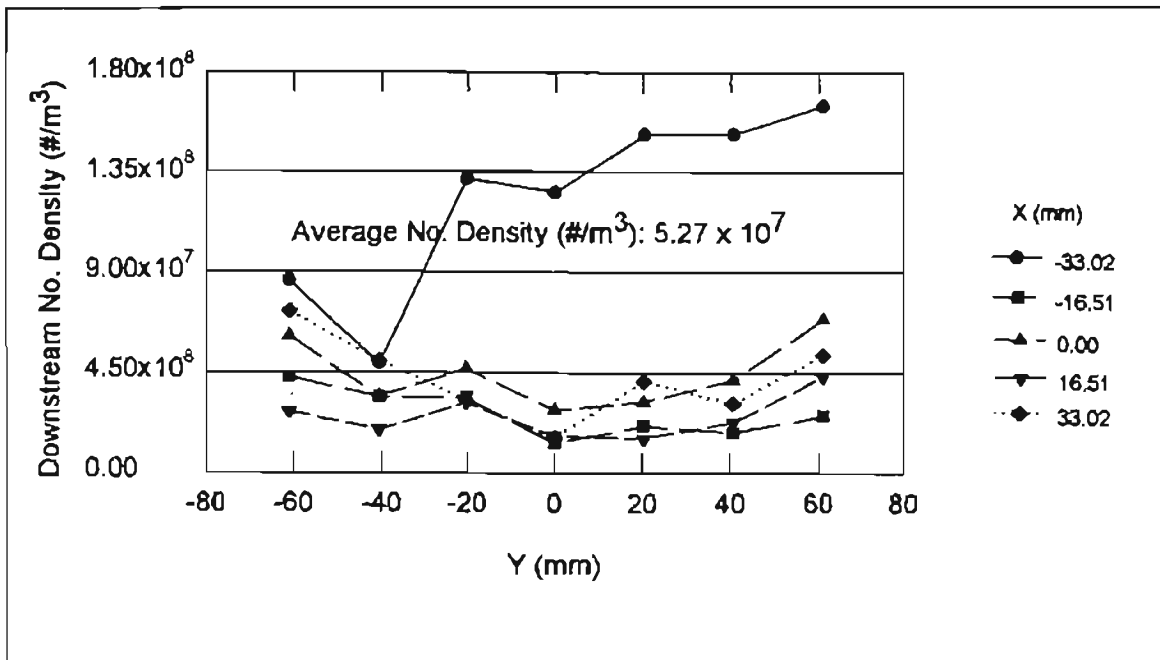


Figure 5.18: Downstream Number Density for Test SAE 200_1_2 at $314.73 \text{ m}^3/\text{hr}$

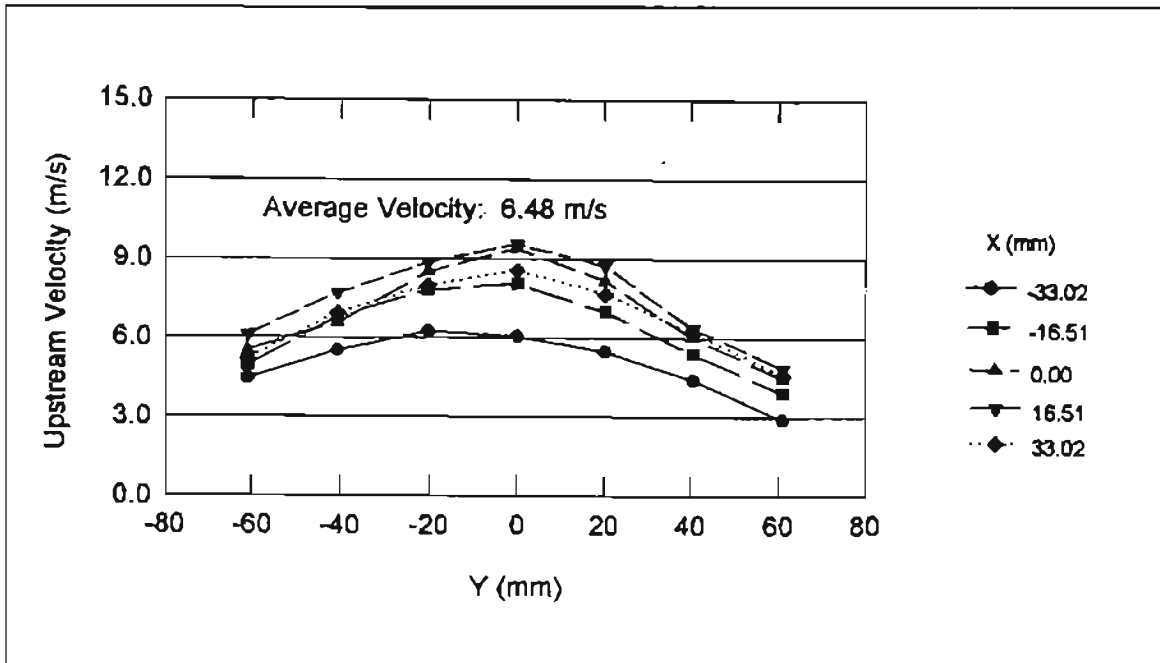


Figure 5.19: Upstream Velocity Profile for Test SAE 200_1_2 at 314.73 m³/hr

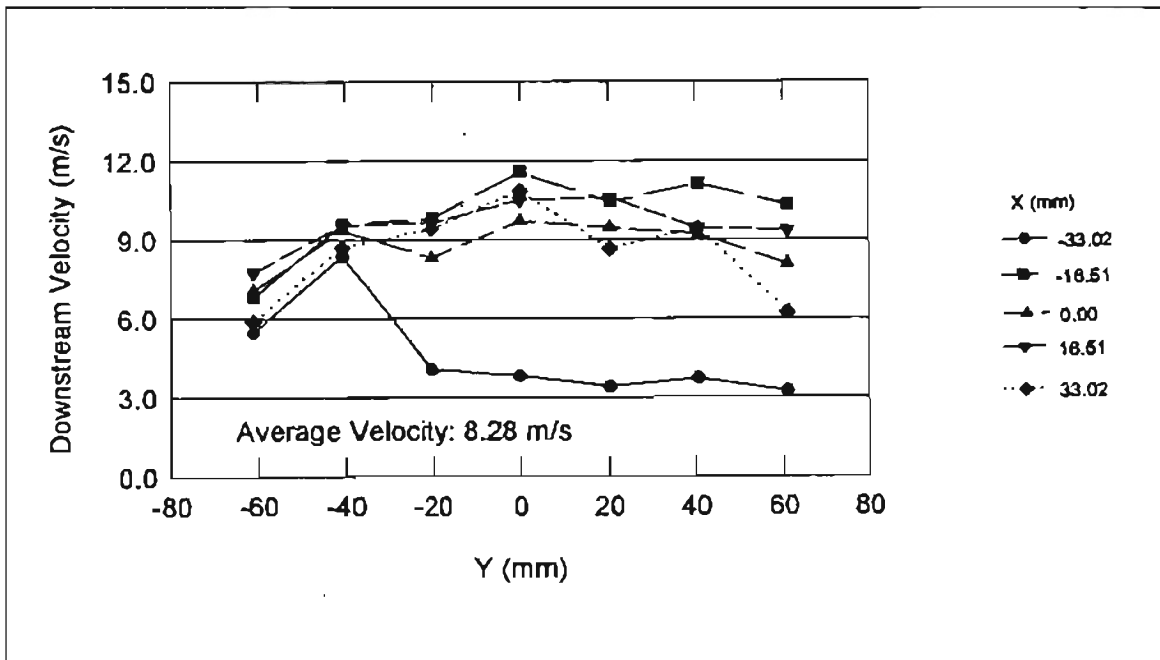


Figure 5.20: Downstream Velocity Profile for Test SAE 200_1_2 at 314.73 m³/hr

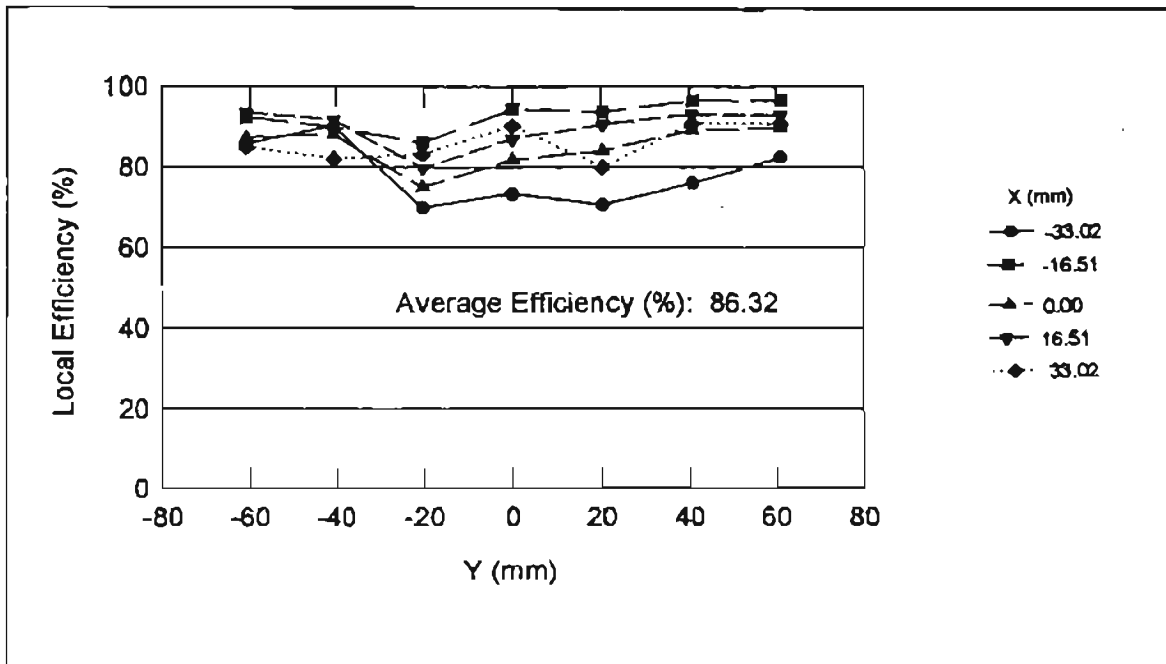


Figure 5.21: Pleated Filter Efficiency for Test SAE 200_1_2 at 314.73 m³/hr

The results in the present study are plotted against the Stokes number in Fig. 5.22 and results from Natarajan [1995] are given in Fig. 5.23. The present results show a trend similar to the expected “S” type curve. However the results of Natarajan do not exhibit similar trend. Though the efficiencies increase with an increase with the flow rate, Natarajan did not show a substantial increase in the efficiencies at higher flow rates. Natarajan [1995] mentions that the filter was not changed for any of the experiments. Contrary to that, as part of this study, a new filter was used for every experiment. This was done to guarantee that the filtration process was not affected by the increase in pressure drop across the filter. Further, the difference in the results may be explained due to the inconsistent laser power, which may have affected the data collection and hence the measured efficiencies.

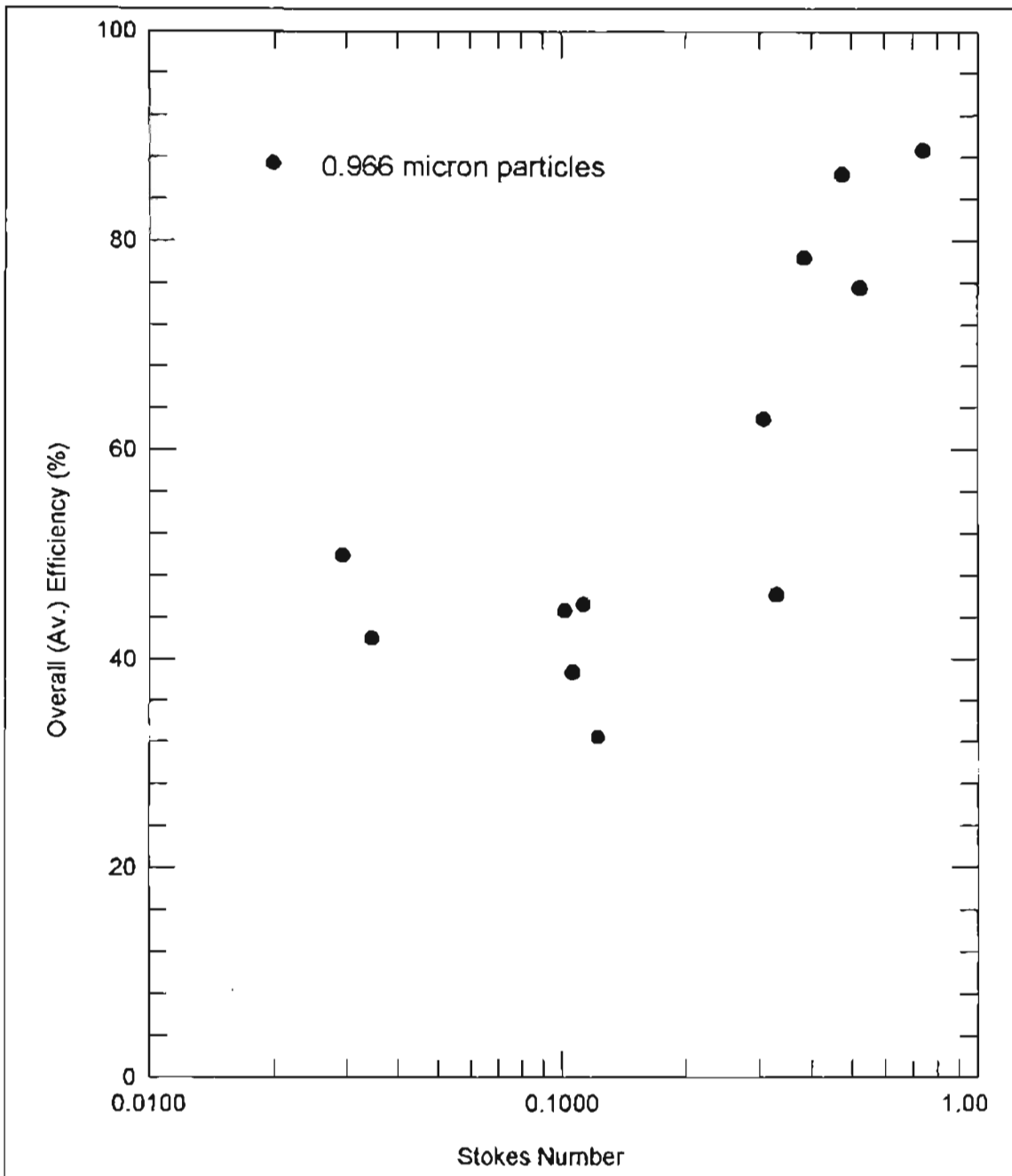


Figure 5.22: Variation of Filtration Efficiency with Stokes Number for SAE J726 Housing

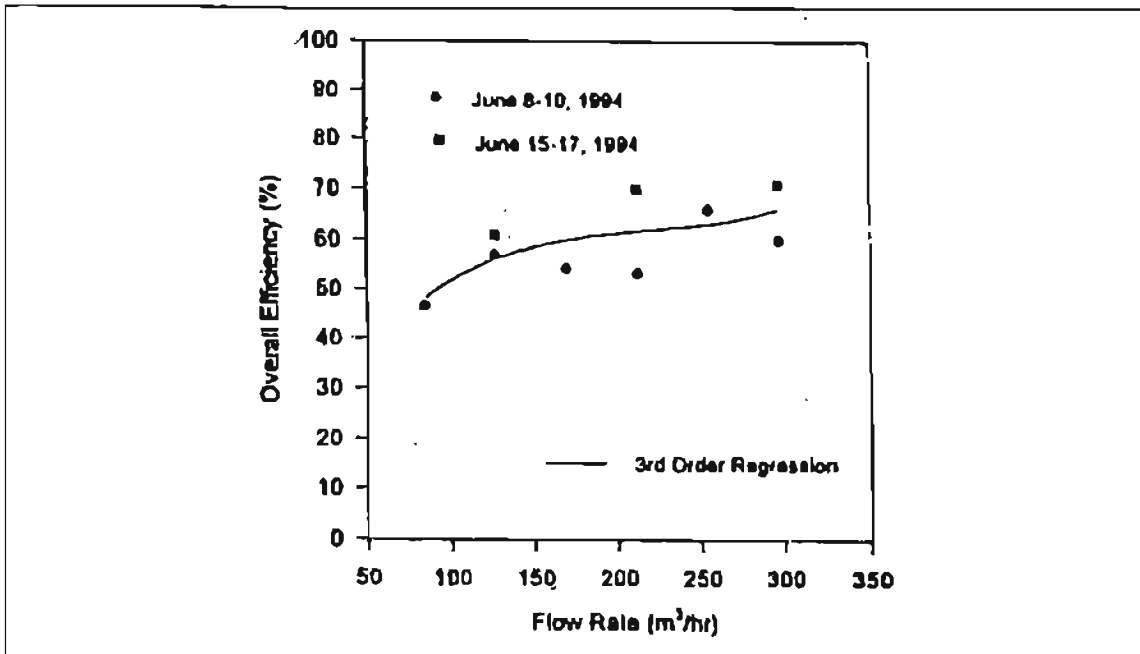


Figure 5.23: Overall Efficiency vs. Flow Rate for the SAE Housing (0.966 μm Particles) [Natarajan, 1995]

5.4 Simulated Automotive Filter Housing Measurements

Co-researchers on this project [Al-Sarkhi et al., 1997] have designed this housing [Fig. 3.14]. This housing is used for studying the flow patterns over the filter with a test housing which is a close representation of an actual filter housing in an automobile. It provides an opportunity to test the theoretical predictions in the actual test setup. It is seen in Fig. 5.24 that the number densities measured in this housing tend to exhibit a slight increase in the local number densities in the direction away from the entrance ($Y = 60 \text{ mm}$) of the housing. The number density profile downstream [Fig. 5.25] of the filter is fairly regular since the lower half of the Small Angle Diffuser housing is used as the bottom half of this test setup.

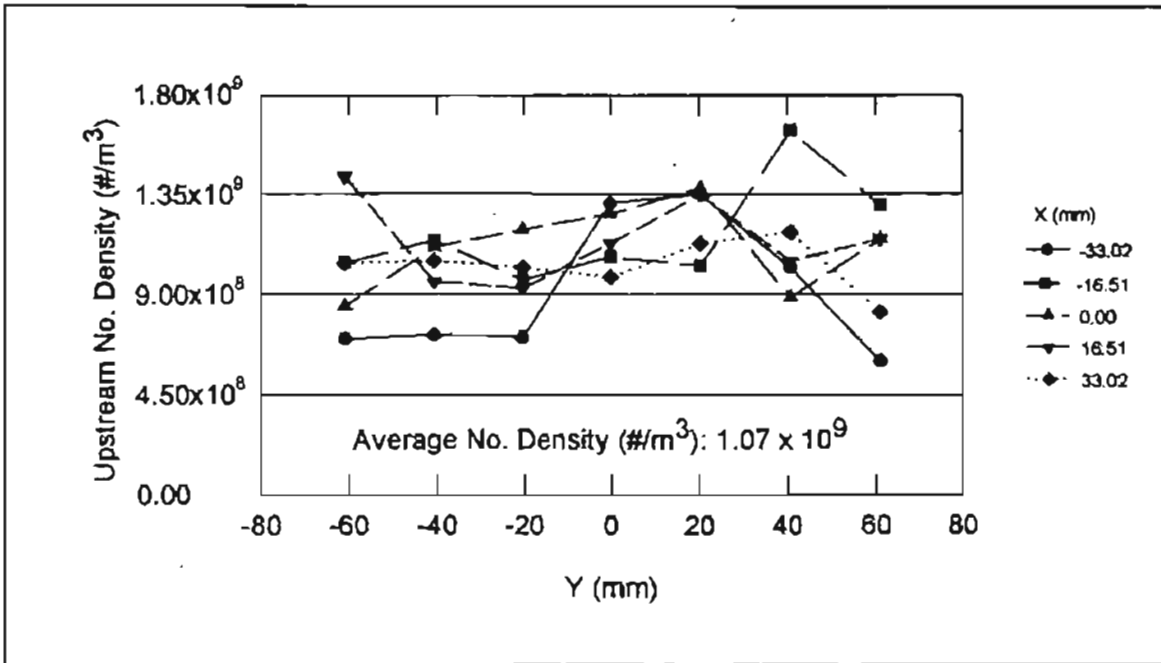


Figure 5.24: Upstream Number Density for Test SAF15_1_1 at 21.55 m³/hr

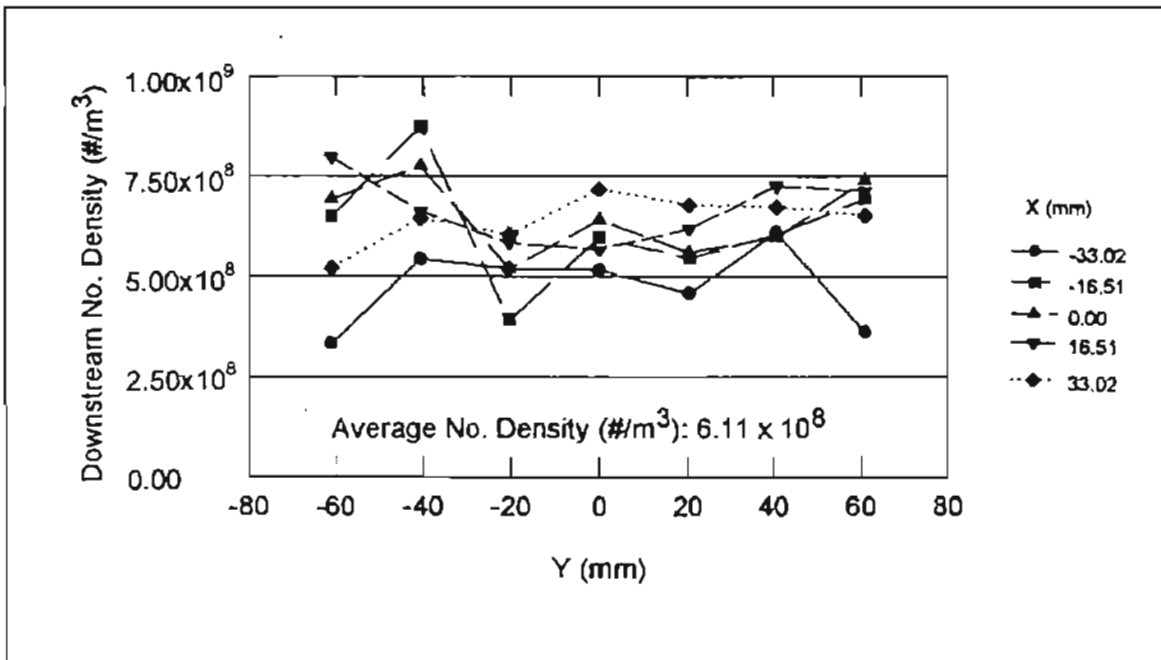


Figure 5.25: Downstream Number Density for Test SAF15_1_1 at 21.55 m³/hr

The entrance above the filter ($Y = -95$ mm) is horizontal, and therefore the transverse component of the velocity is larger than the axial component. Figure 5.26

shows the upstream velocity profile across the filter surface. At the point where the flow enters the housing, the velocity is higher than that at the opposite end of the housing. Equation (H-1) shows the dependence of the local number density on the local velocity. In the case of the SAF housing, the local velocity decreases substantially across the surface of the filter; but there is not a very large change in the number densities across the filter (unlike the change in the SAE housing as seen in Figs. 5.17 and 5.19). It is possible that the higher transverse component of the velocity in the SAF housing is causing this different number density variation across the filter surface. The downstream velocity profile [Fig. 5.27] is fairly regular. The local filtration efficiency profile is shown in Fig. 5.28. The plots for different flow rates in this housing are shown in Appendix E.

As was shown in Figs. 5.11 and 5.22, the overall filtration efficiency for the Small Angle Diffuser housing and the SAE J726 housing displays a typical "S" shaped curve. However in the case of the Simulated Automotive Filter housing, the overall efficiency for different flow rates does not appear to follow the expected trend (Figs. 5.29 and 5.30). The overall efficiency continues to be in a range of 20 - 60% over different flow rates without exhibiting a definite trend (some additional tests need to be conducted around 140 m³/hr in order to be certain about this conclusion). As already mentioned, in the Simulated Automotive Filter housing, the flow enters with a much larger transverse velocity component than the axial component. It is possible that this typical flow pattern is affecting the filtration process and hence causes an atypical variation in the filtration efficiencies with an increase in flow rates. The velocities plotted in Figs. 5.26 and 5.27 are the resultant of both the axial and the transverse components of the velocity as measured by the LDV system with its two channels.

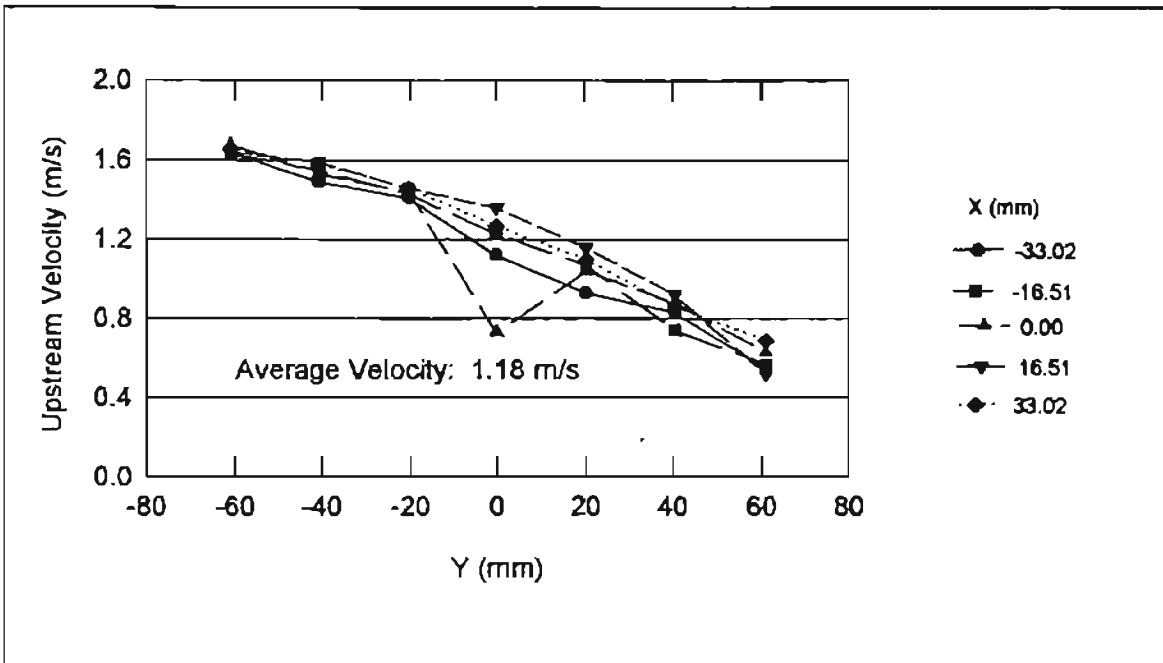


Figure 5.26: Upstream Velocity Profile for Test SAF15_1_1 at 21.55 m³/hr

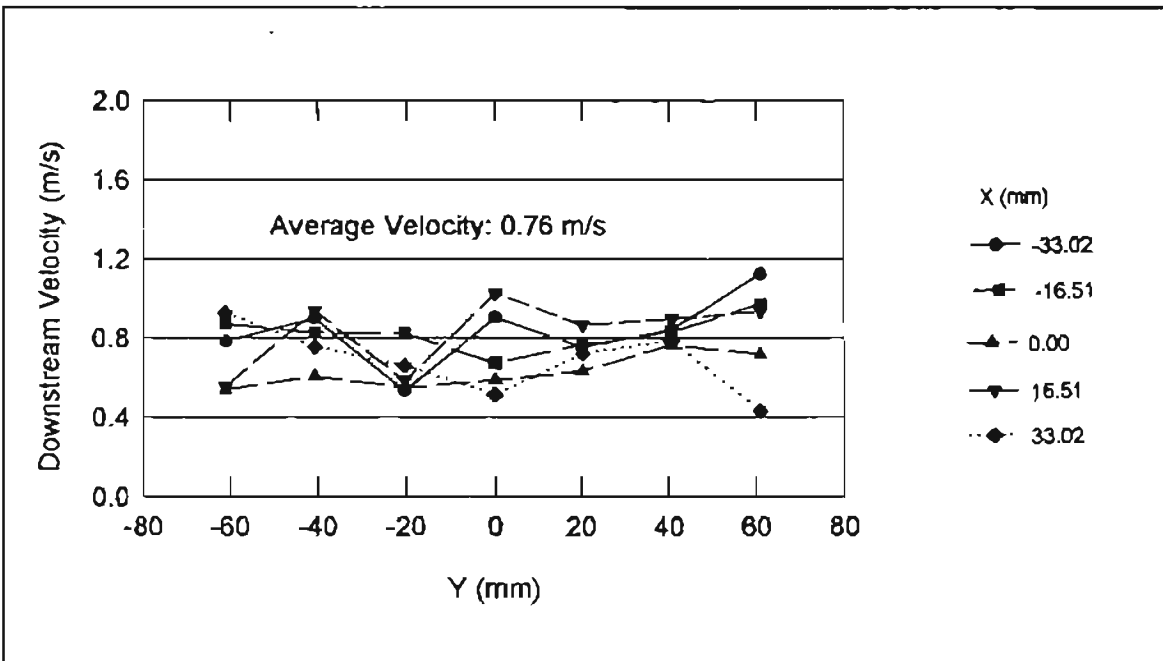


Figure 5.27: Downstream Velocity Profile for Test SAF15_1_1 at 21.55 m³/hr

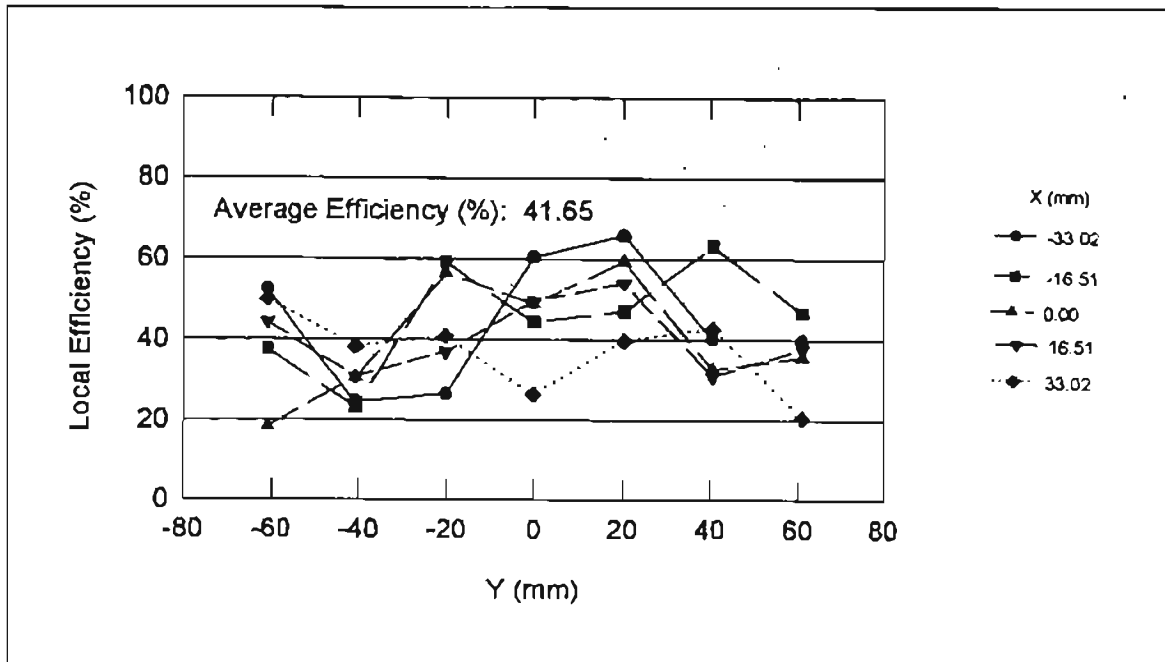


Figure 5.28: Pleated Filter Efficiency for Test SAF15_1_1 at 21.55 m³/hr

The overall filtration measurements at different flow rates have been tabulated in Table 5.5. At all of the local measurement points, the resultant of the axial and transverse component of the velocity (as measured by the LDV system) was used. The average of this resultant velocity at all the 35 points was computed and then substituted into Eq. 2.9 for calculating the Stokes number. By this approach, it was ensured that both of the velocity components were accounted for. Another approach in calculating the Stokes number could have been the use of only the axial component of the velocity for calculating the Stokes number, thereby neglecting the transverse component of the velocity. The author however used the former method of calculating the average particle velocity for all three housings at different flow rates.

The TSI "Upstream Average Particle Velocity" in Table 5.5 was computed by dividing the flow rate by the cross sectional area of the filter exposed to the flow, but the

LDV “Upstream Average Particle Velocity” was computed using the resultant velocity (both the axial and transverse velocity) from the LDV. Above a flow rate of 146.36 m³/s, the flow above the filter is very turbulent, and the velocities are very high in the transverse direction. Collection of data is very difficult for these flow rates and above, since the particle rebound off the walls and the data collection may not be accurate because of the possible double counting of the particles. Because of the large transverse component of the velocity, the particles may not follow an exact vertical path of movement. Instead, the particles after rebounding from the wall, may move to different positions above and below the filter, causing a possible double counting of the particles, thereby affecting the number density measurements and hence the filtration efficiency values.

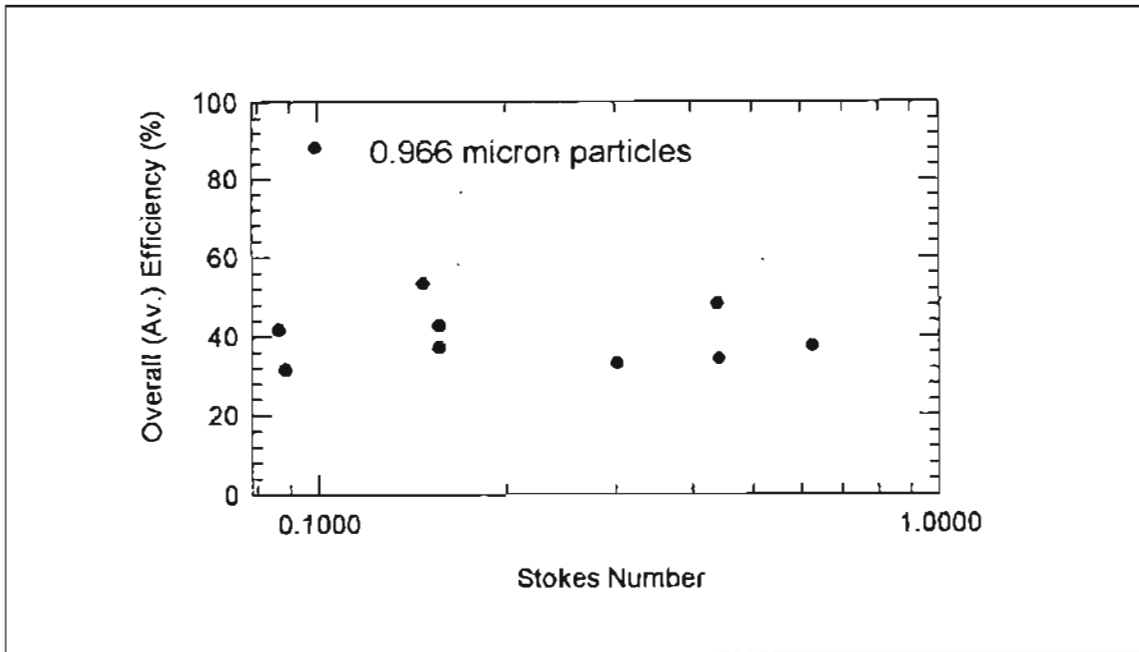


Figure 5.29: Variation of Filtration Efficiency with Stokes Number for Simulated Automotive Filter (SAF) Housing

Table 5.5: Summary of Simulated Automotive Filter Housing Results for 0.966 μm Particles

Test Number	Test Date	Flow Rate TSI (m^3/hr)	Upstream Average Particle Velocity TSI [LDV] (m/s)	Upstream Average Axial Particle Velocity (m/s)	Samples Taken	Time Taken (seconds)	Expected (Actual) Number Density ($\#/\text{m}^3$)	Average Overall Efficiency (%)	Stokes Number Based on Resultant Velocity [Axial]
SAF15_1_1	11/13/97	21.55	0.320 [1.18]	0.358	500	20	1.39 (1.07) $\times 10^9$	41.65	0.0865 [0.0264]
SAF15_1_2	11/22/97	21.55	0.320 [1.21]	0.389	500	20	1.39 (1.37) $\times 10^9$	31.61	0.0887 [0.0286]
SAF20_1_1	11/20/97	29.48	0.436 [2.01]	0.681	500	25	8.91 (7.46) $\times 10^8$	53.31	0.1474 [0.0499]
SAF25_1_1	11/13/97	37.42	0.545 [2.23]	0.677	500	25	6.24 (4.71) $\times 10^8$	42.71	0.1636 [0.0497]
SAF25_1_2	11/21/97	37.42	0.545 [2.13]	0.730	500	25	8.47 (7.79) $\times 10^8$	37.23	0.1562 [0.535]
SAF45_1_1	11/14/97	70.07	0.925 [4.12]	1.255	500	25	1.66 (9.25) $\times 10^9$	33.19	0.3015 [0.0921]
SAF60_1_1	11/14/97	79.00	1.37 [6.03]	1.97	500	30	4.62 (3.67) $\times 10^8$	48.49	0.4423 [0.1445]
SAF60_1_2	11/15/97	79.00	1.37 [6.00]	1.80	500	30	3.25 (2.54) $\times 10^8$	34.47	0.4405 [0.1320]
SAF100_1_1	11/21/97	146.36	2.18 [8.54]	3.32	500	30	2.14 (1.84) $\times 10^8$	37.55	0.6264 [0.2435]

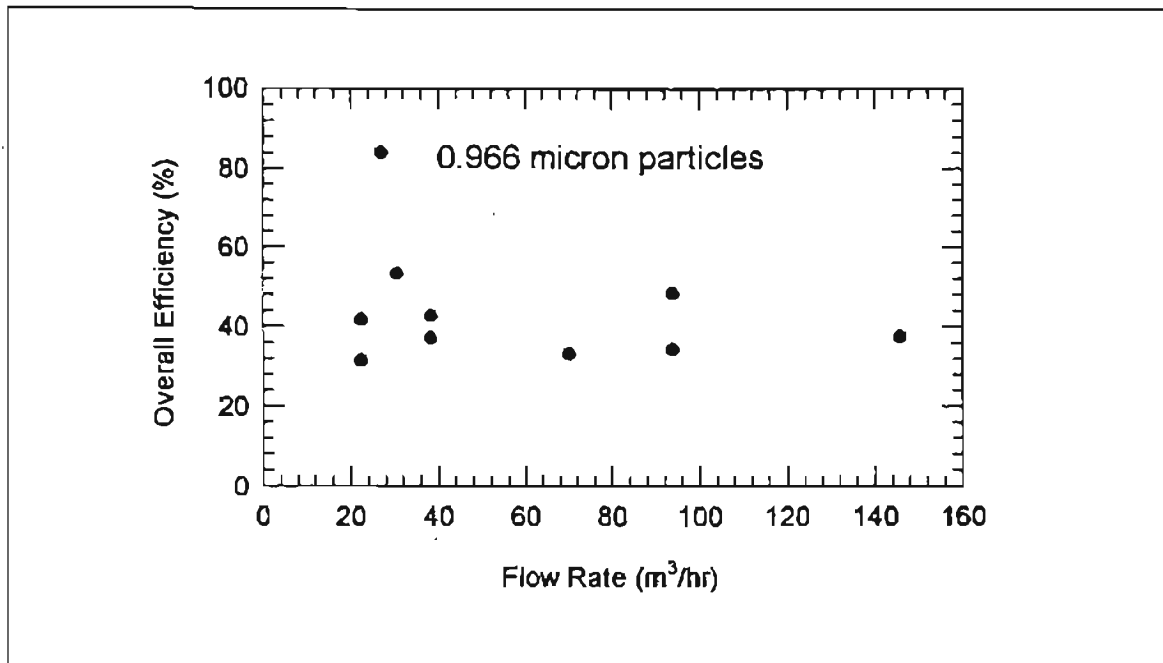


Figure 5.30: Variation of Filtration Efficiency with Flow Rate for SAF Housing

5.5 Glass Beads

The PSL particles, which were used as the test contaminant, are expensive. For a particle size of 2.04 μm and above and at high flow rates (314.73 m^3/hr), more of these particles are needed for getting good signals. The author carried out a few experiments to explore the possibility of using glass beads instead of the PSL particles for the experiments. These glass beads have a specific gravity of 2.5 (other characteristics in App. J) and therefore tend to settle quickly with time. Efforts were therefore made to ensure that the particles remained suspended in solution and a steady number density was maintained during the course of the experiments. The preliminary results were promising since reasonable number densities and good quality signals were obtained by using only about 3 - 7 grams of the glass beads in 1000 ml. of water (which makes it very cost effective). These results have been tabulated and plotted in Appendix F.

Chapter 6

SUMMARY AND RECOMMENDATIONS

6.1 Summary

The results and the conclusions that can be drawn from the experiments are summarized below.

1. The upstream velocity profile for the Small Angle Diffuser Housing above the filter is reasonably regular. A regular velocity profile results in consistent number densities above the filter. However at low flow rates ($13.61 \text{ m}^3/\text{hr}$) the bandwidth, over which the number densities are distributed, is not very narrow, but this bandwidth becomes fairly tight at intermediate ($77.07 \text{ m}^3/\text{hr}$) and at higher flow rates ($146.36 \text{ m}^3/\text{hr}$).
2. Small variation in the velocities (say 0.05 m/s) at low flow rates ($13.61 \text{ m}^3/\text{hr}$) can cause as much as a 25% variation in the number densities, thereby affecting the measured efficiencies. As a result, the number densities and the measured filtration efficiency profile at low flow rates are spread over a larger bandwidth than those at higher flow rates. This accounts for the relatively large bandwidth of number densities above the filter as mentioned in point #1 above.

3. The variation in the measured filtration efficiencies for 2.04 μm particles are consistent with the theoretical predictions for flow rates between 29.48 m^3/hr and 188.45 m^3/hr . However, for lower flow rates (lower than 16.78 m^3/s), the efficiency increases significantly. At lower flow rates, the phenomenon of diffusion may become important. At these flow rates, the anomaly in the results may be attributable to this additional mechanism of filtration, leading to an increase in the measured efficiency.
4. The filter appears to get clogged faster by small particles. The filtration efficiency increases with flow rate. At higher flow rates, more particles get deposited on the filter and a stronger cake of (0.497 μm particles) is formed on the filter, thereby may be clogging it and thus registering a sharp increase in the measured efficiency.
5. The measured efficiencies in the Small Angle Diffuser housing and the standard J726 housing vary according to the typical "S" shaped theoretical curve with an increase in flow rate. The efficiencies measured in the Simulated Automotive Filter housing do not appear to vary considerably at different flow rates. The overall efficiency continues to be in a range of 20 - 60% over different flow rates without exhibiting a definite trend. It is possible that since in the Simulated Automotive Filter housing, the flow enters with a much larger transverse velocity component than the axial component the flow pattern is affecting the filtration process and hence the atypical variation in the filtration efficiencies with increase in flow rates. However as mentioned earlier, some more experiments need to be conducted at and around the flow rate of 140 m^3/hr in order to be convinced of this conclusion (drawn on the basis of the present study).

6. Results show that the Small Angle Diffuser housing provided a regular flow across the filter surface and hence a regular velocity profile above the filter. This regular flow profile translated into a fairly narrow bandwidth of local filtration efficiency variation across the filter surface. In the case of the standard SAE J726 housing, the velocity profile was dependent on the location across the filter surface. As is seen from Eq. (H-1), the measured local number density is dependent upon the velocity at that point. At the points where the velocity is higher, there should be a corresponding decrease in the measured number density. This variation in the number densities consequently affects the measured local filtration efficiency. In the case of the simulated automotive filter housing, the flow entered the housing in a horizontal direction. Therefore, the velocity near the entrance to the housing was higher than the velocity at the end of the housing. The upstream number densities near the entrance of the filter appear to be lower than the number densities at points away from the entrance to the housing. However the variation in the number densities across the filter surface does not appear to be as pronounced as it is in the case of the SAE J726 housing. It is possible that difference in the number density profiles across the filter for the two housings was due to the vertical entrance of the flow in the SAE J726 housing (higher axial component of the velocity) and horizontal entrance of the flow in the SAF housing (higher transverse component of the velocity). This variation in the upstream number densities had a corresponding effect on the local filtration efficiencies across the filter.

6.2 Recommendations for Future Work

For the first time on this project, the efficiencies for different particle sizes were measured. The results have indicated further studies are needed in certain areas and these have been outlined below.

1. In the SAH housing the sudden increase in the measured efficiency for $0.497\ \mu\text{m}$ particles at high flow rates has not been explained properly. Since the small particles tend to clog the filter faster, it is possible that the increase in the efficiency is attributable to increased pressure drop across the filter. However in the absence of pressure measuring equipment with a least count small enough to display changes in the pressure less than 3 mm of water, it is not possible to authoritatively state the reason for this sudden jump in the measured efficiency. It is imperative therefore; that the pressure measuring setup be more sensitive so that the relationships of the efficiencies to the pressure drop across the filter can be studied further. At lower flow rates when the pressure across the filter is very small (less than 3 mm of water), any change in the pressure is not discernable because of the higher least count of the present manometer.
2. As part of the consistency measurements, it was shown that variation in the room temperature caused the laser power to vary during the course of the experiment. This variation of the laser power adversely affected the data collection. A system for providing more effective room temperature control (as close to $\pm 0.1\ ^\circ\text{C}$ as possible) should be installed.
3. In the SAH housing more experiments are required at lower flow rates (to about $5.68\ \text{m}^3/\text{hr}$) for $2.04\ \mu\text{m}$ particles and at higher flow rates (above $104.26\ \text{m}^3/\text{hr}$) for

0.497 μm particles to correctly identify the reasons for the unexpected deviation in the measured efficiencies. There was disparity between the expected and the actual results at and above these flow rates for these particles. It is possible that discrepancy was there due to the influence of increased pressure drop across the filter during the course of the experiment. However test runs at higher flow rates with 0.497 μm and smaller particles will enable a definite analysis of the reason for the deviation in the measured efficiencies.

4. From the literature review, it was found that the temperature and humidity of the fluid under study have an effect on the efficiency of the filter. A change in these two characteristics has an effect on the electrostatic charge associated with the filter fibers and the particles being used for the measurement. This affects the measured efficiencies of the filter. The effect of electrostatics on filtration needs to be studied further. Since, for larger particle diameter, the charge increases [Chapter 2], it will have an effect on the measurements. Though humidity and temperature variation for the fluid by itself do not affect the filtration efficiency substantially [Chapter 2], the effect of relative humidity and temperature on electrostatic charge needs to be studied. The usage of an electrostatic charge discharge system will help in measuring the efficiencies without the effect of electrostatics on the filtration process.
5. Dust measurements need to be conducted. The present apparatus of feeding dust to the system is not suitable since the dust cake in the dust feeder cracks when the dust feeder is in operation, resulting in an irregular feed rate to the system. In order to form a strong cake in this dust feeder, usage of a hydraulic or a pneumatic

- hammer is recommended for enabling the formation of a strong and compact dust cake, which does not crack when the scraper removes the dust from the dust cake.
6. More tests need to be carried out on the Small Angle Diffuser housing, standard SAE J726 housing and the Simulated Automotive Filter housing for different particle sizes (besides 0.497, 0.966 and 2.04 μm diameter particles) for verifying the results of this study and understanding the trends thoroughly. For different particle sizes, it should however be noted that the measured number densities are of the order of 10^8 at flow rates of 100-150 m^3/hr . If the number densities are lower, then longer time periods are needed for data collection; and longer test run time may not be suitable for running the experiment on a clean filter, since the filter may start getting partially clogged.
 7. PSL particles that are currently used as the contaminant during the experiments are very expensive (approximately \$700 per 100 ml of particles in solution). For larger particle sizes, a greater quantity of these particles (20 ml per 1000 ml of solution) is needed in order to obtain sufficient signals. An alternative, in the form of glass beads, is available from Powder Technologies Inc. (see Appendix J). These glass beads are quite inexpensive (available for approximately \$50 per 25 gm - an experiment requires about 3-5 gm per 1000 ml of solution), and are available in specific size ranges. The normalized size distribution for these glass beads is not as narrow as that of the PSL particles, but these can still be tried for the purpose of local efficiency measurements. These glass beads have a specific gravity (2.5) higher than that of water, so they tend to settle after some time. This problem can however be alleviated by making use of a magnetic stirrer, which will

assist in keeping these particles in suspension and thus provide a constant feed rate of the particles to the system.

8. For making measurements in the Simulated Automotive Filter housing, it is imperative that due consideration also be given to the fact that the particles in the flow have a significant component of transverse velocity. This component causes the particles to move away from a vertical direction of motion across the filter. This may result in double counting of the particles and hence influence the number density measurements. It may be advisable to discuss and investigate the feasibility of the concept of measuring only the axial velocity and using this for the number density calculations.

REFERENCES

Aerometrics Inc. (A Division of TSI Inc.) (1992), Doppler Signal Analyzer for Phase Doppler Particle Applications User's Manual, Sunnyvale, CA, draft 2.

Al-Sarkhi, A., Yao, S. H. and Chambers, F. W. (1997), "Flow Distribution Dependence on Housing Geometry for Tangential Inlet Automotive Air Filter Housings," *Advances in Filtration and Separation Technology - Advancing Filtration Solutions*, Proceedings of the Annual National Technical Conference of the American Filtration and Separations Society, Minneapolis, Minnesota, April 29 – May 2, 1997, pp. 210-215.

Anand, S., Jadbabaei, F. M. and Dougherty, R. L. (1997), "Comparison of Filtration Efficiency Measurements for Pleated and Flat Sheet Filters," presented at the 1997 SAE International Congress and Exposition, SAE Technical Paper #970671, Topics in Automotive Filtration Design (SP-1252), Conference of SAE Inc., Detroit, MI

Benarie, M. (1963), "Einfluss der Porenstruktur auf den Abscheidegrad in Faserfiltern," *Staub*, Vol. 29, No. 2, pp. 74-78.

Brown, R. C. (1993), Air Filtration: An Integrated Approach to the Theory and Applications of Fibrous Filters, Pergamon Press, Oxford.

Bugli, N. J. (1997), "Filter Performance Requirements for Engine Air Induction Systems," SAE Technical Paper #970556, Topics in Automotive Filtration Design (SP-1252) SAE, Inc., Warrendale, PA.

Chen, C. Y. (1955), "Filtration of Aerosols by Fibrous Media," *Chemical Review*, Vol. 55, No. 3, pp. 595-623.

Chen, Y. K. and Yu, C. P. (1993), "Particle Deposition from Duct Flows by Combined Mechanisms," *Aerosol Science and Technology*, Vol 19, pp. 389 - 395.

Chen, D. R., Pui, D. Y. H. and Tang Y. M. (1996), "Filter Pleating Design for Cabin Air Filtration," SAE Technical Paper #960941, Aspects of Automotive Filtration (SP-1165), Conference SAE Inc., Warrendale, PA.

Davies, C. N. (1952), "The Separation of Airborne Dust and Particles," Proceedings of The Institute of Mechanical Engineers (Part B), Vol. 1b, pp. 185 – 213.

Davies, C. N. (1973), Air Filtration, Academic Press, New York.

Duran, R. (1995), "Improvement of Flow Uniformity and Modeling of Filtration Efficiencies for Automotive Air Filter Test Housings," M. S. Thesis, School of Mechanical and Aerospace Engineering, Oklahoma State University, Stillwater, Oklahoma.

Fitzgerald, J. J. and Detwiler, (1957), *American Industrial Hygiene Association Quarterly*, Vol. 18, No. 47.

Friedlander, S. K. (1958), "Theory of Aerosol Filtration," *Industrial Engineering Chemistry*, Vol. 50, pp. 1161-1164.

Fuchs, N. A. (1964), *The Mechanics of Aerosols*, Pergamon Press, Oxford.

Gebreegziabher, T. (1998), "Effect of Electrostatic Charges as a Function of Temperature and Humidity, on the Filtration Efficiency of Pleated Automotive Air Filters (tentative title)," M. S. Thesis (to be published), School of Mechanical and Aerospace Engineering, Oklahoma State University, Stillwater, Oklahoma.

Gillespie, T. (1955), "The Role of Electric Forces in the Filtration of Aerosols by Fiber Filters," *Journal of Colloid Science*, Vol. 10, pp. 299-314.

Gustavsson, J. (1996), "Cabin Air Filters: Performances and Requirements," SAE Technical Paper #960941, *Aspects of Automotive Filtration (SP-1165)*, Conference of SAE Inc., Warrendale, PA.

Hamaker, H. C., (1937), *Physica*, Vol. 4, pp. 1058+.

Harrop, J. A. (1969), "The Effect of Fiber Configuration on the Efficiency of Aerosol Filtration," PhD Thesis, Loughborough University of Technology, Loughborough, England.

Jadbabaei, F. M. (1997), "Filtration Efficiency Measurements on Pleated Filters," M. S. Thesis School of Mechanical and Aerospace Engineering, Oklahoma State University, Stillwater, Oklahoma.

Jaroszcyk, T. (1987), "Experimental Study of Nonwoven Filter Performance Using Second Order Orthogonal Design," *Particulate Science and Technology*, Vol. 5, Hemisphere Publishing Corporation, pp. 271-287.

Jaroszcyk, T. and Wake, J. (1991), "Critical Aerosol Velocity in Nonwoven Filtration," TAPPI Proceedings, Nonwoven Conference, pp. 125-135.

Jaroszcyk, T., Ptak, T. J., Fallon, S. L. and Wake, J. (1993a), "Particulate and Odor Control Systems in Car Ventilation Systems," SAE Technical Paper #940321, Conference of SAE Inc., Warrendale, PA.

Jaroszcyk, T., Wake, J. and Connor, M. J. (1993b), "Factors Affecting the Performance of Engine Air Filters," American Society of Mechanical Engineers, Energy Sources Technology Conference and Exhibition, Houston, Texas.

Jaroszcyk, T., Ptak, T.J. and Wake, J. (1994), "An Experimental Evaluation of the Factors Influencing the Performance of Car Interior Air Filters," SAE #940321, International Congress and Exposition, Detroit, MI.

Kline, S. J. and McClintock, F. A. (1953), "Describing Uncertainties in Single-Sample Experiments," *Mechanical Engineering*, January, pp. 3-8.

Landahl, H. D. and Hermann, R. G. (1949), "Sampling of Liquid Aerosols by Wires, Cylinders, and Slides, and the Efficiency of Impaction of the Droplets," *Journal of Colloidal Science*, Vol. 4, pp. 103-136.

Langmuir, I. (1942), "Report on Smokes and Filters," Section I US Office of Scientific Research and Development Report, no. 865, part IV.

Lee, K. W. (1977), "Filtration of Submicron Aerosols by Fibrous Filters," Ph.D. Thesis, University of Minnesota, Twin Cities, Minnesota.

Lee, K. W. and Liu, B. Y. H. (1982a), "Experimental Study of Aerosol Filtration by Fibrous Filters," *Aerosol Science and Technology*, Elsevier Science Publishing Co., Amsterdam, Vol. 1, pp. 25-76.

Lee, K. W. and Liu, B. Y. H. (1982b), "Theoretical Study of Aerosol Filtration by Fibrous Filters," *Aerosol Science and Technology*, Elsevier Science Publishing Co., Amsterdam, Vol. 1, pp. 147-161.

Lee, S. E. (1996), "In-Vehicle Performance of New and Used Automotive Cabin Air Filters," SAE Technical Paper #960541, Aspects of Automotive Filtration (SP-1165), Conference of SAE Inc., Warrendale, PA.

Liang, F. (1997), "Particle Counting and Sizing with LDV for Automotive Air Filters," Ph.D. Thesis, School of Mechanical and Aerospace Engineering, Oklahoma State University, Stillwater, Oklahoma.

Liang, F., Natarajan, B., Tian, Y. and Dougherty, R. L. (1995), "Local Efficiency Measurements Applicable to Both Automotive Engine and Cabin Filtration," *Particulate Science and Technology*, Taylor and Francis Publishers, Vol. 12, No. 4, April, pp. 333-350.

Lindeken, C. L., Morgin, R. L. and Petrock, K. F. (1963), *Health Phys.*, Vol 9, pp. 305+.

Marteson, M. J. (ed.), (1987), Filtration - Principles and Practices, Marcel Dekker, New York, New York.

Maus, R. and Umhauer H. (1996), "Determination of the Fractional Efficiencies of Fibrous Filter Media by Optical In - Situ Measurements," *Aerosol and Technology*, Vol. 24, pp. 161-173, April.

McDonald, B., Gogins, M., Rothman, J. and Scott, J. (1997), "Discriminating Tests for Automobile Cabin Air Filter Media," SAE Technical Paper #970670, Topics in Automotive Filtration Design (SP-1252), Conference of SAE Inc., Warrendale, PA.

Natarajan, B. (1995), "Local Efficiency Measurements of Automotive Air Filters Using Laser Doppler Velocimetry," M. S. Thesis, School of Mechanical and Aerospace Engineering, Oklahoma State University, Stillwater, Oklahoma.

Natarajan, B., Liang, F., Williams, J. C., and Dougherty, R. L. (1995), "Local Efficiency Measurements Flat Filter Media: Application to Automotive Cabin and Engine Air Filters," presented at the American Filtration and Separation Society Meeting, April 24-36, Nashville, Tennessee.

Natanson, G. L. (1957), "Deposition of Aerosol Particles by Electrostatic Attraction upon a Cylinder Around which They Are Flowing," *Dokl. Akad. Nauk SSSR*, Vol. 112, pp. 696-699 (in Russian), HSE Translation 7222 (1977).

Newport Catalog (1993).

Nicholson, R. M. and Weisert, L. E. (1986), "A Review of the Use of SAE Standard J726 in Heavy Duty Engine Air Cleaner Testing," *Fluid Filtration: Gas*, ASTM STP 975, American Society for Testing and Materials, Philadelphia, Vol. 1, pp. 266-274.

Omega Catalog (1997), Vol. 28.

Pich, J (1966), "The Effectiveness of the Barrier Effect in Fiber Filters at Small Knudsen Numbers," *Staub*, Vol. 26, pp. 1-4.

Pich, J. (1966), "Theory of Aerosol Filtration by Fibrous and Membrane Filters," *Aerosol Science*, (C.N. Davies, ed.) Academic Press, New York, New York, pp. 223-285.

Pich, J. (1969), "Pressure Characteristics of Fibrous Aerosols Filters," *Journal of Colloid Interface Science*, Vol. 37, pp. 912-917.

Pich, J. (1971), paper presented at the 45th National Colloid Symposium, Atlanta, Georgia, June 21-23.

Pich, J. (1987), Filtration - Principles and Practices, (M.J. Matteson, ed.), Marcel Dekker, New York, New York.

Poon, W. S. and Liu, B. Y. H. (1997), "Fractional Efficiency and Particle Mass Loading Characteristics of Engine Air Filters," presented at 1997 SAE International Congress and Exposition, SAE Technical Paper #970673, Topics in Automotive Filtration Design (SP-1252), Conference of SAE Inc., Warrendale, PA.

Poon, W. S. and Liu, B. Y. H. (1997), "A Bimodal Loading Test for Engine and General Purpose Air Cleaning Filters," presented at 1997 SAE International Congress and Exposition, SAE Technical Paper #970674, Topics in Automotive Filtration Design (SP-1252), Conference of SAE Inc., Warrendale, PA.

Ptak, T. J. and Jaroszczyk, T. (1990), "Theoretical-Experimental Aerosol Filtration Model for Fibrous Filters at Intermediate Reynolds Numbers," Proceedings of the Fifth World Filtration Congress, Nice, France, pp. 566-572.

Ptak, T. J., Wake, J. and Jaroszczyk, T. (1994), "An Experimental Evaluation of the Factors Influencing the Performance of Car Interior Air Filters," SAE Technical Paper #930014, Conference of SAE Inc., Warrendale, PA.

Reinhart, C. O. and Weisert, L. E. (1983), "Measurement of Engine Air Cleaner Efficiency Using Airborne Particle Size Analysis," SAE Technical Paper #831262, International Off-Highway Meeting and Exposition, Milwaukee, Wisconsin, September.

Rodman, C. A. and Lessmann, R. C. (1988), "Automotive Nonwoven Filter Media: Their Constructions and Filter Mechanisms," *Tappi Journal*, pp. 161-168, April.

Sabnis, R. D. (1993), "Effects of Non-Uniform Air Flow Through Filters on Filtration Efficiency," M. S. Thesis, School of Mechanical and Aerospace Engineering, Oklahoma State University, Stillwater, Oklahoma.

Sabnis, R. D., Cai, Q., Chambers F. W. (1994), "Diagnosis of the Flow Fields in a Housing for Automotive Air Filter Performance Testing," AIAA Paper #94-0117, AIAA 32nd Aerospace Sciences Meeting, Reno, Nevada.

Sabnis, R. D., Cai, Q., Chambers F. W. (1994), "Flow Distribution Effects Upon Air Filter Performance Measurements," SAE 1994 Transactions, *Journal of Engines*, Section 3, pp. 386-397.

Shobokshy, E. and Mohammed S. (1994), "Computer Simulation of Monodisperse Aerosol Collection in Fibrous Filters," *Aerosol Science and Technology*, Elsevier Science Publishing Co., Amsterdam, Vol. 20, pp. 149-160.

Society of Automotive Engineers (1987), "SAE J726 Air Cleaner Test Code - SAE Recommended Practice," SAE Inc., Warrendale, PA.

Society of Automotive Engineers (1993), "SAE J1669 Passenger Compartment Air Filter Test Code - SAE Recommended Practice," Proposed Draft, SAE Inc., Warrendale, PA.

Stechkina, I. B. (1964), *Inzh. Fiz. Zh.*, Vol. 7, pp. 128+ (In Russian).

Stenhouse, J. I. T. (1975), "Filtration of Air by Fibrous Filters," *Filtration and Separation*, pp. 268-274, May/June.

Stinson, J. A., Meyers, M. N., Jaroszczyk, T. and Verdegan, B. M. (1988), "Temporal Changes in Oil and Air Filter Performance due to Dust Deposition," *Filtration and Separation*, Sept./Oct., pp. 368-371.

Stern, S. T., Zeller, H. W. and Schekman, A. I. (1960), "The Aerosol Efficiency and Pressure Drop of a Fibrous Filter at Reduced Pressures," *Journal of Colloid Interface Science*, Vol. 15, pp. 546-562.

Tian, Y. (1995), "TSTEP - Three Dimensional Traverse Software," performed as part of the OCAST Applied Research Project on Automotive Air Filtration, Oklahoma State University, Stillwater, Oklahoma.

Wake, J. and Jaroszczyk, T. (1991), "Experimental Study of Dust Filtration in Surface-Type Nonwovens," *Particulate Science and Technology*, Hemisphere Publishing Corporation, Vol. 9, pp. 31-44.

Walker, M. and Ptak, T. J. (1996), "Particulate Filter Performance in the North American Environment," SAE Technical Paper #960940, Aspects of Automotive Filtration (SP-1165), Conference of SAE Inc., Warrendale, PA.

Whitby, K. T. (1965), "Calculation of Clean Fractional Efficiency of Low Media Density Filter," *ASHRAE J.*, Vol. 7, pp. 56-64.

Whitby K. T. (1973), "On the Multimodal Nature of Atmospheric Aerosol Size Distributions," *Particle Technology*, Publication No. 218, pp. 576-585.

Whitby, K. T., Lundgren, D. A., Jordan, R. C. and McFarland, A. R. (1961), "Evaluation of Air Cleaners for Occupied Spaces," *Journal of Air Pollution Control Association*, Vol. 11, No. 11, pp. 503-515.

Williams, J. C. (1996), "In-Situ Measurements of Local Efficiency for Flat Automotive Air Filter Media," M. S. Report, School of Mechanical and Aerospace Engineering, Oklahoma State University, Stillwater, Oklahoma.

Wilson, W. E. (1977), "General Motors Sulfate Dispersion Experiment: Summary of EPA Measurements," *J. Air Pollution Control Assoc.*, Vol. 27, No. 1, pp. 225-234.

Yeh, H. C. (1972), "A Fundamental Study of Aerosol Filtration by Fibrous Filters," Ph.D. Thesis, University of Minnesota, Twin Cities, Minnesota.

Yeh, H. C., and Liu, B. Y. H. (1974), "Aerosol Filtration by Fibrous Filters - I. Theoretical," *Aerosol Science*, Pergamon Press, Great Britain, Vol. 5, pp. 191-204.

APPENDIXES

APPENDIX A

Stokes Number Calculation

An example of the Stokes number calculation using Eq. (2-9) is presented in this appendix. The variables in Eq. (2-9) are:

- Density of the PSL particles (ρ_p), which is within the range of 1000 to 1050 kg/m³.
- Cunningham slip corrections factor (C_n), which is considered to be one for particle diameter greater than 1 μm and is given by the following relation [Brown, 1993]

$$C_n = 1 + \frac{2A^*\lambda}{D_p} + \frac{2Q^*\lambda}{D_p} \exp\left(-\frac{B^*D_p}{2\lambda}\right),$$

where $A^* = 1.246$, $Q^* = 0.42$, $B^* = 0.87$, λ (mean free path of molecules at NTP) = 0.065 μm .

- Air viscosity (μ_a) which is 18.6×10^{-6} Pa-s at 30° Centigrade.
- Air velocity (U). As an example, the overall average velocity upstream the filter for test SAH50_05_1 (flow rate of 77.07 m³/hr, Fig. 5.8) was used (2.3 m/s).
- Fiber diameter. The exact value of the average fiber diameter is not known, but a value of 38 microns was used (Natarajan, 1995).

From Eq. (2-9), the Stokes number is calculated as:

$$\text{St} = \frac{C_n D_p^2 \rho_p U}{18 \mu_o D_f} \quad (2-9)$$

Substituting in the above listed values, the Stokes number will be:

$$\text{St} = \frac{(1)[(0.497)(10^{-6})]^2 (1000)(2.3)}{18(18.6)(10^{-6})(38)(10^{-6})} = 0.0328$$

APPENDIX B

RESULTS FOR 0.497 μm DIAMETER PSL PARTICLES IN THE SMALL ANGLE DIFFUSER HOUSING

Some of the test results for 0.497 μm diameter PSL spheres have been shown and discussed in Chapter 5. The other test results are presented in this appendix. The results presented here are the upstream and downstream local velocity measurements, the upstream and downstream local number densities, and the local efficiencies for each of the additional tests.

The tests have alphanumeric designations, which specify the housing, flow rates, particle size and the repeat number. SAH75_05_2 stands for the Small Angle Housing experiment for 75 cfm (104.26 m^3/hr) with 0.497 μm particles (rounded to 0.5) and is the second experiment conducted for that flow rate. The files have named as explained in Chapter 4.

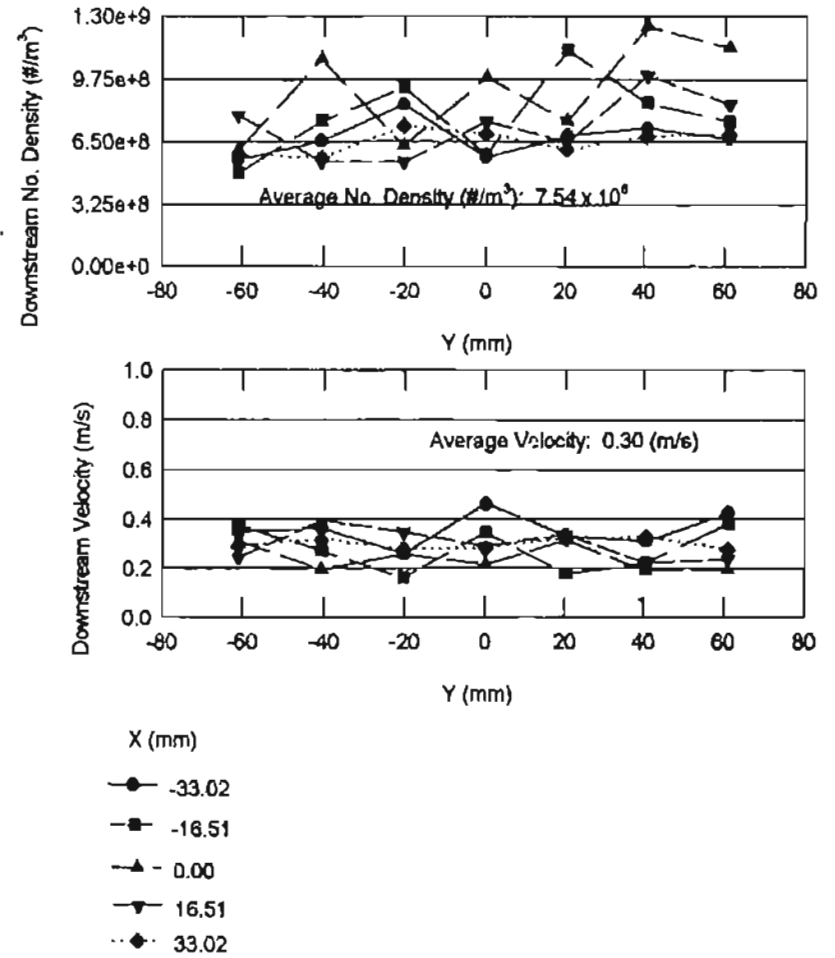
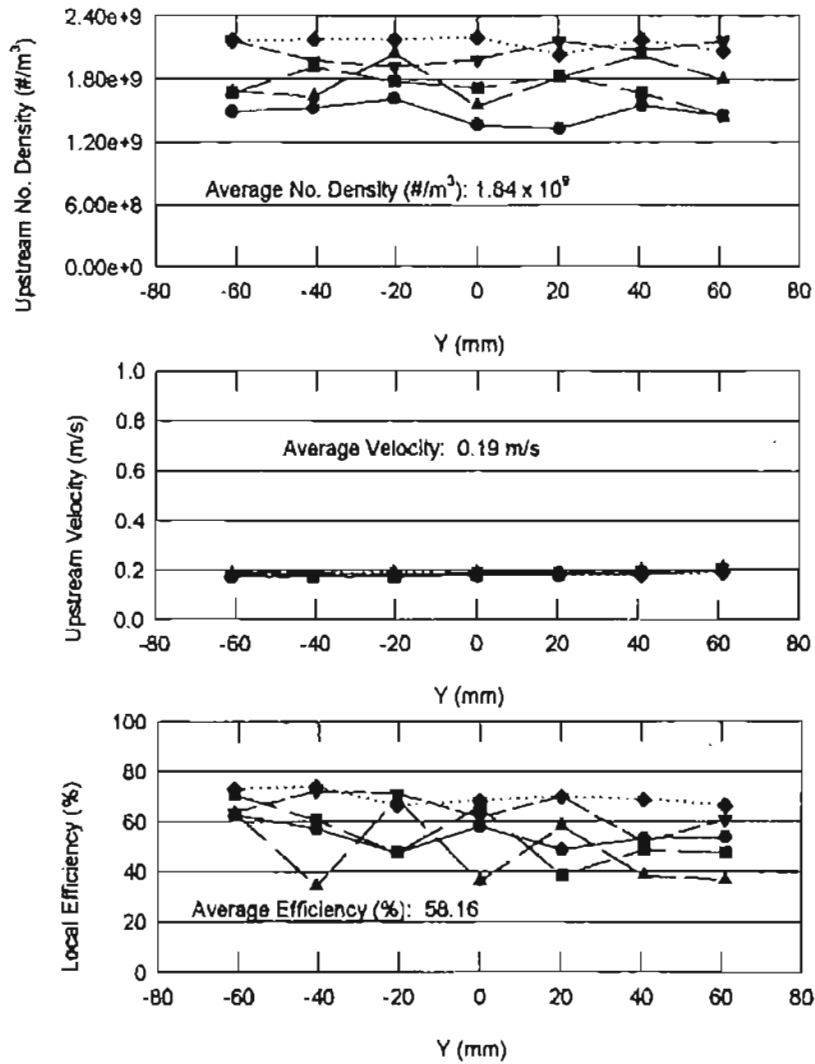
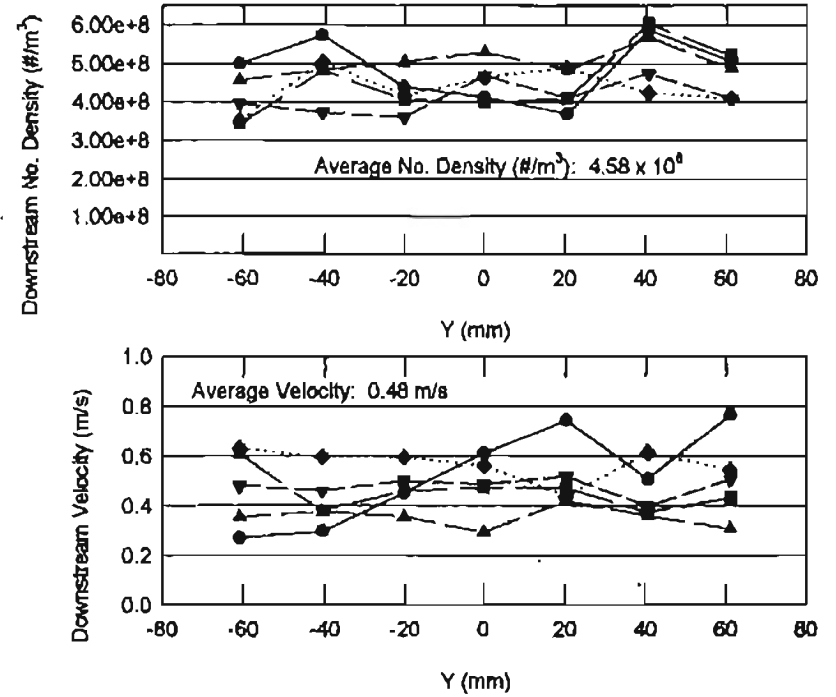
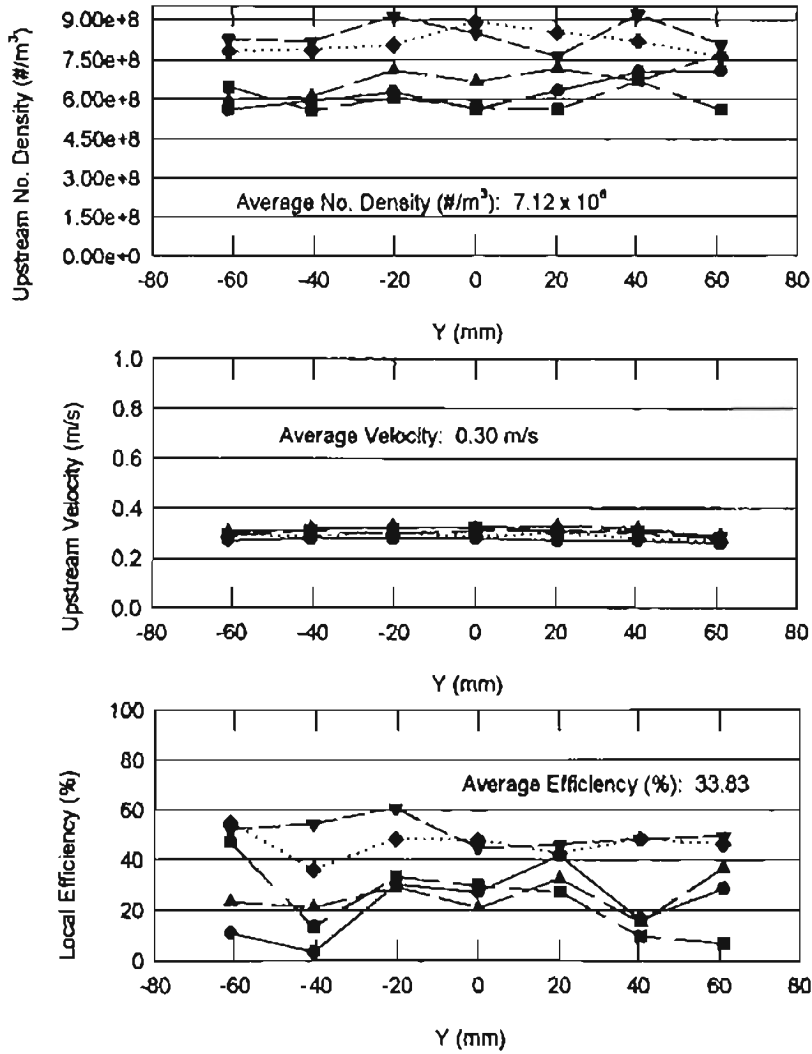


Figure B-1: Pleated Filter Efficiency for Test SAH10_05_2 at 13.61 m³/hr



- X (mm)
- -33.02
 - -16.51
 - ▲ 0.00
 - ▼ 16.51
 - ◆ 33.02

Figure B-2: Pleated Filter Efficiency for Test SAH15_05_1 at 21.55 m³/hr

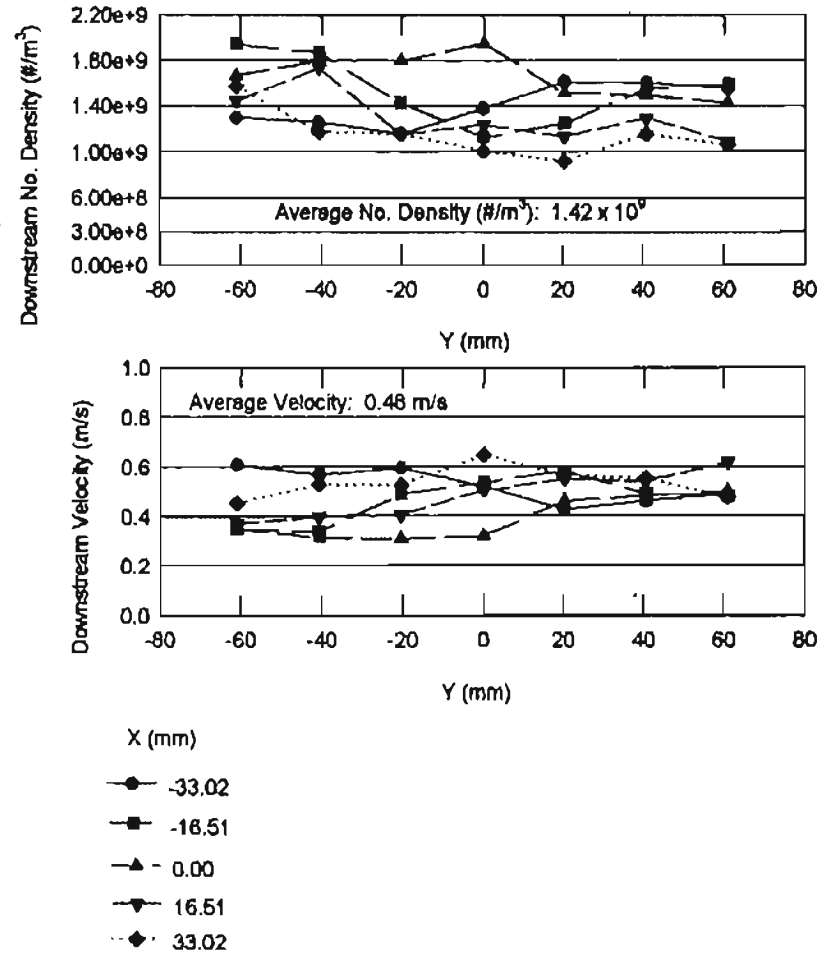
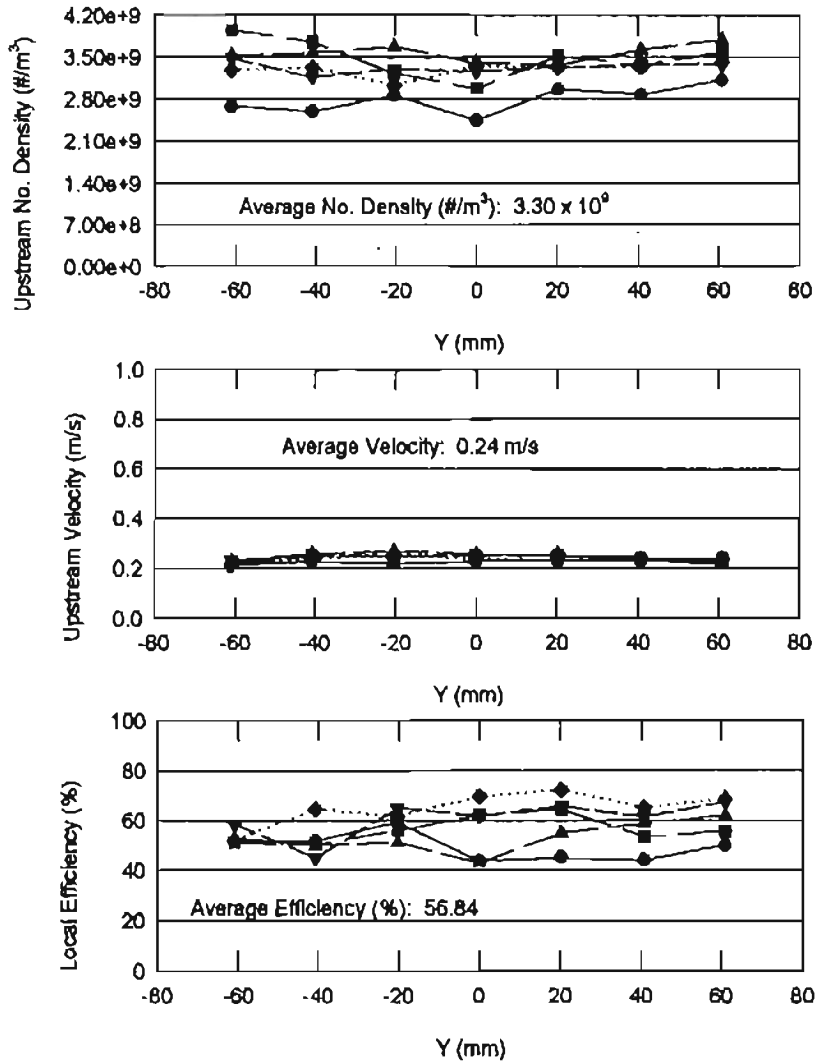


Figure B-3: Pleated Filter Efficiency for Test SAH15_05_2 at 21.55 m³/hr

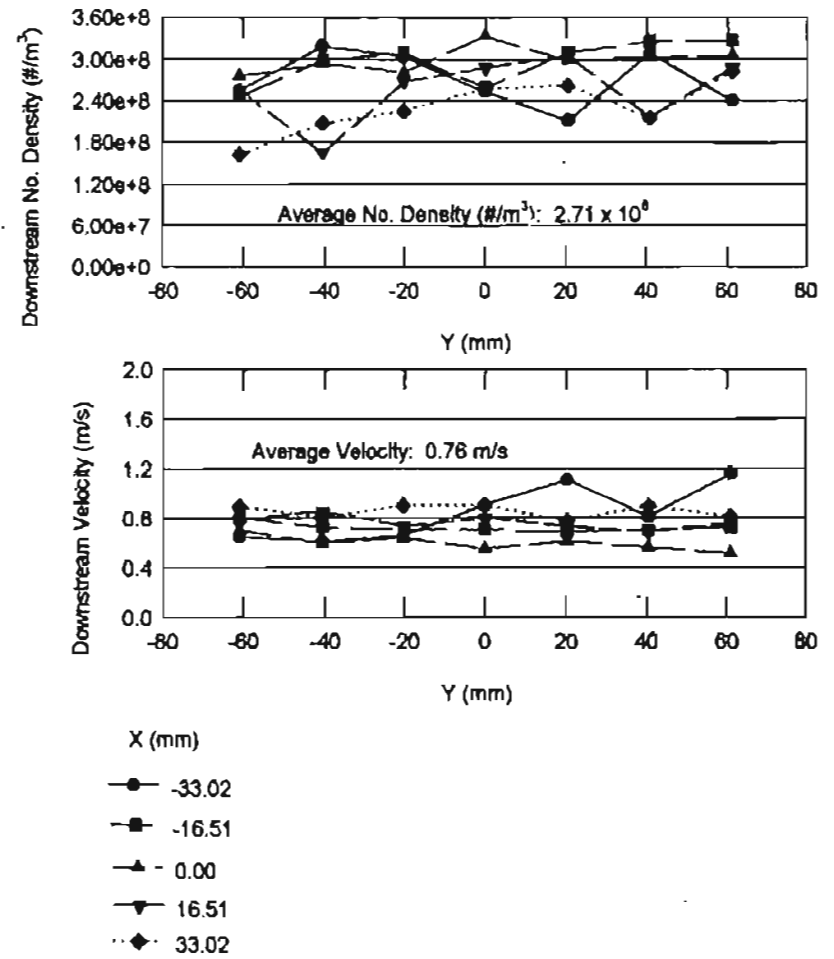
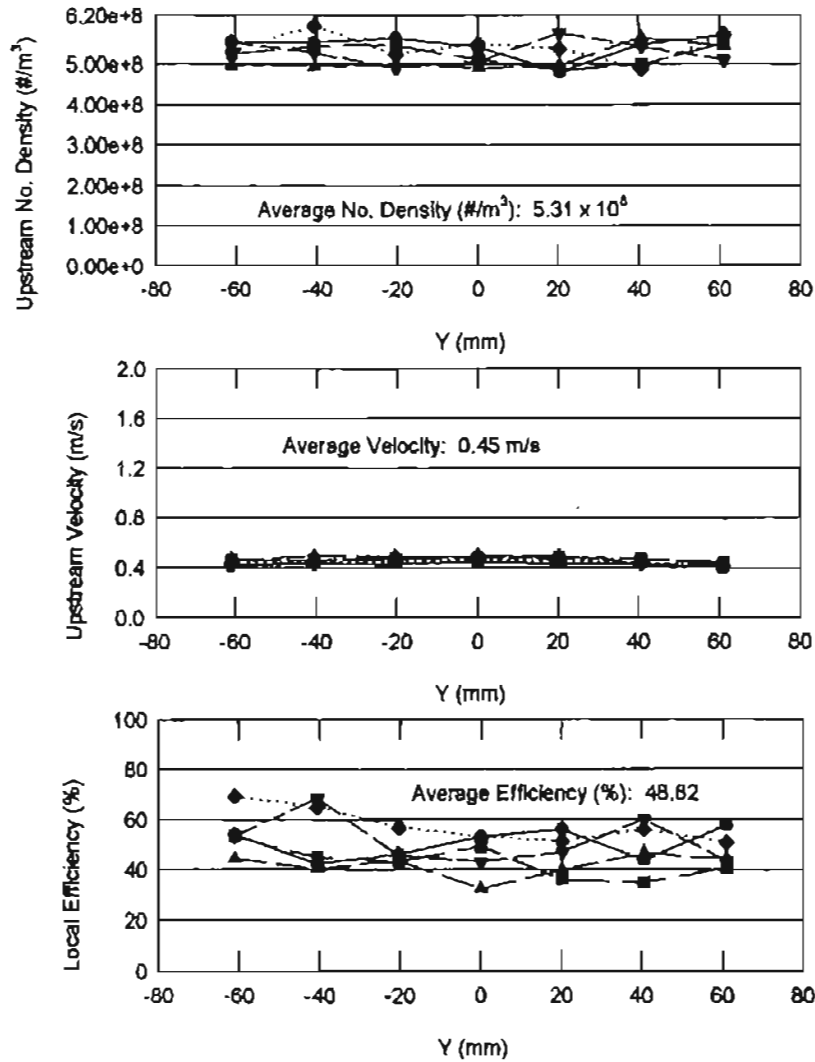
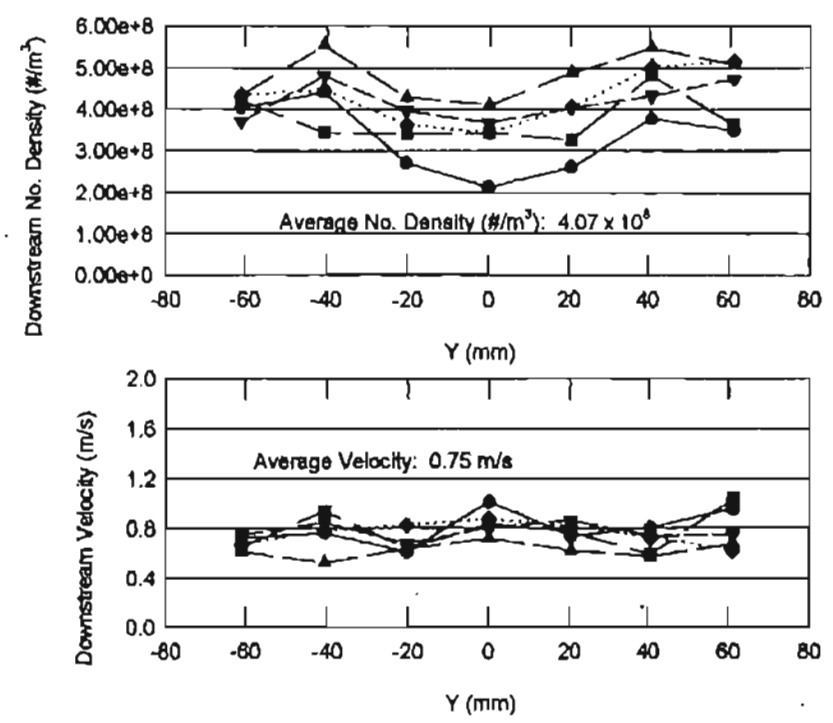
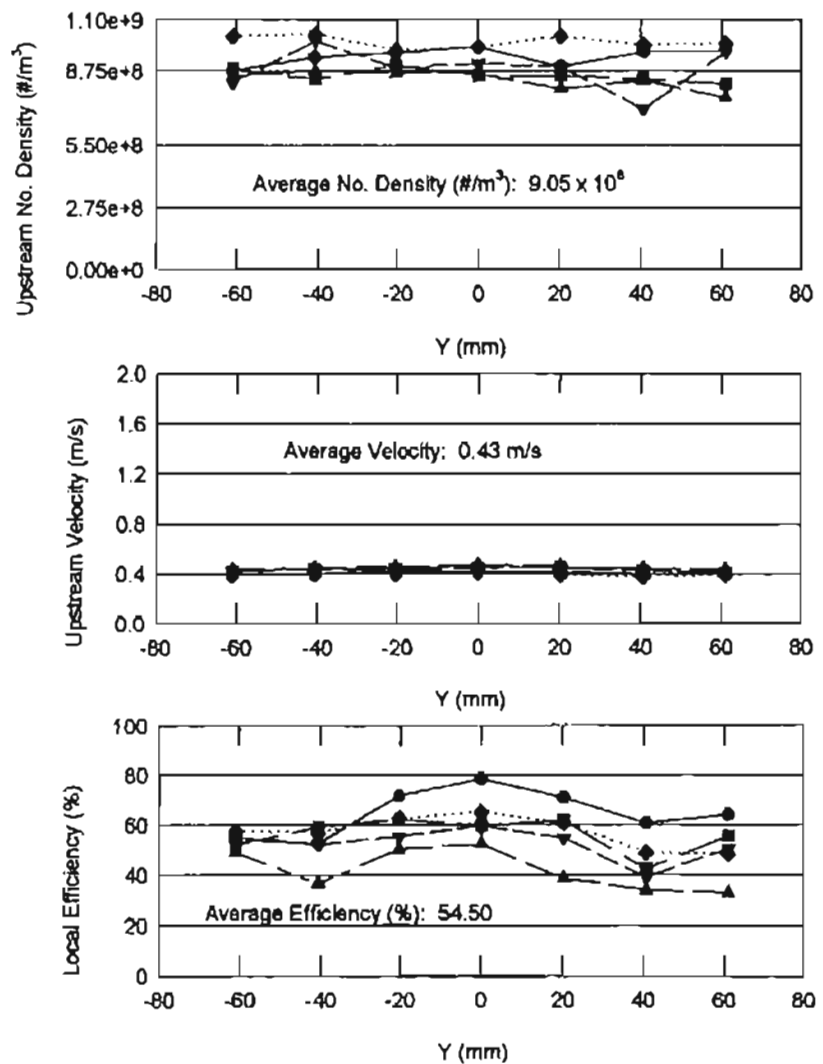


Figure B-4: Pleated Filter Efficiency for Test SAH20_05_1 at 29.48 m³/hr



- X (mm)
- -33.02
 - -16.51
 - ▲ 0.00
 - ▼ 16.51
 - ◆ 33.02

Figure B-5: Pleated Filter Efficiency for Test SAH20_05_2 at 29.48 m³/hr

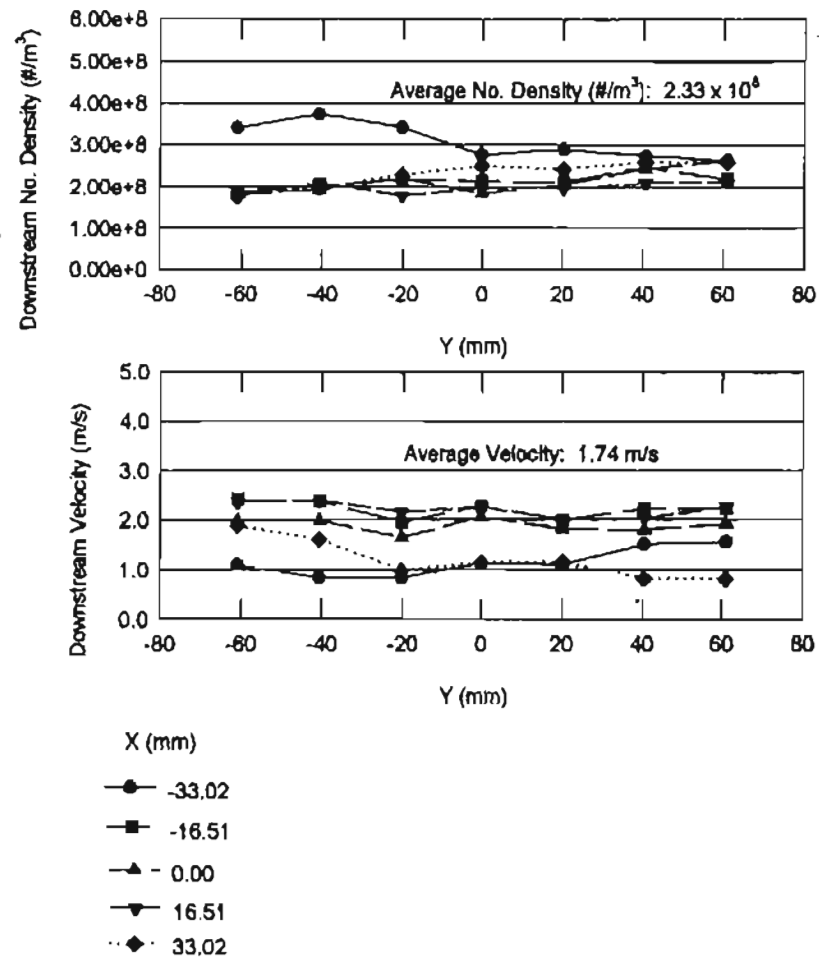
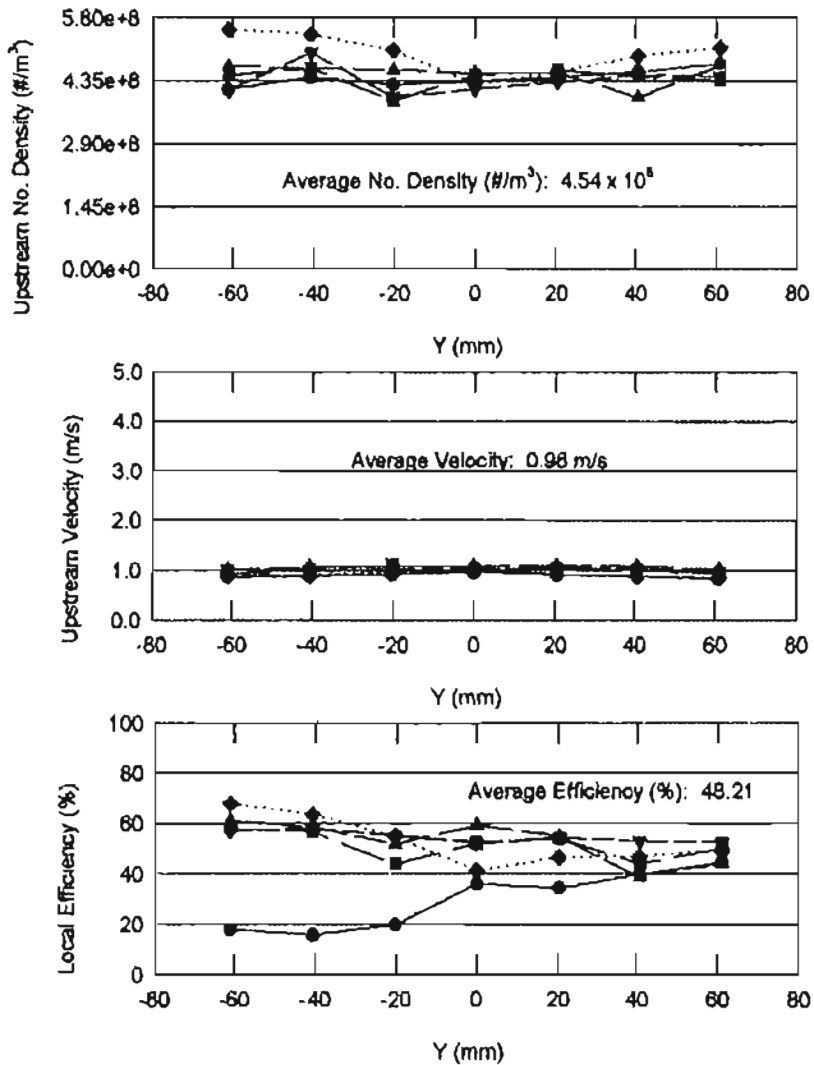


Figure B-6: Pleated Filter Efficiency for Test SAH25_05_1 at 37.42 m³/hr

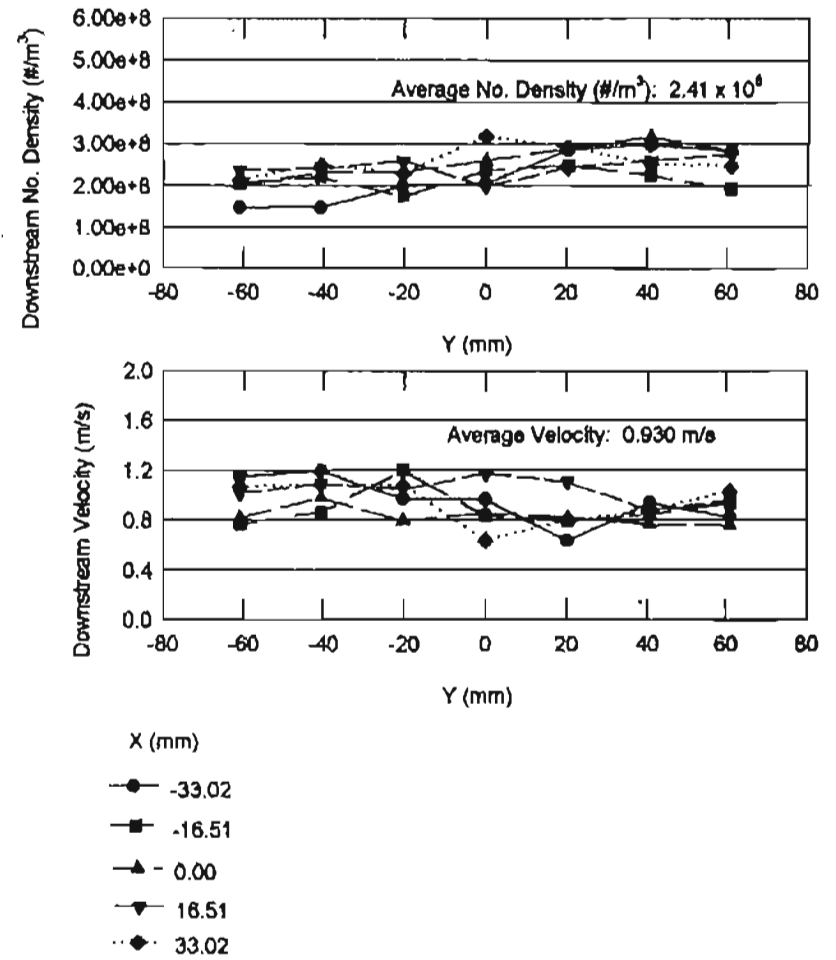
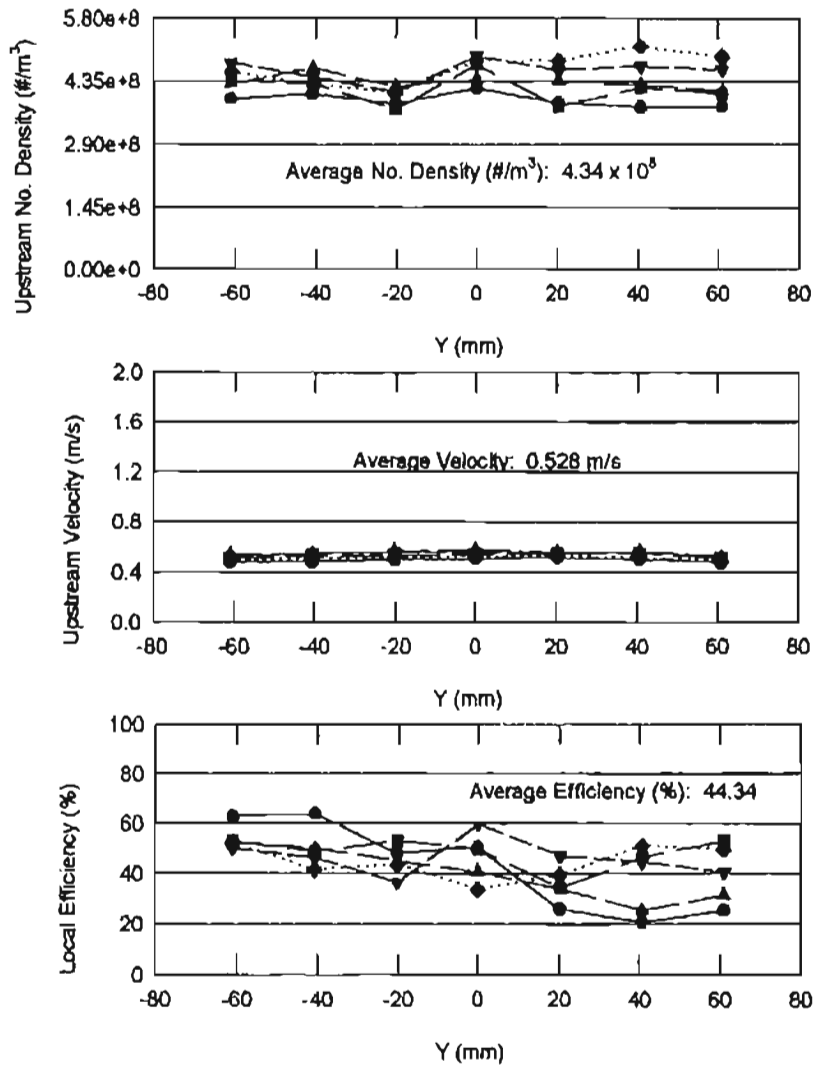
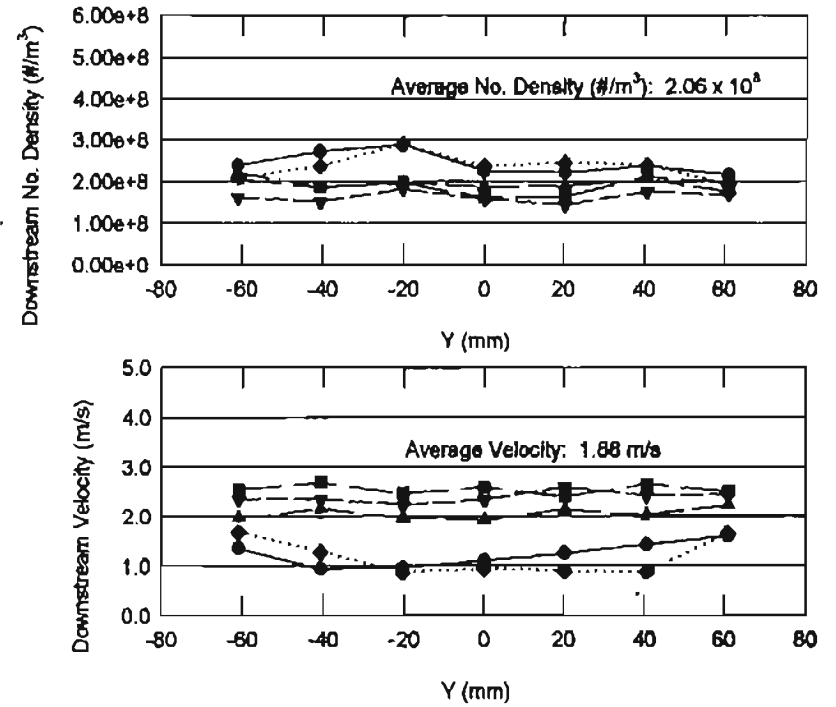
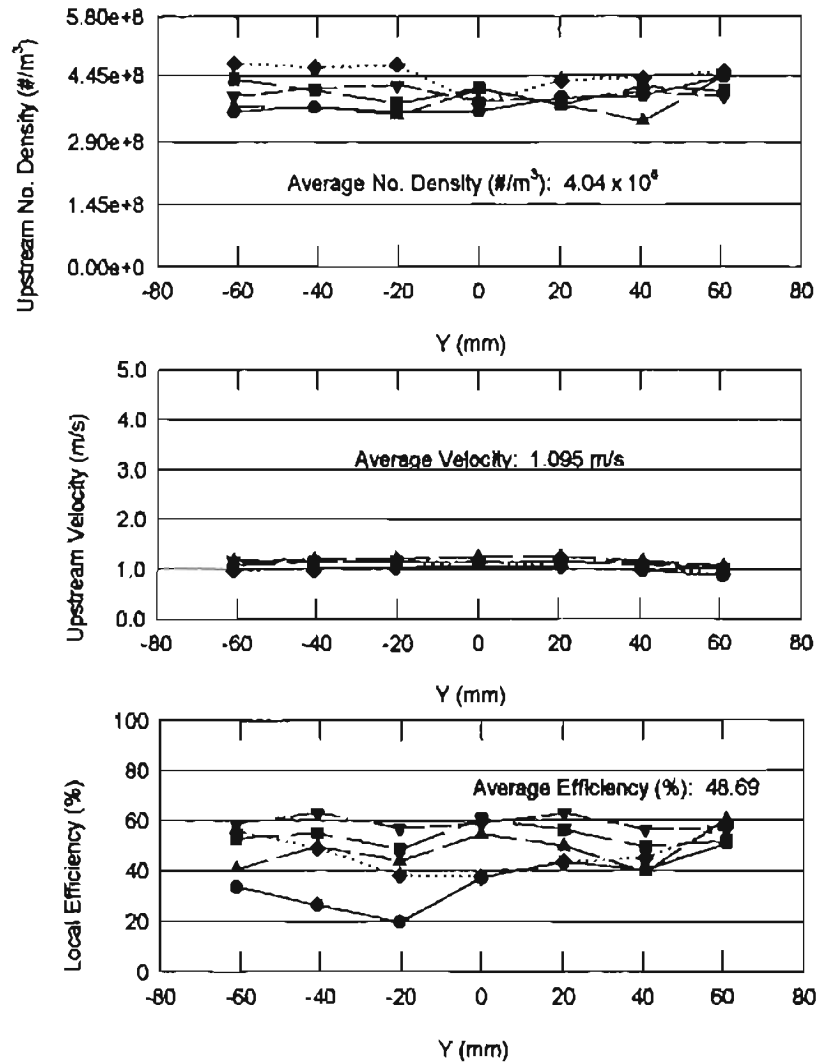


Figure B-7: Pleated Filter Efficiency for Test SAH25_05_2 at 37.42 m³/hr



- X (mm)
- -33.02
 - -16.51
 - ▲ 0.00
 - ▼ 16.51
 - ◆ 33.02

Figure B-8: Pleated Filter Efficiency for Test SAH30_05_1 at 45.35 m³/hr

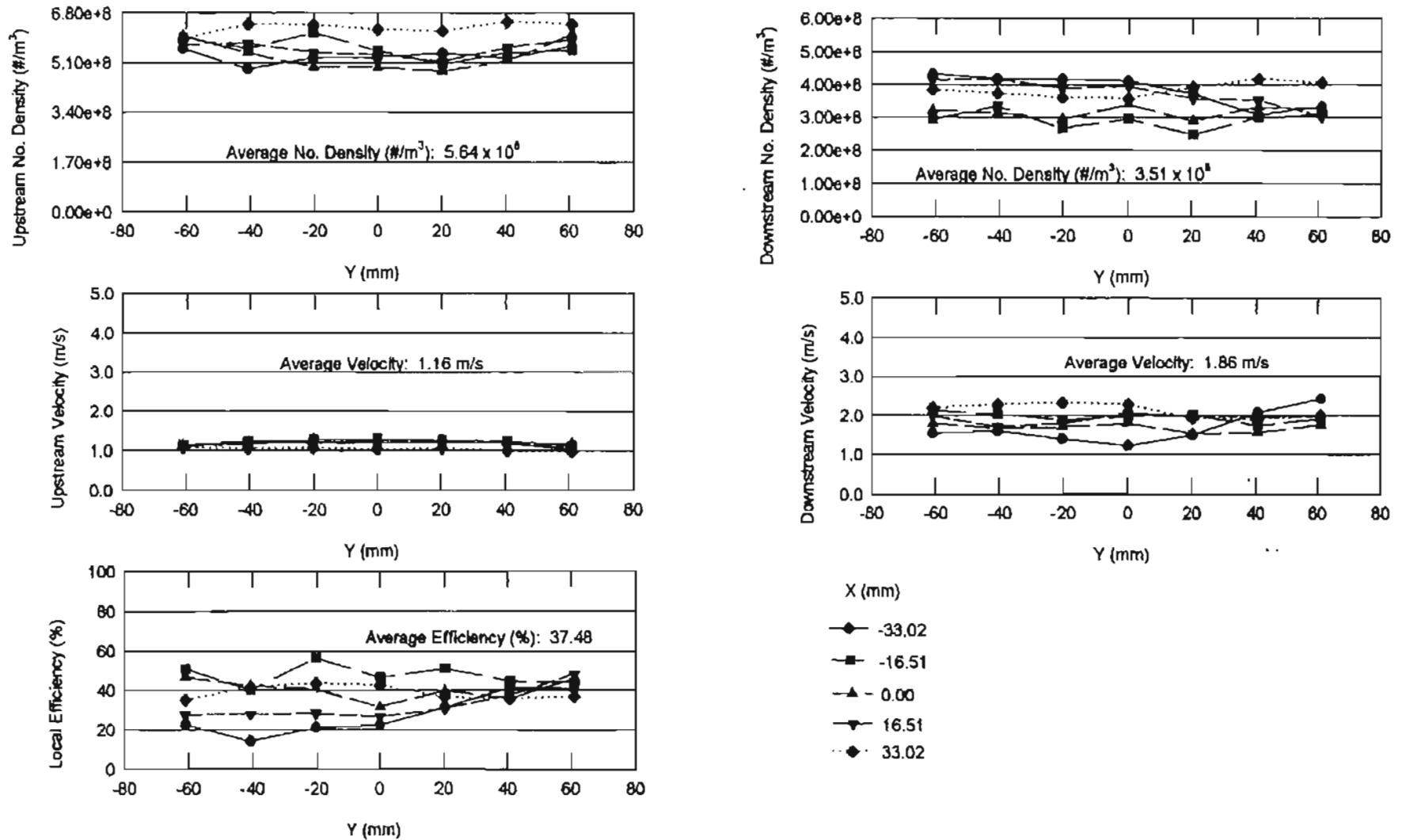
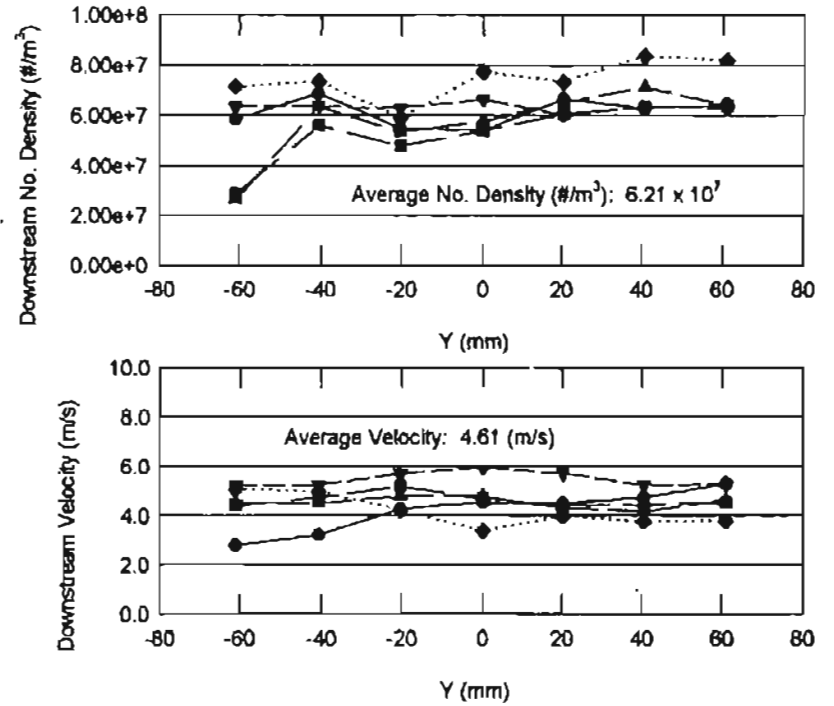
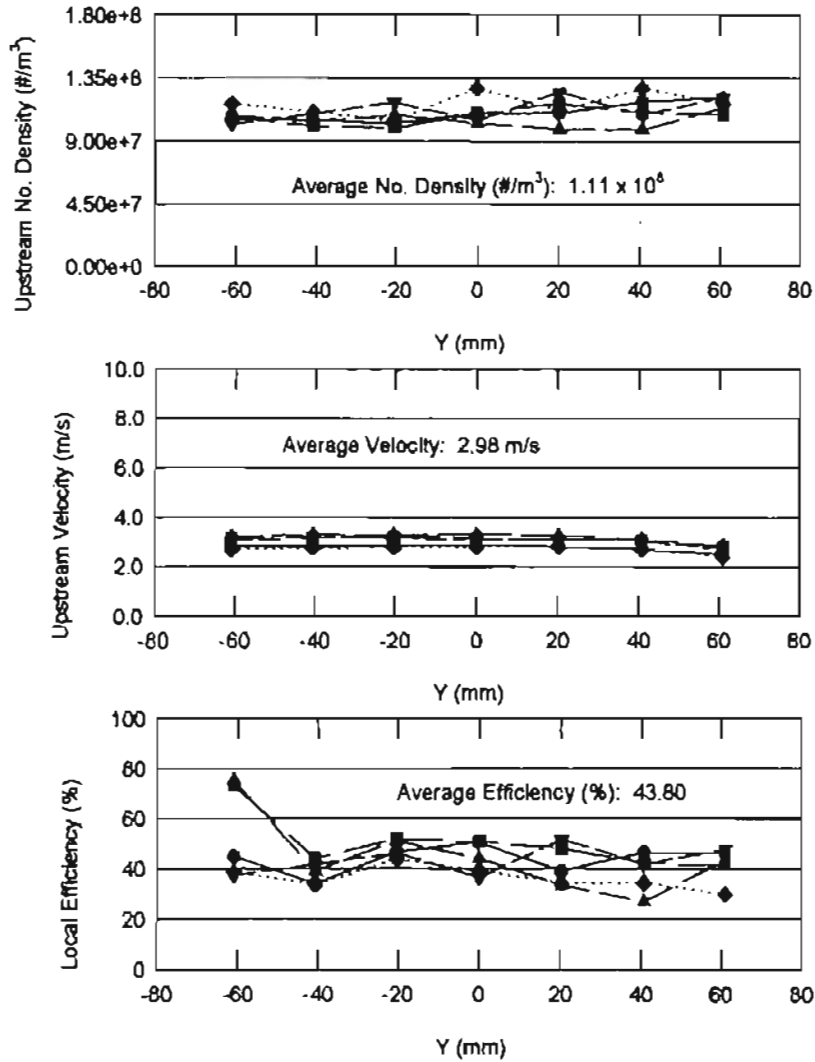
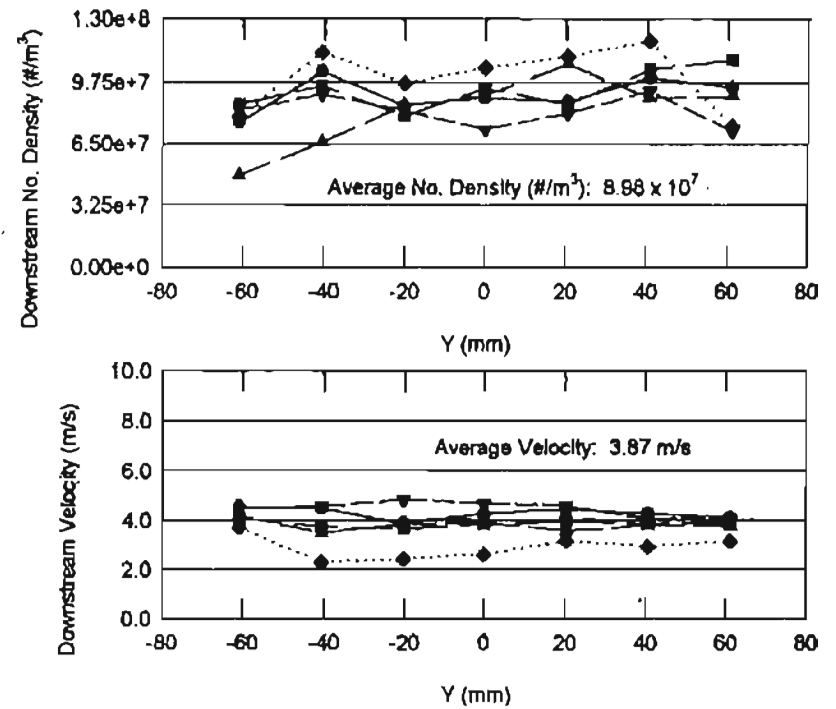
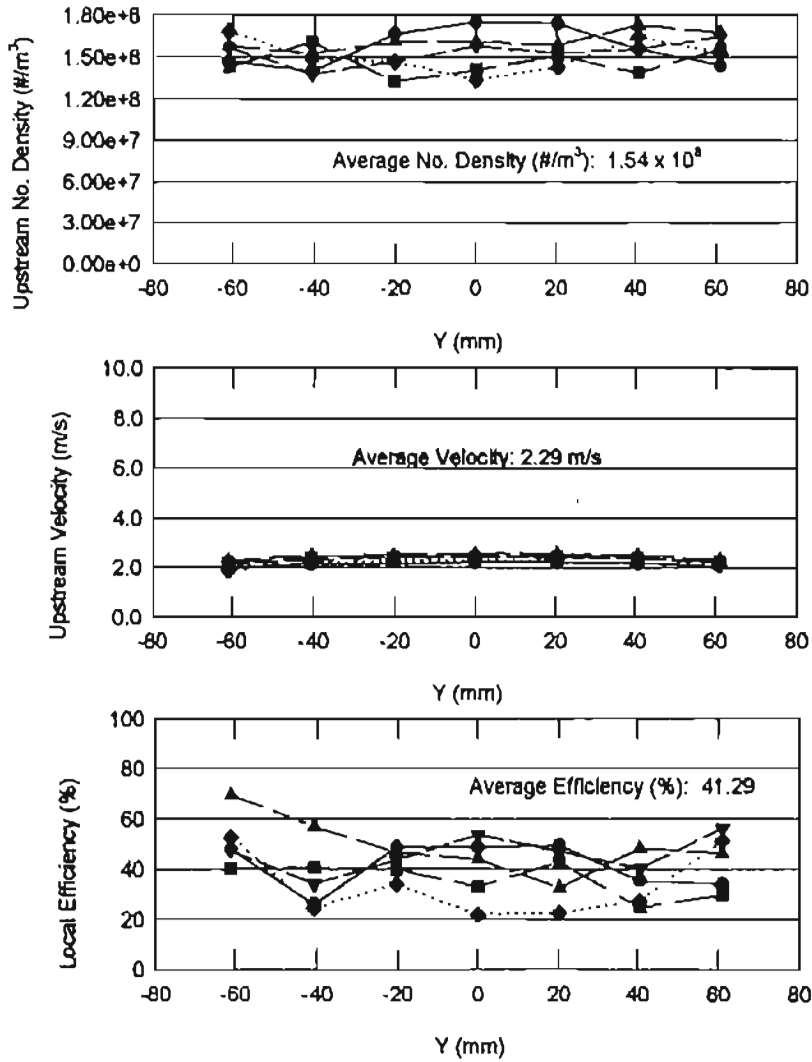


Figure B-9: Pleated Filter Efficiency for Test SAH30_05_2 at 45.35 m³/hr



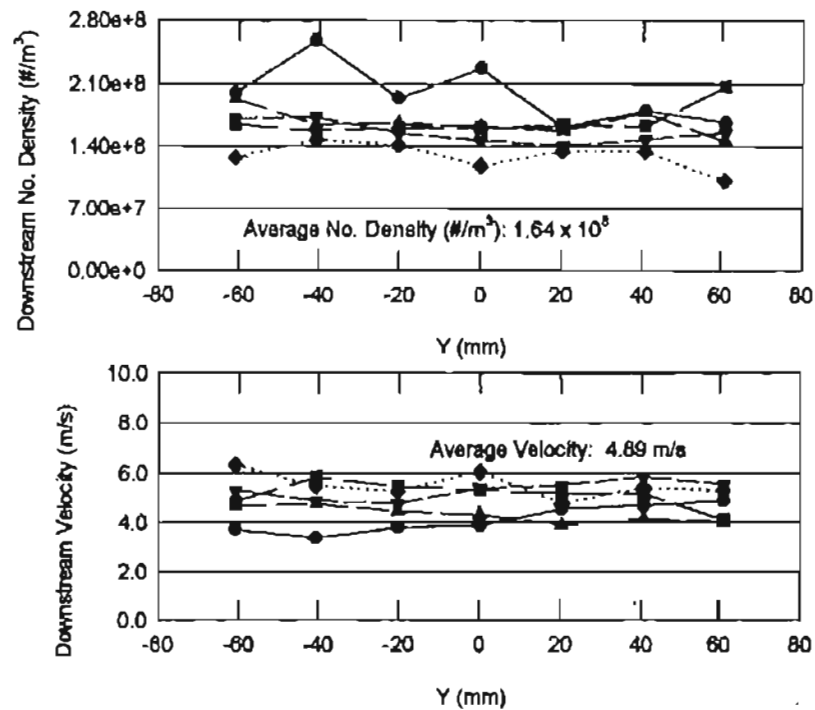
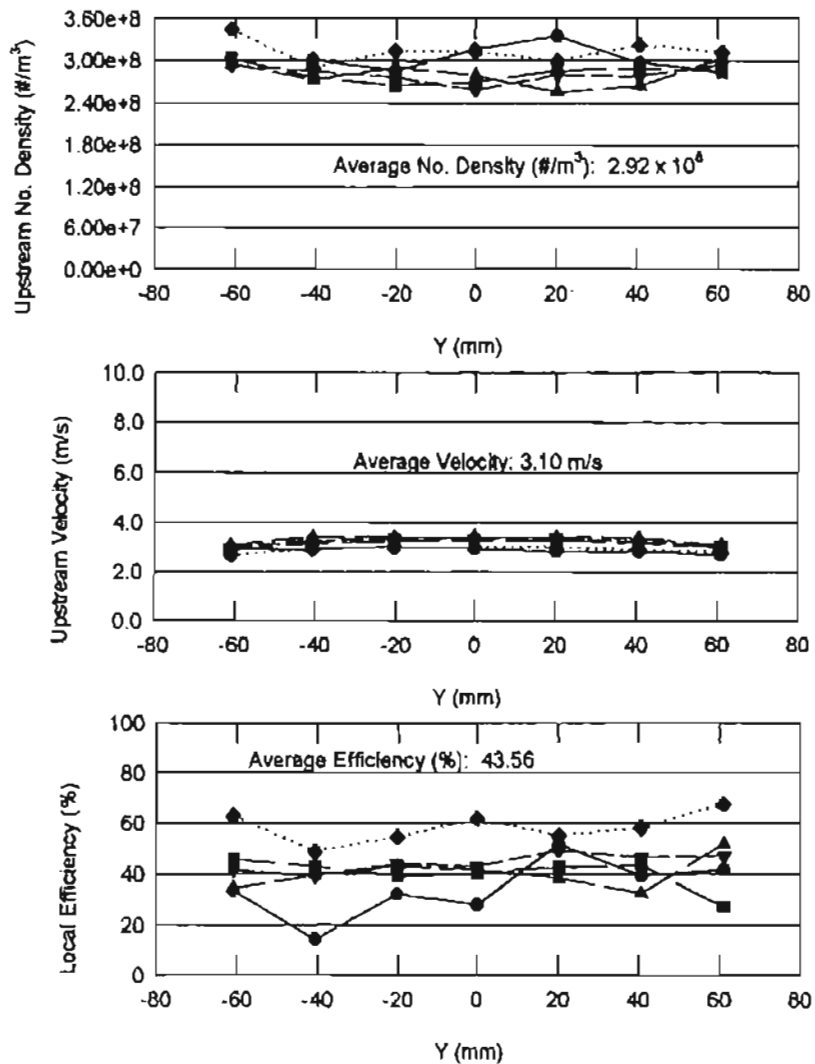
- X (mm)
- -33.02
 - -16.51
 - ▲ 0.00
 - ▼ 16.51
 - ◆ 33.02

Figure B-10: Pleated Filter Efficiency for Test SAH50_05_2 at 77.07 m³/hr



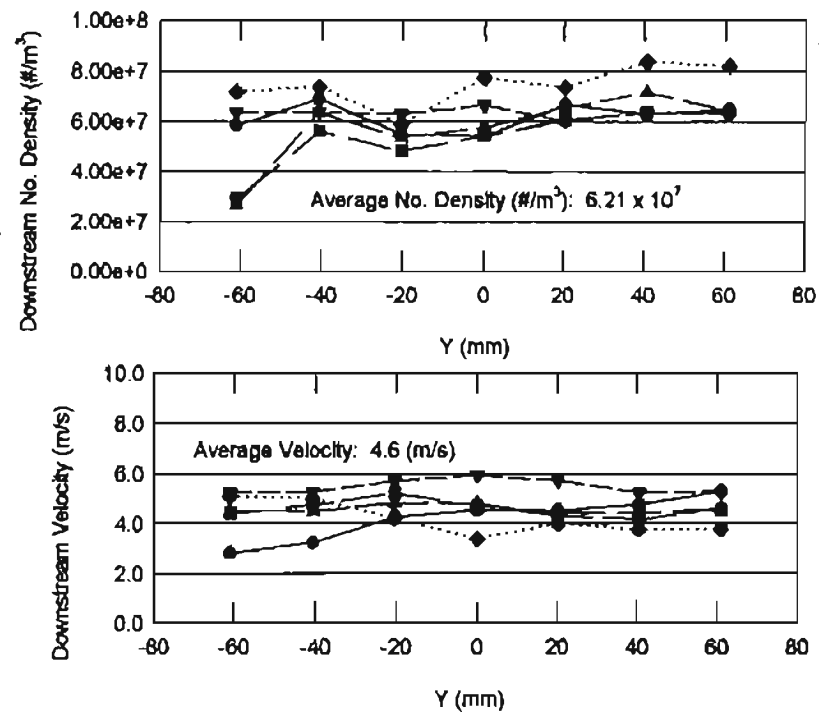
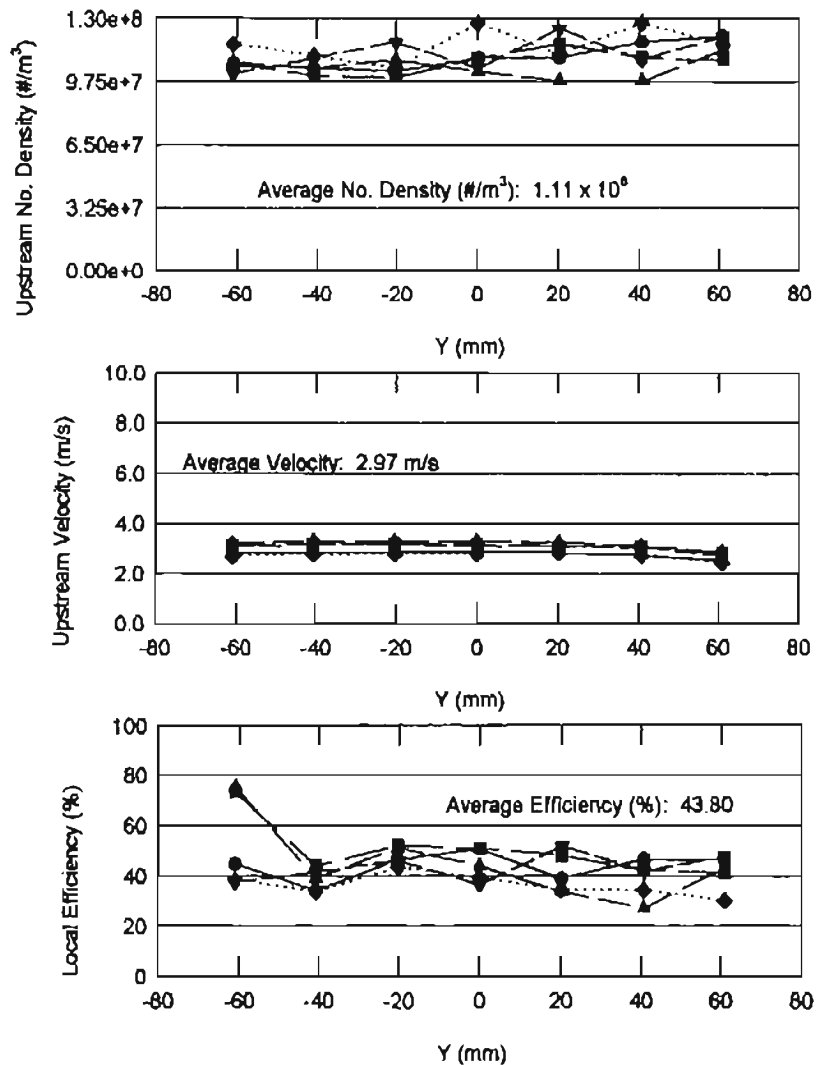
- X (mm)
- -33.02
 - -16.51
 - ...△... 0.00
 - ▽- 16.51
 - ...◇... 33.02

Figure B-11: Pleated Filter Efficiency for Test SAH75_05_1 at 104.26 m³/hr



- X (mm)
- -33.02
 - -16.51
 - ▲ 0.00
 - ▼ 16.51
 - ◆ 33.02

Figure B-12: Pleated Filter Efficiency for Test SAH75_05_2 at 104.26 m³/hr



- X (mm)
- -33.02
 - -16.51
 - ▲ 0.00
 - ▼ 16.51
 - ◆ 33.02

Figure B-13: Pleated Filter Efficiency for Test SAH100_05_1 at 146.36 m³/hr

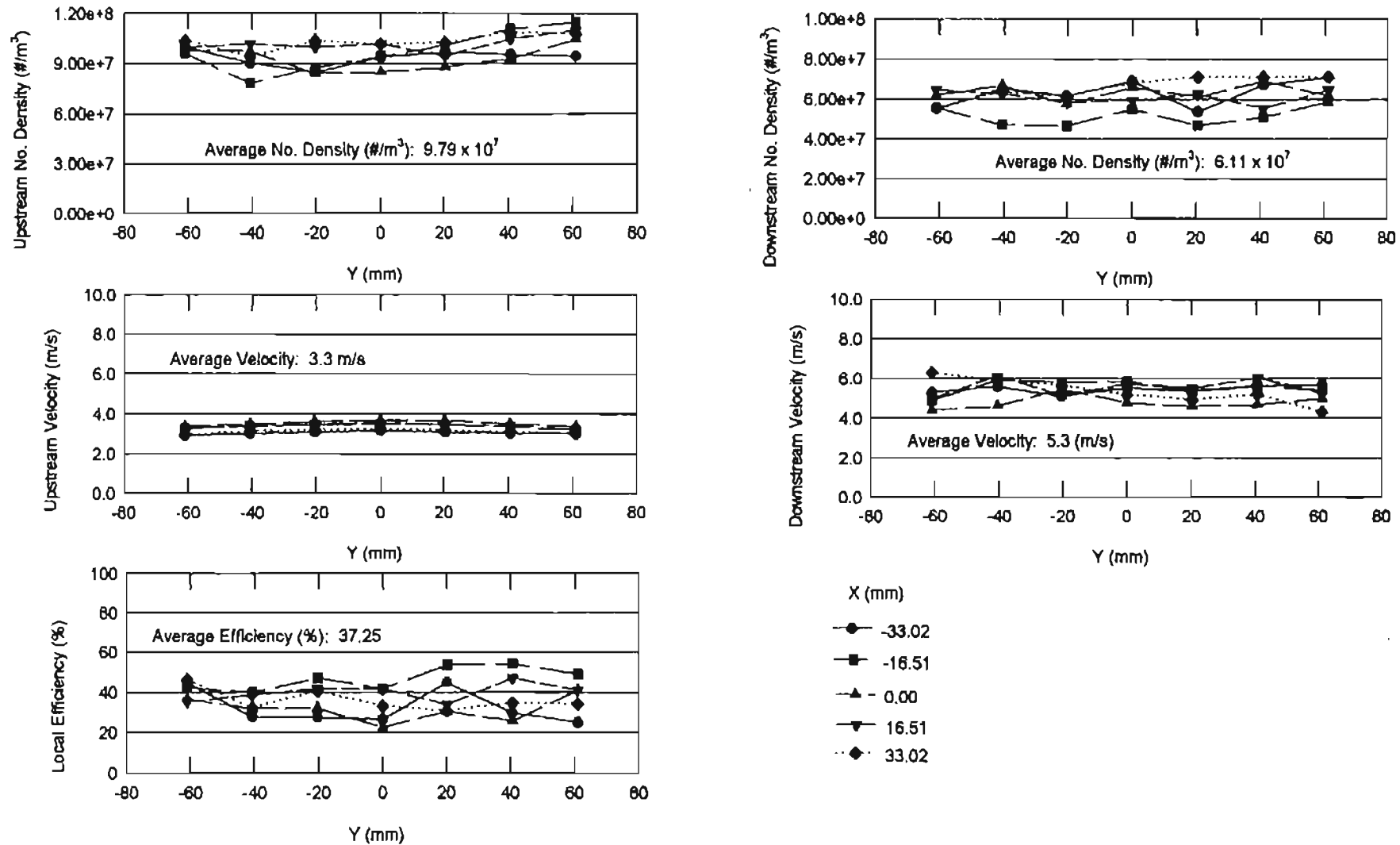
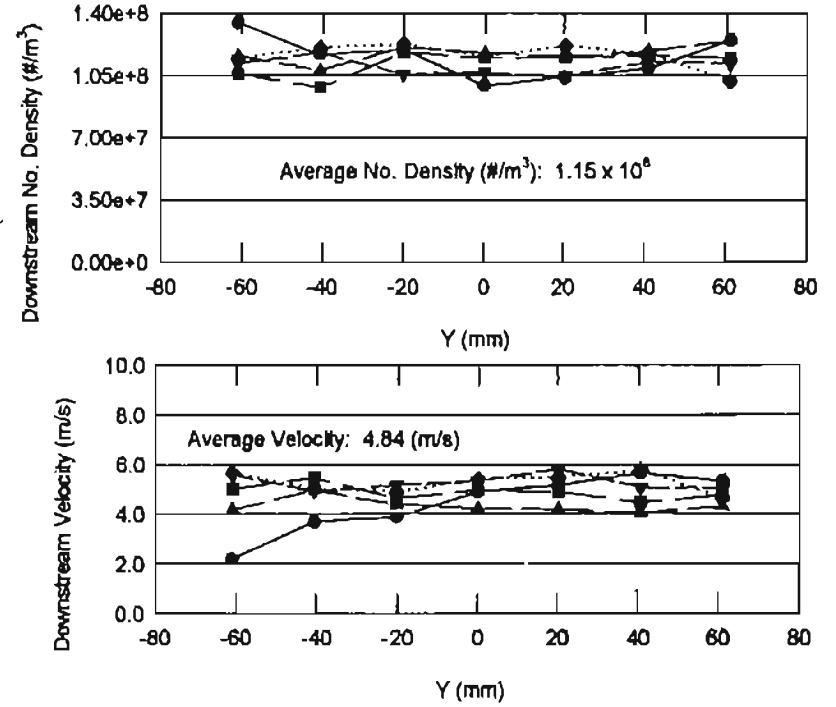
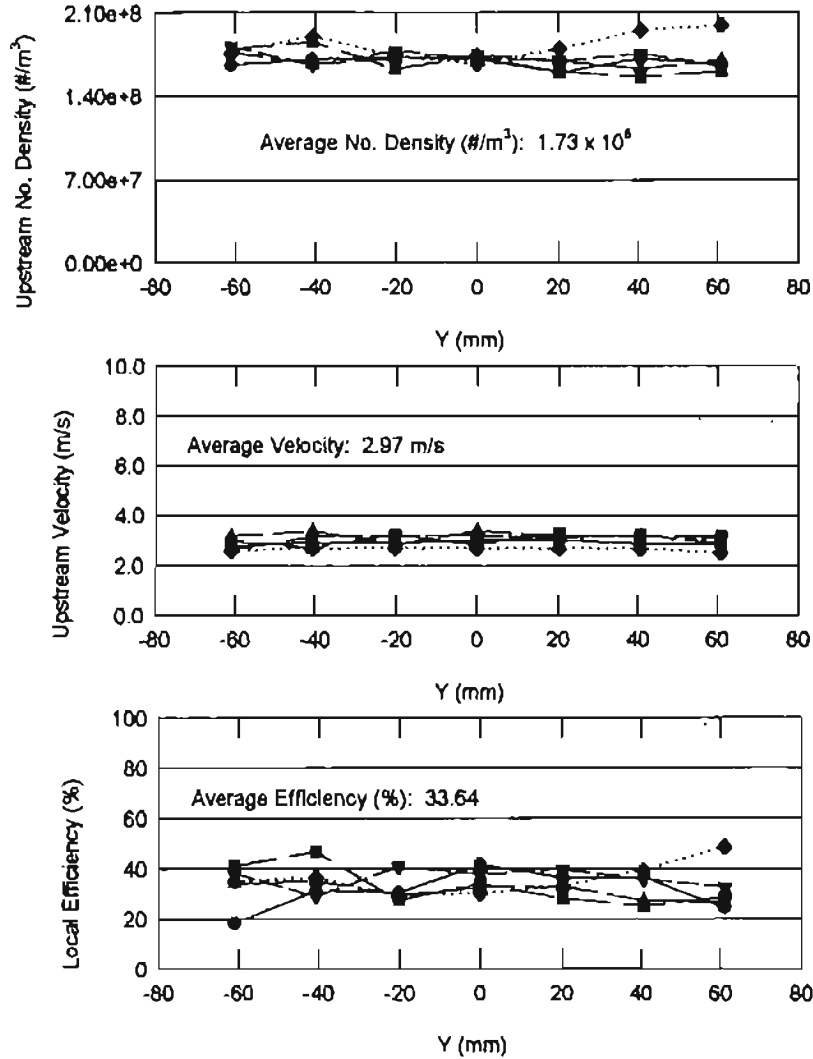


Figure B-14: Pleated Filter Efficiency for Test SAH100_05_2 at 146.36 m³/hr



- X (mm)
- -33.02
 - -16.51
 - ▲ - 0.00
 - ▼ 16.51
 - ◆ 33.02

Figure B-15: Pleated Filter Efficiency for Test SAH100_05_3 at 146.36 m³/hr

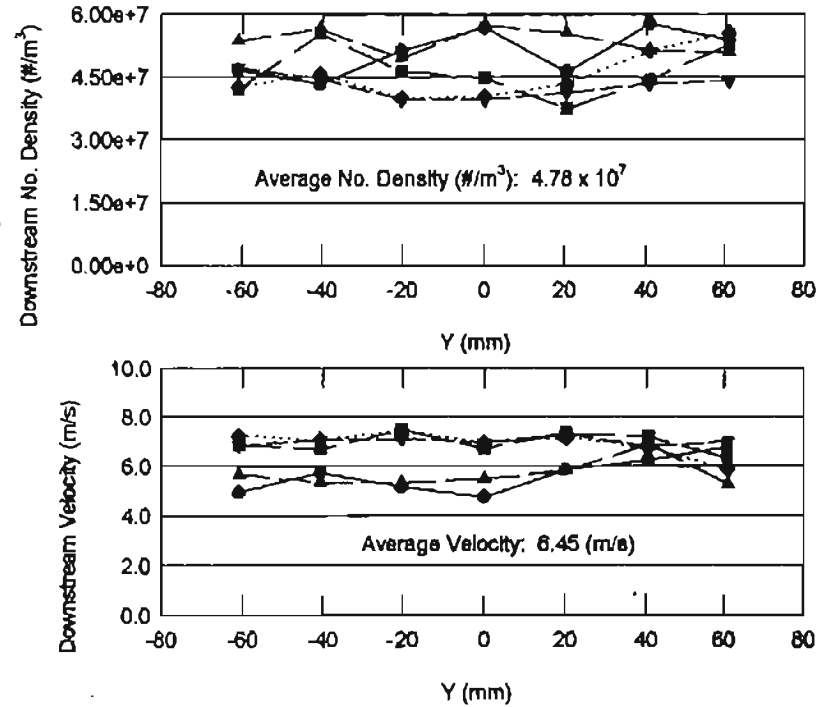
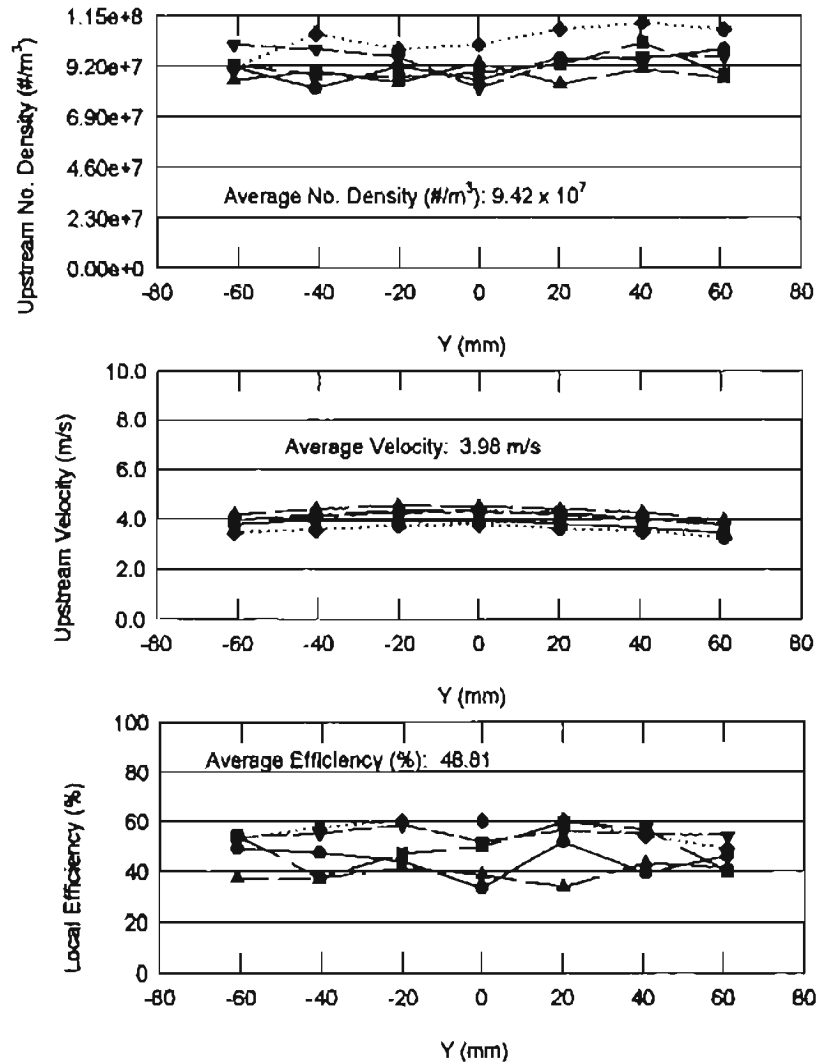
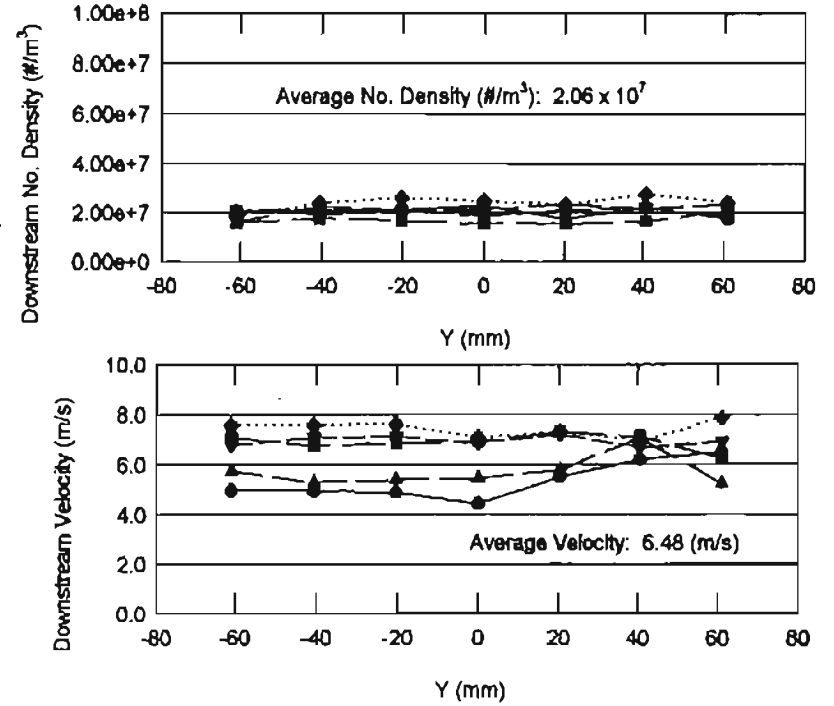
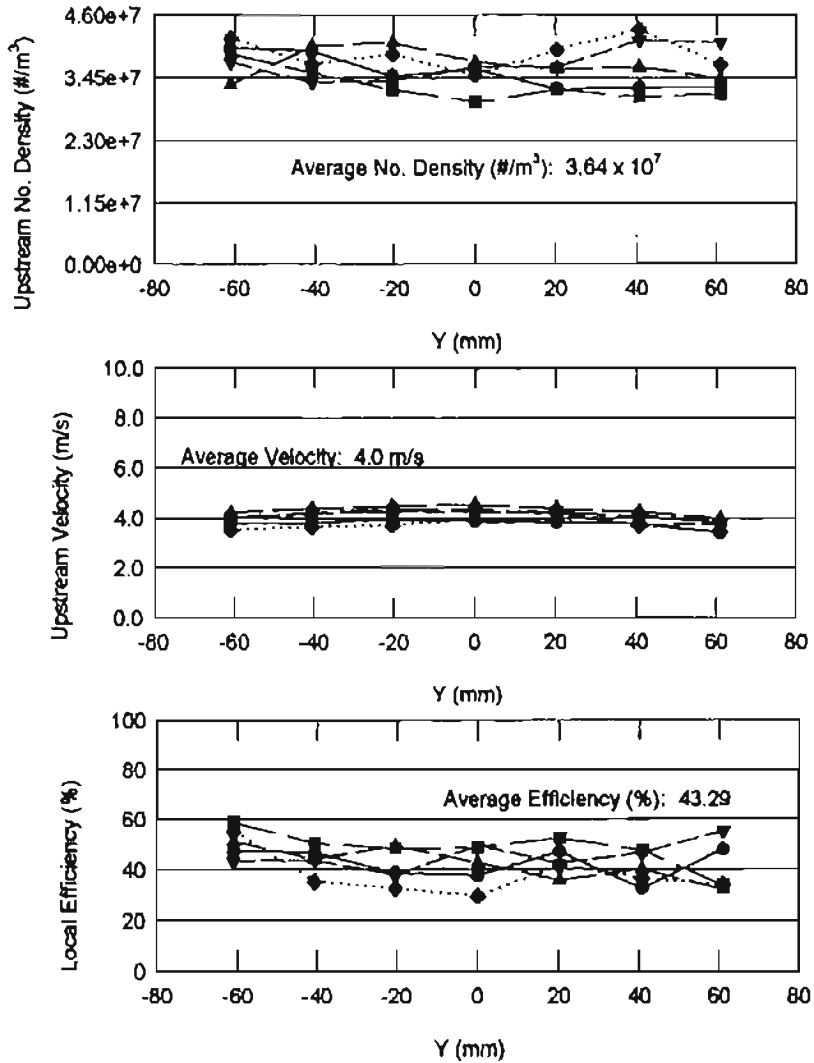


Figure B-16: Pleated Filter Efficiency for Test SAH125_05_1 at 188.45 m³/hr



- X (mm)
- -33.02
 - -16.51
 - ▲ 0.00
 - ▼ 16.51
 - ◆ 33.02

Figure B-17: Pleated Filter Efficiency for Test SAH125_05_2 at 188.45 m³/hr

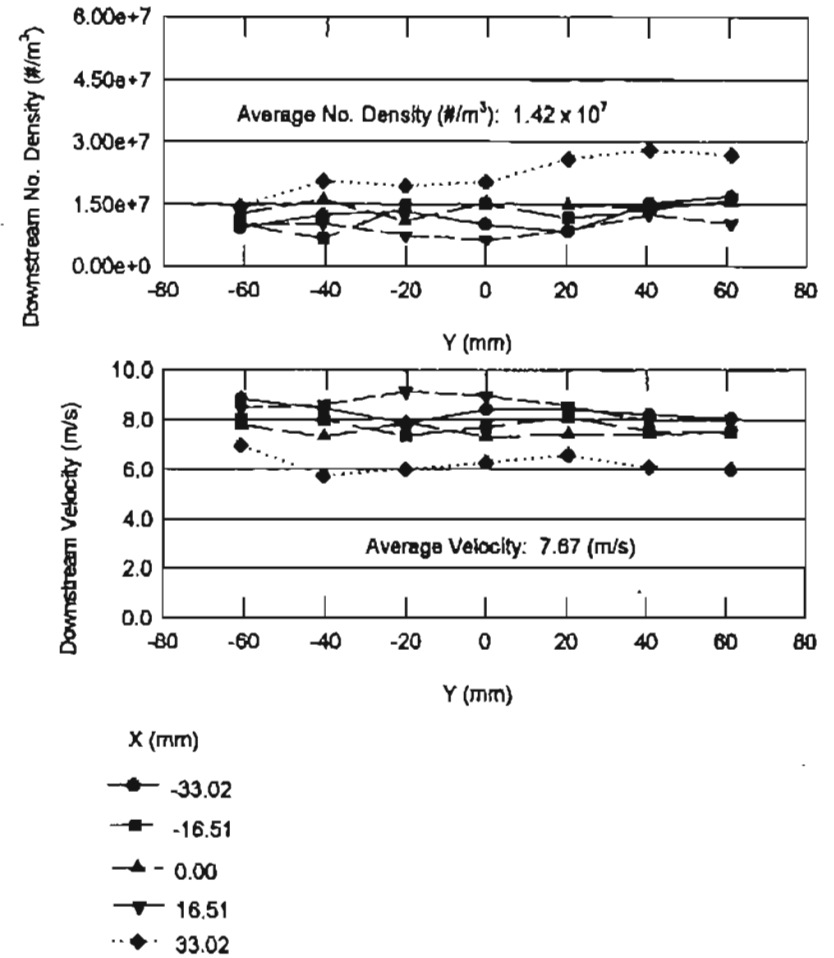
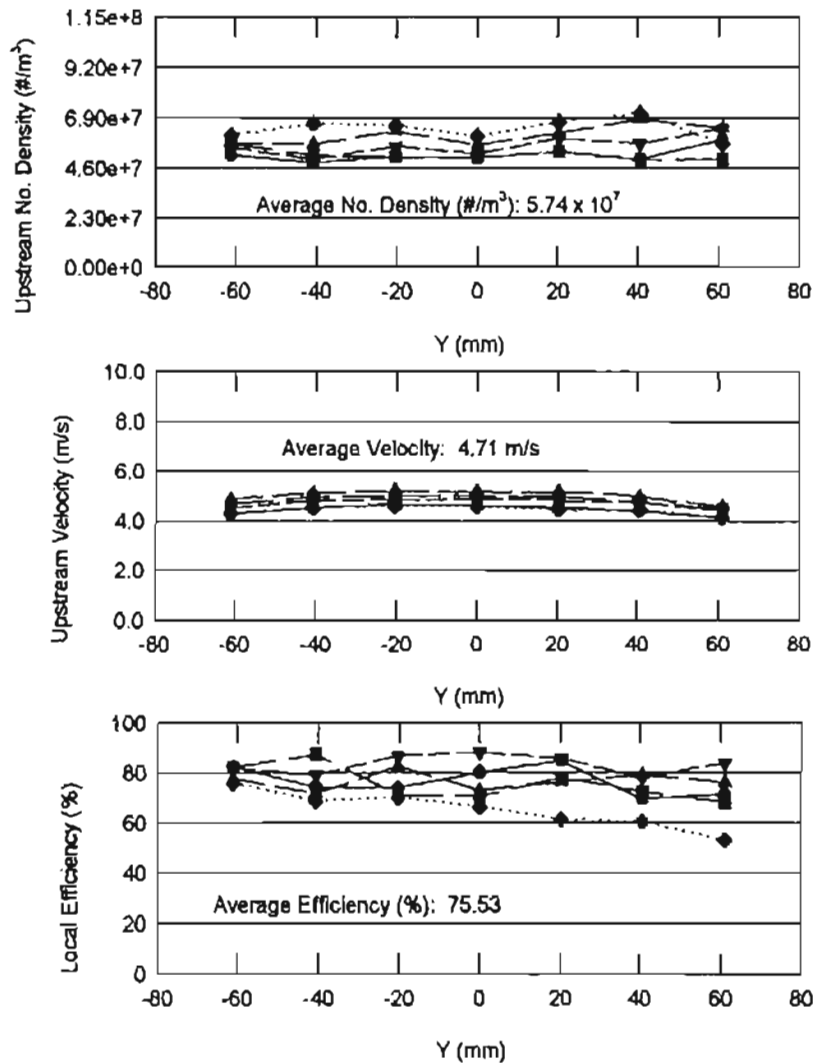


Figure B-18: Pleated Filter Efficiency for Test SAH150_05_1 at 230.54 m³/hr

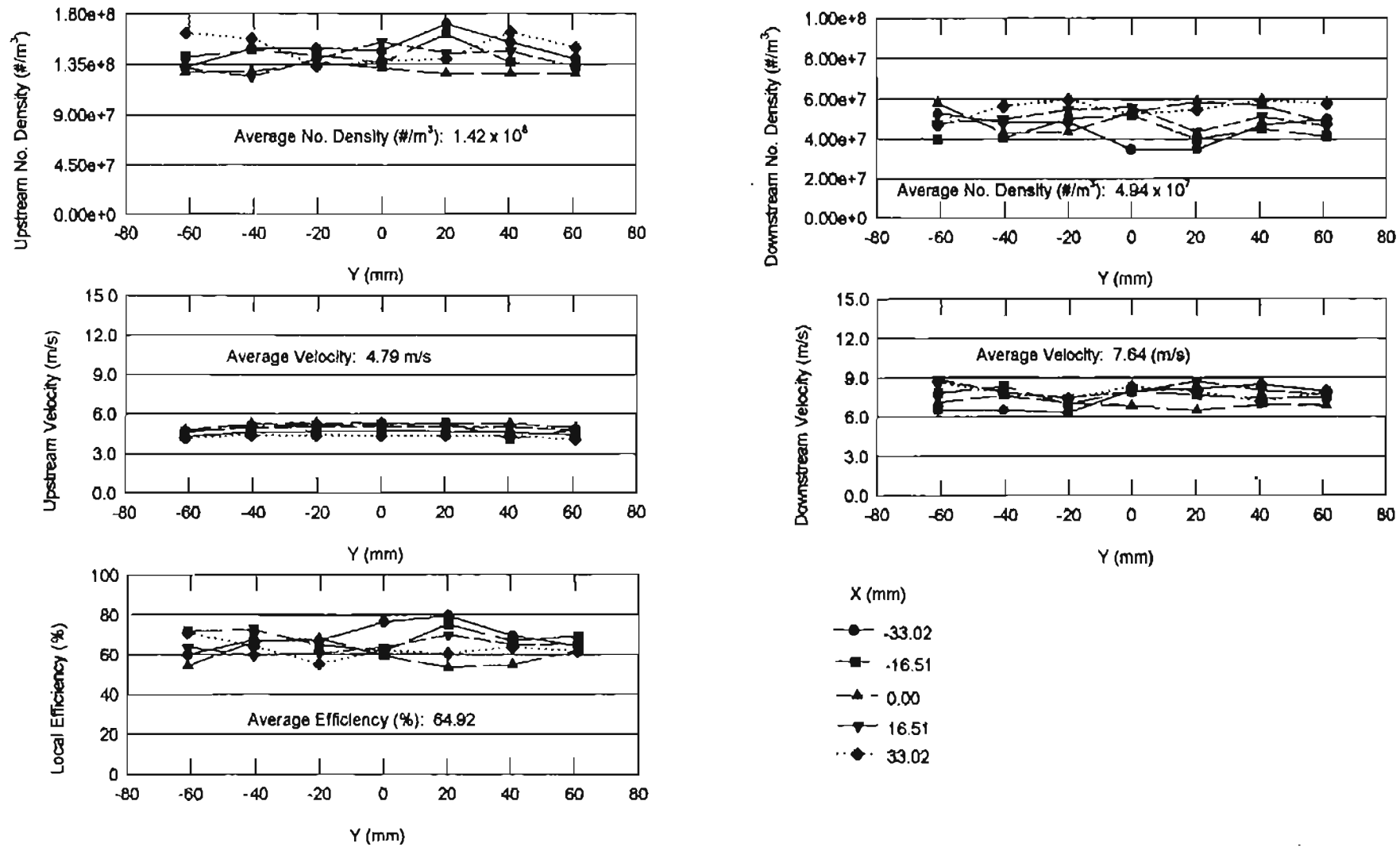


Figure B-19: Pleated Filter Efficiency for Test SAH150_05_2 at 230.54 m³/hr

APPENDIX C

RESULTS FOR 2.04 μm DIAMETER PSL PARTICLES IN THE SMALL ANGLE DIFFUSER HOUSING

Some of the test results for 2.04 μm diameter PSL spheres have been shown and discussed in Chapter 5. The other test results are presented in this appendix. The results presented here are the upstream and downstream local velocity measurements, the upstream and downstream local number densities, and the local efficiencies for each of the additional tests.

The tests have been alphanumeric designations, which specify the housing, flow rates, particle size and the repeat number. SAH75_2_2 stands for Small Angle Housing experiment for 75 cfm (104.26 m^3/hr) with 2.04 μm particles (rounded to 2) and is the second experiment conducted for that flow rate. Files have been named as explained in Chapter 4 of this thesis.

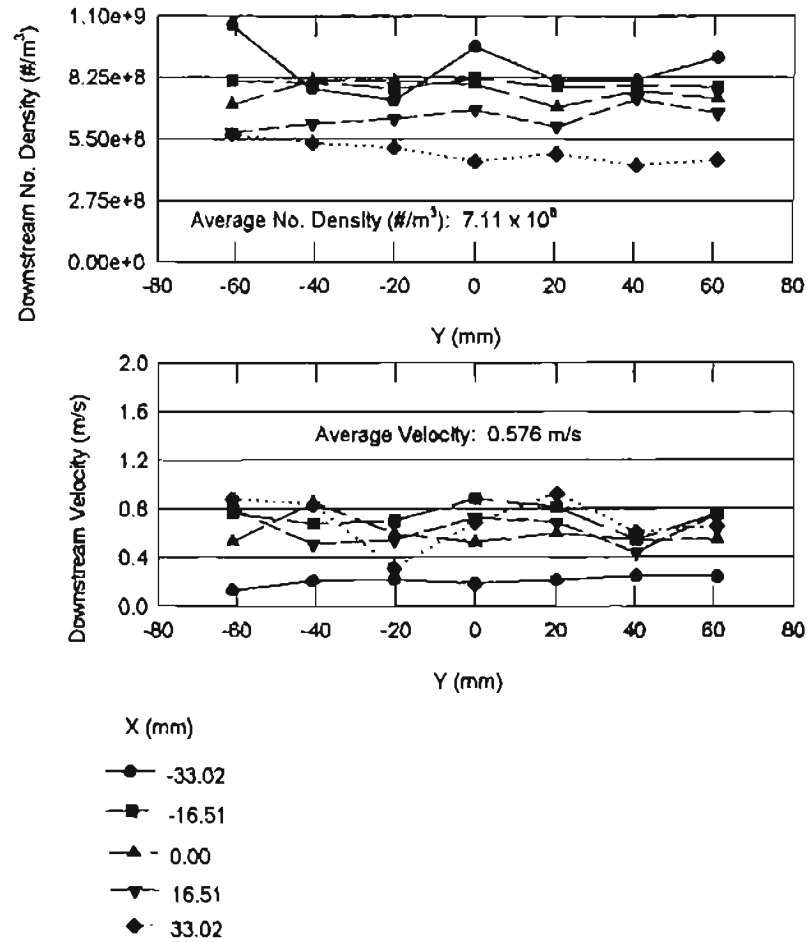
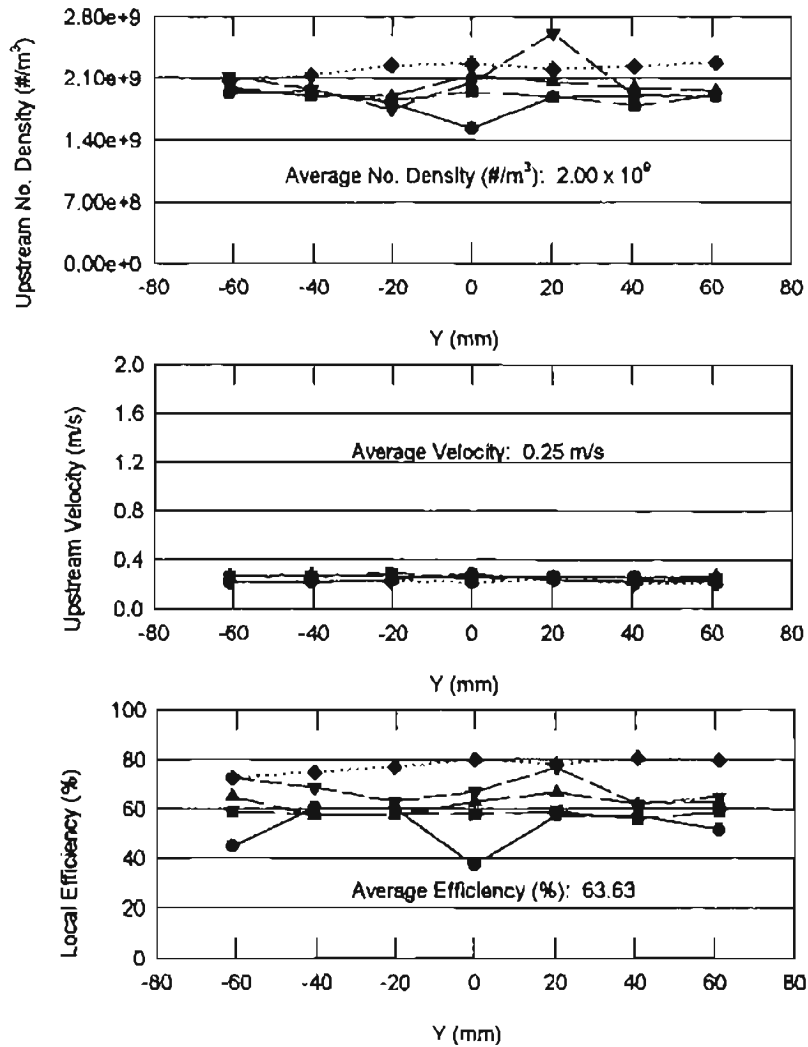
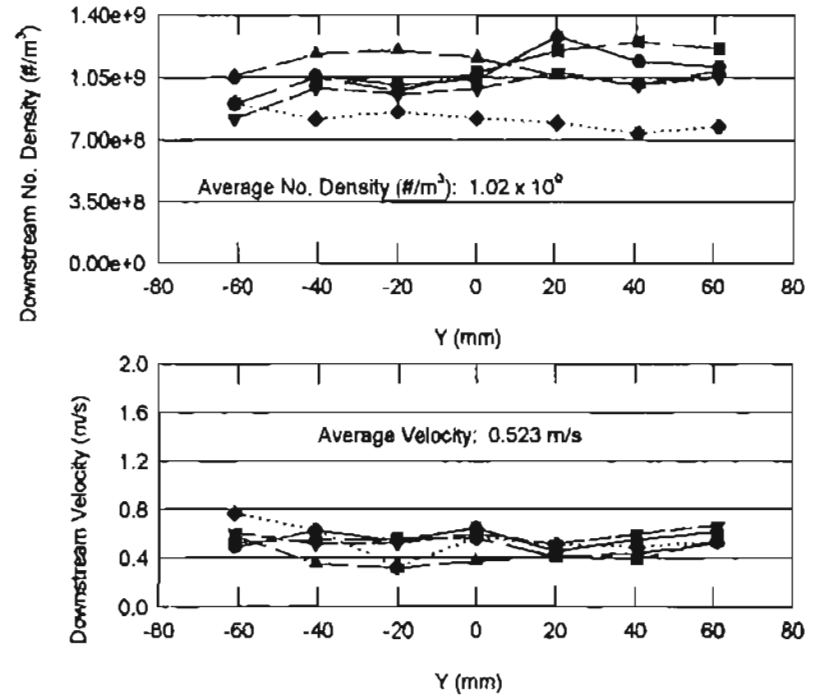
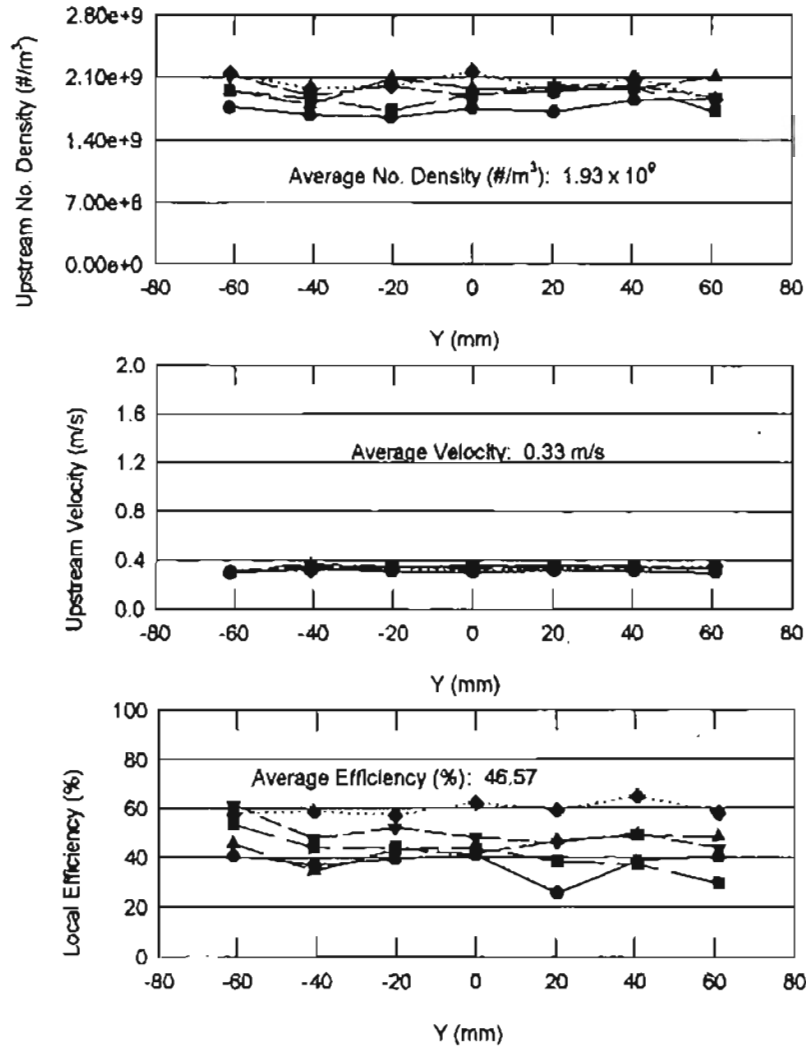


Figure C-1: Pleated Filter Efficiency for Test SAH12_2_1 at 16.78 m³/hr



- X (mm)
- -33.02
 - -16.51
 - ▲ 0.00
 - ▼ 16.51
 - ◆ 33.02

Figure C-2: Pleated Filter Efficiency for Test SAH12_2_2 at 16.78 m³/hr

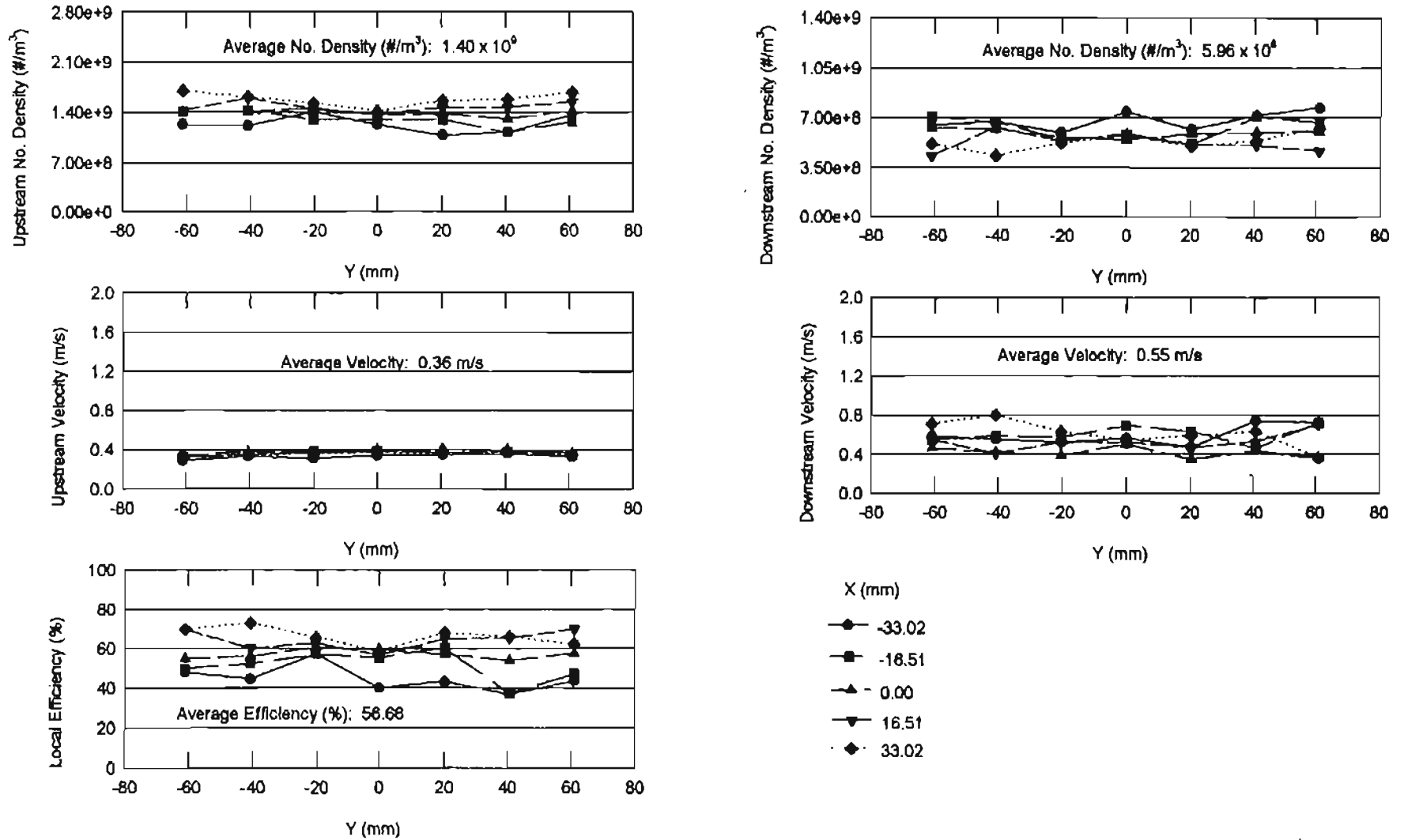


Figure C-3: Pleated Filter Efficiency for Test SAH12_2_3 at 16.78 m³/hr

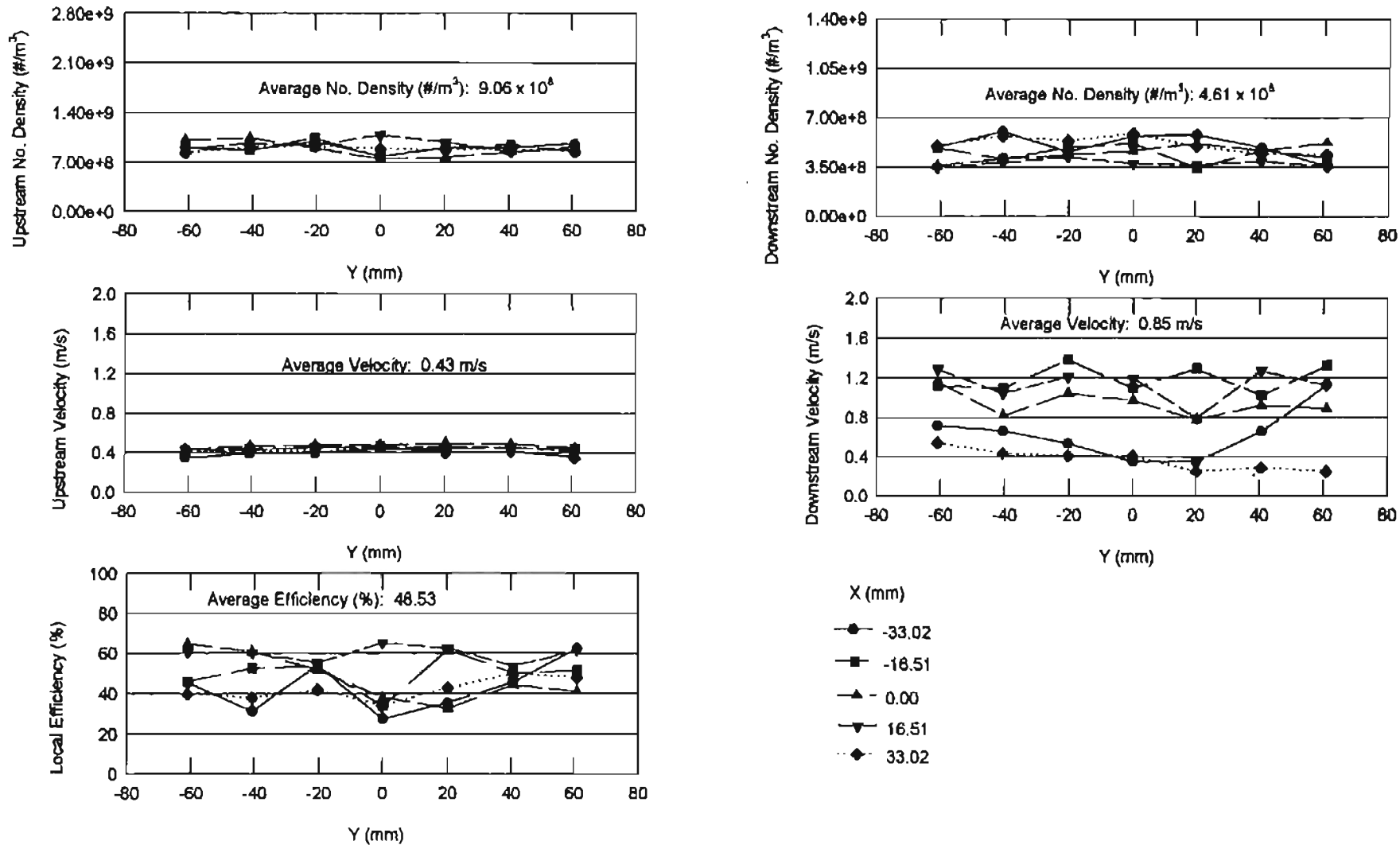


Figure C-4: Pleated Filter Efficiency for Test SAH15_2_1 at 21.55 m³/hr

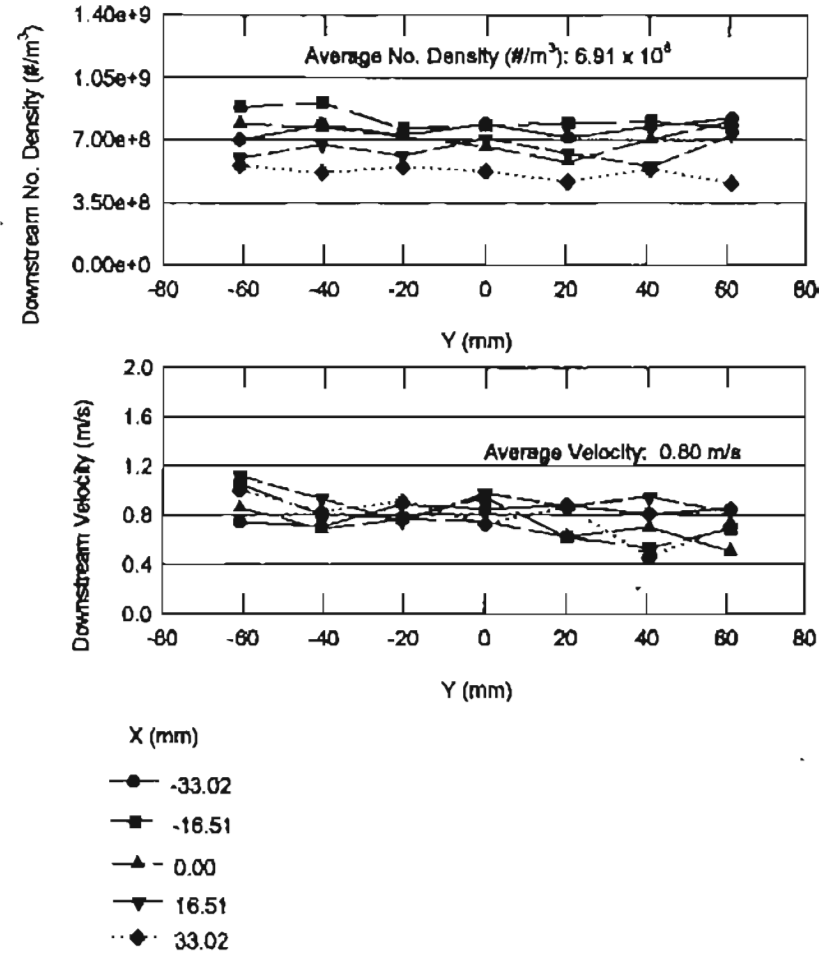
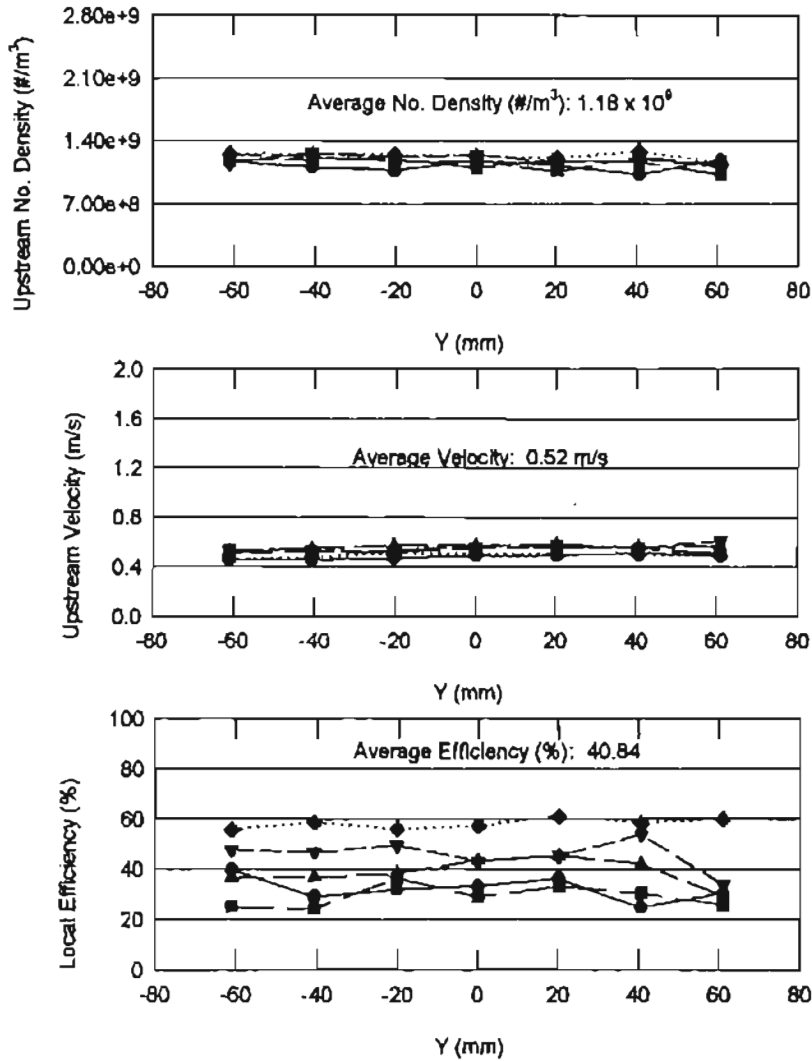


Figure C-5: Pleated Filter Efficiency for Test SAH15_2_2 at 21.55 m³/hr

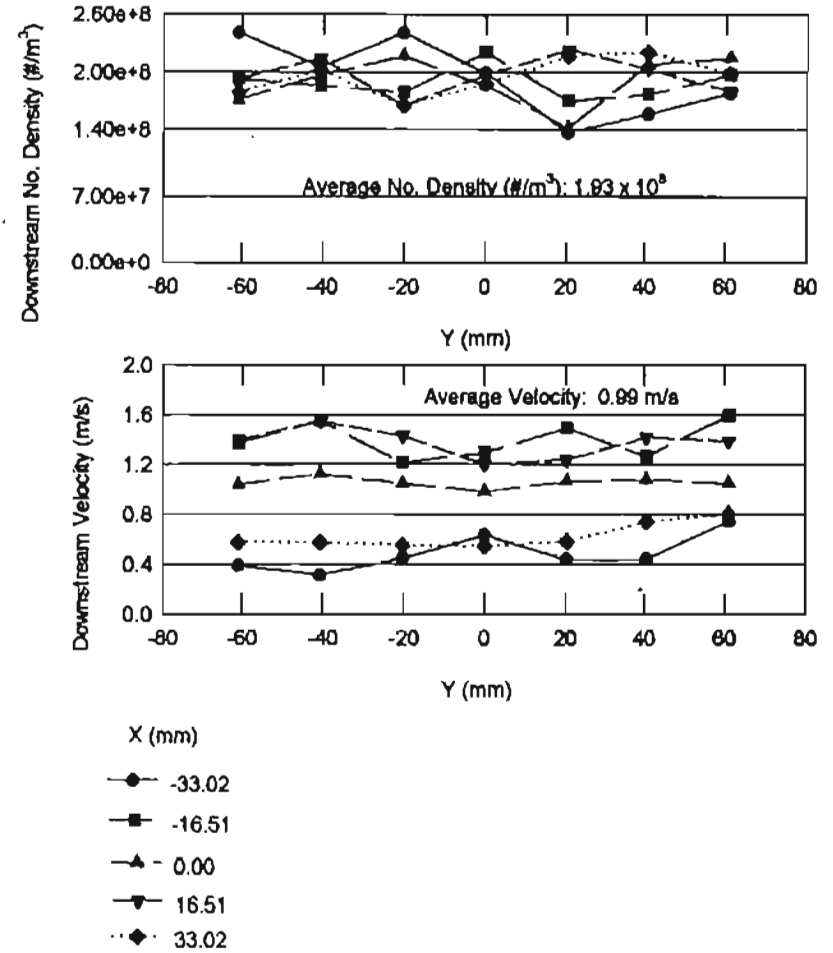
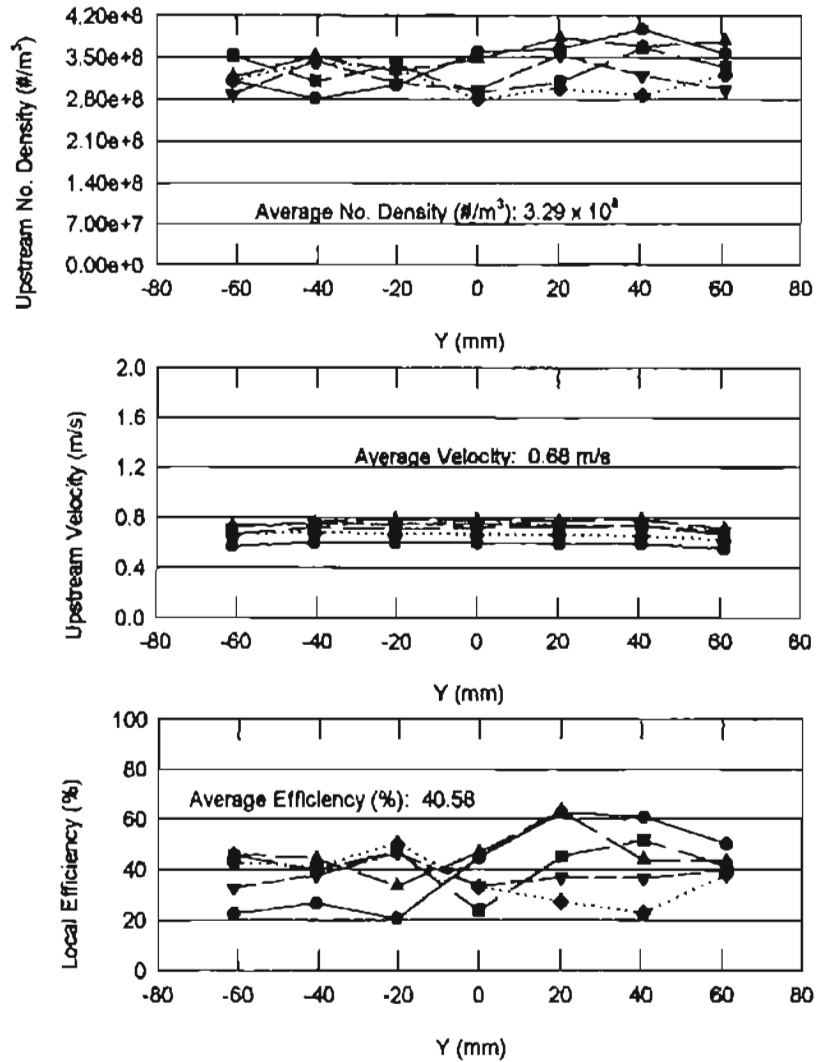


Figure C-6: Pleated Filter Efficiency for Test SAH20_2_1 at 29.48 m³/hr

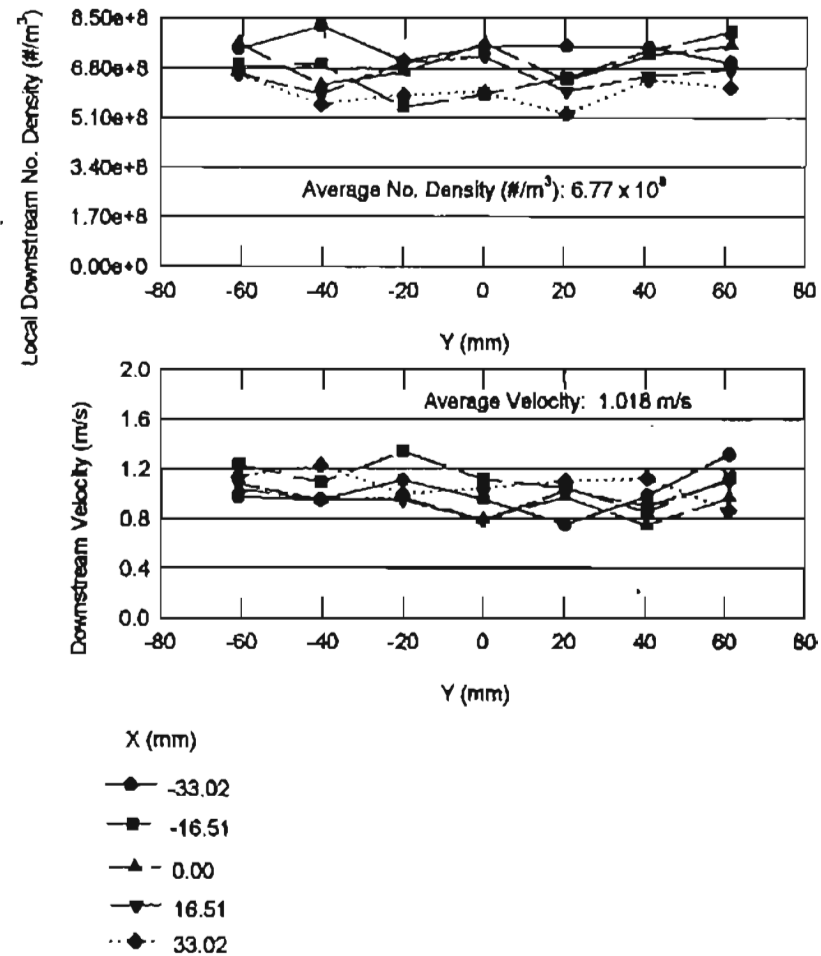
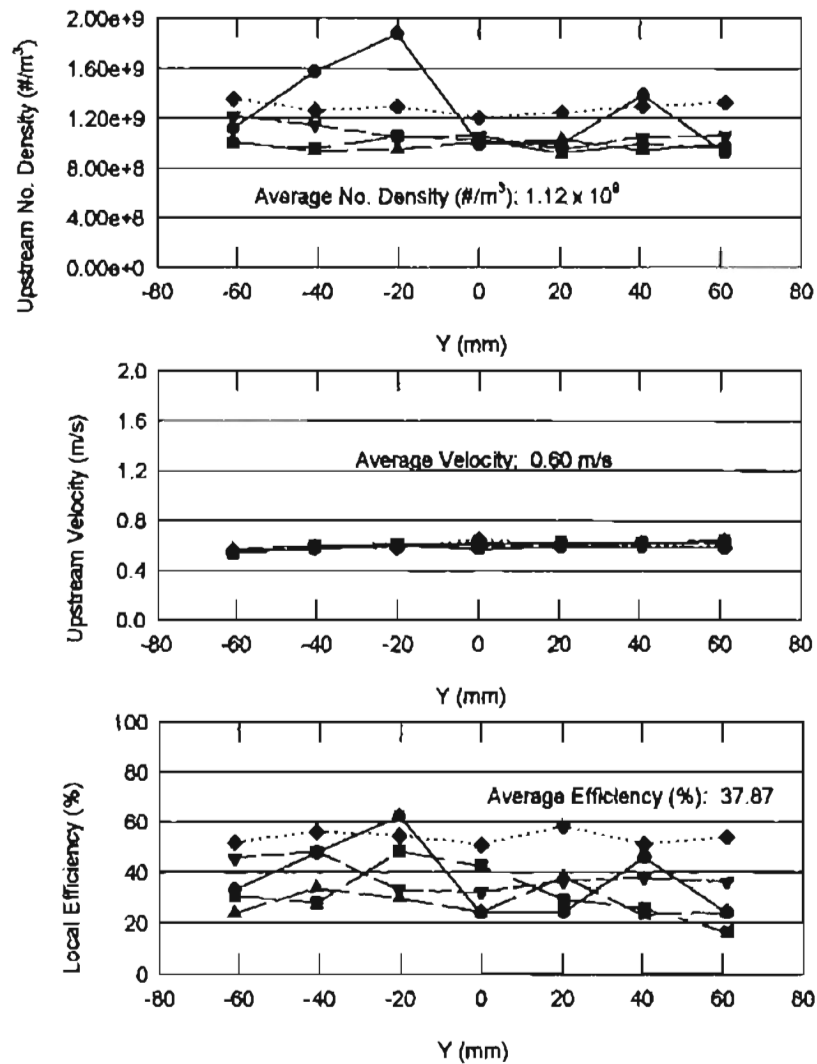


Figure C-7: Pleated Filter Efficiency for Test SAH20_2_2 at 29.48 m³/hr

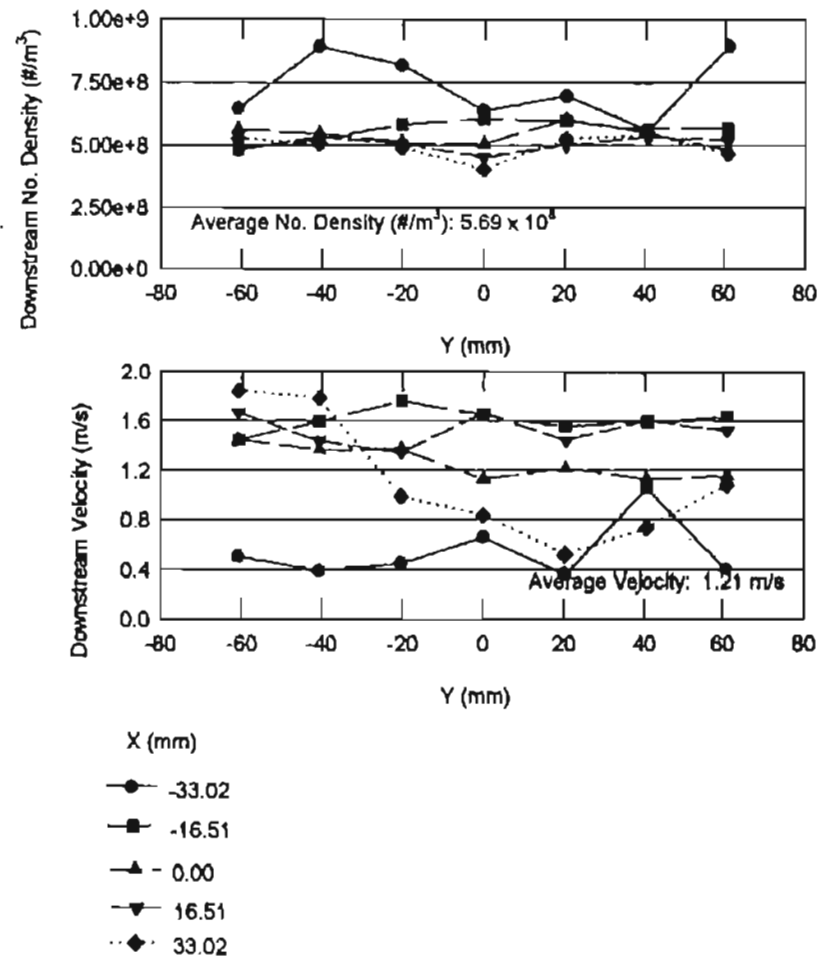
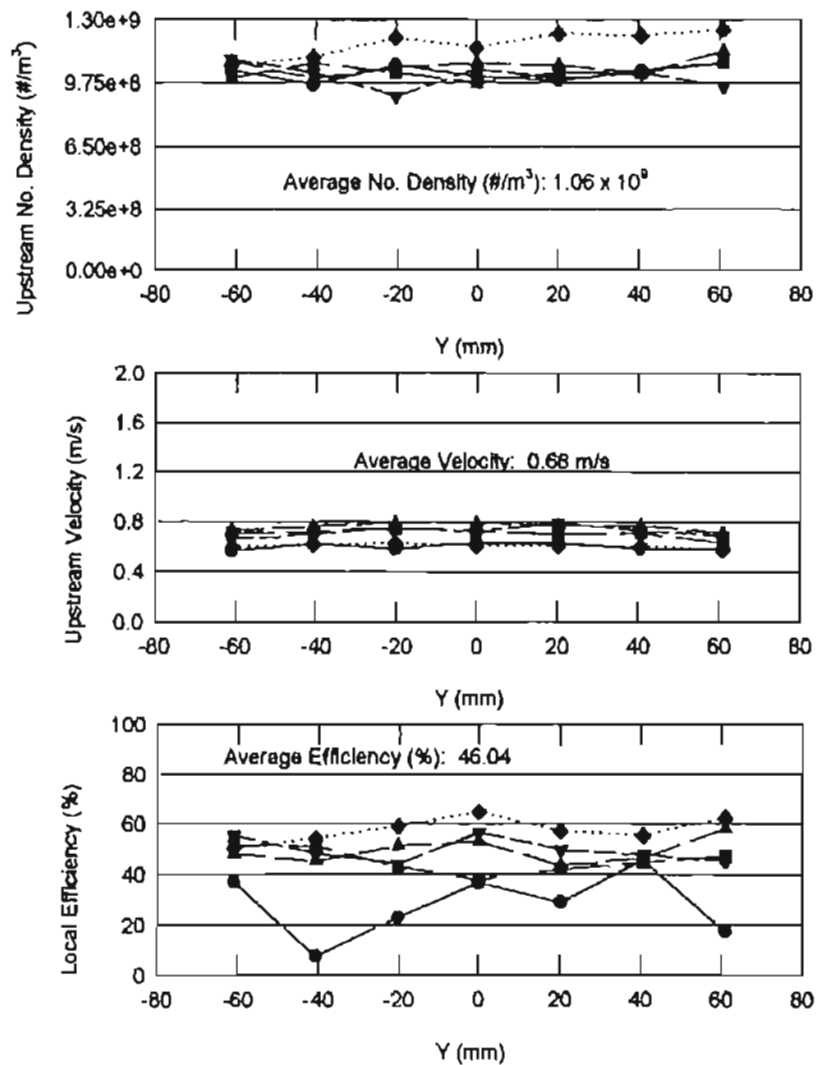


Figure C-8: Pleated Filter Efficiency for Test SAH25_2_1 at 37.42 m³/hr

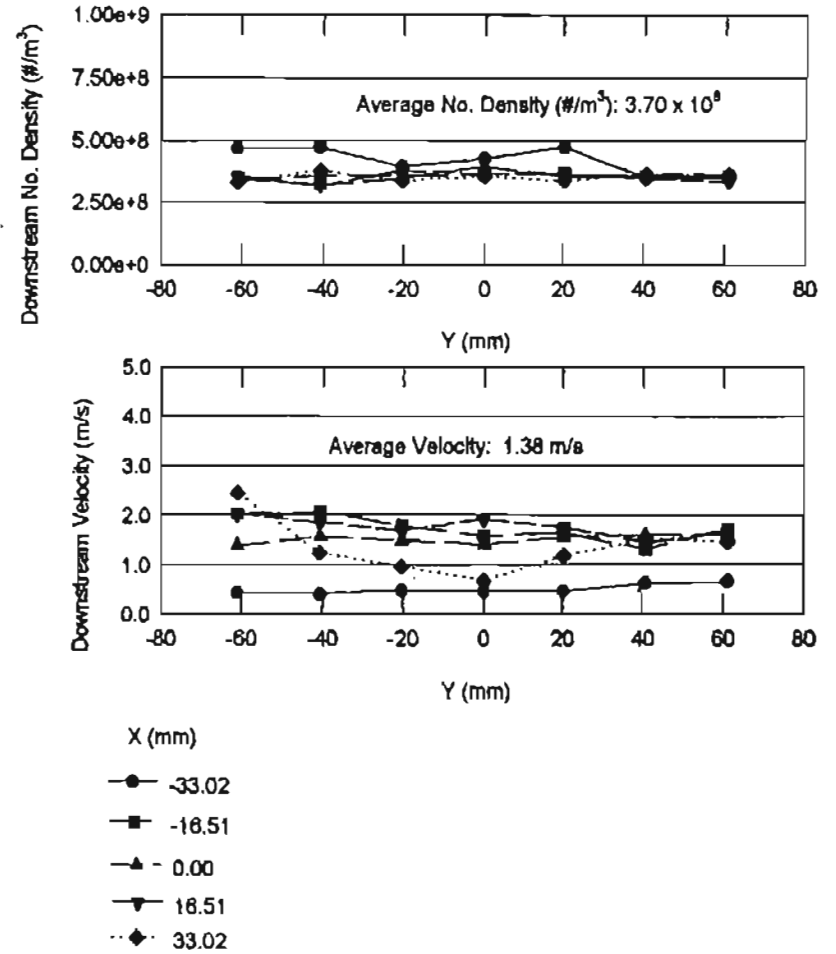
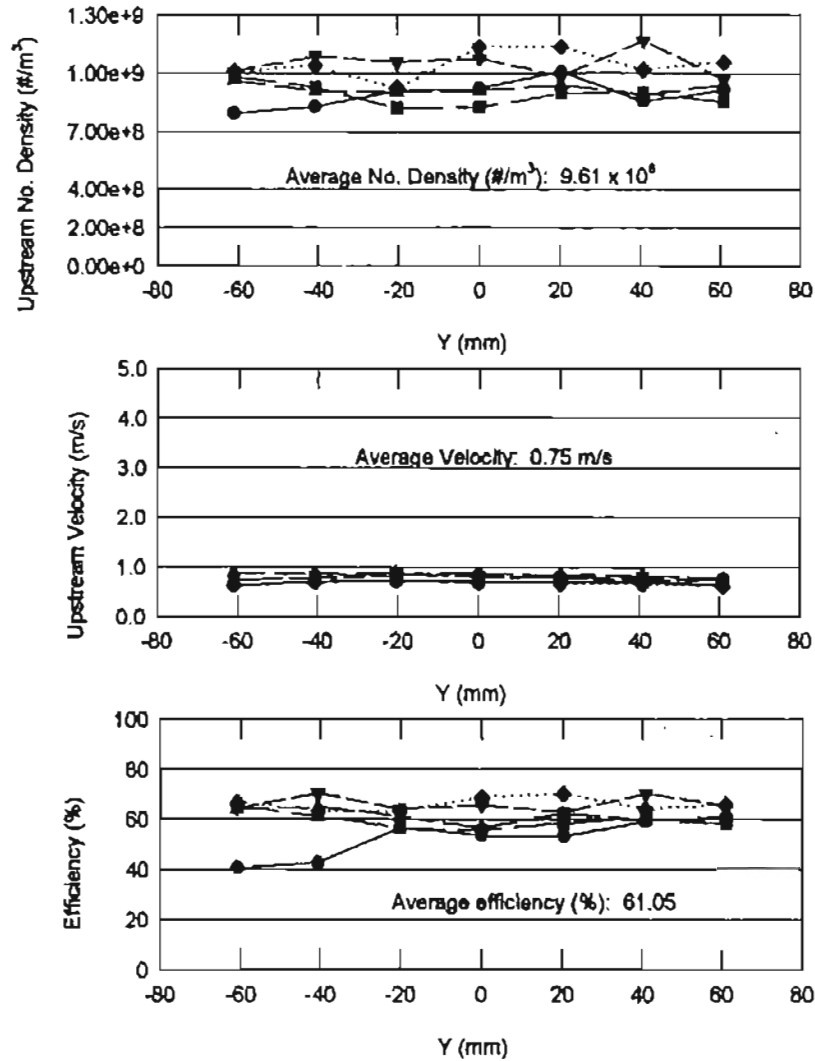


Figure C-9: Pleated Filter Efficiency for Test SAH25_2_2 at 37.42 m³/hr

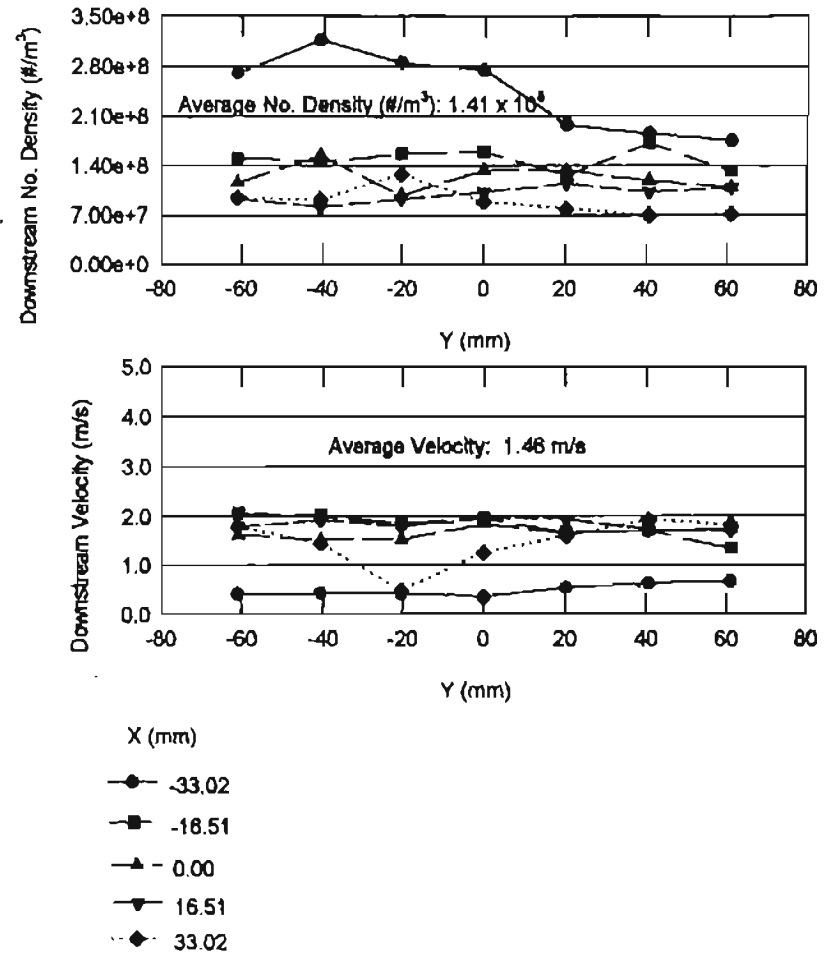
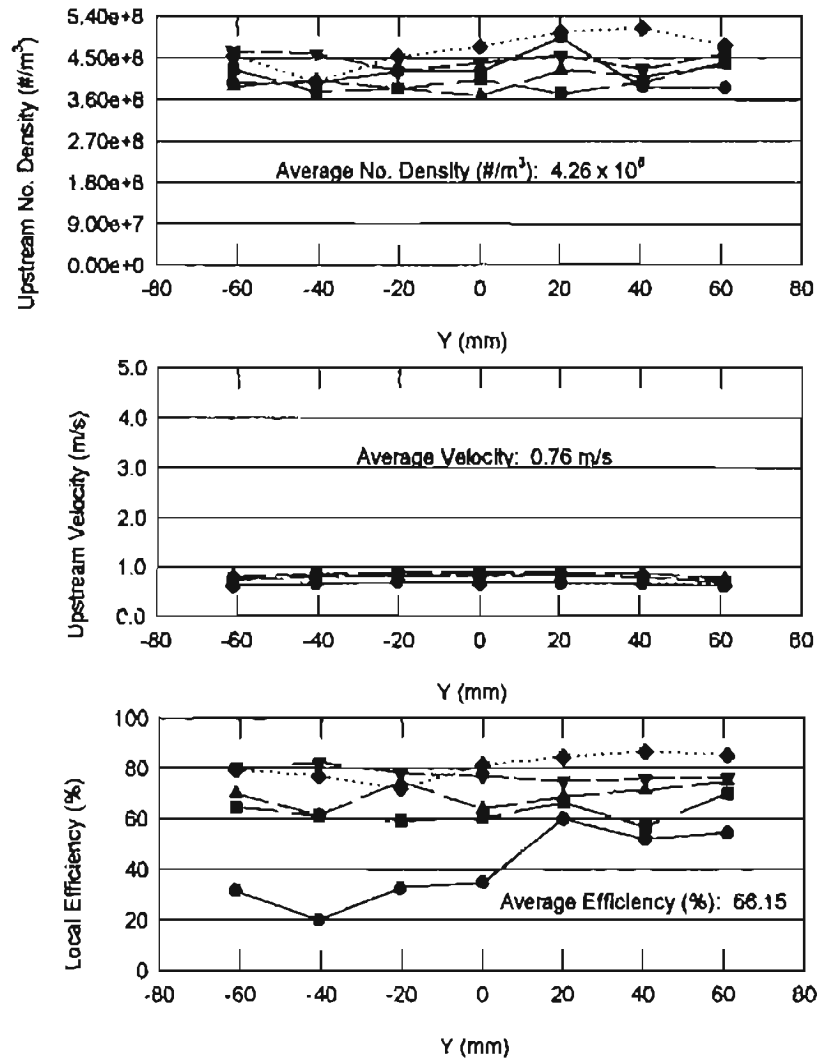


Figure C-10: Pleated Filter Efficiency for Test SAH40_2_1 at 61.20 m³/hr

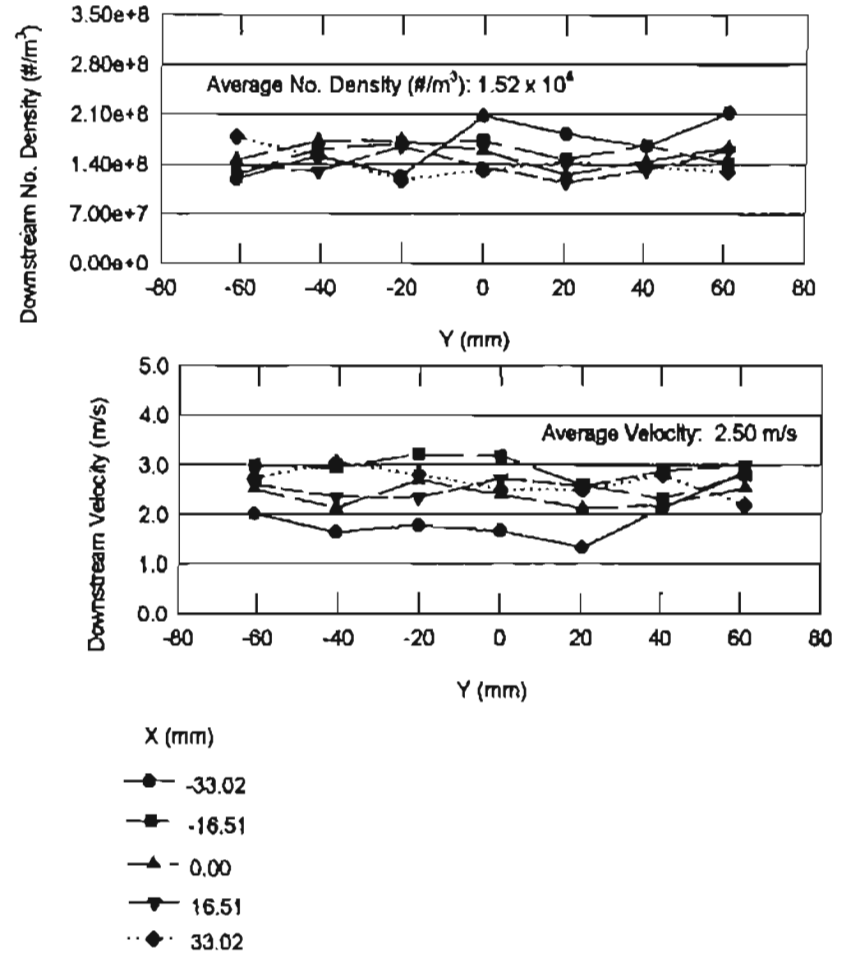
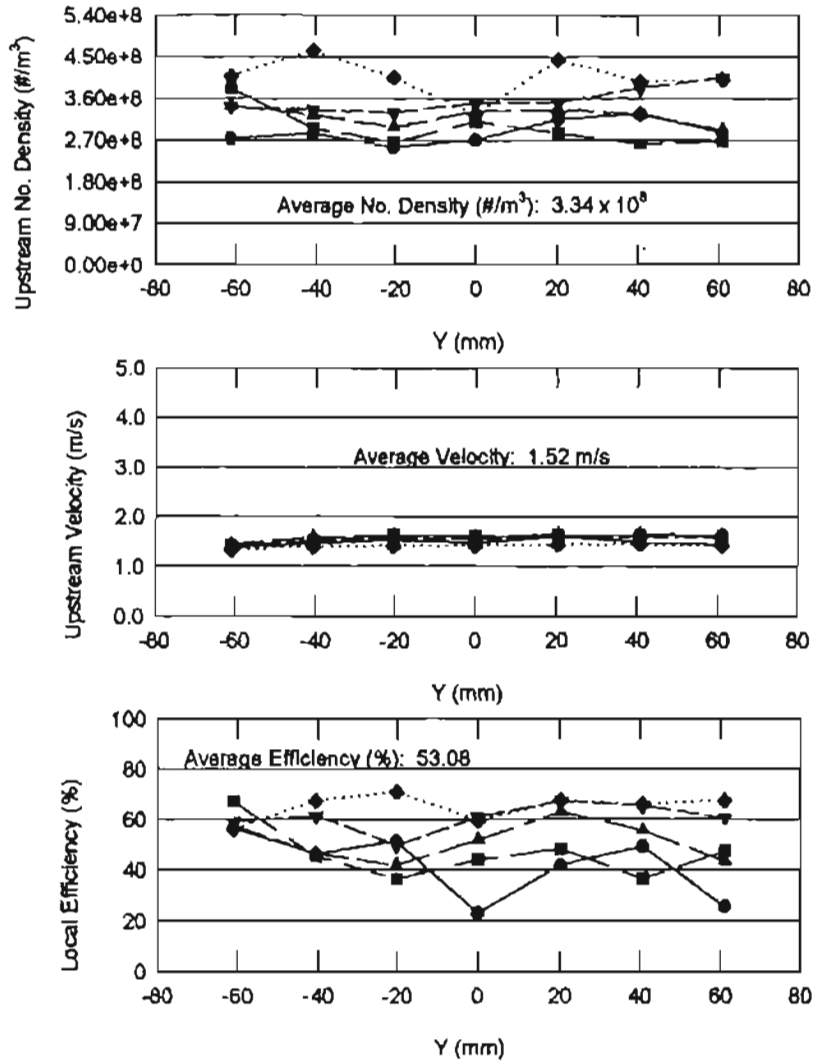


Figure C-11: Pleated Filter Efficiency for Test SAH40_2_2 at 61.20 m³/hr

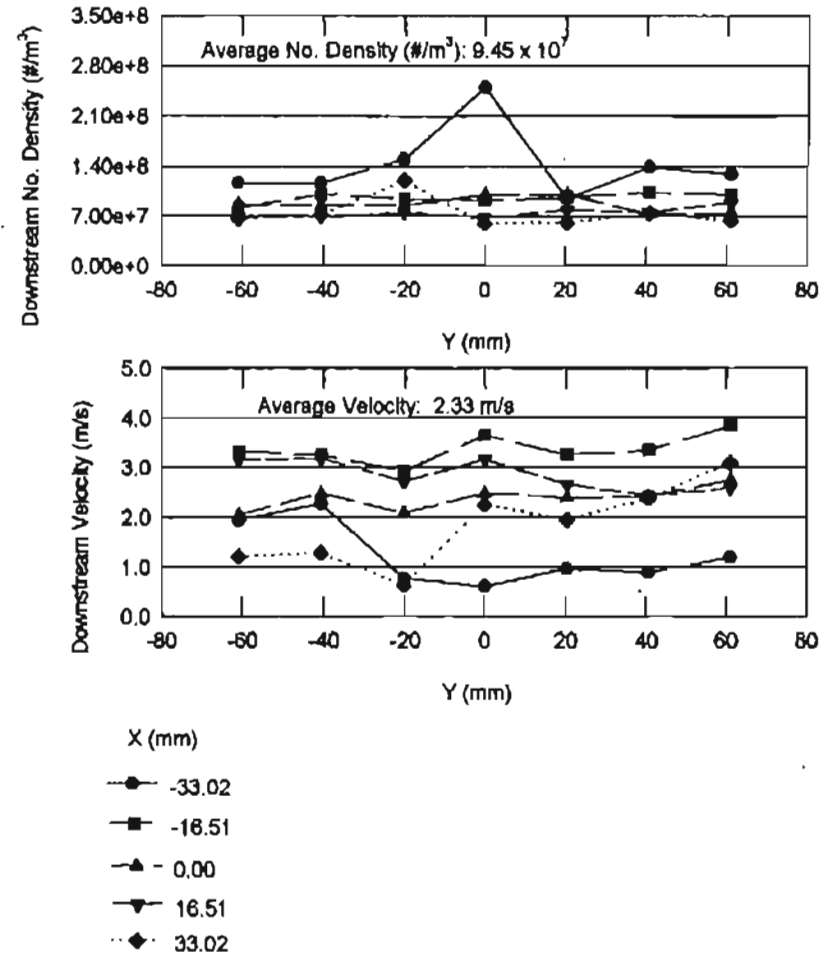
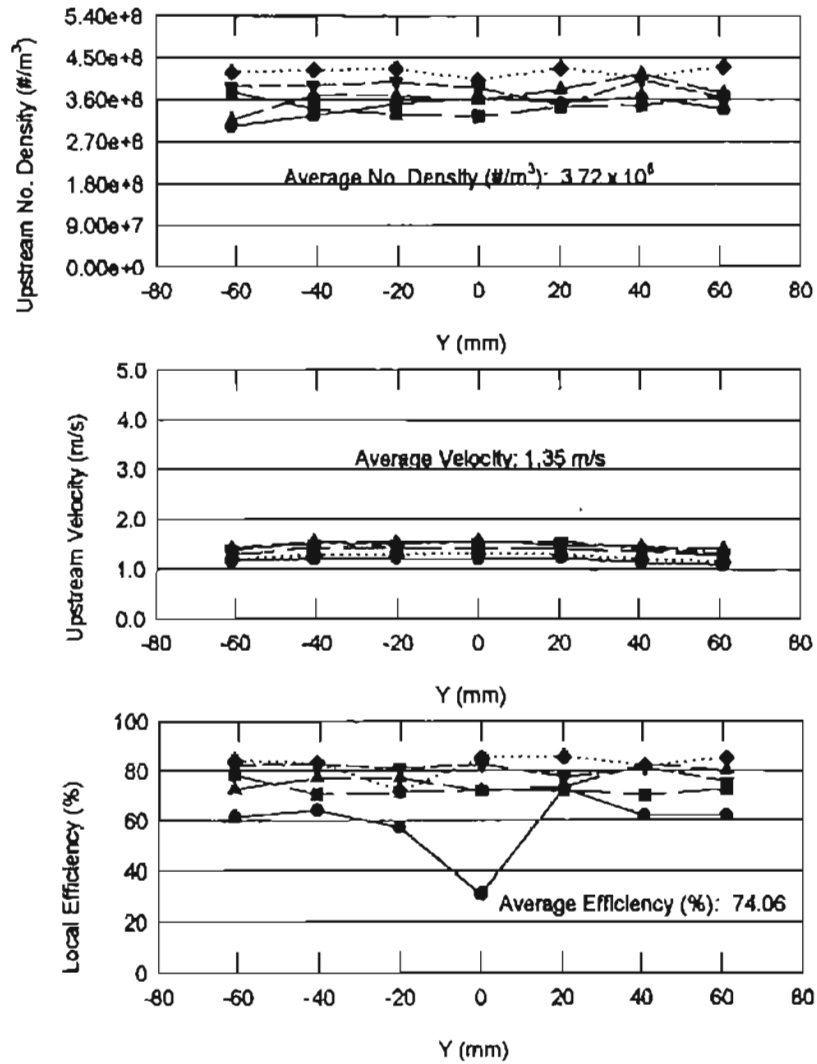


Figure C-12: Pleated Filter Efficiency for Test SAH50_2_1 at 77.07 m³/hr

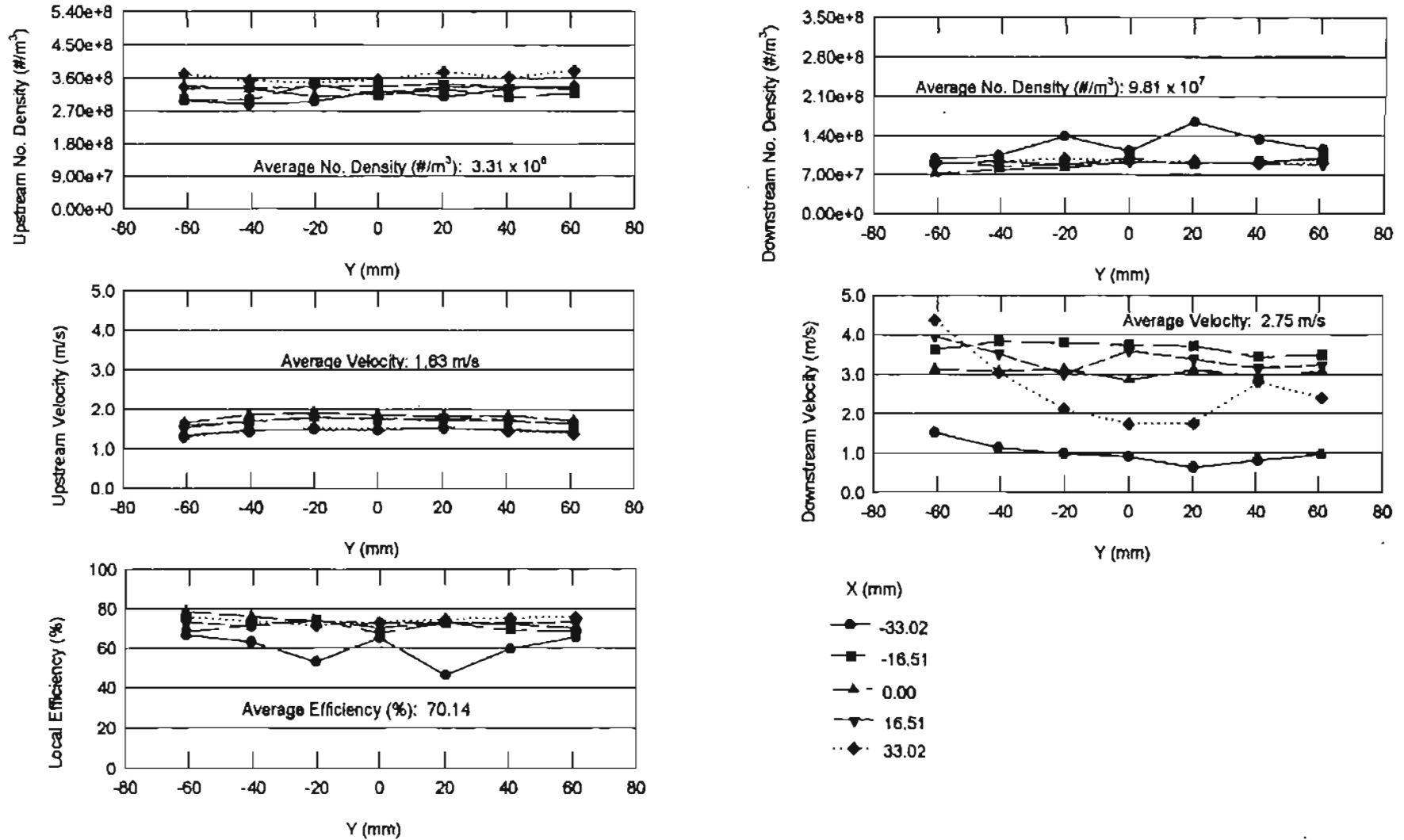
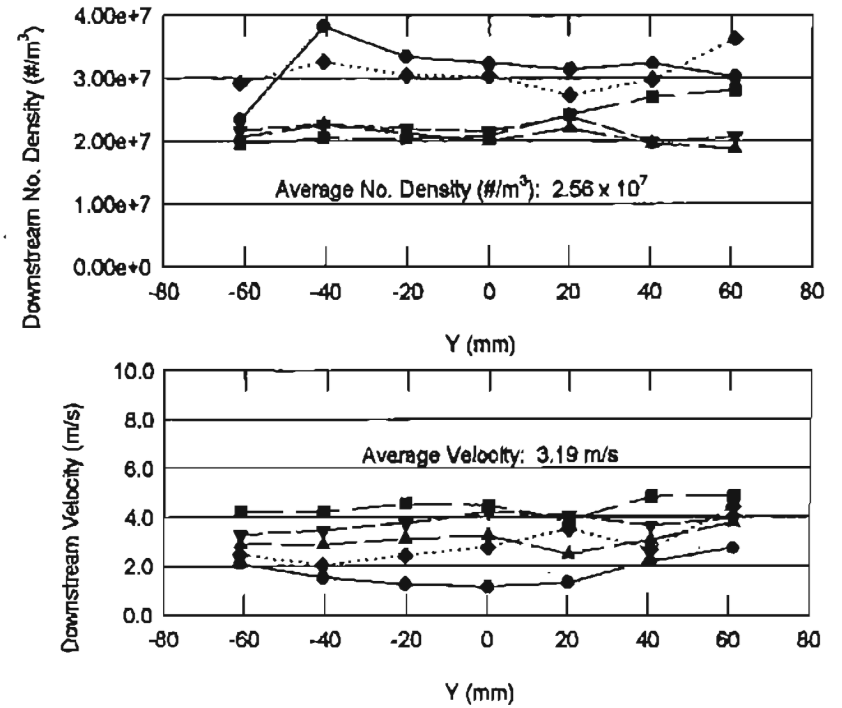
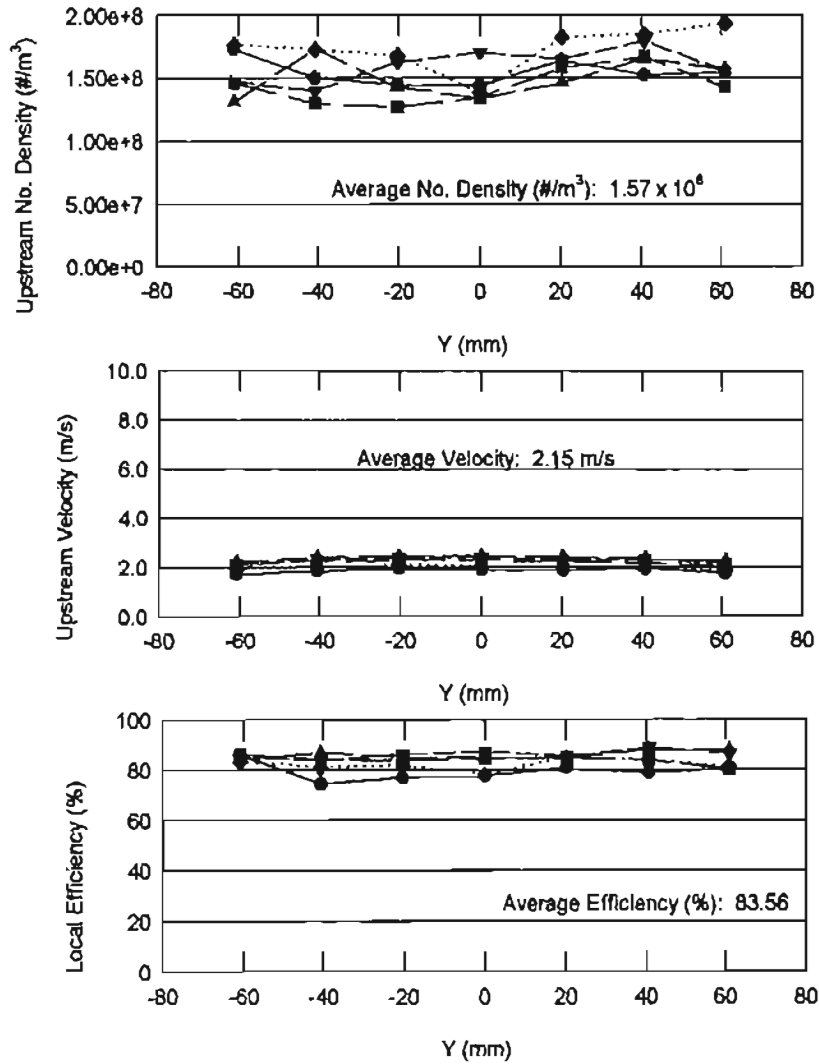


Figure C-13: Pleated Filter Efficiency for Test SAH50_2_2 at 77.07 m³/hr



- X (mm)
- -33.02
 - -16.51
 - ▲ 0.00
 - ▼ 16.51
 - ◆ 33.02

Figure C-14: Pleated Filter Efficiency for Test SAH75_2_1 at 104.26 m³/hr

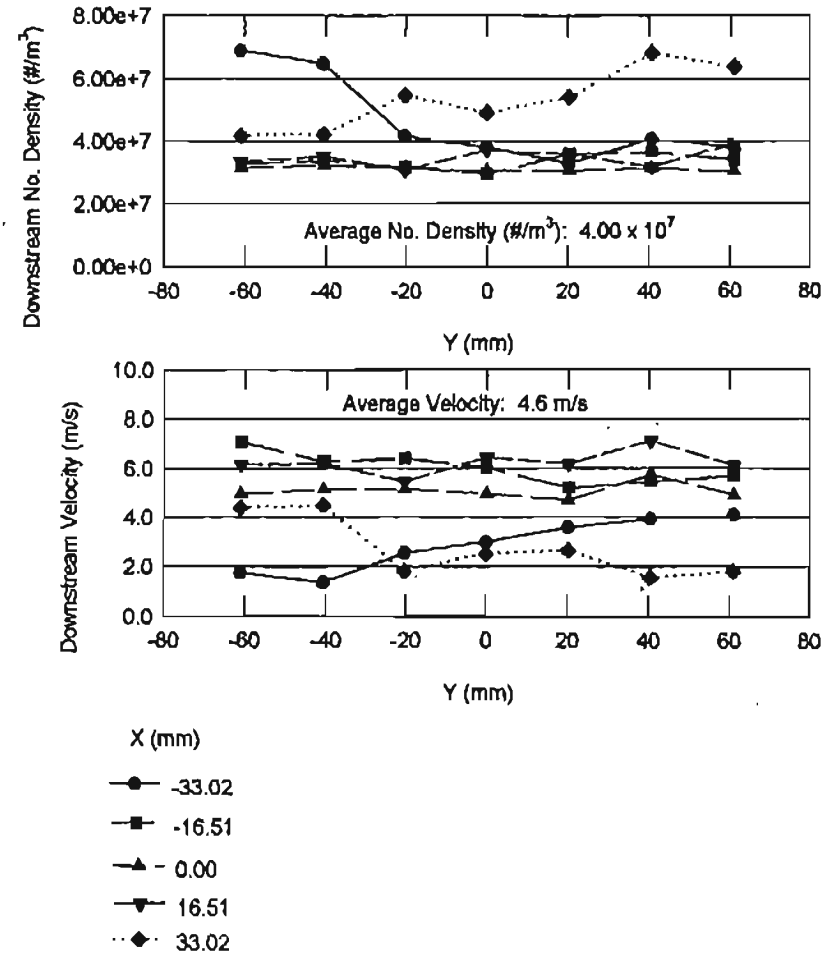
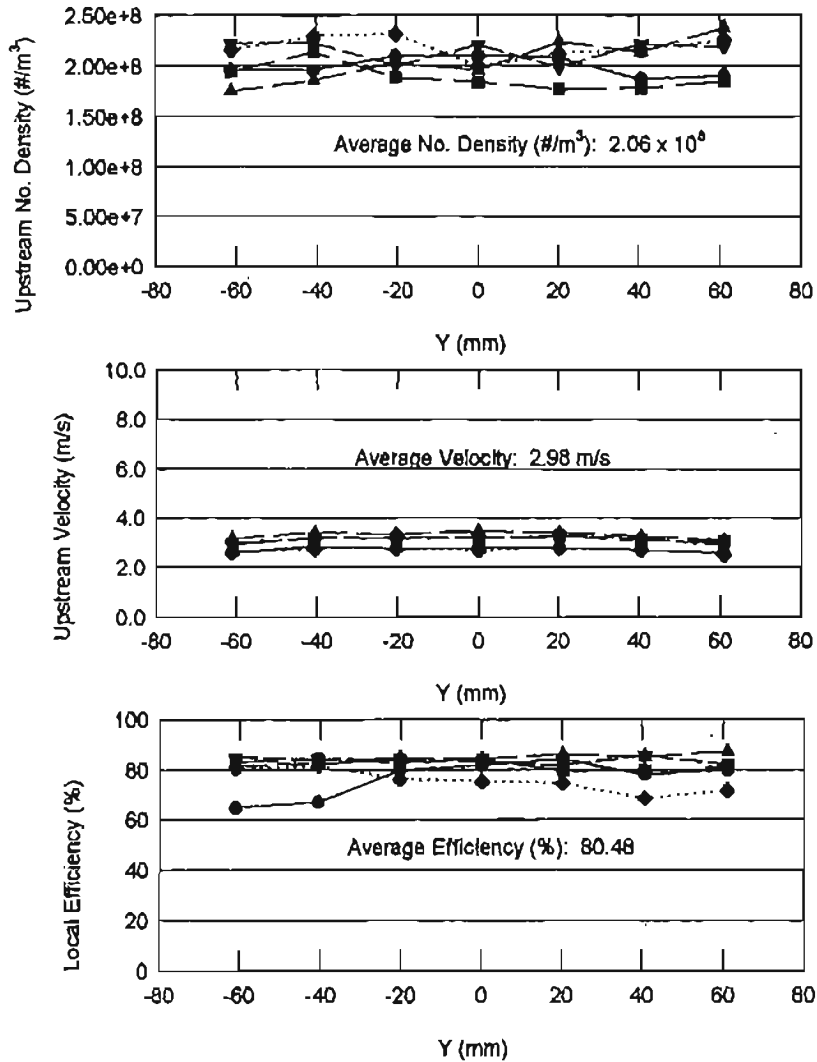
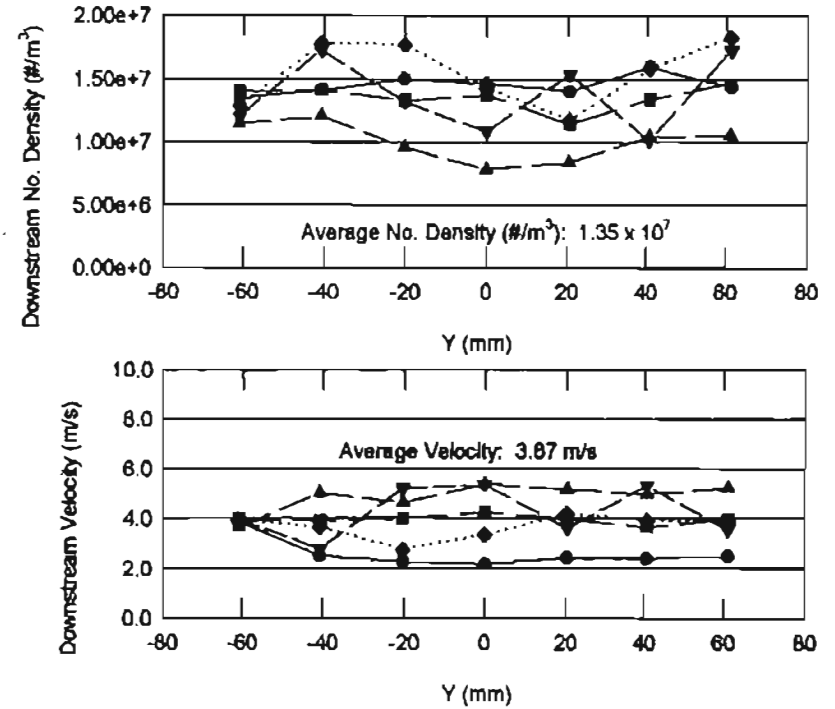
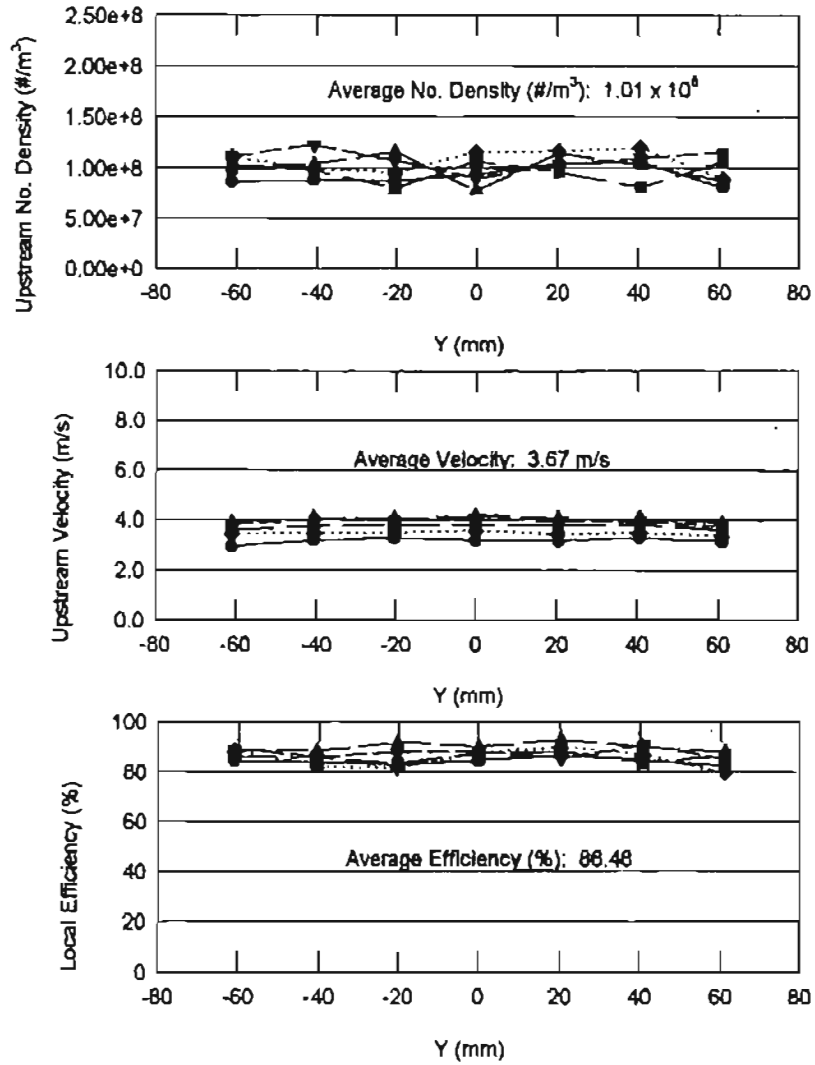
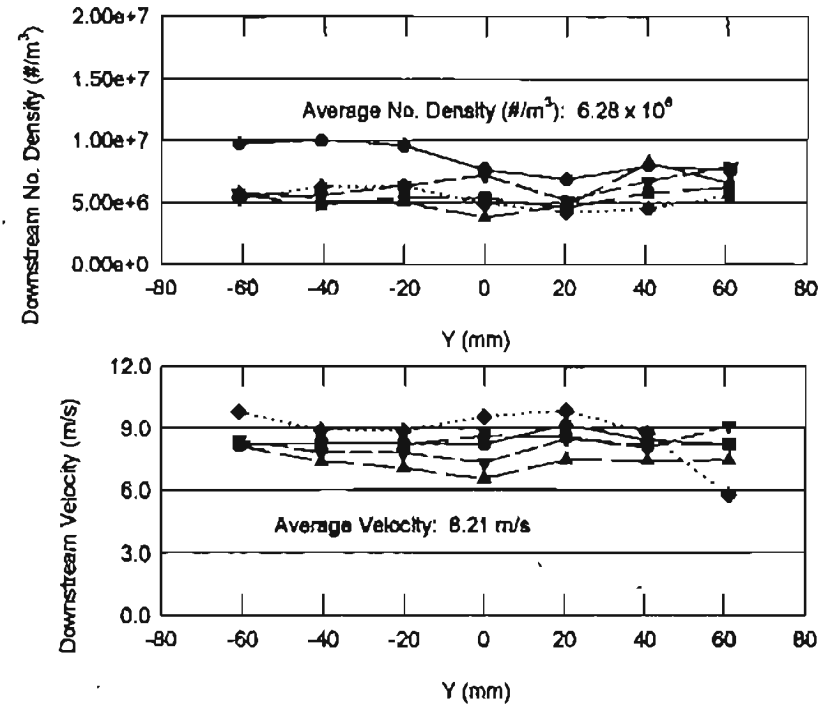
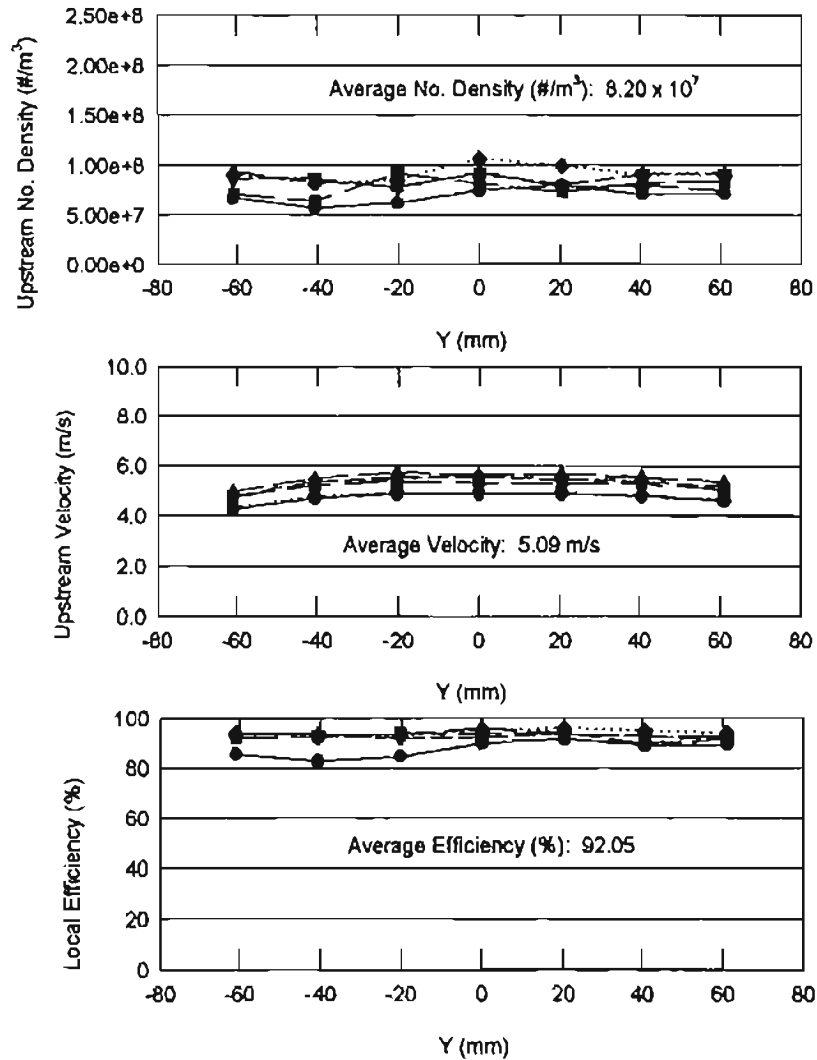


Figure C-15: Pleated Filter Efficiency for Test SAH75_2_2 at 104.26 m³/hr



- X (mm)
- -33.02
 - -16.51
 - ▲ 0.00
 - ▼ 16.51
 - ◆ 33.02

Figure C-16: Pleated Filter Efficiency for Test SAH125_2_1 at 188.45 m³/hr



- X (mm)
- -33.02
 - -16.51
 - ▲ 0.00
 - ▼ 16.51
 - ◆ 33.02

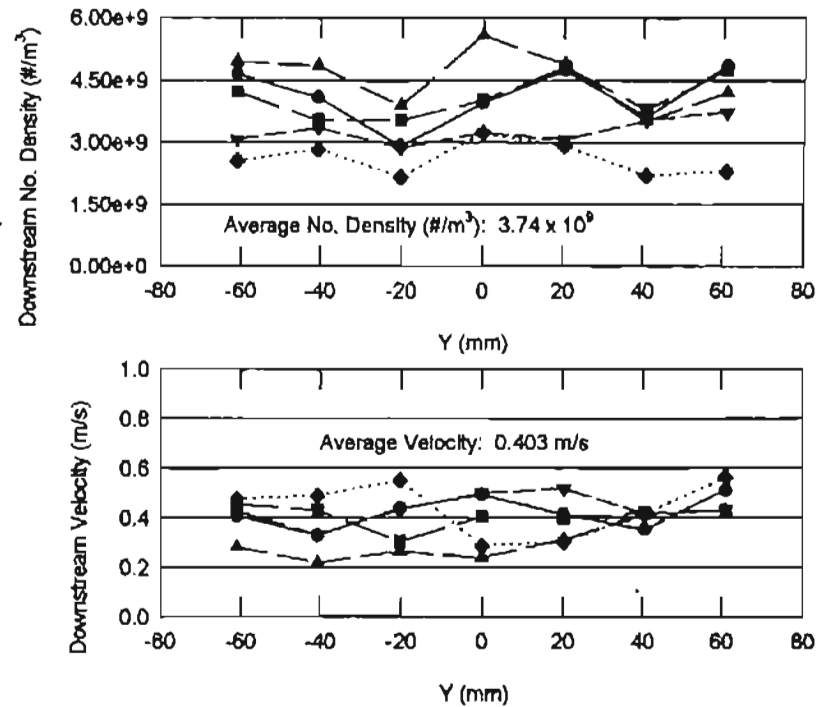
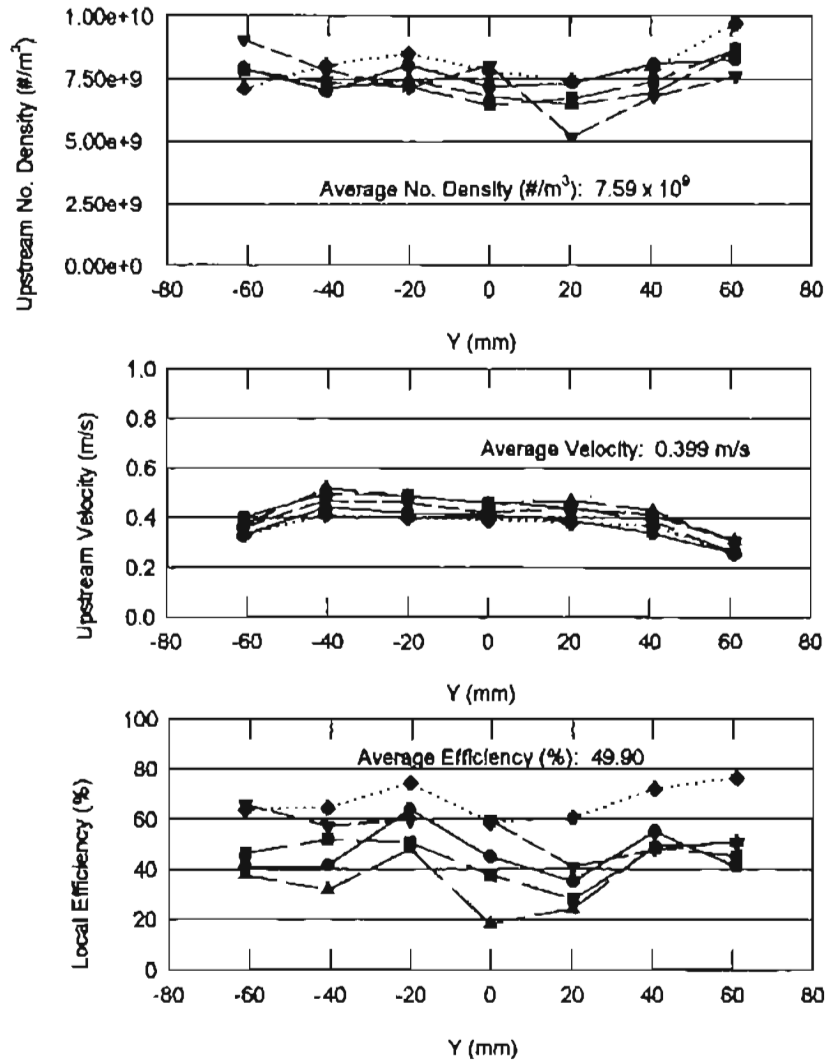
Figure C-17: Pleated Filter Efficiency for Test SAH125_2_2 at 188.45 m³/hr

APPENDIX D

RESULTS FOR 0.966 μm DIAMETER PSL PARTICLES IN THE SAE J726 HOUSING

Some of the test results for 0.966 μm diameter PSL spheres have been shown and discussed in Chapter 5. The other test results are presented in this appendix. The results presented here are the upstream and downstream local velocity measurements, the upstream and downstream local number densities, and the local efficiencies for each of the additional tests.

The tests have alphanumeric designations, which specify the housing, flow rates, particle size and the repeat number. SAE75_1_2 stands for SAE J726 Housing experiment for 75 cfm (104.26 m^3/hr) with 0.966 μm particles (rounded to 1) and is the second experiment conducted for that flow rate. The files have been named as explained in Chapter 4.



- X (mm)
- -33.02
 - -16.51
 - ▲ -0.00
 - ▼ 16.51
 - ◆ 33.02

Figure D-1: Pleated Filter Efficiency for Test SAE10_1_1 at 13.61 m³/hr

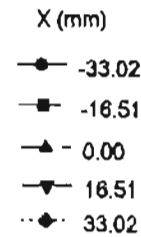
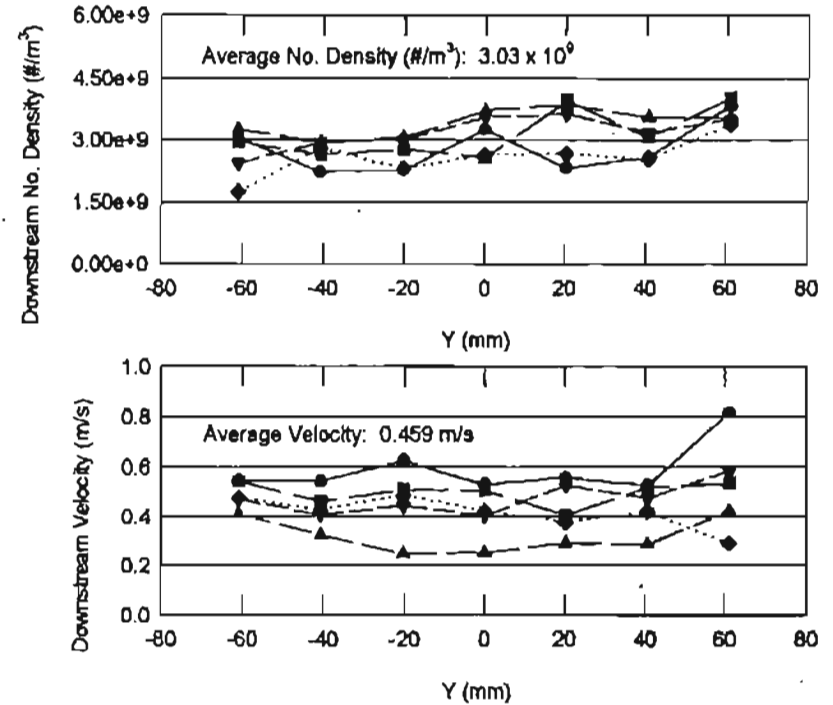
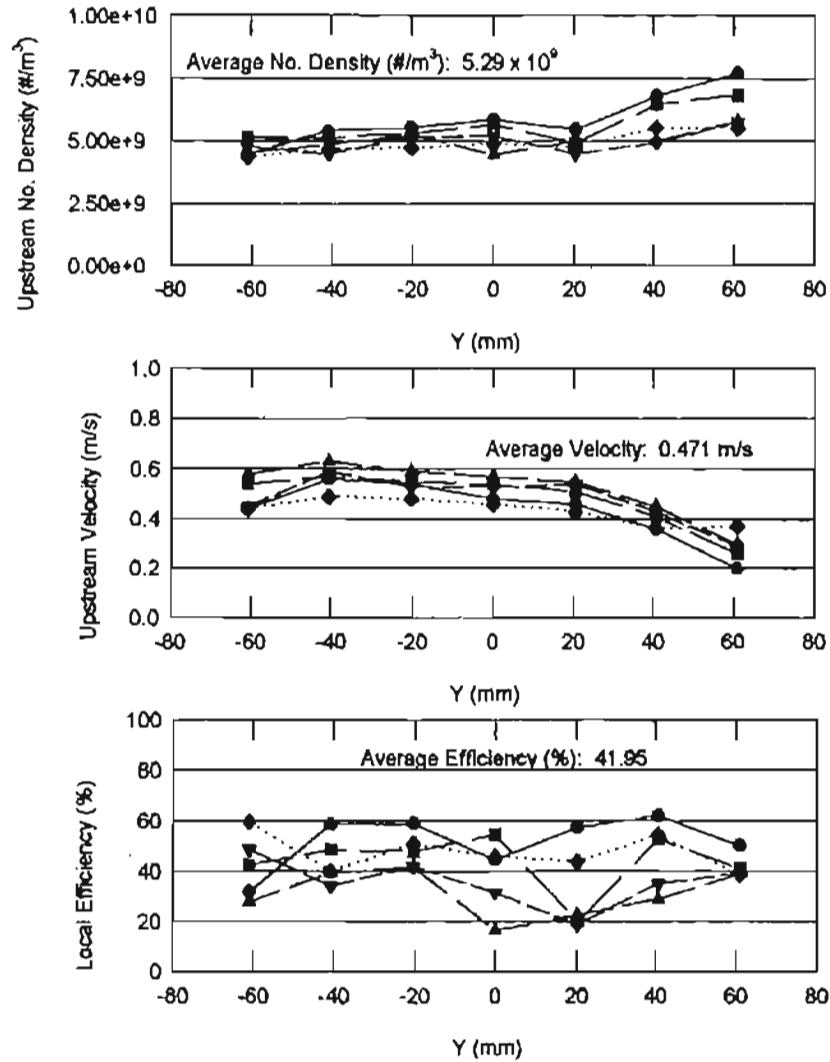


Figure D-2: Pleated Filter Efficiency for Test SAE10_1_2 at 13.61 m³/hr

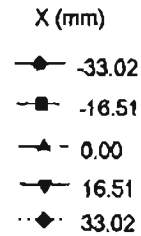
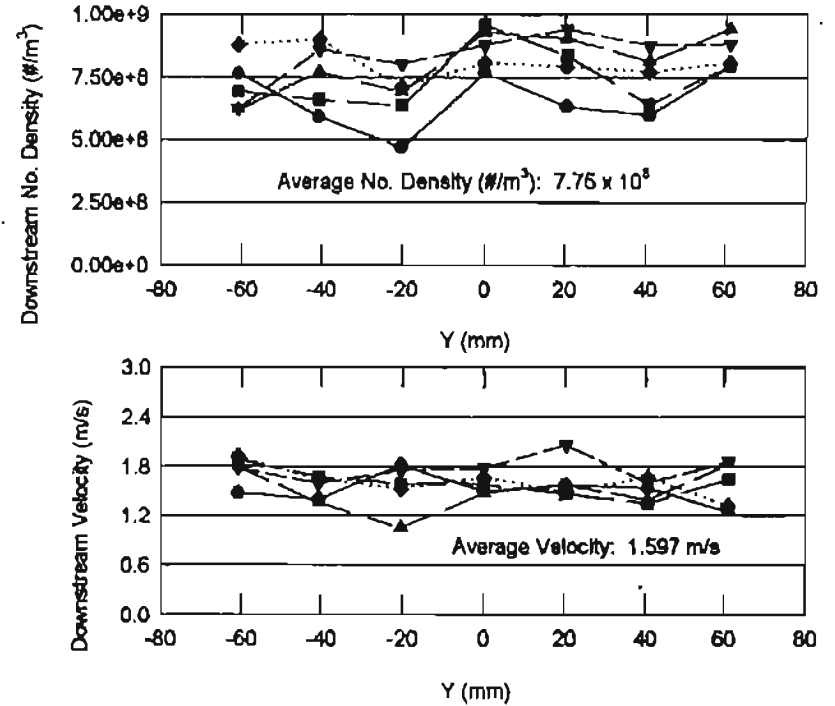
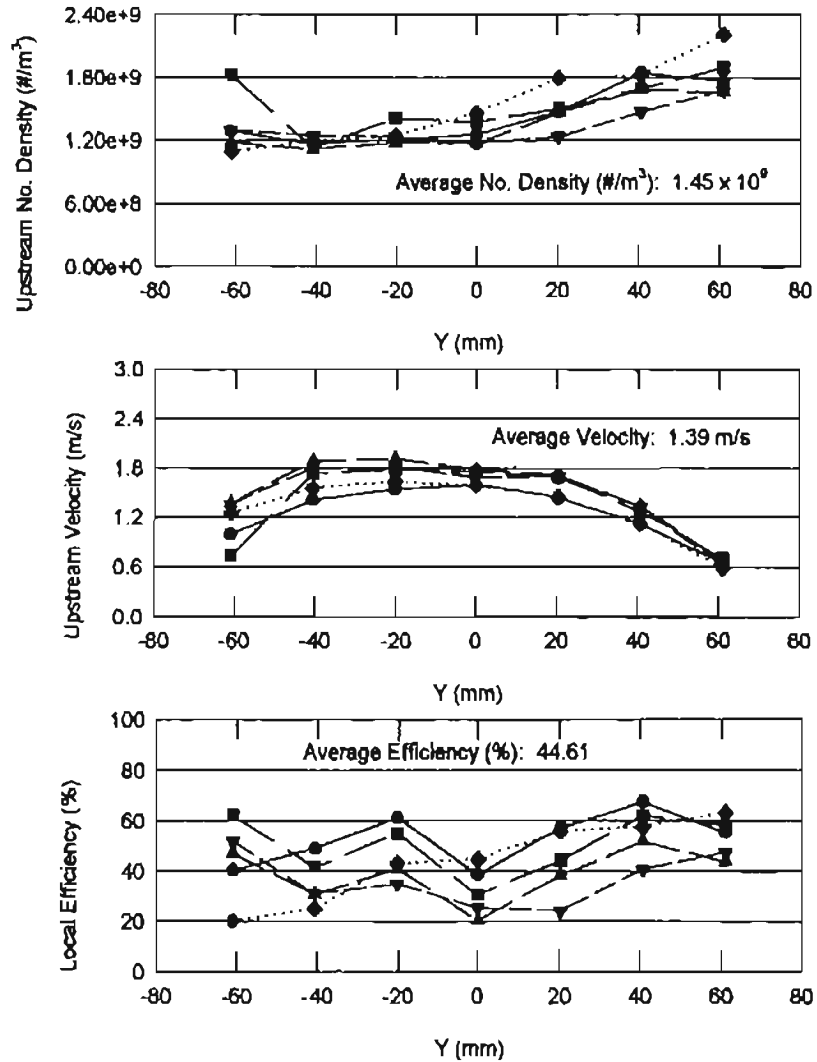
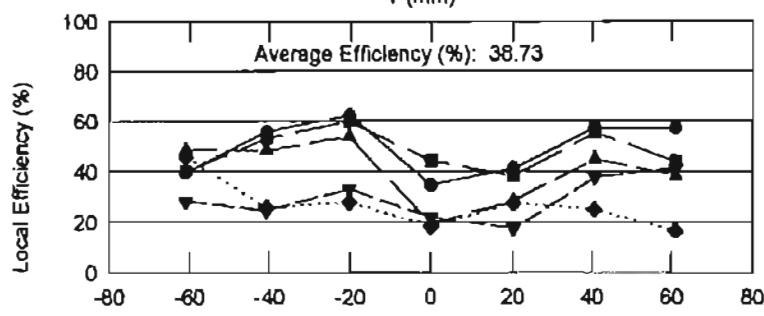
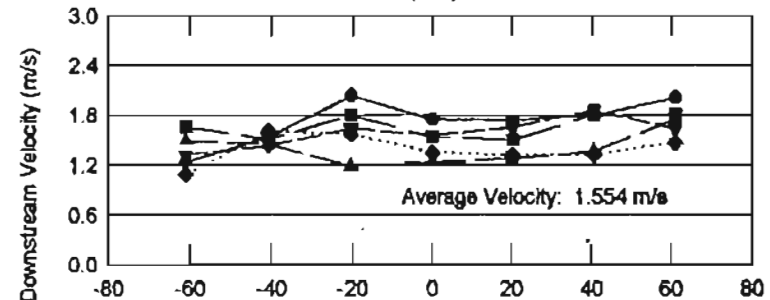
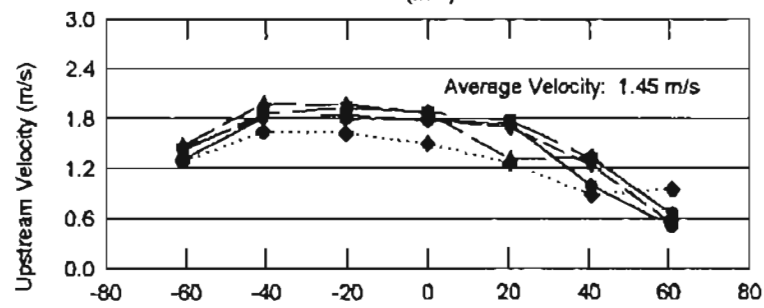
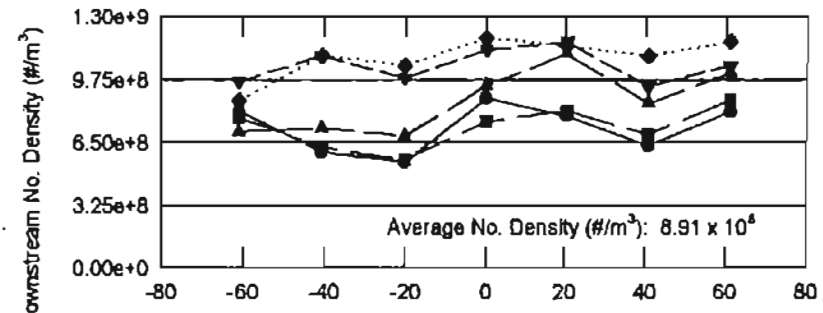
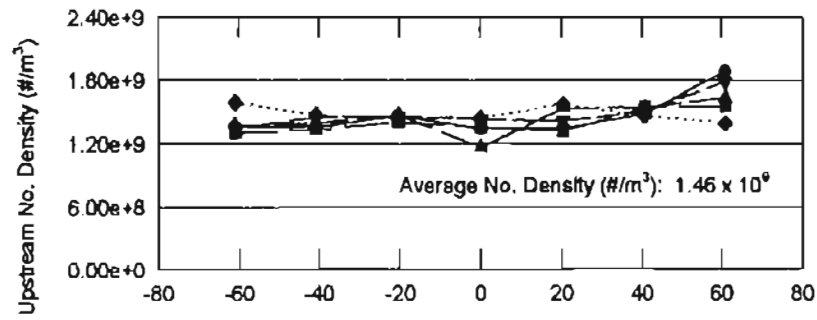


Figure D-3: Pleated Filter Efficiency for Test SAE25_1_1 at 37.42 m³/hr



- X (mm)
- -33.02
 - -16.51
 - ▲ 0.00
 - ▼ 16.51
 - ◆ 33.02

Figure D-4: Pleated Filter Efficiency for Test SAE25_1_2 at 37.42 m³/hr

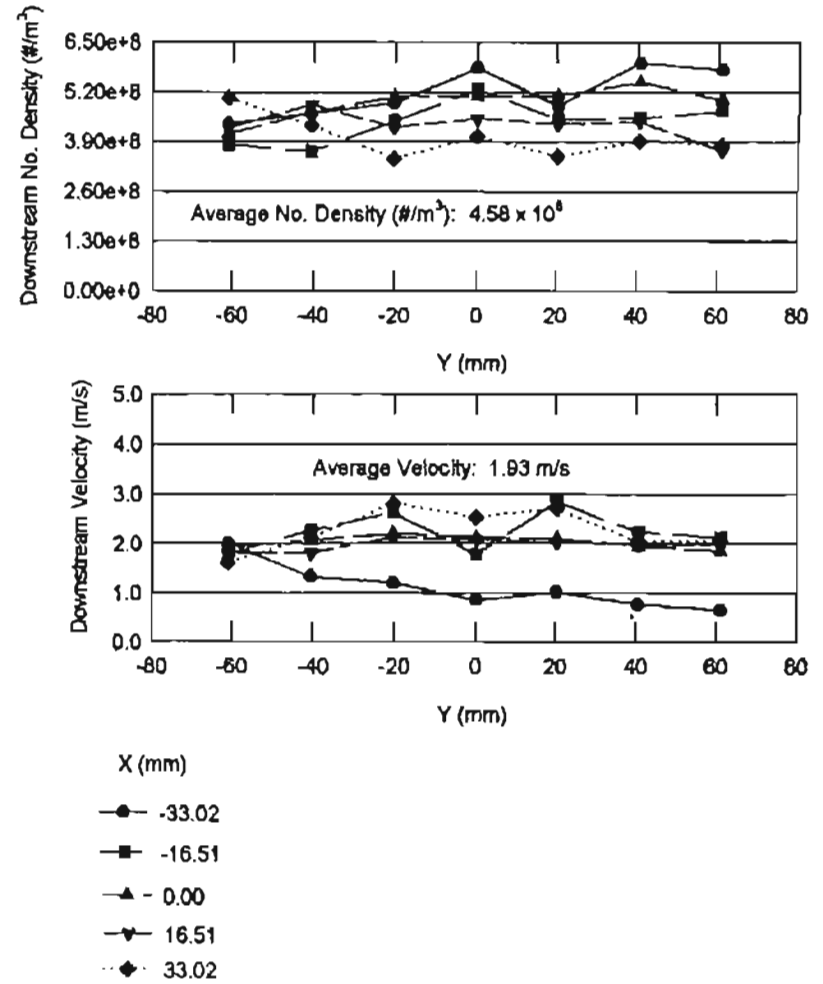
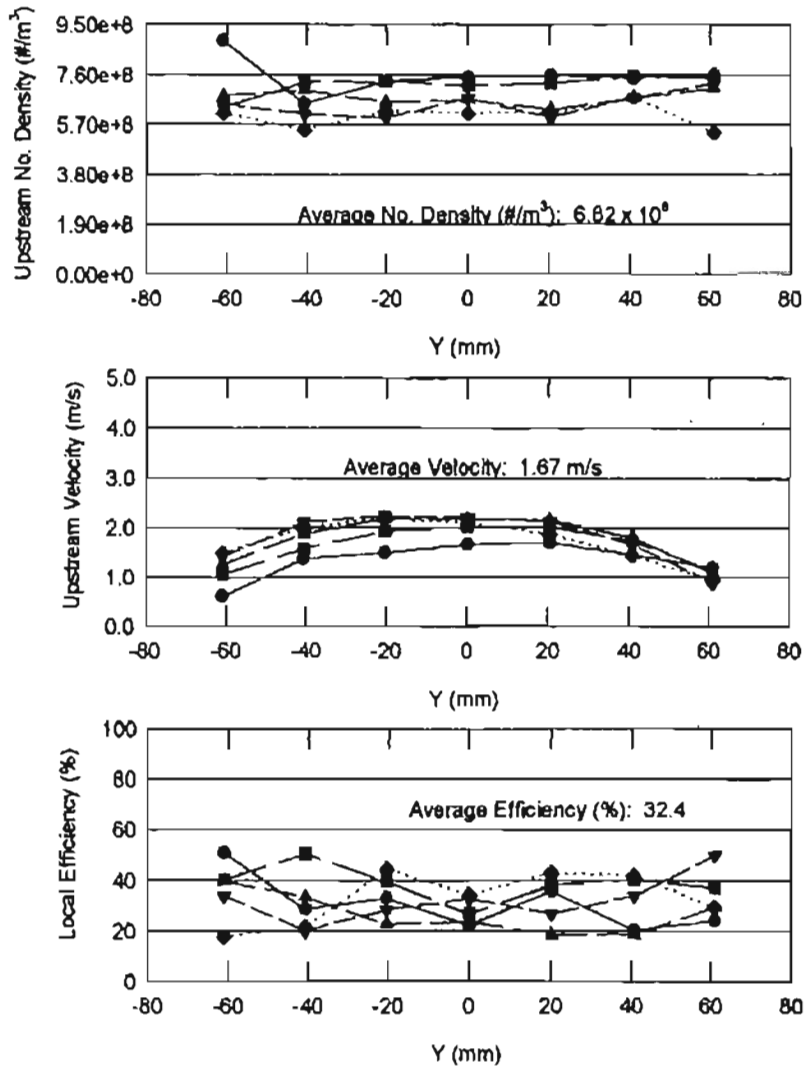


Figure D-5: Pleated Filter Efficiency for Test SAE40_1_1 at 61.20 m³/hr

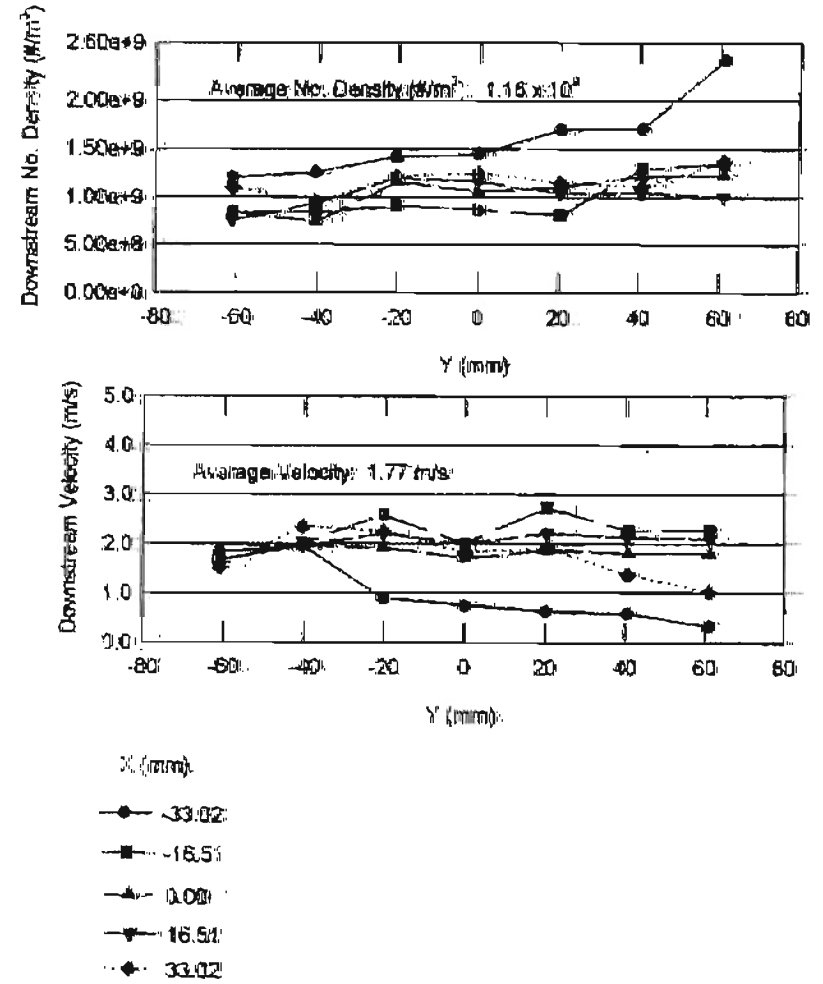
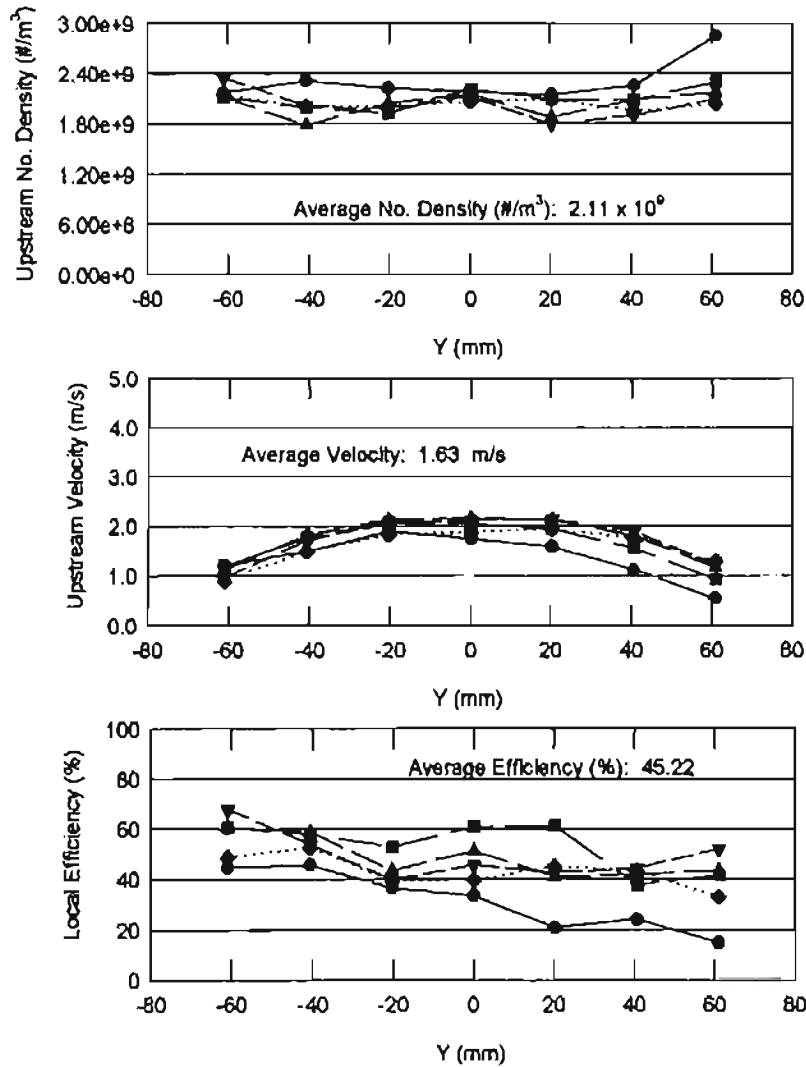


Figure D-6: Pleated Filter Efficiency for Test SAE40_1_2 at 61.20 m³/hr

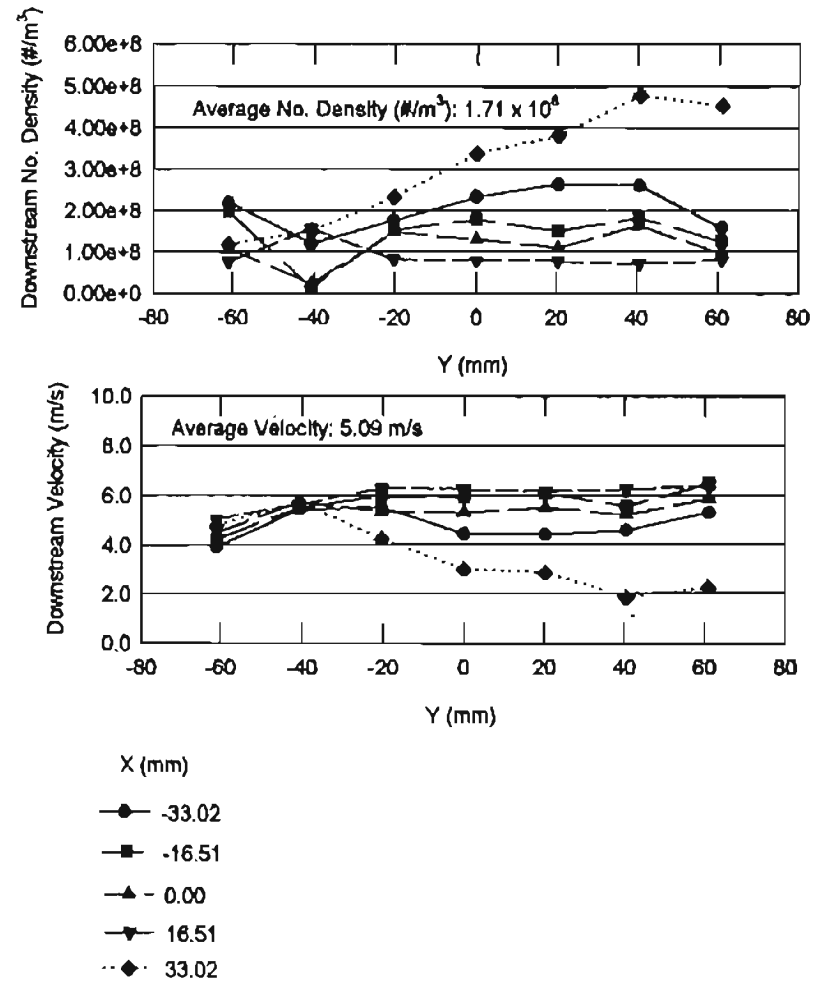
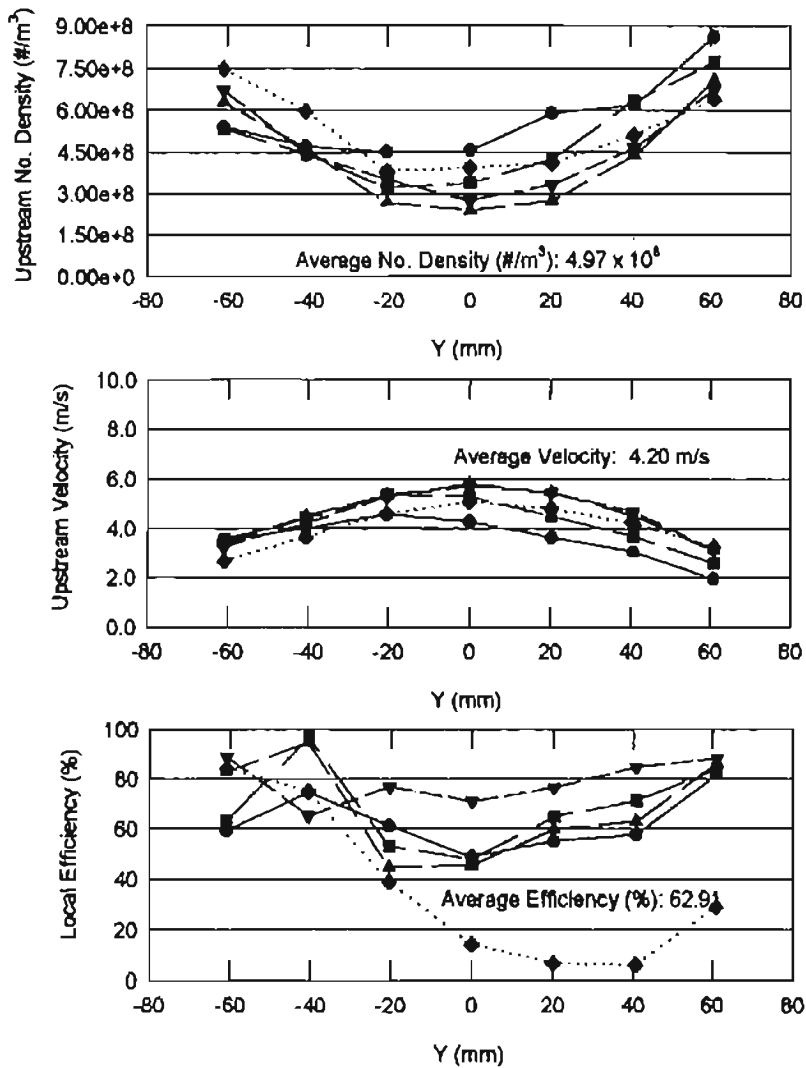


Figure D-7: Pleated Filter Efficiency for Test SAE120_1_1 at 180.03 m³/hr

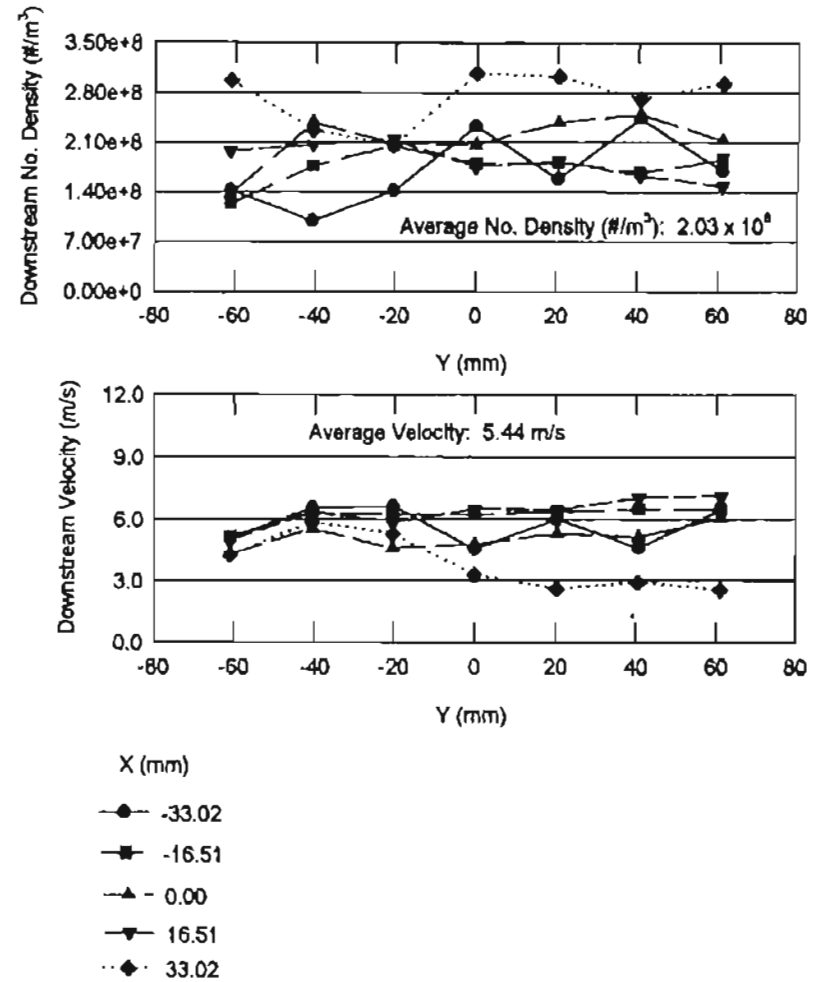
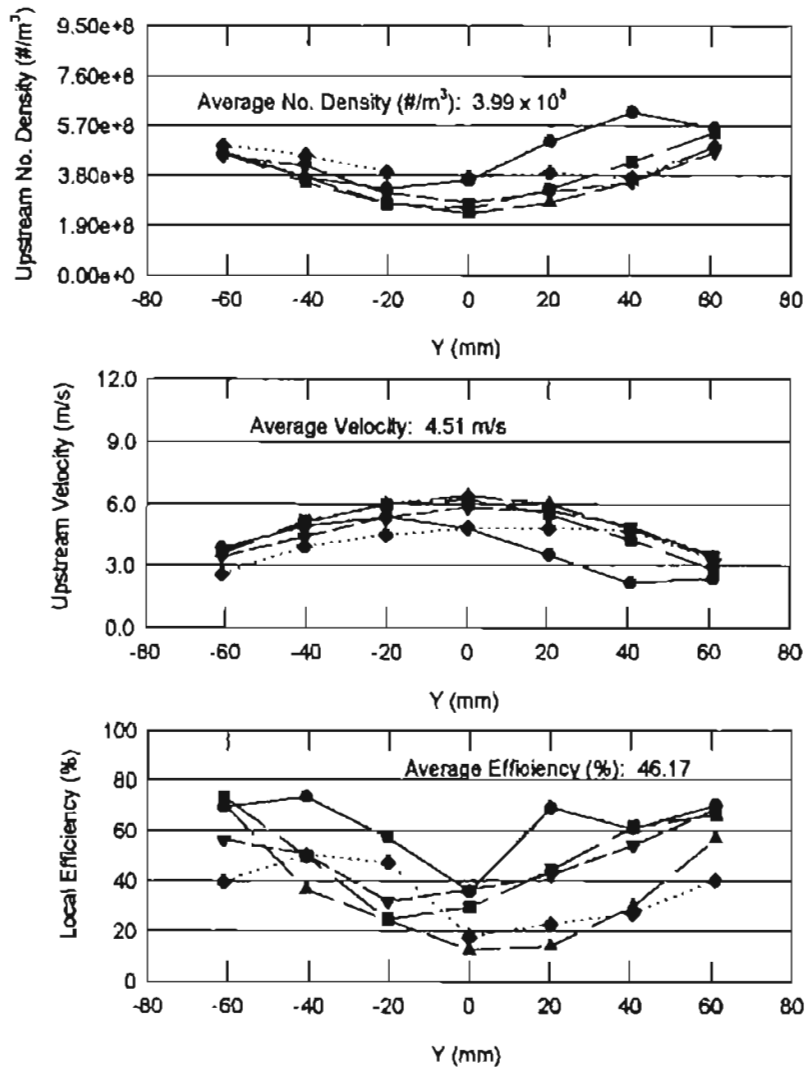


Figure D-8: Pleated Filter Efficiency for Test SAE125_1_1 at 188.45 m³/hr

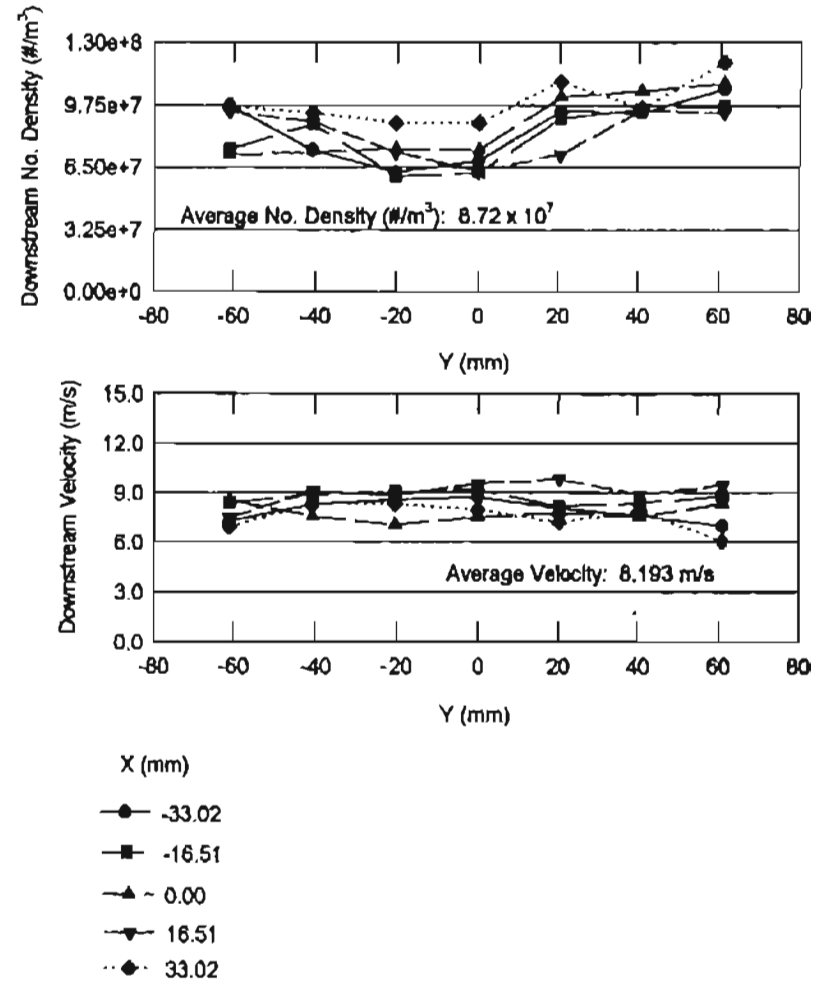
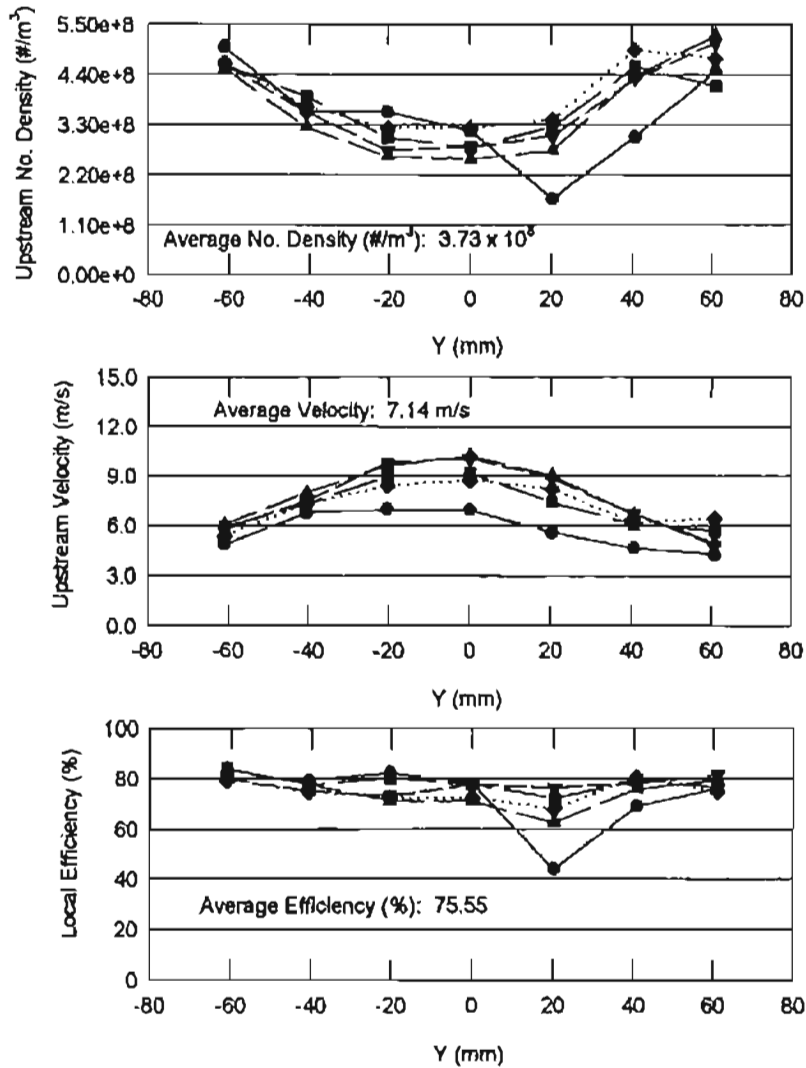
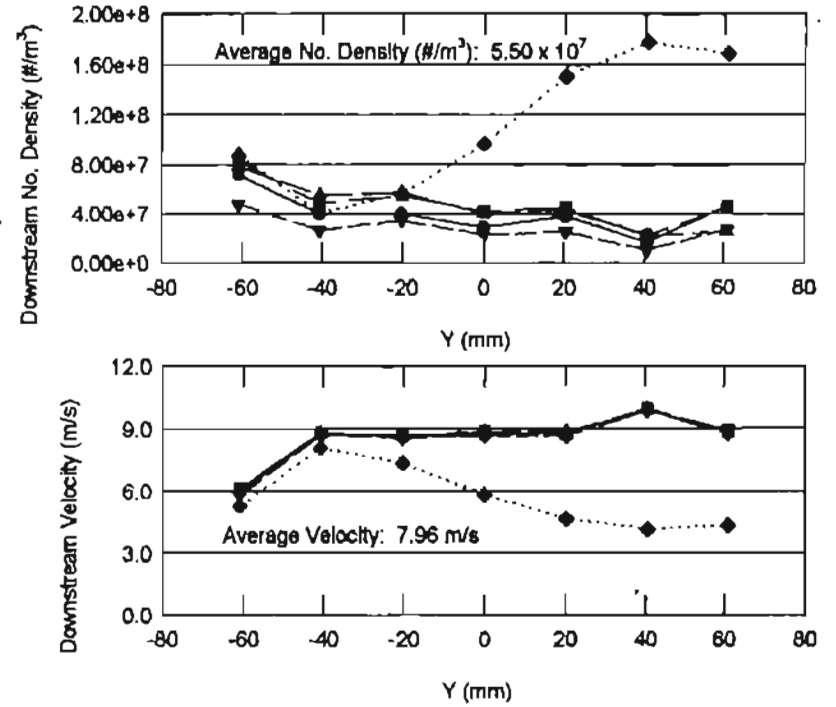
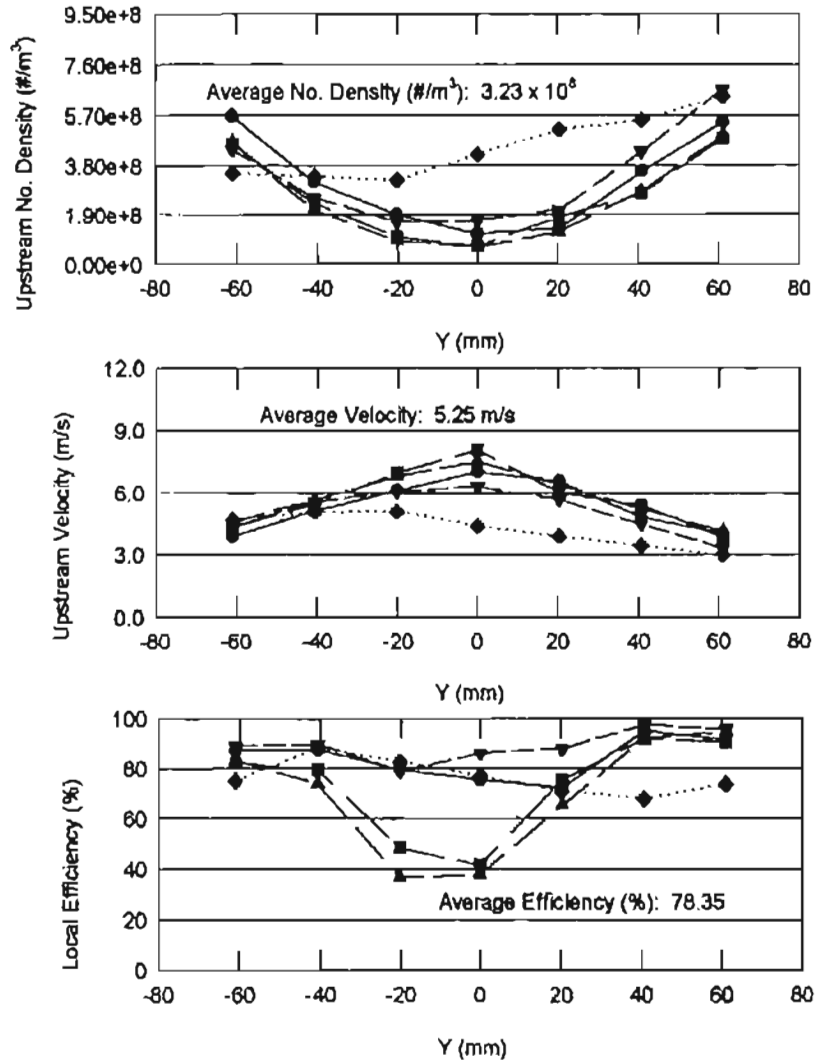
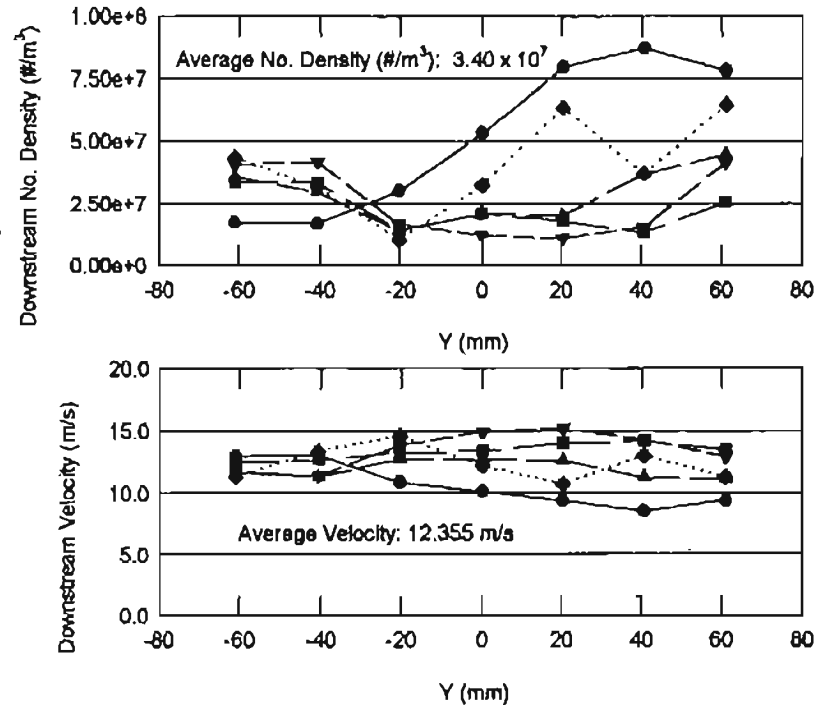
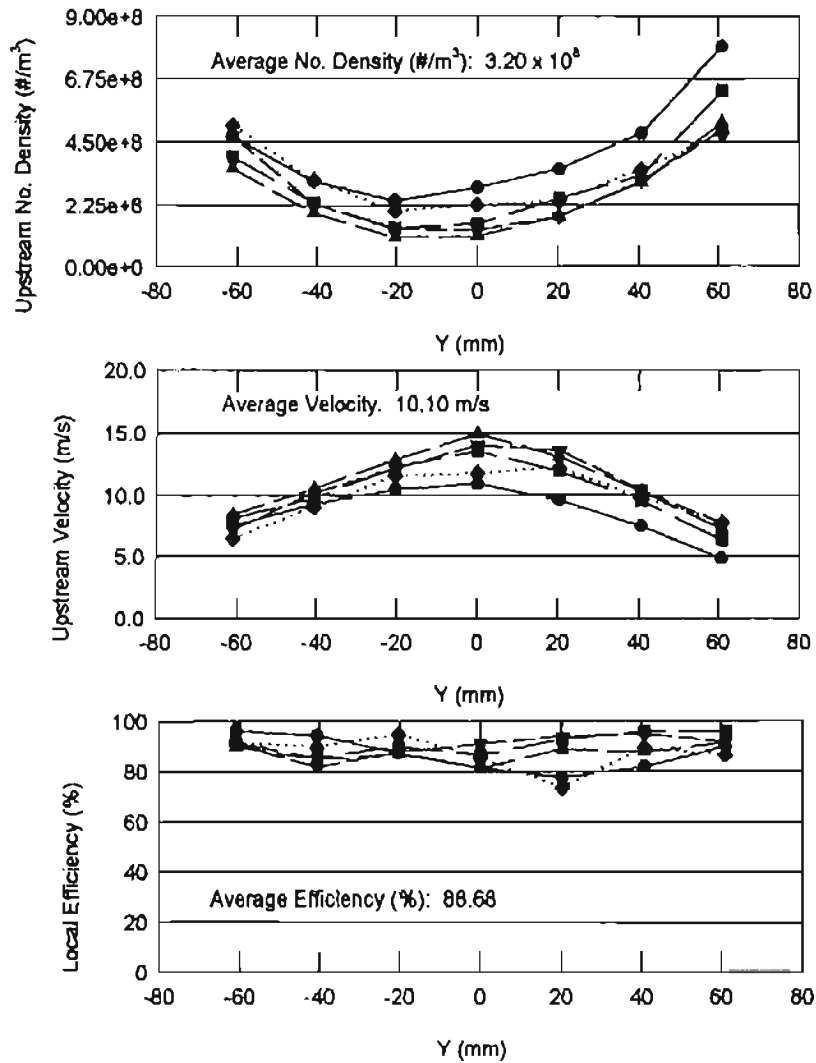


Figure D-9: Pleated Filter Efficiency for Test SAE125_1_2 at 188.45 m³/hr



- X (mm)
- -33.02
 - -16.51
 - ▲ 0.00
 - ▼ 16.51
 - ◆ 33.02

Figure D-10: Pleated Filter Efficiency for Test SAE200_1_1 at 314.73 m³/hr



- X (mm)
- -33.02
 - -16.51
 - ▲ 0.00
 - ▼ 16.51
 - ◆ 33.02

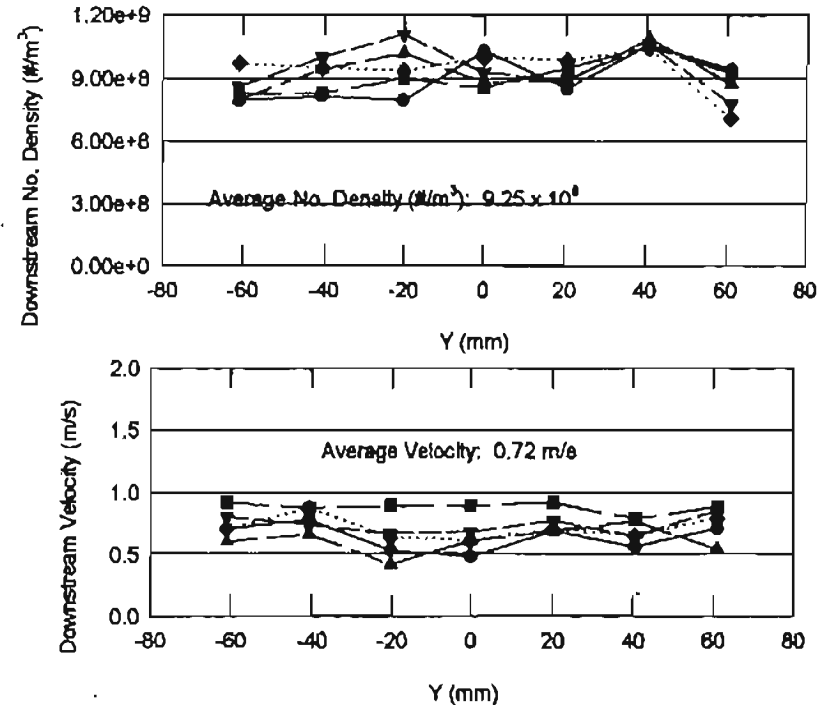
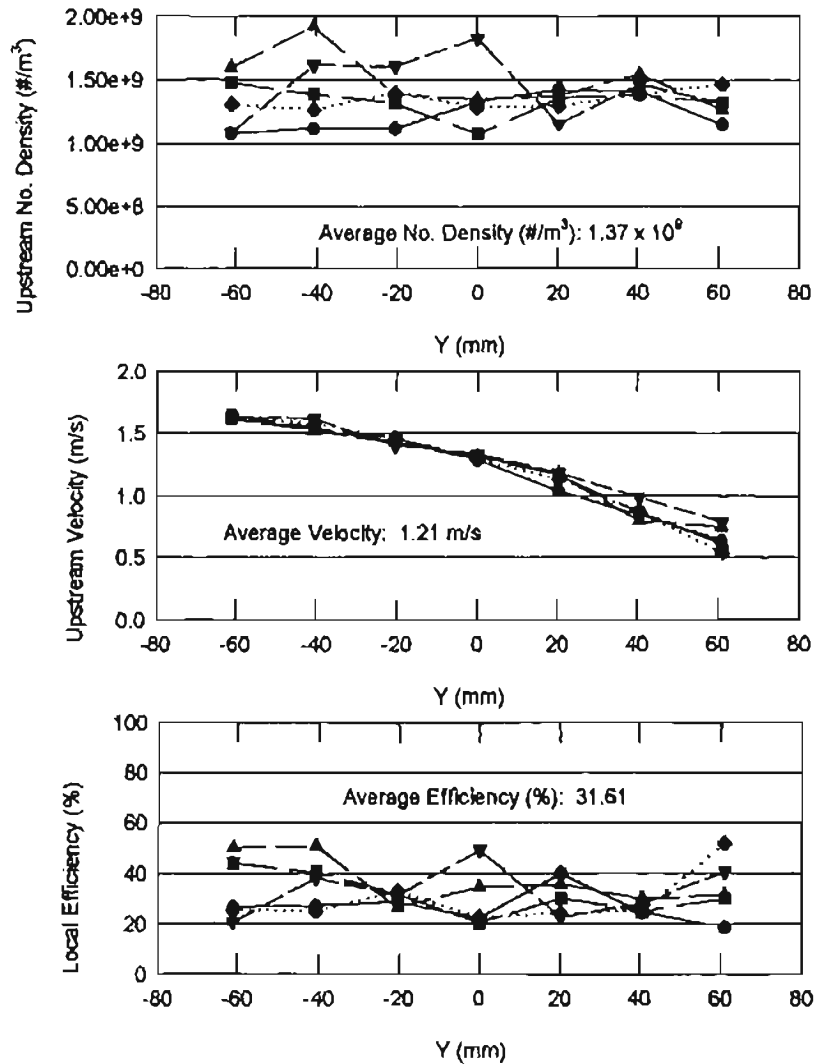
Figure D-11: Pleated Filter Efficiency for Test SAE200_1_3 at 314.73 m³/hr

APPENDIX E

RESULTS FOR 0.966 μm DIAMETER PSL PARTICLES IN THE SIMULATED AUTOMOTIVE FILTER HOUSING

Some of the test results for 0.966 μm diameter PSL spheres have been shown and discussed in Chapter 5. The other test results are presented in this appendix. The results presented here are the upstream and downstream local velocity measurements, the upstream and downstream local number densities, and the local efficiencies for each of the additional tests.

The tests have alphanumeric designations, which specify the housing, flow rates, particle size and the repeat number. SAF75_1_2 stands for Simulated Automotive Filter Housing experiment with 75 cfm (104.26 m^3/hr) for 0.966 μm particles (rounded to 1) and is the second experiment conducted for that flow rate. The files have been named as explained in Chapter 4.



- X (mm)
- -33.02
 - -16.51
 - ▲ 0.00
 - ▼ 16.51
 - ◆ 33.02

Figure E-1: Pleated Filter Efficiency for Test SAF15_1_2 at 21.55 m³/hr

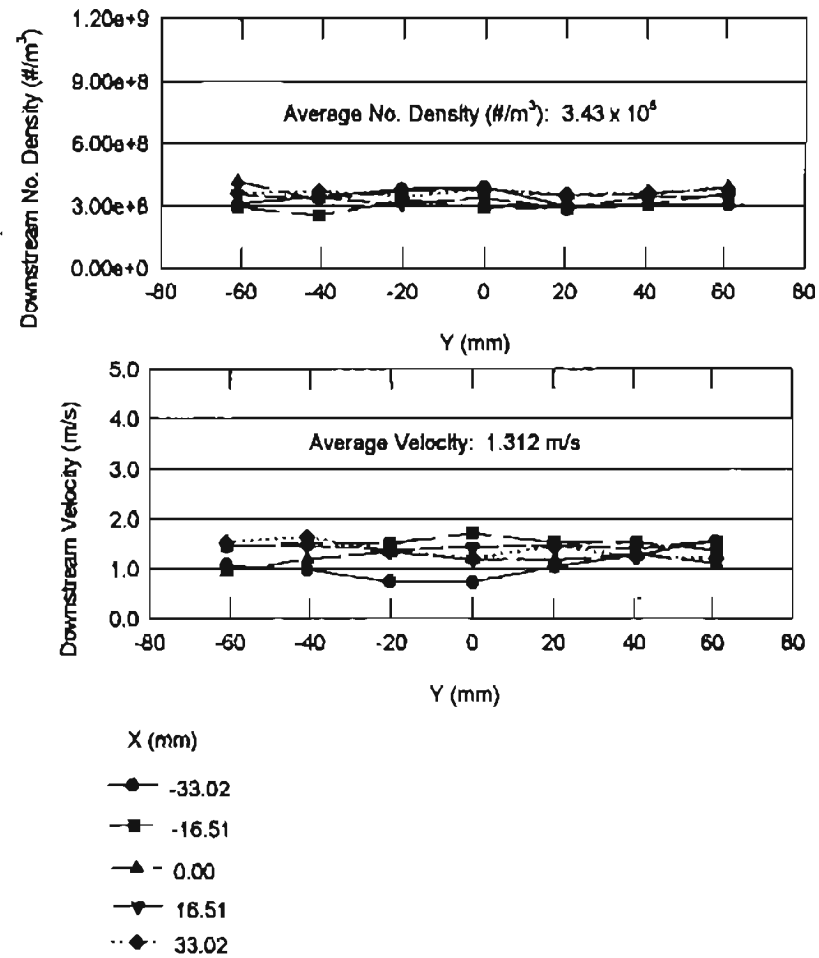
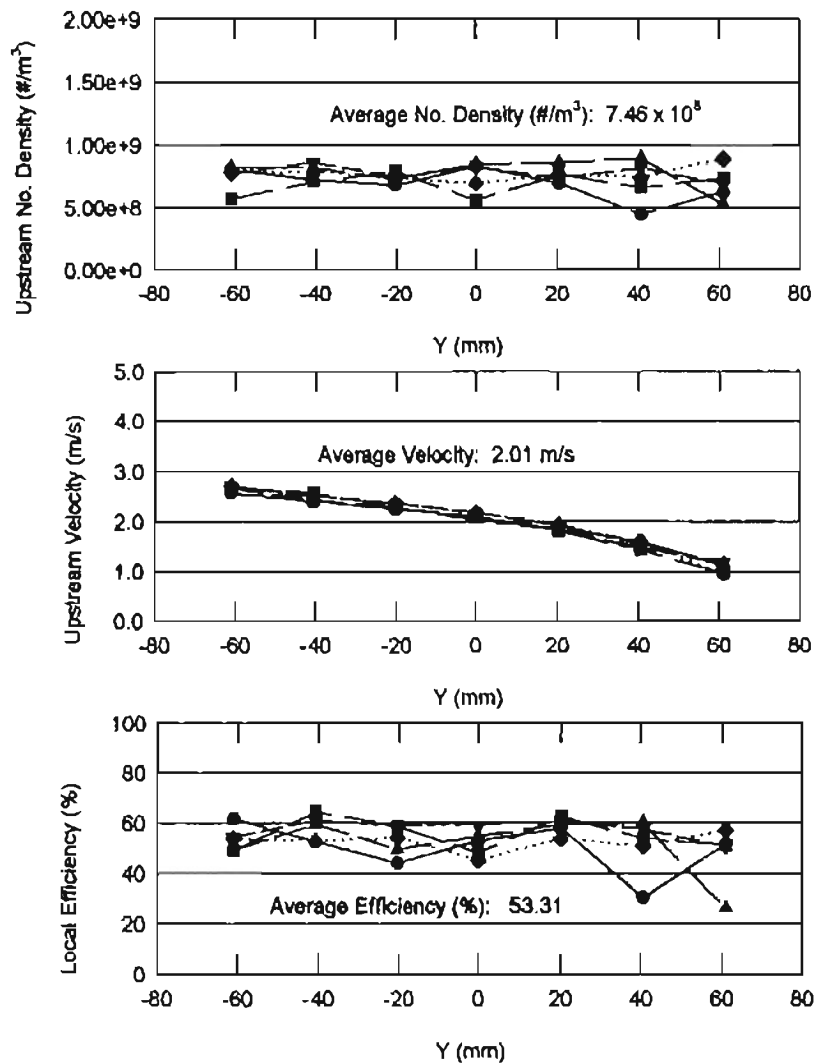
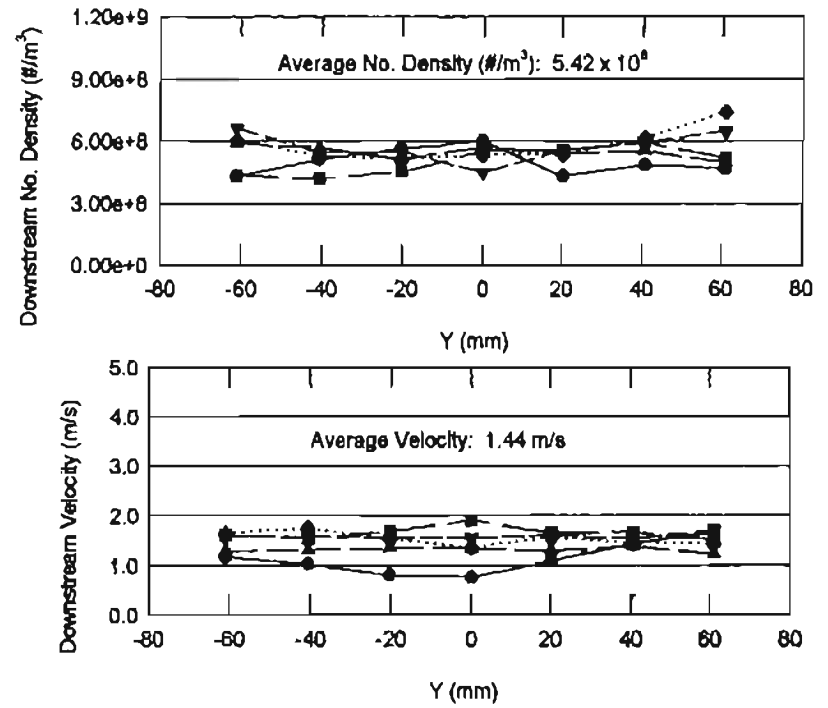
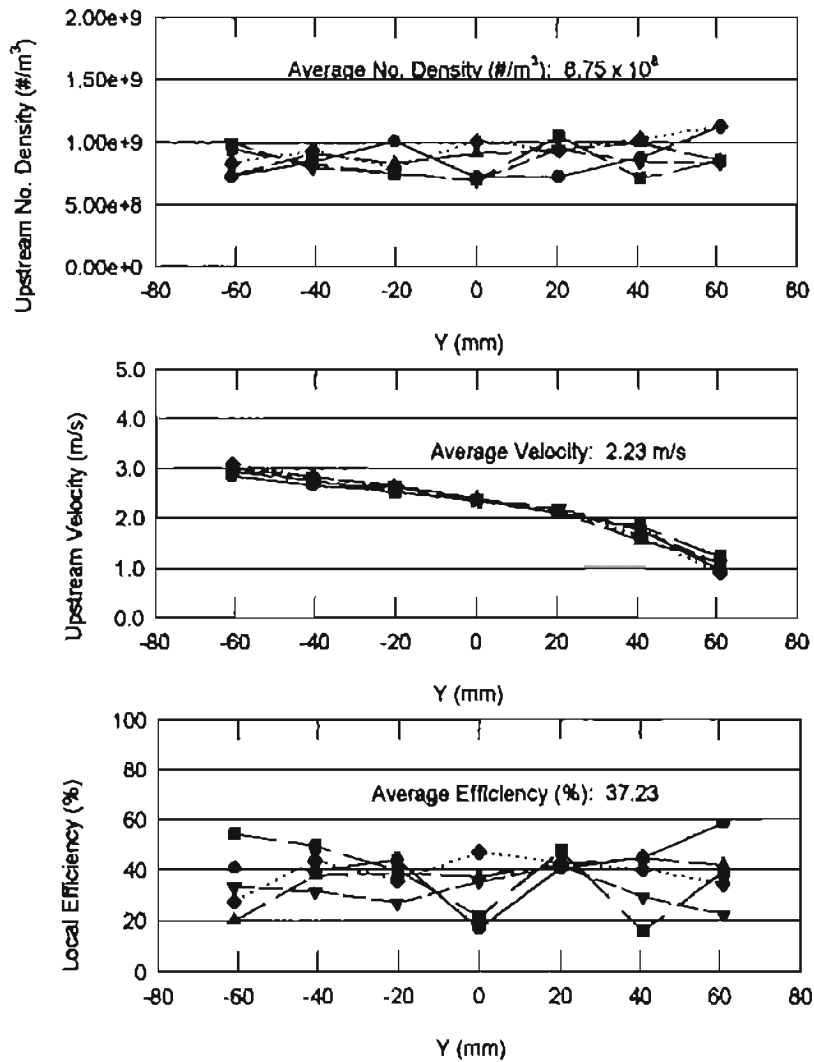
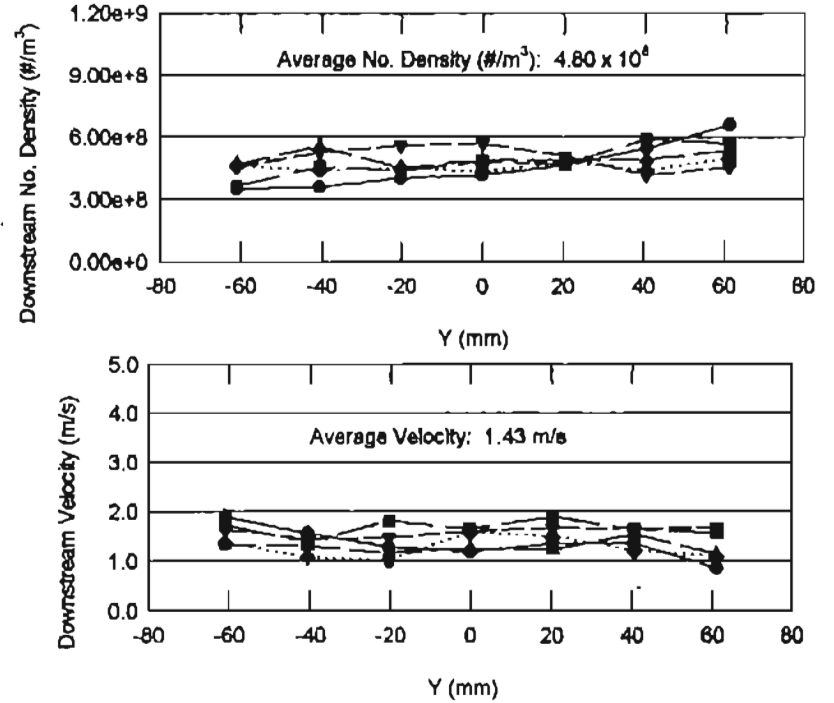
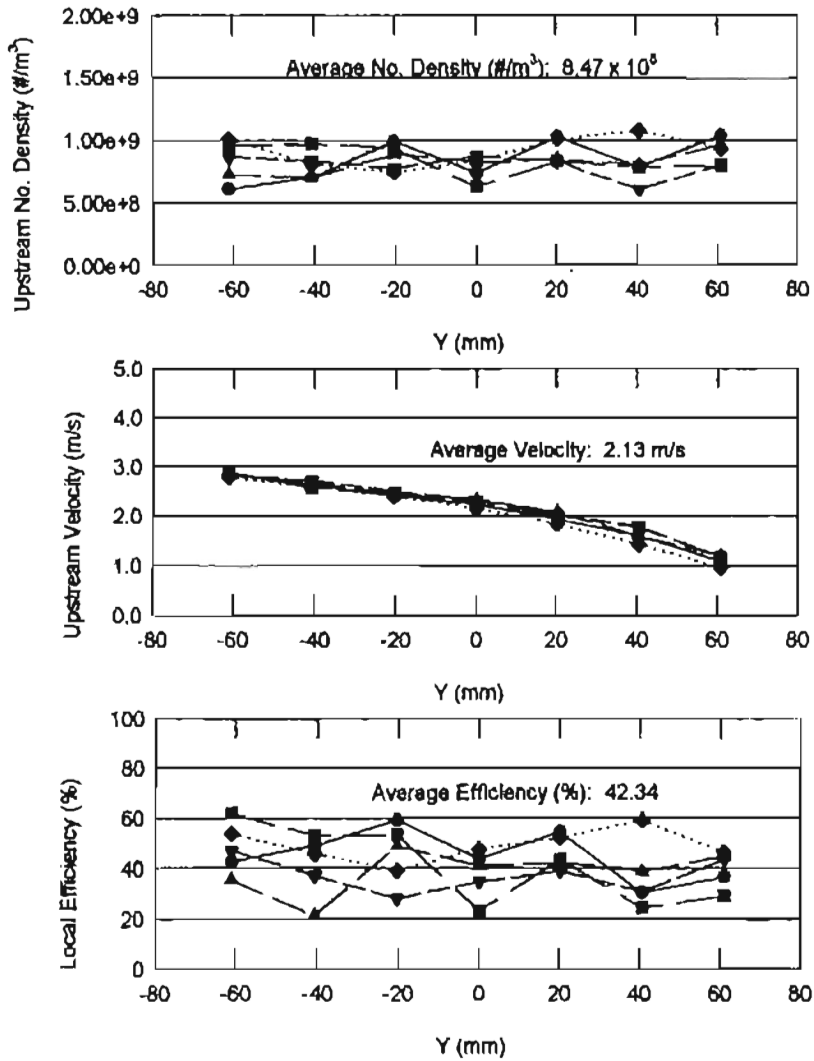


Figure E-2: Pleated Filter Efficiency for Test SAF20_1_1 at 29.48 m³/hr



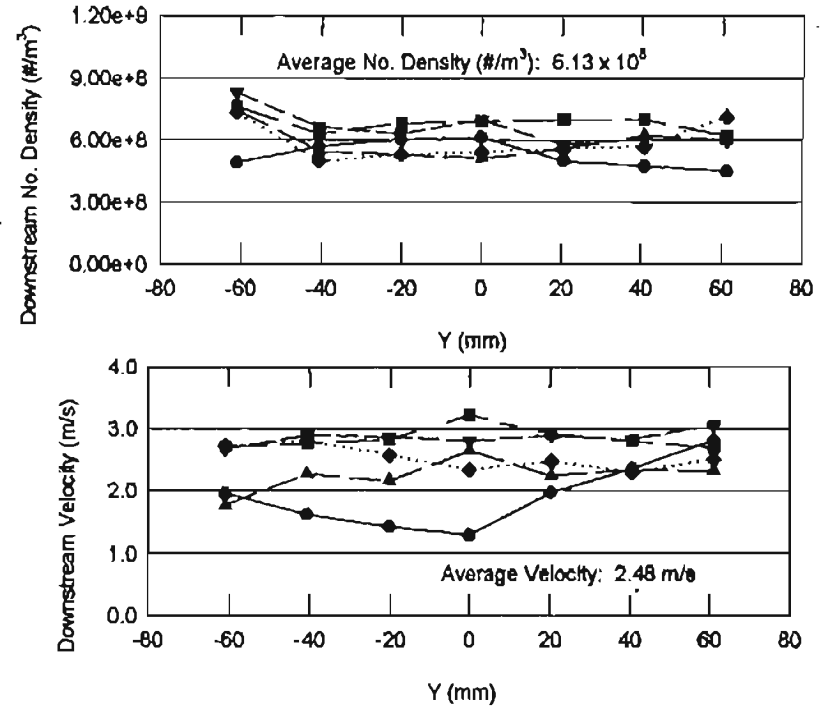
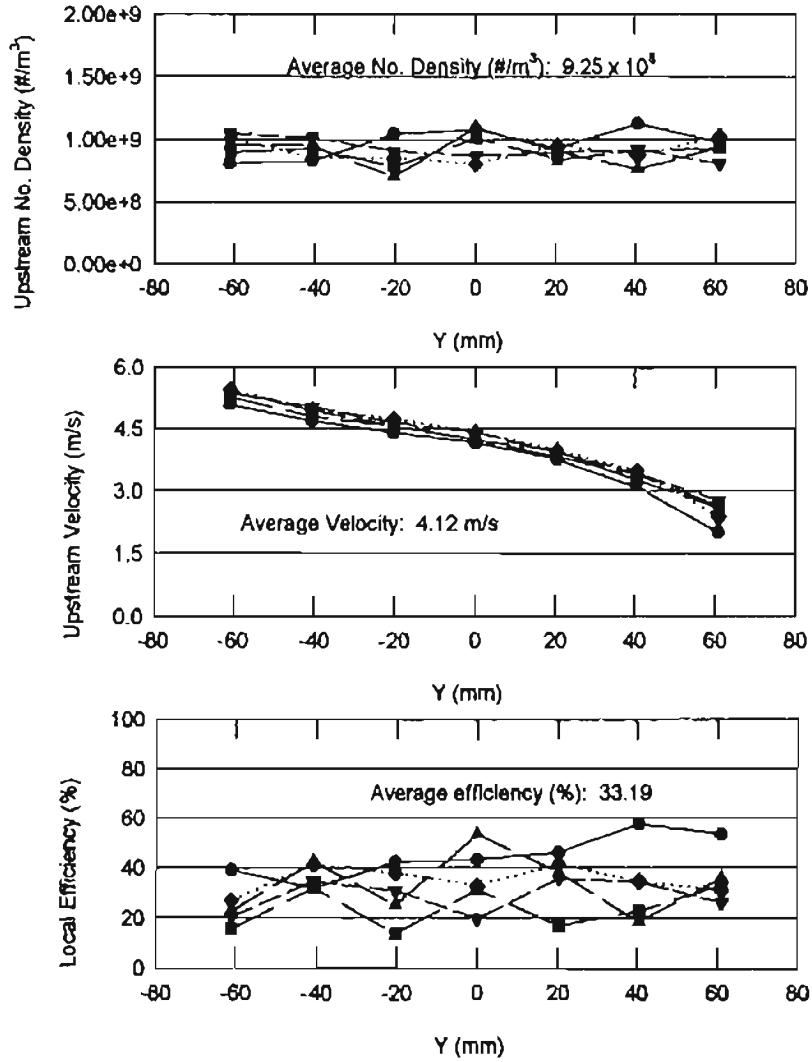
- X (mm)
- -33.02
 - -16.51
 - ▲ 0.00
 - ▼ 16.51
 - ◆ 33.02

Figure E-3: Pleated Filter Efficiency for Test SAF25_1_1 at 37.42 m³/hr



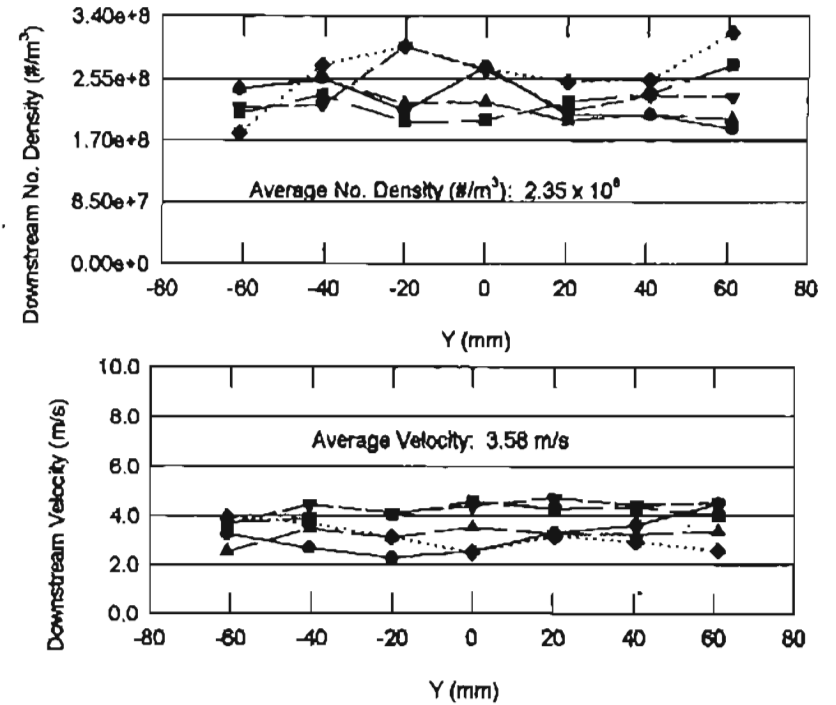
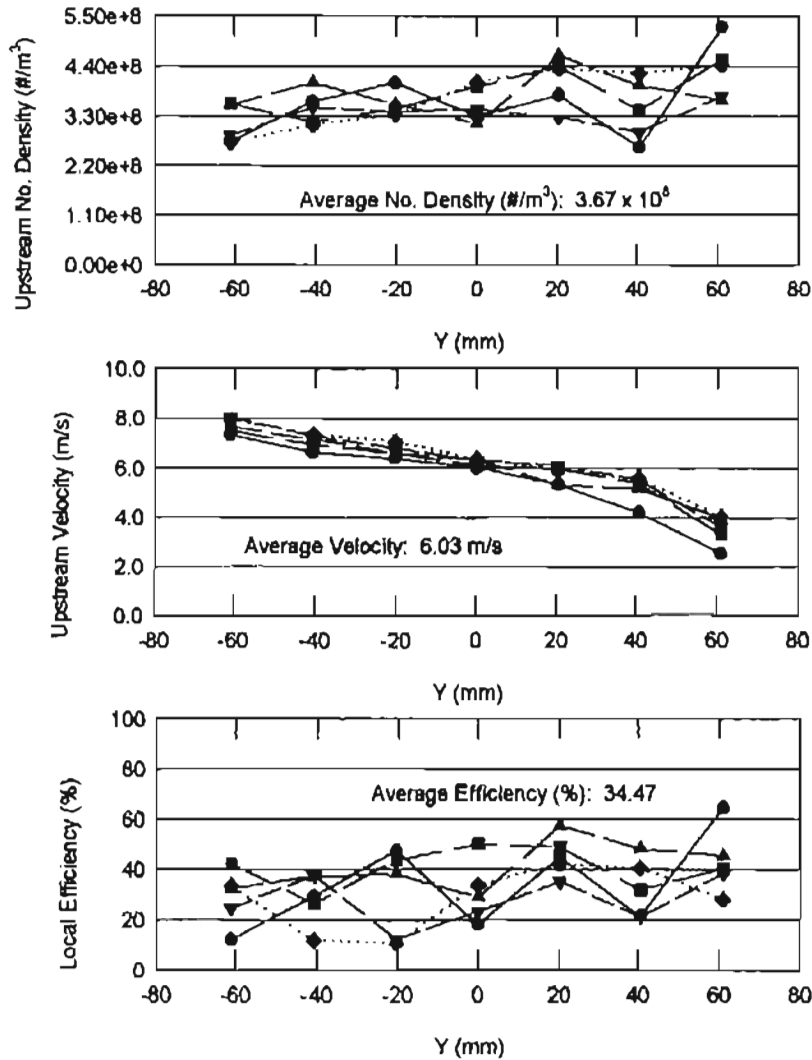
- X (mm)
- -33.02
 - -16.51
 - ▲ 0.00
 - ▼ 16.51
 - ◆ 33.02

Figure E-4: Pleated Filter Efficiency for Test SAF25_1_2 at 37.42 m³/hr



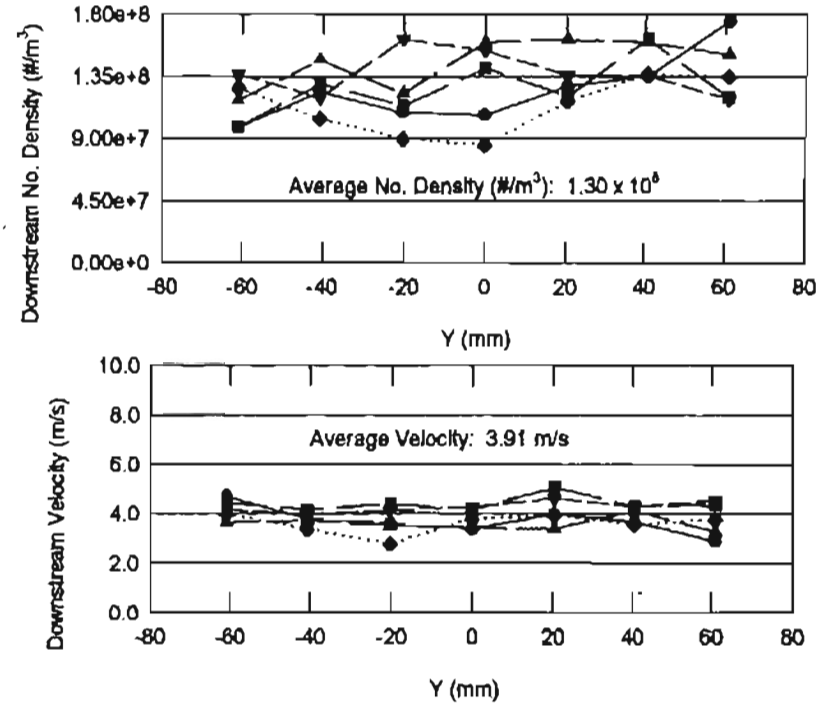
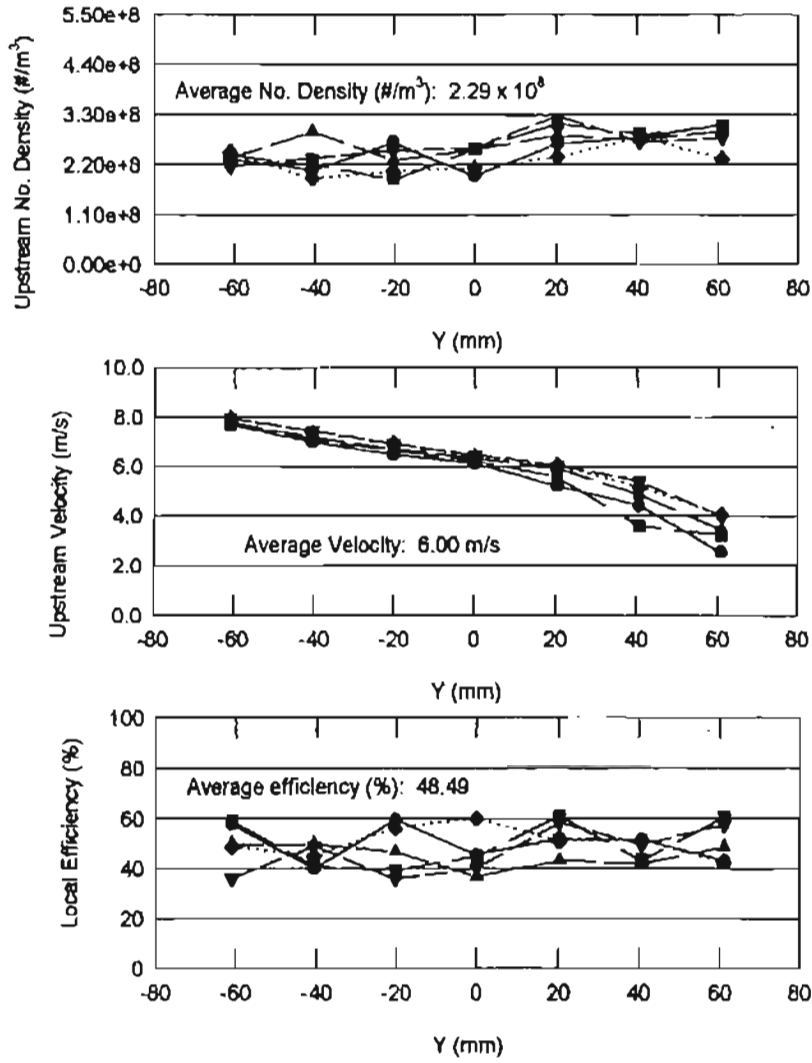
- X (mm)
- -33.02
 - -18.51
 - ▲ 0.00
 - ▼ 16.51
 - ◆ 33.02

Figure E-5: Pleated Filter Efficiency for Test SAF45_1_1 at 70.07 m³/hr



- X (mm)
- -33.02
 - -16.51
 - ▲ 0.00
 - ▼ 16.51
 - ◆ 33.02

Figure E-6: Pleated Filter Efficiency for Test SAF60_1_1 at 79 m³/hr



- X (mm)
- -33.02
 - -16.51
 - ▲ 0.00
 - ▼ 16.51
 - ◆ 33.02

Figure E-7: Pleated Filter Efficiency for Test SAF60_1_2 at 79 m³/hr

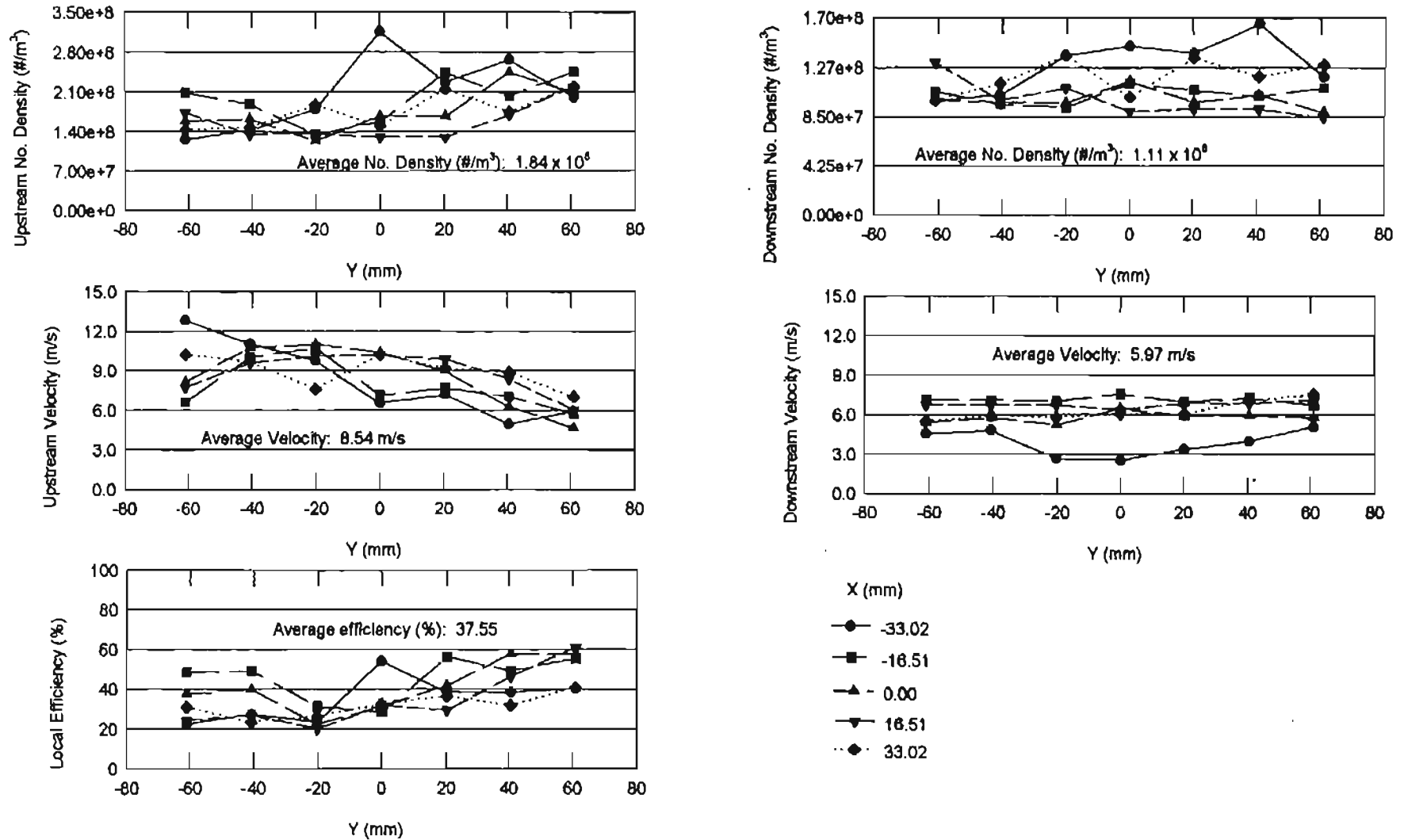


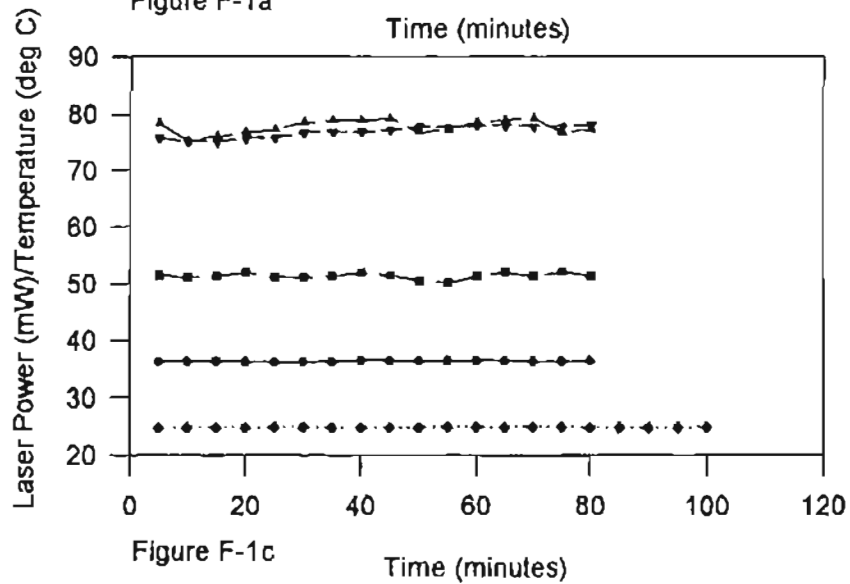
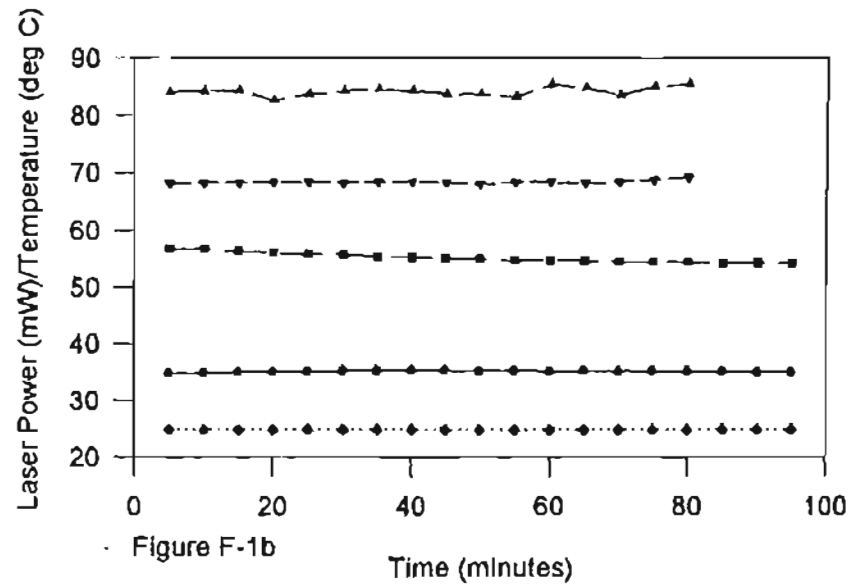
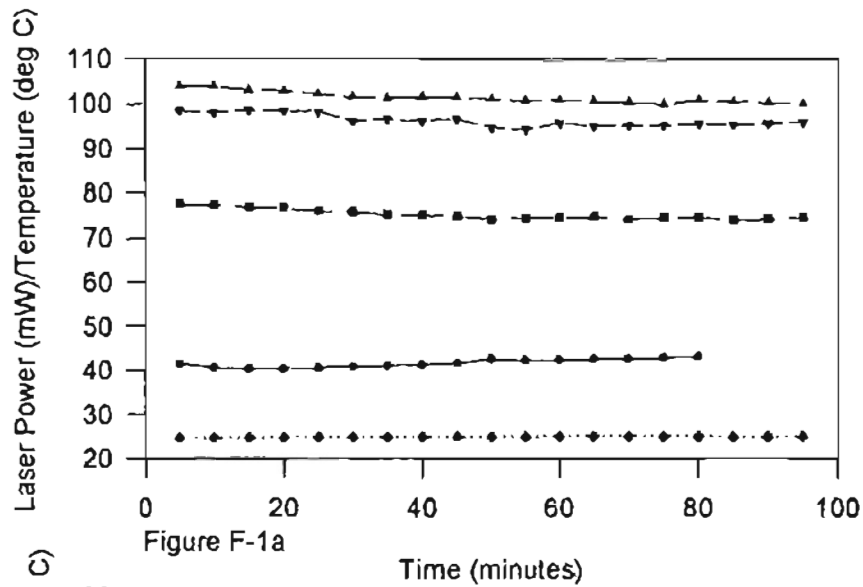
Figure E-8: Pleated Filter Efficiency for Test SAF100_1_1 at 146.36 m³/hr

APPENDIX F

CONSISTENCY MEASUREMENTS FOR THE LASER, THE ATOMIZER AND THE GLASS BEADS

The data has been tabulated such that the response of individual beams to the variation in the temperature of the Plexiglas box (which houses the laser) can be compared. For this purpose, the individual responses have been plotted on the same graph. The approximate dates on which the experiments were carried out are given along with the tabulated data. The consistency experiments on the laser have been performed jointly with author's research partner T. Gebreegziabher.

The consistency measurements for the glass beads were taken, in order to verify the suitability of the glass beads for filtration efficiency measurements. The normalized number densities for the glass beads were plotted to ascertain the maximum error in the number densities which gives an estimate of the error in the measured efficiencies (just due to the glass bead size variation).



- Blue (Shifted)
- Blue (Unshifted)
- ▲— Green (Unshifted)
- ▼— Green (Shifted)
- ...◆... Temperature

Figure F-1: Laser Power Measured at the Transceiver When the Temperature in the Plexiglas Box Is Controlled

Table TF-1a: Data for Figure F-1a (Date: May 28 - May 29, 1997)

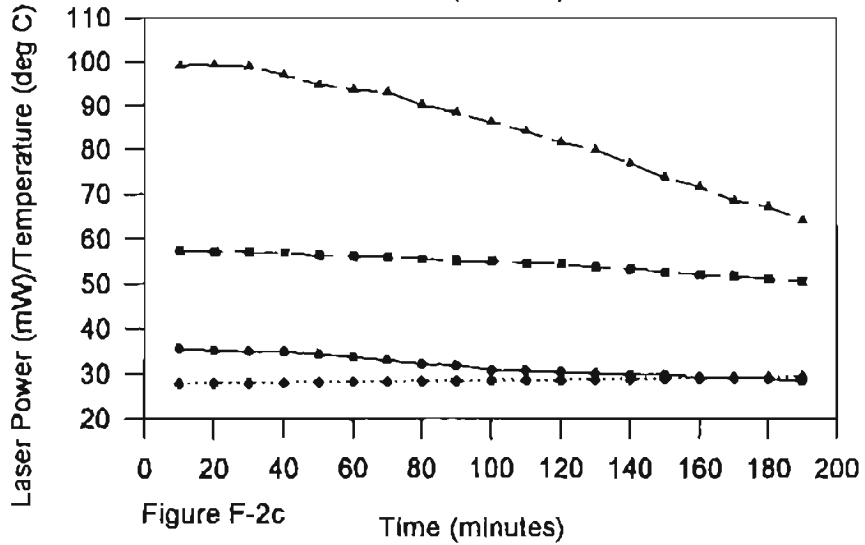
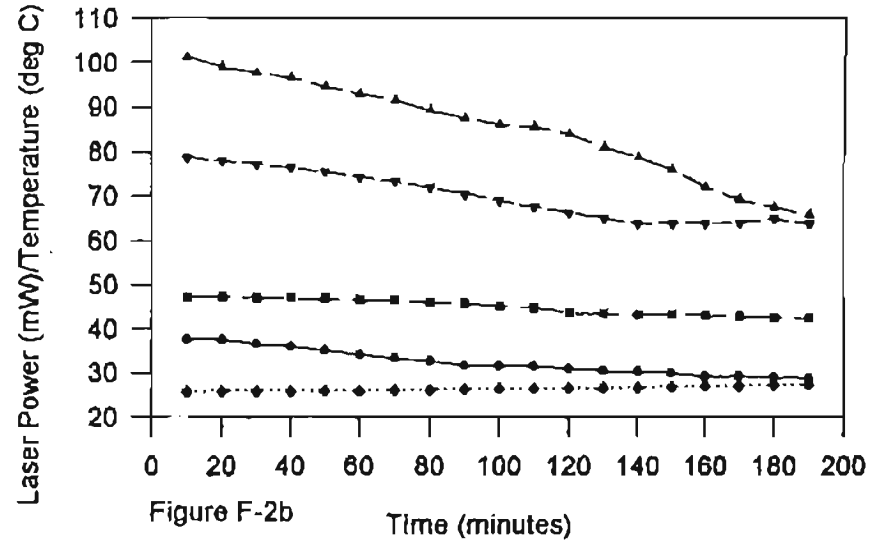
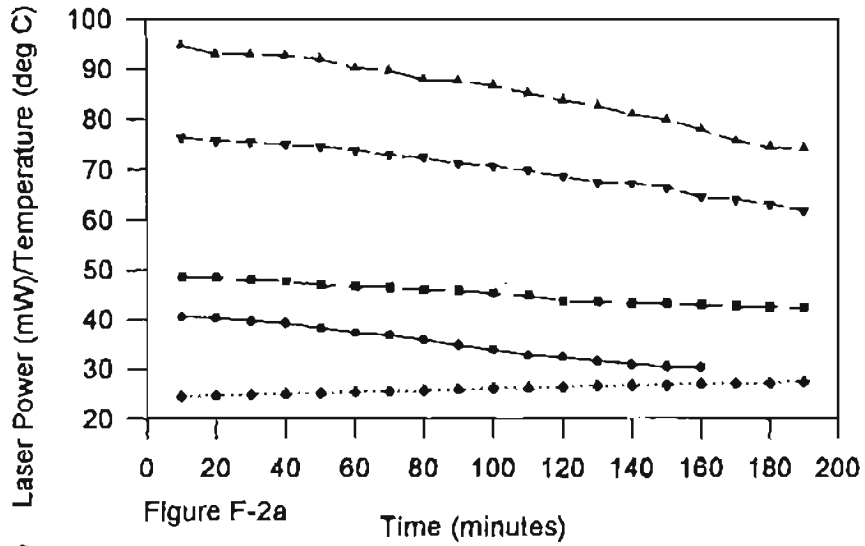
TIME (minutes)	Green (Unshifted) [mW]	Blue (Shifted) [mW]	Green (Shifted) [mW]	Blue (Unshifted) [mW]	Temperature (°C)
5	103.91	41.45	98.53	77.66	24.9
10	103.89	40.6	98.09	77.47	24.9
15	103.12	40.38	98.53	77.01	24.9
20	102.89	40.38	98.4	76.75	24.9
25	102.31	40.52	98.26	76.15	25.0
30	101.65	40.86	96.16	75.96	25.0
35	101.48	41.05	96.67	75.3	24.8
40	101.53	41.24	96.1	75.17	24.9
45	101.58	41.58	96.62	74.88	24.9
50	101.06	42.57	94.65	74.13	24.9
55	100.78	42.3	94.28	74.41	25.0
60	100.92	42.38	95.64	74.48	25.0
65	100.61	42.58	94.99	74.78	24.9
70	100.42	42.66	95.09	74.1	24.8
75	100	42.89	95.03	74.5	24.8
80	100.89	43.16	95.33	74.61	24.9
85	100.59		95.25	74	24.9
90	100.28		95.51	74.22	25.0
95	100.02		95.87	74.52	24.9

Table TF-1b: Data for Figure F-1b (Date: June 16 - June 22, 1997)

TIME (minutes)	Blue (Shifted) [mW]	Blue (Unshifted) [mW]	Green (Unshifted) [mW]	Green (Shifted) [mW]	Temperature (°C)
5	34.82	56.82	84.2	68.28	24.9
10	34.9	56.92	84.46	68.34	24.9
15	35	56.49	84.6	68.35	24.9
20	35.1	56.12	82.76	68.42	25.0
25	35.18	55.92	83.92	68.44	25.0
30	35.24	55.85	84.45	68.33	25.0
35	35.26	55.38	84.78	68.49	24.8
40	35.35	55.4	84.52	68.51	24.9
45	35.33	55.17	83.89	68.38	24.9
50	35.22	55.02	83.92	68.14	24.9
55	35.3	54.78	83.52	68.48	25.0
60	35.15	54.78	85.65	68.49	25.0
65	35.27	54.71	84.98	68.37	24.9
70	35.22	54.56	83.79	68.56	24.8
75	35.23	54.51	85.17	68.92	24.9
80	35.15	54.53	85.72	69.29	24.8
85	35.12	54.32			24.9
90	35	54.35			24.9
95	35.02	54.22			24.9

Table TF-1c: Data for Figure F-1c (Date: June 23 - July 07, 1997)

TIME (minutes)	Blue (Shifted) [mW]	Blue (Unshifted) [mW]	Green (Unshifted) [mW]	Green (Shifted) [mW]	Temperature (°C)
5	36.45	51.48	78.35	75.78	25.0
10	36.41	51.13	75.28	75.1	25.0
15	36.38	51.27	75.98	75.18	25.0
20	36.29	51.97	76.71	75.75	25.0
25	36.22	51.13	77.2	75.85	25.0
30	36.27	51.11	78.53	76.78	25.1
35	36.28	51.27	78.87	76.81	25.1
40	36.53	51.97	78.87	76.82	25.0
45	36.53	51.46	79.23	77.1	25.0
50	36.45	50.54	76.71	77.72	25.0
55	36.48	50.12	77.2	77.56	24.9
60	36.48	51.27	78.53	77.87	24.9
65	36.4	51.97	78.87	77.95	25.0
70	36.41	51.27	79.23	77.85	25.0
75	36.33	51.97	76.71	77.85	25.0
80	36.45	51.27	77.2	77.86	25.0



- Blue (Shifted)
- Blue (Unshifted)
- ▲— Green (Unshifted)
- ▼— Green (Shifted)
- ◆— Temperature

Figure F-2: Laser Power Measured at the Transceiver When the Temperature in the Plexiglas Box Is Not Controlled

Table TF-2a: Data for Figure F-2a (Date: May 21 - May 23, 1997)

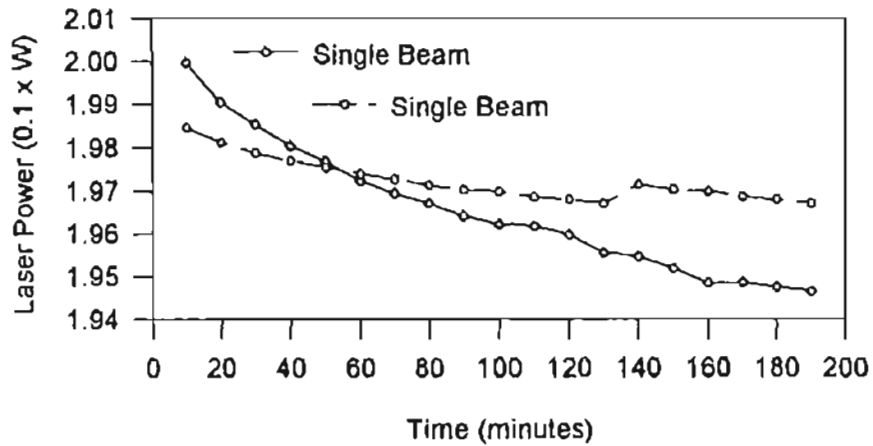
TIME (minutes)	Blue (Shifted) [mW]	Blue (Unshifted) [mW]	Green (Unshifted) [mW]	Green (Shifted) [mW]	Temperature (°C)
10	40.64	48.68	94.85	76.4	24.6
20	40.35	48.51	93.22	75.81	24.7
30	39.68	48.06	93.05	75.58	24.9
40	39.2	47.65	92.8	75.09	25.0
50	38.25	46.97	92.1	74.67	25.2
60	37.35	46.67	90.3	74.02	25.4
70	36.8	46.53	89.71	73.02	25.6
80	35.95	46.01	88.02	72.6	25.7
90	34.8	45.79	87.65	71.25	25.9
100	33.92	45.23	86.7	70.78	26.1
110	32.78	44.83	85.22	69.89	26.2
120	32.28	43.65	83.82	68.65	26.4
130	31.56	43.51	82.7	67.4	26.6
140	30.91	43.21	81.02	67.24	26.7
150	30.45	43.24	80	66.51	26.8
160	30.28	42.95	77.95	64.6	27.0
170		42.75	75.75	64.08	27.1
180		42.55	74.47	63.14	27.2
190		42.33	74.28	61.95	27.4

Table TF-2b: Data for Figure F-2b (Date: May 25 - May 27, 1997)

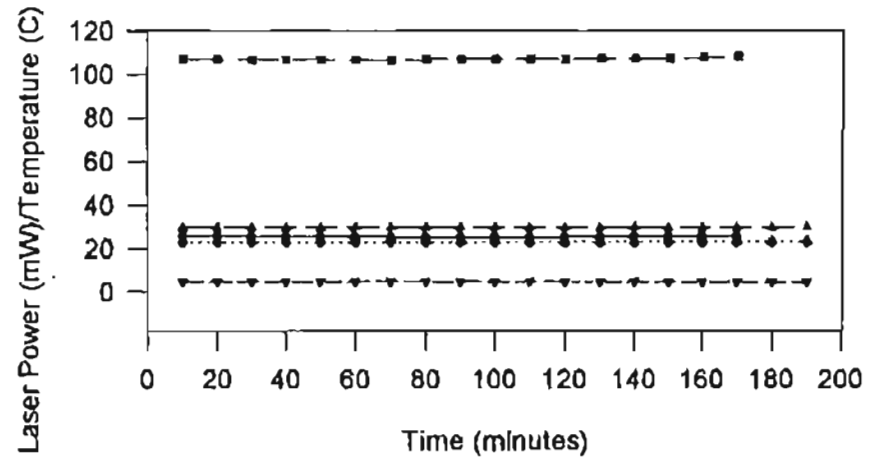
TIME (minutes)	Blue (Shifted) [mW]	Blue (Unshifted) [mW]	Green (Unshifted) [mW]	Green (Shifted) [mW]	Temperature (°C)
10	37.65	47.28	101.4	78.85	25.8
20	37.58	47.23	99.01	78.04	25.9
30	36.6	47.05	97.72	77.36	25.9
40	36	47.17	96.65	76.54	25.9
50	35.11	46.97	94.65	75.48	26.0
60	34.13	46.67	92.97	74.35	26.0
70	33.36	46.53	91.58	73.35	26.1
80	32.69	46.01	89.3	72	26.2
90	31.65	45.79	87.55	70.6	26.3
100	31.71	45.23	86.03	69.15	26.4
110	31.56	44.83	85.65	67.75	26.5
120	30.91	43.65	83.97	66.43	26.5
130	30.45	43.51	80.98	65.12	26.6
140	30.28	43.21	78.9	63.95	26.7
150	29.95	43.24	76.01	64.02	26.8
160	29.13	42.95	72.09	64	27.0
170	29.3	42.75	69.35	64.13	27.1
180	28.94	42.55	67.63	64.98	27.2
190	28.69	42.33	65.91	63.9	27.3

Table TF-2c: Data for Figure F-2c (Date: June 06 - June 10, 1997)

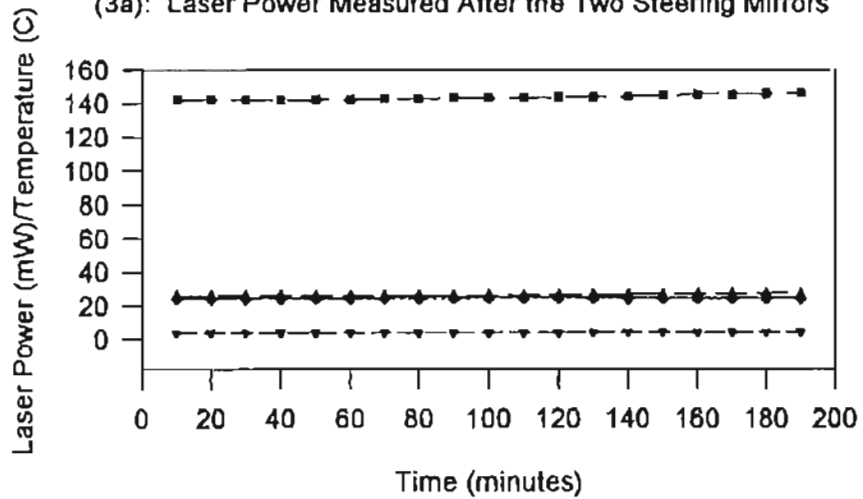
TIME (minutes)	Blue (Shifted) [mW]	Blue (Unshifted) [mW]	Green (Unshifted) [mW]	Temperature (°C)
10	35.5	57.2	98.99	27.8
20	35.1	57.07	99.3	27.9
30	34.9	56.95	98.81	27.9
40	34.8	56.75	96.92	28.0
50	34.2	56.16	94.65	28.1
60	33.6	56.06	93.52	28.2
70	32.9	55.95	93.02	28.2
80	32.1	55.5	90.12	28.4
90	31.8	55.06	88.35	28.4
100	30.8	54.96	86.17	28.5
110	30.7	54.55	83.98	28.6
120	30.4	54.41	81.5	28.6
130	30	53.58	79.78	28.7
140	29.7	53.2	76.75	28.8
150	29.7	52.52	73.64	28.8
160	29.2	52.05	71.54	28.9
170	29.1	51.68	68.35	29.0
180	28.8	51.05	67.05	28.1
190	28.3	50.5	64.05	29.2



(3a): Laser Power Measured After the Two Steering Mirrors



(3b): Laser Power Measured After the Optical Fiber Drive



(3c): Laser Power Measured After the Optical Fiber Drive

Figure F-3: Laser Power Measured at Different Points Before the Transceiver

Table TF-3a: Data for Figure F-3a (Date: May 29 - June 01, 1997)

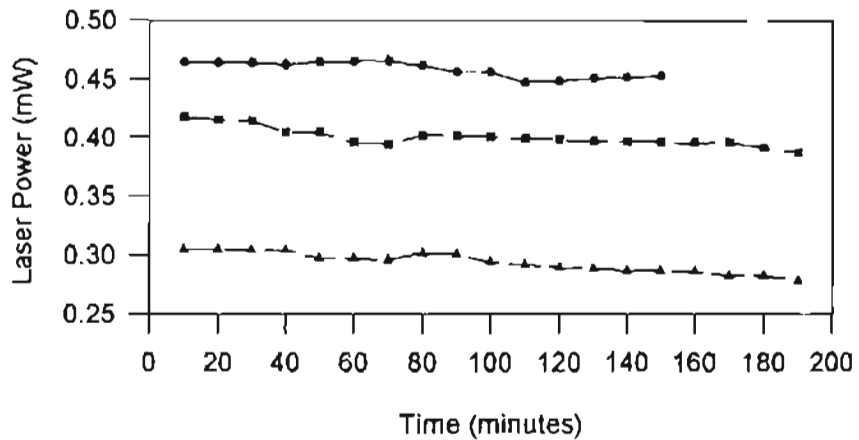
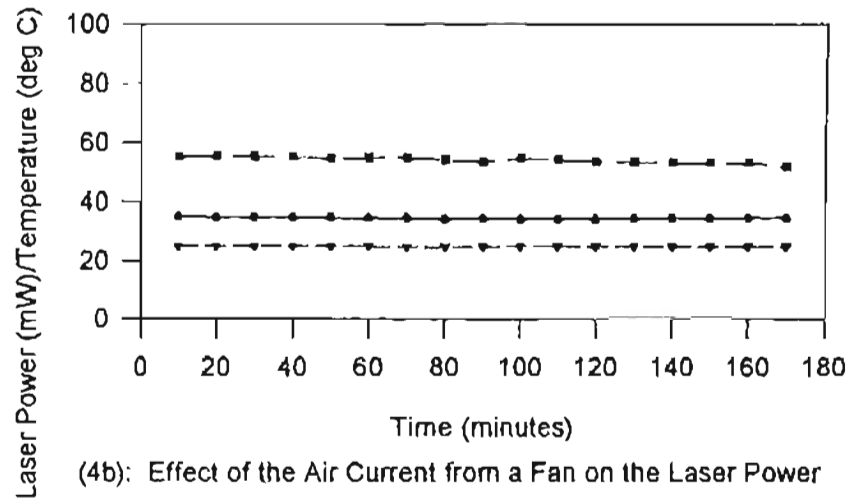
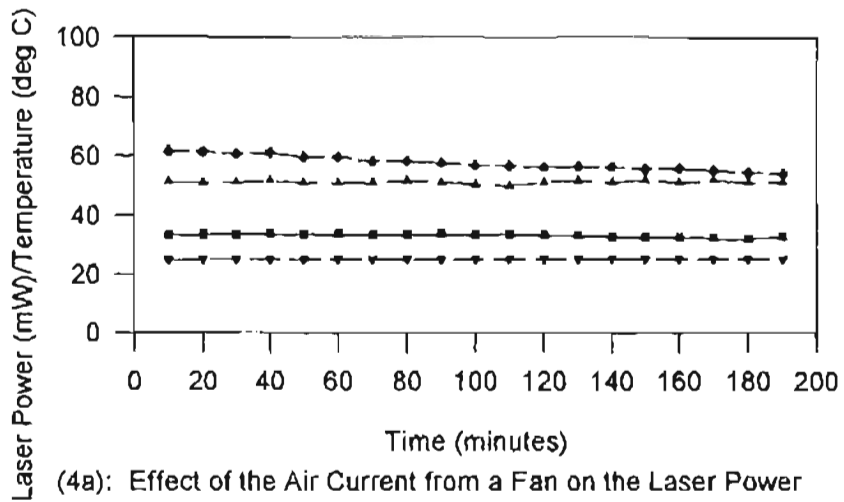
TIME (minutes)	Laser Power Measured after Steering Mirrors (x 0.1 W)	Laser Power Measured after Steering Mirrors (x 0.1 W)	Temperature (°C)
10	1.9998	1.9846	24.9
20	1.9905	1.9813	24.9
30	1.9854	1.9788	24.8
40	1.9805	1.977	24.8
50	1.9768	1.9755	24.9
60	1.9724	1.974	24.9
70	1.9695	1.9728	24.9
80	1.9672	1.9714	24.9
90	1.9642	1.9703	24.9
100	1.9623	1.9699	24.9
110	1.9618	1.9686	24.9
120	1.9598	1.968	24.9
130	1.9555	1.9671	25.0
140	1.9547	1.9714	25.0
150	1.9519	1.9703	25.0
160	1.9485	1.9699	24.9
170	1.9487	1.9686	24.9
180	1.9476	1.968	25.0
190	1.9466	1.9671	25.1

Table TF-3b: Data for Figure F-3b (Date: June 02 - June 03, 1997)

TIME (minutes)	Blue (Shifted) Measured After the Couplers (mW)	Blue (Unshifted) Measured After the Couplers (mW)	Green (Unshifted) Measured After the Couplers (mW)	Green (Shifted) Measured After the Couplers (mW)	Temperature (°C)
10	25.93	107.1	29.64	4.694	25.6
20	25.73	107.1	29.67	4.675	25.8
30	25.66	106.85	29.67	4.683	25.7
40	25.54	106.9	29.67	4.662	25.7
50	25.48	106.87	29.67	4.683	25.7
60	25.39	106.69	29.65	4.678	25.7
70	25.36	106.63	29.67	4.665	25.8
80	25.28	107.22	29.71	4.67	25.8
90	25.27	107.04	29.71	4.676	25.8
100	25.28	107.12	29.73	4.662	25.8
110	25.3	107.28	29.68	4.675	25.8
120	25.38	107	29.63	4.679	25.8
130	25.41	107.35	29.73	4.664	25.9
140	25.44	107.55	29.75	4.667	25.9
150	25.53	107.55	29.6	4.672	25.8
160	25.58	107.95	29.58	4.665	25.8

Table TF-3c: Data for Figure F-3c (Date: June 04 - June 07, 1997)

TIME (minutes)	Blue (Shifted) Measured After the Couplers (mW)	Blue (Unshifted) Measured After the Couplers (mW)	Green (Unshifted) Measured After the Couplers (mW)	Green (Shifted) Measured After the Couplers (mW)	Temperature (°C)
10	24.78	142.58	26.22	3.914	22.8
20	24.72	142.5	26.17	3.913	22.7
30	24.68	142.62	26.16	3.92	22.9
40	24.63	142.25	26.15	3.922	22.8
50	24.63	142.53	26.08	3.925	22.8
60	24.66	142.58	26.15	3.925	22.9
70	24.75	142.85	26.24	3.925	22.9
80	24.81	142.85	26.27	3.923	22.9
90	24.91	143.19	26.22	3.929	22.9
100	24.97	143.19	26.26	3.934	22.8
110	24.97	143.45	26.3	3.937	22.8
120	24.96	143.8	26.45	3.939	22.8
130	24.89	143.98	26.63	3.959	22.8
140	24.81	144.08	26.72	3.963	22.8
150	24.68	145.11	26.89	3.965	22.8
160	24.58	145.5	26.98	3.971	22.9
170	24.48	145.45	27.04	3.971	22.7
180	24.45	145.63	27.12	3.971	22.6
190	24.43	146.23	27.21	3.981	22.7
100	24.43	146.17	27.08	3.981	22.8
105	24.18	145.54	26.93	3.979	22.8
110	24.16	145.89	26.89	3.977	22.9
	24.2	145.84	26.82	3.983	22.8
	24.27	145.2	26.8	3.984	22.7
	24.27	145.23	26.83	3.986	22.7



- ◆ Blue (Shifted)
- Blue (Unshifted)
- ▲ Green (Unshifted)
- ▼ Temperature

Figure F-4: Laser Power Measured for Verifying the Effects of Air Current and Alignment of Couplers

Table TF-4a: Data for Figure F-4a (Date: July 11 - July 12, 1997)

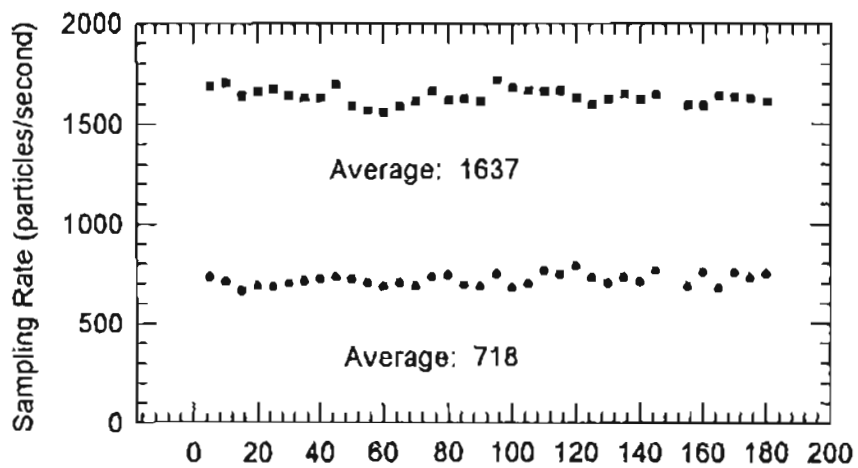
TIME (minutes)	Blue (Shifted) (mW)	Blue (Unshifted) (mW)	Green (Shifted) (mW)	Temperature (°C)
10	33.46	51.48	61.78	25.0
20	33.63	51.13	61.55	25.2
30	33.77	51.27	60.92	25.0
40	33.94	51.97	61.39	25.0
50	33.79	51.13	59.85	25.0
60	33.87	51.11	59.98	25.1
70	33.6	51.27	58.5	25.1
80	33.75	51.97	58.54	25.0
90	33.92	51.46	57.92	25.0
100	33.72	50.54	57.06	25.0
110	33.76	50.12	56.85	24.9
120	33.53	51.27	56.45	24.9
130	33.29	51.97	56.59	25.0
140	32.87	51.27	56.43	25.0
150	32.86	51.97	55.84	25.0
160	32.67	51.27	55.92	25.0
170	32.44	51.97	55.33	25.0
180	32.15	51.13	54.52	25.1
190	32.87	51.27	54.14	25.2

Table TF-4b: Data for Figure F-4b (Date: July 14 - July 15, 1997)

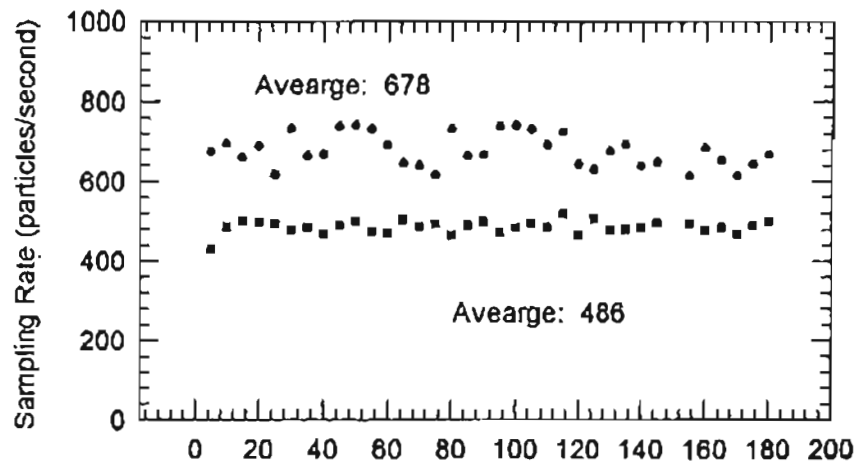
TIME (minutes)	Blue (Shifted) (mW)	Blue (Unshifted) (mW)	Temperature (°C)
10	34.95	55.05	22.9
20	34.71	55.51	22.9
30	34.74	55.26	22.8
40	34.64	55.08	22.7
50	34.64	54.62	22.8
60	34.34	54.92	22.9
70	34.43	54.81	22.9
80	34.08	54.05	22.9
90	34.21	53.37	23.0
100	34.12	54.74	23.0
110	34.1	54.22	23.0
120	34.12	53.66	23.0
130	34.27	53.22	22.9
140	34.43	53.4	22.9
150	34.42	53.12	22.9
160	34.55	53.08	22.9
170	34.52	52.05	22.9

Table TF-4c: Data for Figure F-4c (Date: July 17 - July 18, 1997)

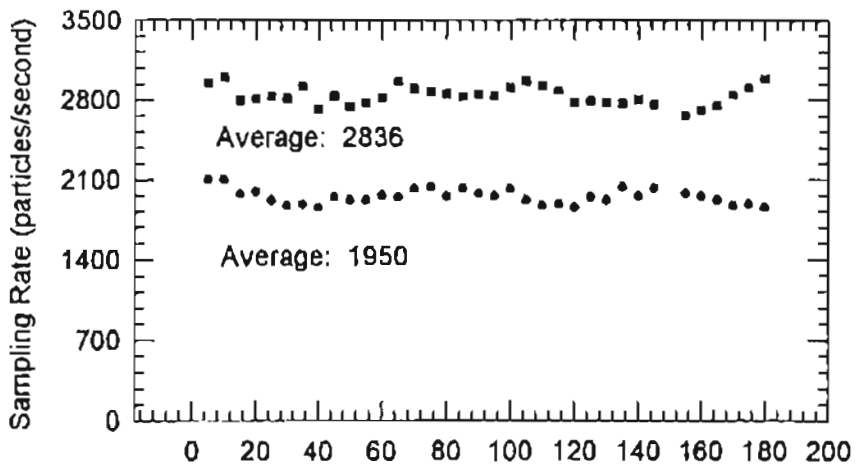
TIME (minutes)	Blue (Shifted) (mW)	Green (Unshifted) (mW)	Green (Shifted) (mW)	Temperature (°C)
10	0.4644	0.4172	0.3042	23.1
20	0.464	0.4151	0.3042	23.1
30	0.4638	0.414	0.3039	23.1
40	0.4625	0.4046	0.3037	23.1
50	0.4642	0.4042	0.297	23.2
60	0.4652	0.396	0.2968	23.2
70	0.4656	0.3945	0.2958	23.1
80	0.4614	0.4017	0.3015	23.0
90	0.4559	0.4016	0.3007	23.0
100	0.456	0.4006	0.2937	23.0
110	0.4473	0.399	0.2912	23.1
120	0.4485	0.3982	0.2889	23.1
130	0.4506	0.3972	0.2879	23.1
140	0.4514	0.3965	0.2862	23.1
150	0.453	0.3961	0.2861	23.1
160		0.3955	0.2855	23.1
170		0.3954	0.2817	23.2
180		0.3912	0.282	23.2
190		0.3872	0.2776	23.1



(5a): 2.04 micron particles Time (minutes)



(5b): 0.497 micron particles Time (minutes)



(5c): 0.966 micron particles Time (minutes)

Figure F-5: Atomizer Consistency Measurements for 0.497, 0.966 and 2.04 Micron Particles

Table TF-5a: Sampling Rate for 2.04 Micron Particles
(November 07, 1997 - March 28, 1998)

TIME (minutes)	Sampling Rate @ 25.3 °C	Sampling Rate @ 24.7 °C
5	735.12	1687.33
10	712.79	1704.64
15	666.16	1642.97
20	688.7	1660.53
25	684.18	1675.08
30	700.79	1643.34
35	716.85	1630.23
40	724.31	1630.84
45	733.1	1699.55
50	726.26	1591.97
55	705.42	1568.65
60	686.84	1560.21
65	705.42	1587.66
70	686.84	1614.81
75	736.7	1666.37
80	742.8	1618.92
85	693.05	1629.87
90	684.42	1613.4
95	747.27	1718.81
100	678.16	1682.68
105	699.61	1668.11
110	765.56	1661.81
115	744.01	1668.11
120	789.5	1629.98
125	728.57	1594.07
130	702.51	1622.07
135	732.37	1649.67
140	708.84	1622.76
145	764.86	1647.37
155	686.38	1595.23
160	757.02	1593.86
165	675.85	1642.64
170	754.49	1634.06
175	728.81	1629.44
180	748.06	1612.1

Table TF-5b: Sampling Rate for 0.497 Micron Particles
(November 11, 1997 - March 28, 1998)

TIME (minutes)	Sampling Rate @ 25.4 °C	Sampling Rate @ 24.7 °C
5	674.07	429.34
10	695.51	486.87
15	660.63	501.29
20	689.74	498.22
25	617.61	494.34
30	732.89	479.39
35	664.93	486.61
40	668.95	470.17
45	740.01	491.44
50	742.87	501.39
55	732.87	474.06
60	693.88	472.15
65	646.27	504.39
70	639.91	487.78
75	617.61	495.2
80	732.89	466.17
85	664.93	492.32
90	668.95	500.99
95	740.01	473.25
100	742.87	485.22
105	732.87	495.5
110	693.88	485.99
115	725.92	520.21
120	644.44	466.48
125	631.8	507.82
130	678.39	478.96
135	694.82	481.18
140	640.83	484.67
145	649.57	498.22
155	615.78	494.34
160	685.59	479.39
165	654.64	486.61
170	616.22	470.17
175	645.39	491.44
180	667.77	501.39

Table TF-5c: Sampling Rate for 0.966 Micron Particles
(November 26, 1997 - November 27, 1997)

TIME (minutes)	Sampling Rate @ 25.4 °C	Sampling Rate @ 25.6 °C
5	2102.83	2948.55
10	2100.12	2993
15	1975.78	2797.57
20	1996.39	2812.04
25	1918.33	2823.56
30	1873	2812.46
35	1883.28	2918.72
40	1856.44	2717.65
45	1950.23	2834.55
50	1919.24	2744.65
55	1919.24	2772.76
60	1965.17	2814.19
65	1947.95	2966.79
70	2019.86	2895.74
75	2036.06	2866.61
80	1957.14	2856.01
85	2023.31	2825.44
90	1981.45	2847.81
95	1956.2	2835.84
100	2018.81	2905.37
105	1918.33	2967.7
110	1873	2917.03
115	1883.28	2875.49
120	1856.44	2774.57
125	1950.23	2788.91
130	1919.24	2775.3
135	2036.06	2768.32
140	1957.14	2803.25
145	2023.31	2762.41
155	1981.45	2662.85
160	1956.2	2708.91
165	1918.33	2751.54
170	1873	2841.43
175	1883.28	2899.46
180	1856.44	2982.63

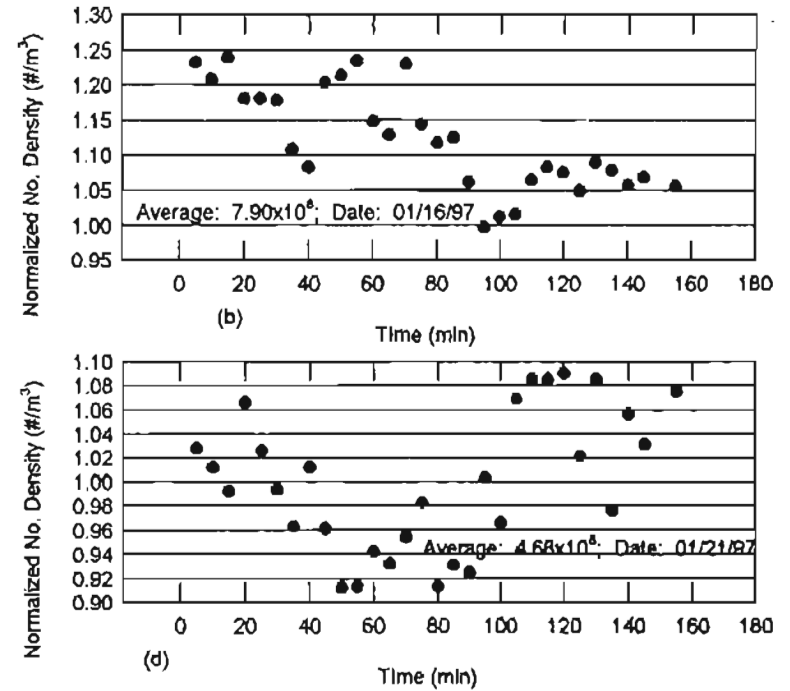
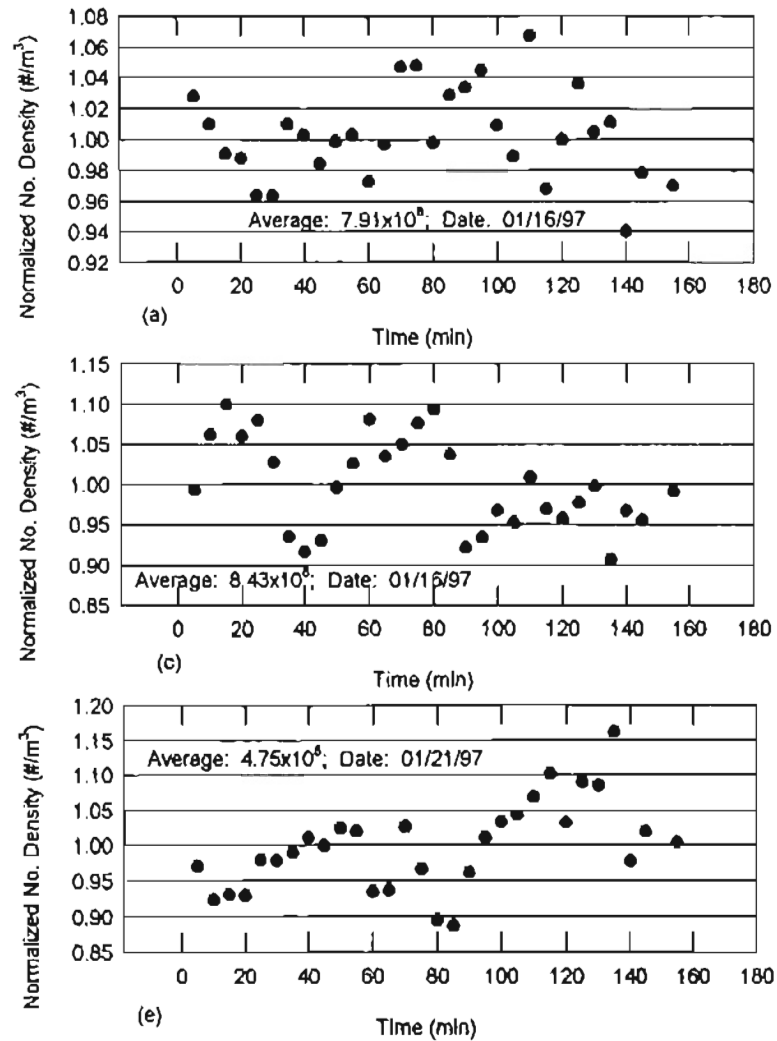


Figure F-6: Consistency Measurements for 1.59 Micron Glass Beads at 103.69 m³/hr

Table TF-6: Data for Figure F-6 for Glass Beads

Time (minutes)	Number Density (Particles/m ³) Date 01/16/97 (a)	Number Density (Particles/m ³) Date 01/16/97 (b)	Number Density (Particles/m ³) Date 01/16/97 (c)	Number Density (Particles/m ³) Date 01/21/97 (d)	Number Density (Particles/m ³) Date 01/21/97 (e)
5	7.85E+08	8.12E+08	8.19E+08	5.76E+08	4.89E+08
10	8.4E+08	8E+08	7.79E+08	5.65E+08	4.8E+08
15	8.69E+08	7.84E+08	7.85E+08	5.79E+08	4.71E+08
20	8.38E+08	8.42E+08	7.84E+08	5.52E+08	4.7E+08
25	8.54E+08	8.11E+08	8.27E+08	5.52E+08	4.59E+08
30	8.12E+08	7.85E+08	8.26E+08	5.51E+08	4.59E+08
35	7.39E+08	7.61E+08	8.35E+08	5.18E+08	4.8E+08
40	7.25E+08	8E+08	8.53E+08	5.06E+08	4.77E+08
45	7.35E+08	7.59E+08	8.43E+08	5.63E+08	4.68E+08
50	7.88E+08	7.21E+08	8.64E+08	5.67E+08	4.75E+08
55	8.11E+08	7.22E+08	8.61E+08	5.77E+08	4.77E+08
60	8.55E+08	7.44E+08	7.89E+08	5.37E+08	4.63E+08
65	8.18E+08	7.36E+08	7.9E+08	5.28E+08	4.74E+08
70	8.3E+08	7.54E+08	8.67E+08	5.75E+08	4.98E+08
75	8.5E+08	7.77E+08	8.16E+08	5.35E+08	4.99E+08
80	8.64E+08	7.22E+08	7.55E+08	5.22E+08	4.75E+08
85	8.2E+08	7.36E+08	7.48E+08	5.26E+08	4.89E+08
90	7.29E+08	7.31E+08	8.12E+08	4.97E+08	4.91E+08
95	7.38E+08	7.93E+08	8.53E+08	4.66E+08	4.97E+08
100	7.65E+08	7.63E+08	8.71E+08	4.73E+08	4.8E+08
105	7.53E+08	8.45E+08	8.79E+08	4.74E+08	4.7E+08
110	7.97E+08	8.58E+08	9.02E+08	4.98E+08	5.07E+08
115	7.66E+08	8.58E+08	9.29E+08	5.06E+08	4.6E+08
120	7.56E+08	8.61E+08	8.7E+08	5.03E+08	4.75E+08
125	7.72E+08	8.07E+08	9.19E+08	4.9E+08	4.93E+08
130	7.88E+08	8.58E+08	9.16E+08	5.09E+08	4.78E+08
135	7.17E+08	7.71E+08	9.8E+08	5.04E+08	4.81E+08
140	7.65E+08	8.35E+08	8.25E+08	4.94E+08	4.47E+08
145	7.55E+08	8.14E+08	8.59E+08	5E+08	4.65E+08
155	7.84E+08	8.5E+08	8.47E+08	4.93E+08	4.61E+08

APPENDIX G

EXPERIMENTS CONDUCTED TO VERIFY THE REPEATABILITY OF THE MEASUREMENTS

In order to ascertain the repeatability of the measurements after the laser system had been received from Aerometrics after maintenance, three different flow rates were run in the Small Angle Diffuser housing; and the results were compared with those of Jadbabaei [1997] as shown in Table 5.3. Further the filtration efficiencies for test SAH75_05_1 and SAH75_05_2 have been plotted on the same graph for comparison of the local efficiencies. As can be seen, almost all of the local efficiencies are fairly close to those of Jadbabaei [1997].

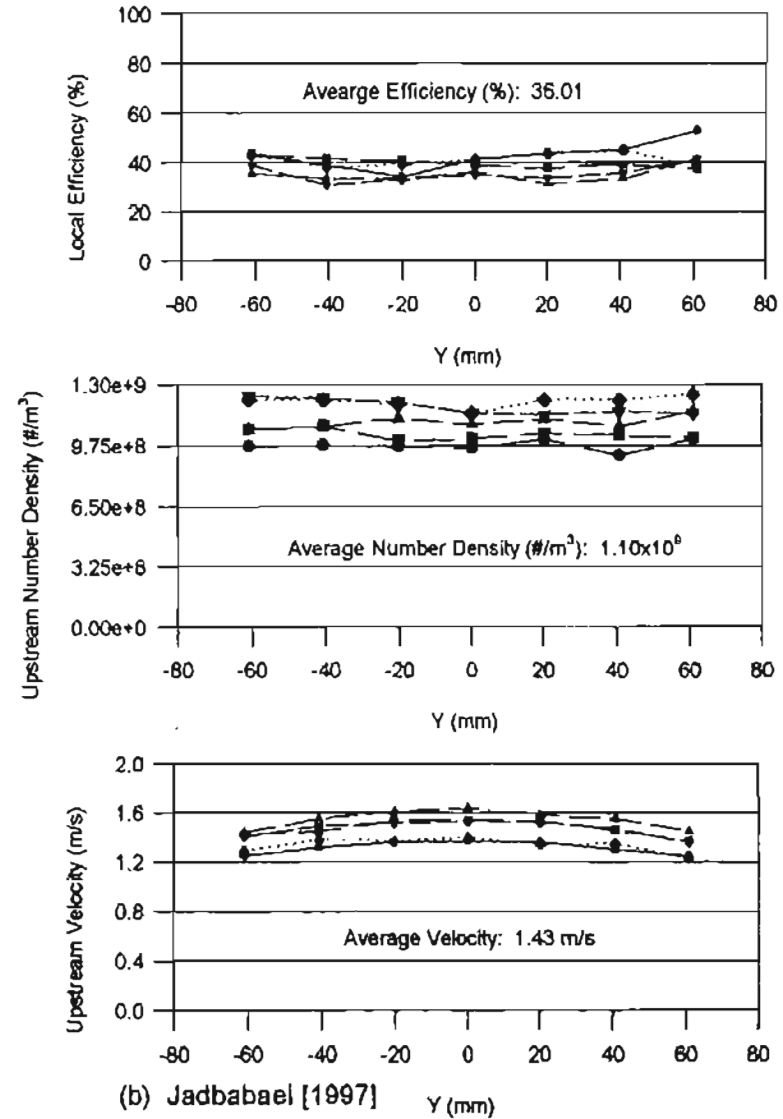
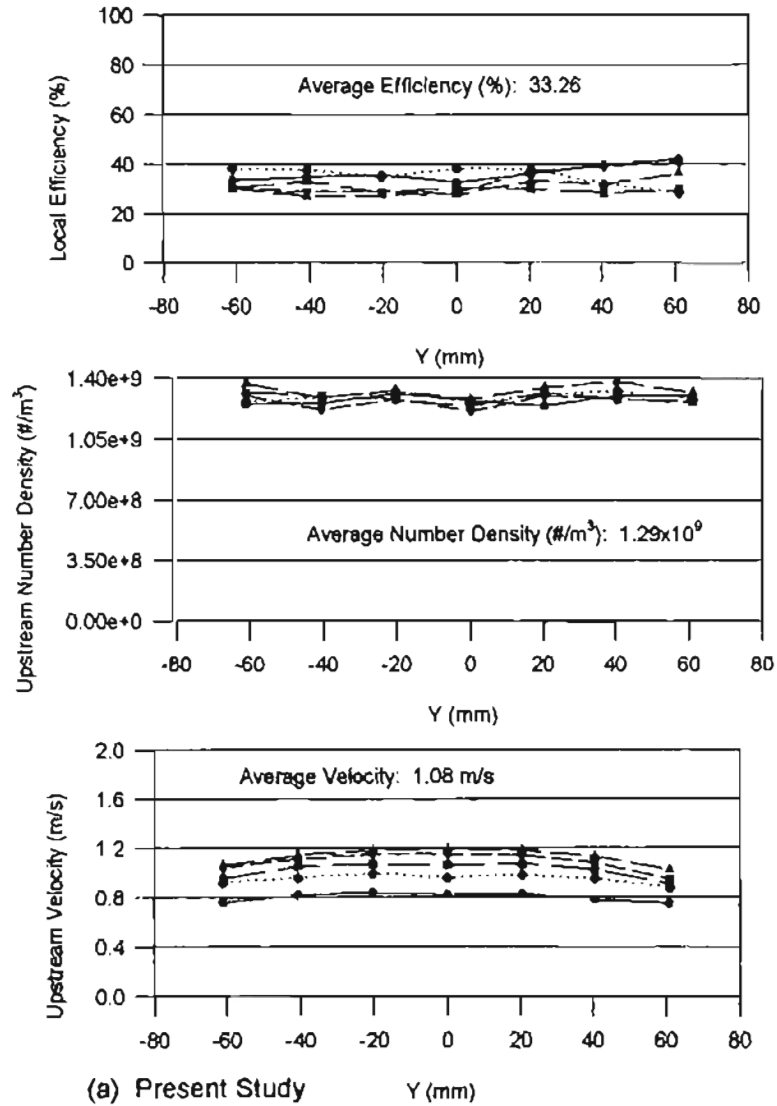


Figure G-1: Comparison of Local Efficiency, Upstream Velocity and Number Density Profiles with Jadbabael [1997] at $77.07 \text{ m}^3/\text{hr}$

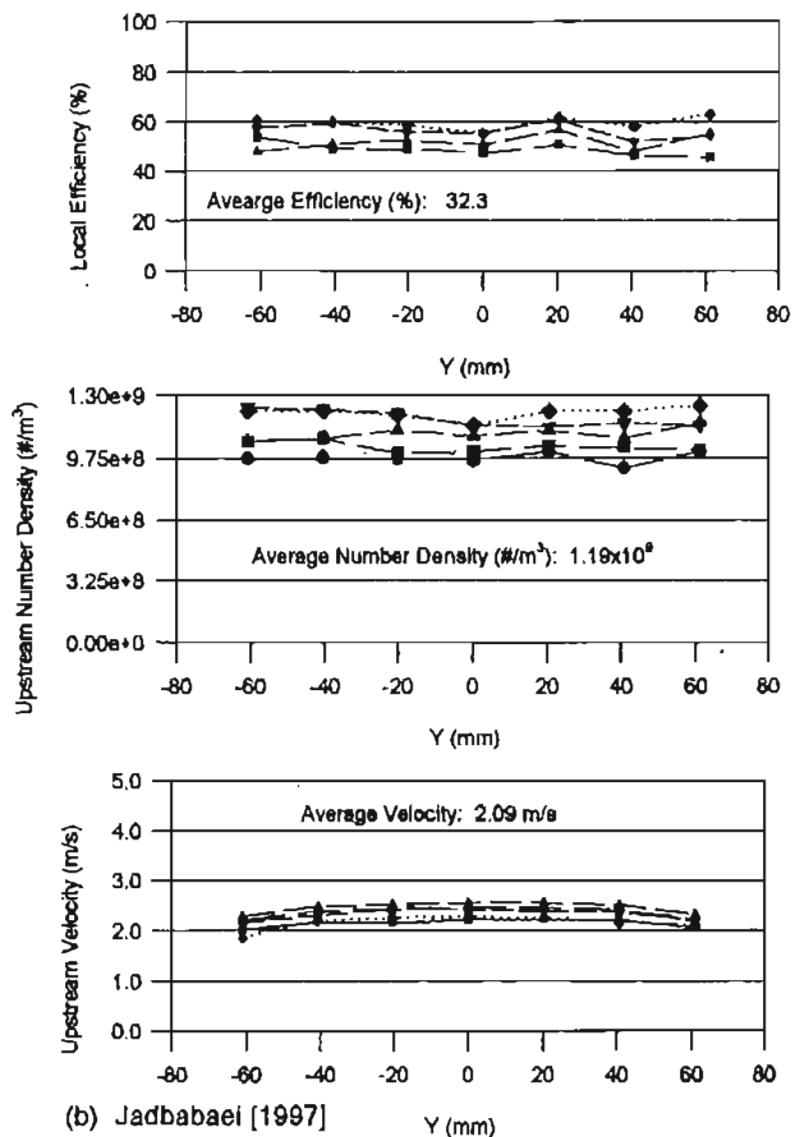
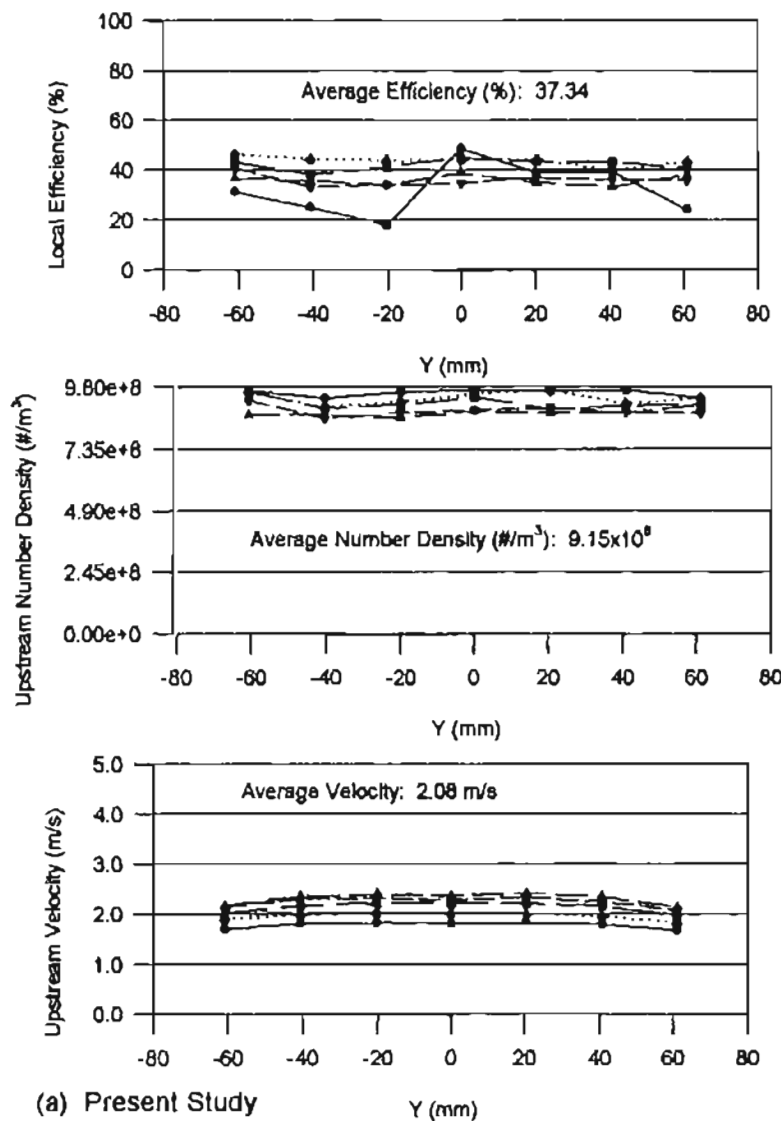


Figure G-2: Comparison of Local Efficiency, Upstream Velocity and Number Density Profile with Jadbabaei [1997] at 103.69 m³/hr

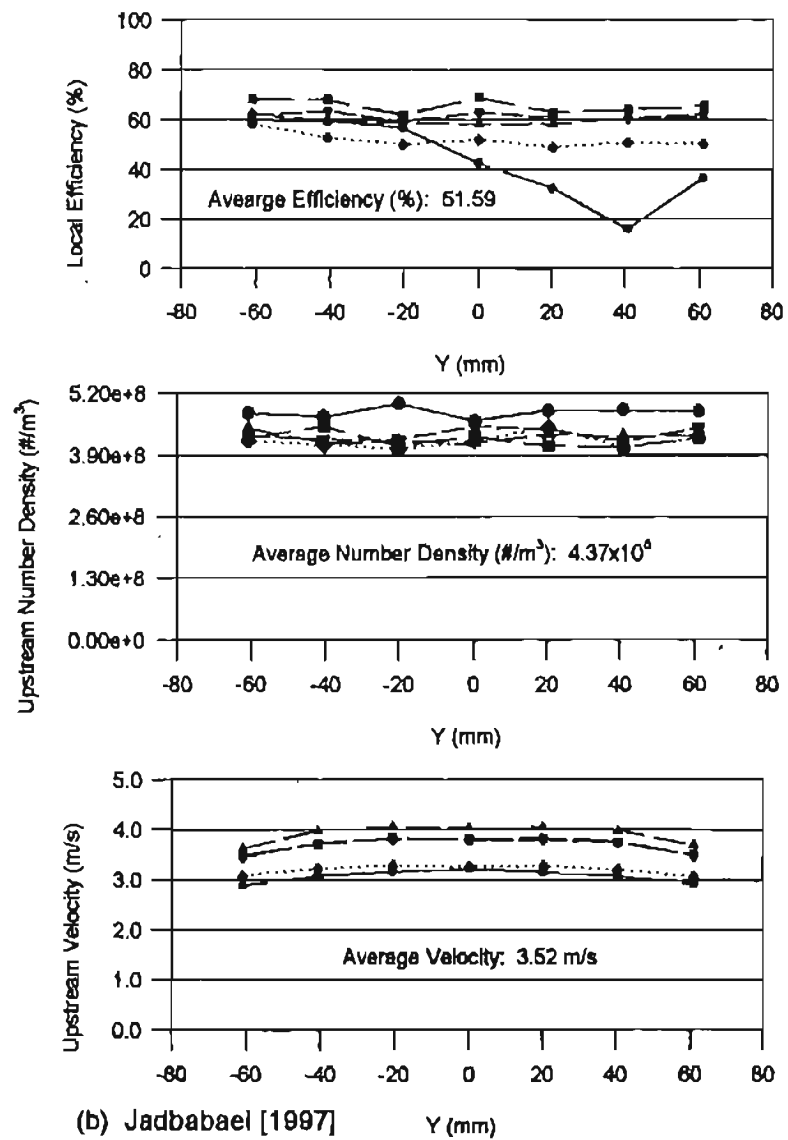
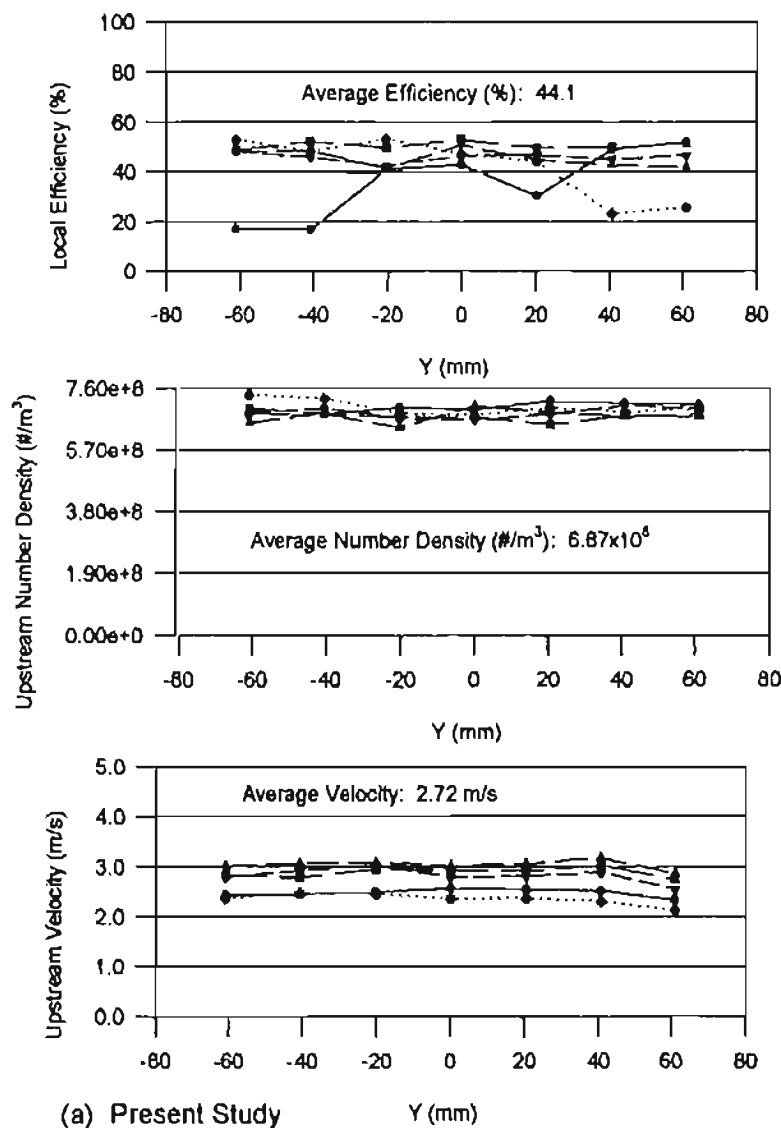


Figure G-3: Comparison of Local Efficiency, Upstream Velocity and Number Density Profiles with Jadbabael [1997] at 188.45 m³/hr

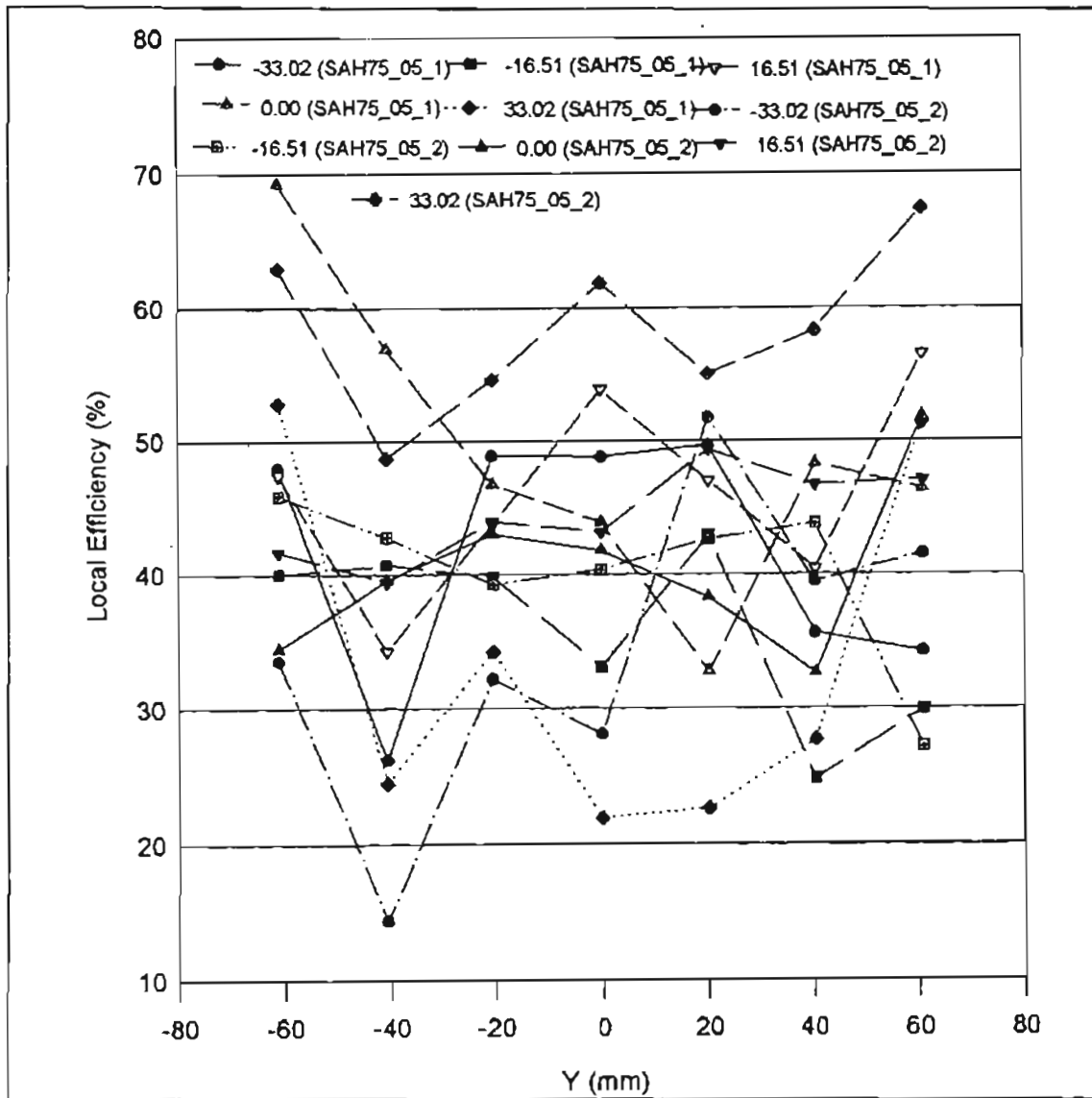


Figure G-4 Comparison of the Local Filtration Efficiencies for Tests SAH75_05_1 and SAH75_05_2

APPENDIX H

SWEPT VOLUME TECHNIQUE

The Swept Volume Technique was developed by Liang [1997] to determine the number density value from the number of particles counted (N_i), their average measured velocity (v_i), the length of time taken to count these particles, and the area of the probe (A) swept to form the volume. The method assumes that all of the particles crossing the probe volume have a velocity equal to the average velocity of all samples measured at a location. Thus, number density is given as

$$n_i = \frac{N_i}{v_i t_i A} \quad (\text{H-1})$$

The probe area is $3.257 \times 10^{-11} \text{ m}^2$ [Liang, 1997]. Figure H-1 shows the concept of the swept volume.

This technique has been shown to fail at very low velocities [Jadbabaei, 1997]. A look at Eq. (G-1) indicates that, for very low velocities like those measured near the walls of the housing, the number density tends to an erroneously large value. Jadbabaei [1997] explains this observation from a physical point of view and discusses a number of different modifications to overcome this difficulty. Jadbabaei [1997] indicates that in regions where there is a recirculating flow, the average velocity of the particles is close to zero, but the velocity distribution is comprised of both positive and negative velocity values. This

technique assumes that the velocity is unidirectional, which is not the case in many situations (for example a recirculating flow). Jadbabaei [1997] suggests the use of root mean squared velocity or absolute value average velocity but is unable to mathematically / physically justify their use. For the present study (Small Angle Diffuser housing, standard SAE J726 housing, Simulated Automotive Filter housing) the flow field was assumed to be uniform in the measurement grid, thus allowing the use of the swept volume technique.

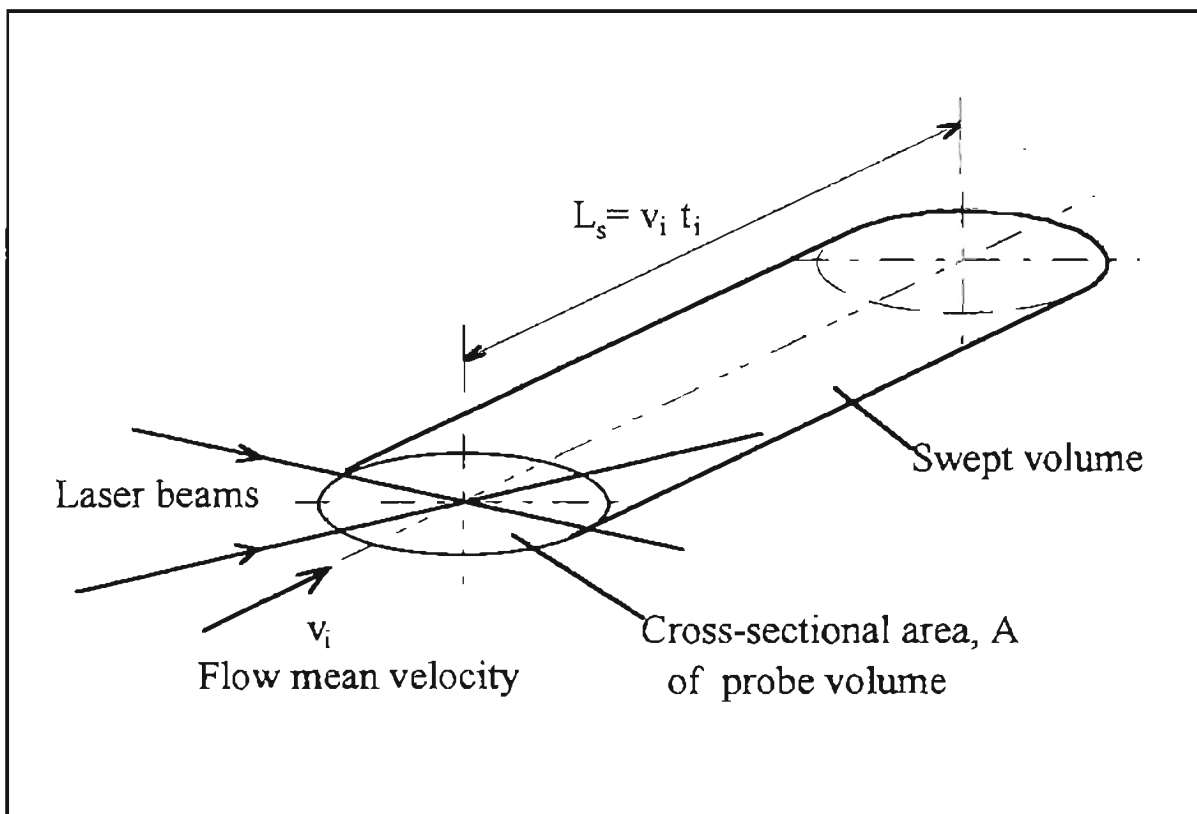


Figure H-1: Swept Volume [Liang, 1997]

APPENDIX I

ERROR ANALYSIS

The error analysis in Section 4.2 was based on simple analysis of the variation in the number density calculation. Anand [1997] has presented error analysis as proposed by Kline and McClintock [1953]. This based on the assumption of a random error in number density measurements. The error in number density due to errors in N, v, t and A has been shown to be equal to

$$\frac{dn}{n} = \left[\left(\frac{dN}{N} \right)^2 + \left(\frac{dv}{v} \right)^2 + \left(-\frac{dt}{t} \right)^2 + \left(-\frac{dA}{A} \right)^2 \right]^{1/2} \quad (\text{I-1})$$

Making use of the error in the number density measurements, the error in the measured efficiencies will be given by the following equation

$$\frac{d\eta}{\eta} = \frac{n_d}{n_u} \left[(c_u)^2 + (c_d)^2 \right]^{1/2} = \sqrt{2} (c_e) R_{nd} \quad (\text{I-2})$$

Where c_e (any constant) is the value of the fractional error values for the upstream (n_u) and downstream number densities (n_d). Anand assumed an error of 2% for the area of the probe volume of the LDV system. Using the test data for Test SAH75_05_2 (Fig. B-12), the error for the various parameters of particle velocity, time taken to take the upstream data, and number of particles counted, the error for the respective parameters was found

to be 8%, 3% and 2% respectively. These are the deviations of the measured parameters assuming a standard deviation of 2σ (confidence level of approximately 97%) for the measured data. Using these error values for the measured values, the error in the calculated number densities was found to be

$$\frac{dn}{n} = \left[(0.08)^2 + (-0.03)^2 + (-0.02)^2 + (-0.02)^2 \right] = 0.09 \text{ or } 9.00\% \quad (\text{I-3})$$

If this error was substituted into Eq. (I-2), then the following relation will give the error in efficiency

$$\frac{d\eta}{\eta} = \sqrt{2}(0.09)R_{nd} = (0.1272)R_{nd} \quad (\text{I-4})$$

Thus the above mentioned errors in the measured values of number count, velocity, time, and probe cross-sectional area result in an efficiency error given by Eq. (I-4).

APPENDIX J

LIST OF EQUIPMENT

1. 5 - Watt Argon Ion laser: Coherent, Model Innova 70-A, Serial No. P/S 92K-1758
2. Remote control for the laser: Coherent, Model I-70, Serial No. 92411171
3. Fiber drive: Aerometrics, Inc., Model FBD1240, Serial No. 026
4. Bragg cell: IntraAction, Inc., Model ME-40H, Serial No. 3247
5. Photomultiplier Tubes: Aerometrics, Inc., Model RCM2200L, Serial No. 029
6. Doppler Signal Analyzer: Aerometrics, Inc., Model DSA3220, Serial No. 044
7. Computer and Monitor: Impression 3, IBM compatible 80486 DX2, 66 MHz
8. Computer for Traverse System and MS-Excel Data Acquisition Files: Gateway 2000, IBM compatible, 80486 DX2, 33 MHz
9. Laser Transceiver: Aerometrics, Inc., Model XRV1212, Serial No. 001
10. Three Stepper Motors (Sanyo Denki, Type: 103-850-11)
11. Oscilloscope: Hewlett Packard, Model 54501A
12. Plexiglas Test Housings: a) Similar to SAE J1669 Small Angle Diffuser Housing, b) Standard J726 housing, c) Simulated Automotive Filter housing.
13. Pleated Test Filters: Dayco-Purolator, Inc., A13192 (formerly AF3192)
14. TSI Mass Flow Sensor: TSI, Model 2018, Serial No. 30644

15. Atomizer: TSI Model 9306, six-jet atomizer
16. SAE J726 Air Stand, Purolator Products, Inc.
17. Rival Compact Heater, Model T114
18. Stepper Motor Drives, Model CMD-40
19. 24 V DC - 6 A Power Supply (Acme Electronics)
20. Connector 3 for Digital Output, Model PCLD-780
21. Ultrasonic Humidifier: Pollenex, Model SH55R
22. Room Air Conditioner: Cooling Capacity 12600 Btu/hr
23. Polystyrene Latex (PSL) Particles: 0.497, 0.966, 2.04 μm particles, accuracy (99.99%), Duke Scientific; \$700 for 100 ml of the particles in a 10% solution
24. Glass Beads: 1.59 μm diameter beads, Standard Deviation: 0.304, Powder Technologies Inc.; \$50 for 25 gm of the particles

VITA

Puneet Saxena

Candidate for the Degree of

Master of Science

Thesis: COMPARISON OF FILTRATION EFFICIENCY OF PLEATED FILTERS
FOR DIFFERENT PARTICLE SIZES

Major Field: Mechanical Engineering.

Biographical:

Personal Data: Born in Lucknow, Uttar Pradesh, India, on March 15, 1972,
son of Arun Saxena and Deepika Arun.

Educational: Graduated from Central School, New Delhi, India in April 1989;
received Bachelor of Engineering degree in Mechanical Engineering
from University of Mysore, India in October 1994. Completed the
requirements for the Master of Science degree with a major in
Mechanical Engineering at Oklahoma State University in July 1998.

Experience: Employed by Oklahoma State University as a graduate research
assistant from August 1996 to May 1998; worked as Factory Quality
Engineer with Hindustan Lever Ltd. from September 1995 to July 1996
and as an Officer Trainee - Technical with Hindustan Lever Ltd from
October 1994 to August 1995.

Professional Memberships: Student Member, ASME and AIAA.